AFFDL-TR-71-50
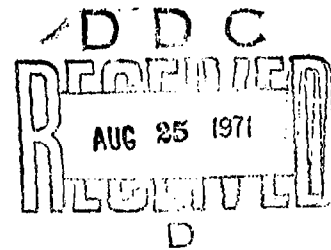
AD728647

THEORY OF AN AIR CUSHION LANDING SYSTEM FOR AIRCRAFT

KENNERLY H. DIGGES

TECHNICAL REPORT AFFDL-TR-71-50

JUNE 1971

AIR FORCE FLIGHT DYNAMICS LABORATORY
AIR FORCE SYSTEMS COMMAND
WRIGHT-PATTERSON AIR FORCE BASE, OHIO

324

13. ABSTRACT

The Air Cushion Landing System is a scheme to replace the wheeled landing gear on aircraft by a peripheral jet air cushion. This concept has been developed through flight testing by Bell Aerosystems and the Air Force Flight Dynamics Laboratory. The concept employs a flexible elastic membrane or "trunk" which is attached to the bottom of the aircraft fuselage. During flight, the trunk shrinks elastically and hugs the bottom of the fuselage like a de-icing boot. When a flow of air is applied to the inside of the trunk, the elastic material stretches and forms an elongated doughnut-shaped protrustion on the underside of the aircraft. The air flow is ducted by the trunk to the fuselage periphery and exhausted through a large number of holes or slots. As a result, a pressure builds up under the aircraft when the ground is approached. The pressure is sufficient to support the aircraft and absorb its vertical landing velocity. This study develops analytical relationships between the variables associated with the Air Cushion Landing System. Included are the following: (a) The derivation of a theory which predicts the static characteristics of the system. (b) Analytical methods for predicting flow, jet height and power requirements. (c) Curves which illustrate the interrelationships among the design variables. (d) Computer programs for predicting the cross-sectional area and shape of the elastic trunk. (e) The development and test of an analytical model which predicts the dynamic response of the system to landing impact. (f) A discussion of the design considerations for the system.

Preliminary experimental data is presented to illustrate that agreement between theory and experiment is good.

NOTICE

When Government drawings, specifications, or other data are used for any purpose other than in connection with a definitely related Government procurement operation, the United States Government thereby incurs no responsibility nor any obligation whatsoever; and the fact that the government may have formulated, furnished, or in any way supplied the said drawings, specifications, or other data, is not to be regarded by implication or otherwise as in any manner licensing the holder or any other person or corporation, or conveying any rights or permission to manufacture, use, or sell any patented invention that may in any way be related thereto.

KEY WORDS						
	ROLE	WT	ROLE	WT	ROLL	WT
Air Cushion Vehicles; landing gear; hover craft						

BLANK PAGE

THEORY OF AN AIR CUSHION LANDING SYSTEM FOR AIRCRAFT

KENNERLY H. DIGGES

FOREWORD

This technical report has been reviewed and is approved.

LEO H. HILDEBRANDT
Chief, Vehicle Equipment Division
AF Flight Dynamics Laboratory

Abstract

The Air Cushion Landing System is a scheme to replace the wheeled landing gear on aircraft by a peripheral jet air cushion. This concept has been developed through flight testing by Bell Aerosystems and the Air Force Flight Dynamics Laboratory.

The concept employs a flexible elastic membrane of "trunk" which is attached to the bottom of the aircraft fuselage. During flight, the trunk shrinks elastically and hugs the fuselage like a de-icing boot. When a flow of air is applied to the inside of the trunk, the elastic material stretches and forms an elongated doughnut-shaped protrusion on the underside of the aircraft. The air flow is ducted by the trunk to the fuselage periphery and exhausted through a large number of holes or slots. As a result, a pressure builds up under the aircraft when the ground is approached. The pressure is sufficient to support the aircraft and absorb its vertical landing velocity.

This study develops analytical relationships between the variables associated with the Air Cushion Landing System. Included are the following:

(a)   The derivation of a theory which predicts the static characteristics of the system.

(b)   Analytical methods for predicting flow, jet height, and power requirements.

(c)   Curves which illustrate the interrelationships among the design variables.

(d)   Computer programs for predicting the cross-sectional area and shape of the elastic trunk.

(e)   The development and test of an analytical model which predicts the dynamic response of the system to landing impact.

(f)   A discussion of the design considerations for the system.

Preliminary experimental data is presented to illustrate that agreement between theory and experiment is good.

iv

TABLE OF CONTENTS

LIST OF ILLUSTRATIONS

x

LIST OF TABLES

LIST OF SYMBOLS

Latin letters

A	piston area, ft^2
A_c	cushion area, ft^2
A_g	cushion area under trunk, ft^2
A_h	cushion area under aircraft hard structure, ft^2
A_I	jet augmentation ratio
A_j	cross-sectional area of the trunk, ft^2
A_3	trunk footprint area, ft^2
a	x coordinate of upper trunk attachment point, ft.
$\bar{a}$	horizontal distance between trunk attachment points, ft
a_D	total area of exhaust nozzle for fan calibration test, ft^2
a_j	total area of all orifices in the trunk, ft^2
a_n	total area of all orifices in the nth segment of the trunk, ft^2
a_r	effective flow area for fan backflow, ft^2
a_3'	effective flow area for the ℓ_3 segment of the trunk, ft^2
b	y coordinate of upper trunk attachment point, ft
C_D	coefficient of discharge for plenum chamber
C_{hd}	power - jet height parameter
C_{ht}	power - thickness parameter
C_p	specific heat at constant pressure, $Btu/lb^o\ F$
C_Q	flow coefficient for pressure distribution across the jets
$(C_Q)_n$	flow coefficient for pressure distribution across the nth row of jets
C_T	percent reduction in flow area of cushion exhaust caused by trunk jets
C_v	coefficient of discharge for the trunk
C_x	coefficient of discharge for the trunk nth row of orifices in the trunk

C_y	flow coefficient associated with vehicle height
C_z	vertical thrust coefficient
D	cushion diameter, ft
D_q	trunk orifice diameter, ft
D_1	cushion width, ft
D_2	cushion length, ft
d	jet height of trunk daylight clearance, ft
d_n	jet height for the nth row of jets, ft
E_t	unit elongation per pound of tension per foot-length in axial direction for the trunk material
e	horizontal distance between lower trunk attachment points, ft
F_j	total vertical thrust from jet exhaust, lb
F_3	total force developed in the trunk footprint, lb
f	arbitrary function
g	acceleration due to gravity, ft/sec^2
g_0	constant from Newton's law, lbm · ft/lbf · sec^2
H	total clearance between vehicle hard structure and the ground, ft
h	specific enthalphy, Btu/lb
hp	power supplied to the air by the fan, horsepower
J	magnitude of the total momentum of the air from all trunk jets, ft-lb/sec
J'	magnitude of the total momentum reaction of all gas exhausting from the trunk, lb
J_n'	magnitude of the total momentum reaction of the gas exhausting from the nth row of jets, lb
K_n	effective length for calculating volume of the nth trunk segment from the cross-sectional area $(A_j)n$, ft
k	ratio of specific heats
L_n	effective length for calculating the footprint area of the nth trunk segment from the footprint length $(\ell_3)_n$, ft

L_s	length of trunk side segment, ft
ℓ	cross-sectional length of trunk, ft
$\bar{\ell}$	trial value of the cross-sectional length of trunk, ft
ℓ_n	length of trunk segment n, ft
ℓ_o	design length of trunk cross-section, ft
M	total number of rows of orifices
M_n	number of rows of orifices
m	mass per unit width of an infinitesimal element of gas in jet (see figure 2-2), slugs/ft
$\dot{m}$	mass flow rate, slugs/sec
N	number of jet orifices per row
n'	effective number of rows or orifices which contribute to cushion exhaust nozzle area reduction
P (p)	pressure, psfa (psfg)
P_a	atmospheric pressure, psfa
P_c (p_c)	cushion pressure, psfa (psfg)
P_j (p_j)	trunk pressure, psfa (psfg)
P_n	static pressure in cushion exhaust nozzle at nth row of trunk orifices, psf
P_c/P_j	cushion to trunk pressure ratio (both pressures in psfa)
p_c/p_j	cushion to trunk pressure ratio (both pressures in psfg)
Q	flow rate, ft^3/sec
Q_c	total flow from the cushion, ft^3/sec
Q_i	total flow from the fan, ft^3/sec
Q_j	total flow from the trunk, ft^3/sec
Q_L	leakage flow, ft^3/sec
Q_n	total flow from the orifices in the $(\ell_n)^{th}$ trunk segment, ft^3/sec
Q_p	total flow from the plenum chamber, ft^3/sec
Q_r	total fan flow at stall pressure, ft^3/sec
$(Q_t)_n$	total flow from the jets in row n through row m, ft^3/sec

R	radius of curvature of jet exhaust, ft
$\bar{R}$	universal gas constant, Btu/lb$^\circ$F
R_n	radius of curvature of nth segment, ft
$\bar{r}_n$	distance between the center of revolution and the centroid of the cross-sectional area $(A_j)_n$ for the nth trunk shape, ft
S	cushion perimeter, ft
S'	effective length of jet, ft
S_g	effective length for calculating cushion area A_g from the length X_o, ft
S_g'	effective length for calculating the volume V_g from the area A_g, ft
S_j	effective length for calculating the trunk volume V_j from the area A_j, ft
S_n	effective length of the nth trunk segment, ft
S_3	peripheral distance around the trunk at cushion nozzle exhaust, ft
s_n	peripheral distance around the trunk at nth row of orifices, ft
T	absolute temperature of air, $^\circ$F
T_t	tension in the trunk material in the tangential direction per unit length in the axial direction, lb/ft
t	thickness of peripheral jet nozzle, ft
t_n	effective thickness of nth jet, ft
U	total internal energy of the gas in the control volume, Btu
u	specific internal energy of the gas in the control volume, Btu/lb
V	volume of gas in the control volume, ft^3
V_c	total cushion volume, ft^3
V_f	total volume of ducting between fan and trunk, ft^3
V_g	portion of cushion volume directly under the trunk, ft^3
V_h	portion of cushion volume directly under the hard structure, ft^3
V_j	total trunk volume, ft^3
v	velocity of the gas, ft/sec
v_n	average velocity of the gas from the nth row of trunk orifices, ft/sec

$(v_t)_n$ — average velocity of the gas from the cushion exhaust nozzle, at the nth row of trunk orifices, ft/sec

W — mass of gas in the control volume, lb

W_A — mass of the aircraft, lb

$\overline{W}_f$ — work done by fan, ft·lb

w — mass flow of the gas, lb/sec

w_i — mass flow into the control volume, lb/sec

w_n — mass flow from the $(\ell_n)^{th}$ segment of the trunk, lb/sec

w_o — mass flow from the control volume, lb/sec

X — jet thickness parameter for concentrated jet

$\overline{X}$ — distance from aircraft c.g. to center of pressure of trunk footprint, ft

X_n — jet thickness parameter for nth jet

X_o — horizontal distance from inside attachment point to inside of trunk footprint, ft

x_o — x coordinate of minimum jet height point, ft

Y_o — trunk clearance, vertical distance between aircraft hard structure and lowest point of the trunk, ft

Y_∞ — vertical distance at which no trunk footprint exists ($\ell_3 = 0$), ft

y — vertical distance, ft

$\dot{y}$ — vertical velocity, ft/sec

$\ddot{y}$ — vertical acceleration, ft/sec^2

y_o — y coordinate of minimum jet height point, ft

Z_n — momentun parameter defined by equation (5-7)

z — dummy variable

Greek letters

α_n — angle of revolution for trunk cross-section to form trunk volume segment n, radians

β_n — angular position of nth row of orifices relative to the vertical, radians

γ_n angle of nth orifice row relative to trunk, radians

δ_n height of nth orifice above the minimum ground clearance of the trunk, ft

ϵ strain in the trunk material in/in

ζ proportionality constant used in calculating trunk volume

η angle through which the peripheral jet is deflected, radians

θ effective jet angle, radians

λ_n distance along the trunk from attachment point (a, b) to the nth row of orifices, ft

ξ trunk porosity

π dimensionless ratio of trunk dimensions used in scaling

ρ density of the gas, lb/ft^3

ϕ_n central angle for nth trunk segment, radians

ψ_z angle between trunk and ground at the edge of the trunk footprint, radians

ψ_1 complementary angle to ϕ_1, radians

Subscripts

A   aircraft

a   atmosphere

c   cushion

e   end section of trunk volume

f   fan

g   cushion volume under trunk

h   cushion volume under hard structure

i   flow into the control volume

j   trunk

k   corner section of trunk volume

l   first row of jet orifices inside the cushion

m   last row of jet orifices inside the cushion

n   arbitrary

o	flow out of the control volume
p	plenum chamber
q	orifices
r	stall condition of the fan
s	side section of trunk volume
t	total value of all parts
0	atmosphere
1	trunk segment inscribed by angle ϕ_1
2	trunk segment inscribed by angle ϕ_2
3	trunk segment flattened against the ground
4	trunk segment associated with the minimum possible value of R_1
∞	distance at which trunk support is negligible ($Y_3 = 0$)

1. INTRODUCTION

1.1   Statement of the Problem

The purpose of this work is to develop design techniques which can predict analytically the power requirements and dynamic response of a unique air suspension system which can be used to replace the landing gear on aircraft. The particular system analyzed will be referred to as the Air Cushion Landing System and abbreviated ACLS. The ACLS was developed jointly by Bell Aerosystems and the Air Force Flight Dynamics Laboratory. It utilizes a flexible skirt or "trunk" and a distributed peripheral jet as described in Section 1.3. The development program for the ACLS is documented by References 1, 2, 3, 4, 5, and 6. The referenced program was largely experimental. This study is intended to present analytical techniques which will be useful in extrapolating the reported experimental results and in designing larger and more efficient air suspension systems for aircraft.

The power requirements for an air suspension system may be stated in terms of pressure versus flow characteristics for the fan which supplies the air for the system. In the following chapters, relationships are developed which relate the pressure and flow to the resulting ground clearance and overpressure beneath the aircraft. For the purposes of this work, the effect of forward velocity is neglected.

The dynamic response of interest in this work is the response of the air cushion trunk to landing impact. It is desired to predict the forces and motions which result from a residual vertical velocity of the aircraft at touchdown. Of particular interest are the maximum acceleration and the maximum trunk deflection for a given aircraft weight and sink rate. For the purpose of this work, only vertical forces and motions are considered.

1

Aerodynamic forces resulting from the aircraft surfaces are neglected as are all moments and angular motions.

Static analyses of the trunk shape and flow characteristics are prerequisites to analytical treatment of both power requirements and the dynamic response of the system. Consequently, these analyses are developed and experimentally verified prior to presenting the dynamic and power system analysis.

The most widely accepted flow theories for predicting the cushion pressure in air cushion vehicles are summarized in Chapter 2. Nondimensional flow parameters are developed in Chapter 3. The prediction of the trunk shape and cross-sectional area is developed in Chapter 4. Flow theories for the combined trunk-jet system are presented in Chapter 5. Experimental results to verify the trunk shape and flow theories are presented in Chapter 6. An analysis of the dynamic response of the trunk system is derived in Chapter 7. Experimental verification of the dynamic system is presented in Chapter 8. A summary of the design considerations, the dynamic response and the power requirements is included in Chapter 9.

The following design tools are presented:

(a)   The power-jet height parameter, C_{hd}, developed in Chapter 3 is valuable dimensionless parameter for comparing the relative effectiveness of competing designs for minimizing horsepower and maximizing jet height. The value of C_{hd} for a design may be determined easily by test, thereby eliminating a complicated analysis. The parameter C_{hd} is also valuable for scaling model test results to full size vehicles.

(b)   The trunk shape analysis developed in Chapter 4 provides the capability of analytically evaluating the effect of trunk length, attachment poi. 1s, material elasticity, cushion pressure and trunk pressure on trunk shape, volume and stiff , the accuracy of this analysis in predicting trunk shape is illustrated by Figure 6-5 (Page 159).

(c)   The resitrictor flow theory developed in Chapter 5 provides the capability of analytically evaluating the effect of jet size, spacing, angle, position on the trunk; aircraft weight, power input, trunk shape and cushion area on the resulting footprint pressure distribution, jet height and flow. The accuracy of the flow restrictor theory in predicting pressure distribution around the trunk is illustrated by Figures 6-8, 6-9, and 6-10 (Pages 168, 169, and 170). The accuracy in predicting flow is illustrated in Figure 7-11 (Page 173). The accuracy in predicting jet height is illustrated by Figure 7-12 (Page 174).

(d)   The dynamic analysis developed in Chapter 7 provides the capability of analytically evaluating the influence of aircraft weight, sink velocity, fan characteristics, trunk shape, trunk length, and trunk orifice area and spacing on the dynamic response of the vehicle under landing impact. The accuracy of this analysis in predicting trunk pressure, deceleration, and displacement during drop test is illustrated by Figures 8-11, 8-12, and 8-13 (Pages 244, 245, and 246), respectively.

1.2   Background

An air suspension system supports a vehicle on a cushion of air trapped between the vehicle underside and the ground. The vehicle weight is uniformly distributed by the air cushion over a large area. Extremely low ground pressure results. Consequently, such a system offers the potential for operating on extremely soft ground and even water.

The two most common air suspension systems are known as the plenum chamber and the peripheral jet. These systems are illustrated in Figures 1-1(a) and 1-1(b), respectively. Both systems rely on "ground effects" or an overpressure caused by the presence of the ground for support. In both systems, input power is required to maintain the air cushion. The major difference between the two systems lies in the mechanism by which the overpressure is maintained. The plenum chamber utilizes a flow restriction, while the peripheral jet maintains the overpressure by a momentum "seal".
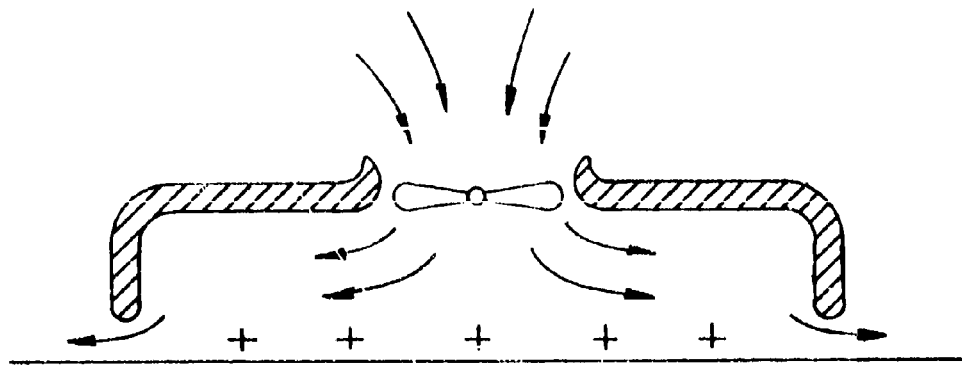
(a) PLENUM CHAMBER
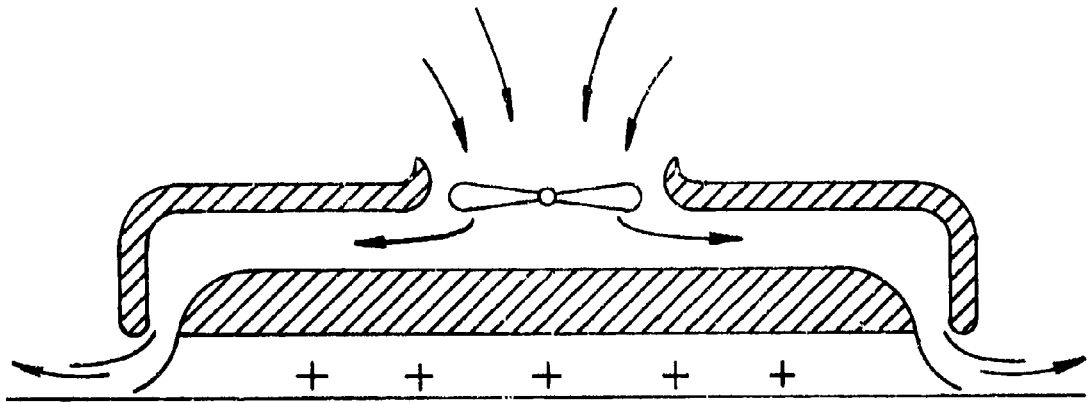
(b) PERIPHERAL JET

AIR CUSHION SUSPENSION SYSTEMS

FIGURE 1-1

In the case of the plenum chamber, air is pumped into the cavity under the vehicle and leaks out through a narrow gap between the periphery of the vehicle and the ground. An overpressure is maintained in the cavity as a consequence of equilibrium between the pressure differential across the gap and the combined acceleration and frictional forces which limit the flow of air through the gap. The result is a flow restriction of the exhaust plane.

In the case of peripheral jet, air is vented in a jet at the periphery to form an air curtain seal. The sealing effect of the jet is a consequence of the equilibrium between the pressure differential across the jet and the centrifugal forces in the curved jet airflow. Pressure in the cushion is maintained by this air curtain seal. In a "pure" peripheral jet air suspension system, all air is introduced at the periphery. In theory, air neither enters nor leaves the cavity when the system is at equilibrium.

The concept of using an air cushion (or ground effects) to support an aircraft during take-off and landing is not new. Machines which utilize this principle are called Ground Effects Take-off and Landing aircraft and are abbreviated GETOL aircraft. Studies of GETOL concepts have been conducted by AVRO Canada, ONERA (France), UTIAS (Canada), DORNIER (Germany) and VERTOL and CONVAIR, and Bell Aerosystems in the United States of America.[7,8]*

Figure 1-2(a) shows the AVROCAR, a peripheral jet concept which was studied by AVRO between 1954 and 1962.[9,10,11,12,13] Research was discontinued because of excessive power consumption (attributed to high duct losses) and instability when out of ground effect.

Figure 1-2(b) shows a GETOL aircraft design proposed by VERTOL. The VERTOL studies indicated that their design is competitive with conventional aircraft in weight and performance.[14,15,16,17,18] However, the static and dynamic stability and control of the craft present major problems.

CONVAIR studied a GETOL aircraft with a thick rectangular wing equipped with a peripheral nozzle.[19,20] The major difficulties anticipated were stability and excessive energy losses.

*Numbers in parentheses refer to references.
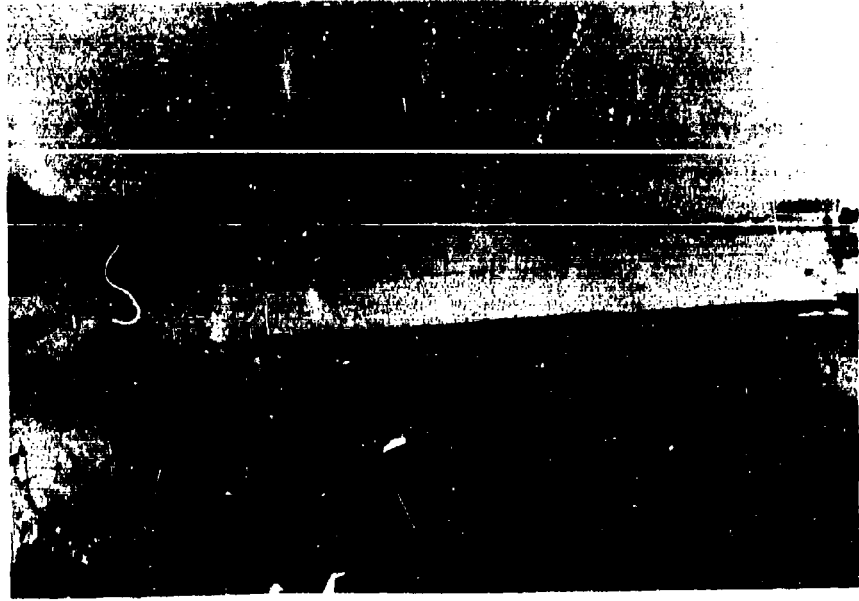
(a) THE AVROCAR
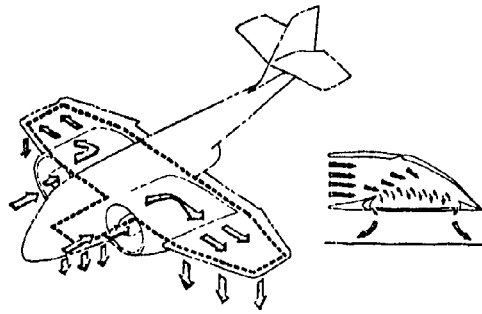
(b) VERTOL PROPOSED GETOL

HISTORICAL GETOL DESIGNS

FIGURE 1-2

ONERA,[21,22] UTIAS[23,24,25,26] and DORNIER[27] have studied wings of various shapes equipped with peripheral nozzles. Each of the studies mentioned above employed a jet height (ground clearance) measurable in feet. Several deficiencies are associated with such large ground clearances. These deficiencies include poor stiffness, poor vertical energy absorptive properties and large power requirements.

The concept developed jointly by Bell and the Air Force Flight Dynamics Laboratory is unique.[1,2,3,4] It utilizes a jet height of less than one inch, thus reducing the power requirements to an acceptable level. The use of flexible skirts around the periphery of the air cushion greatly increases the stiffness and energy absorptive properties of the system.

1.3   The ACLS Concept

The Air Cushion Landing System completely eliminates the conventional aircraft landing gear and replaces it with a cushion of air maintained beneath the fuselage during take-off and landing. An artist's concept of the system is shown in Figure 1-3. The elongated doughnut shown on the bottom of the fuselage is call a trunk. The trunk forms the flexible ducting required to provide a continuous curtain of air around the periphery of the fuselage.

Air is fed into the trunk from a compressor located in the nose wheel well. The air is ducted by the trunk to the fuselage periphery and exhausted through jets in the trunk to form a jet curtain. This jet curtain seals a pressure of one to two psi under the aircraft fuselage when the ground is approached. The trunks are made of rubber and nylon. When inflated, they stretch approximately 300% to assume the shape shown in Figure 1-3. When not pressurized, they shrink and hug the fuselage like a de-icing boot.

A braking system is shown in Figure 1-4. Braking is accomplished by pressing a brake material against the ground. The brake material may be replaced without replacing the rest of the system — just as conventional brakes may be relined without replacing the landing gear. Brakes are actuated by applying pneumatic pressure to the pillow sections shown on the bottom of the trunk. Steering is accomplished by differential braking as in a caterpillar tractor.
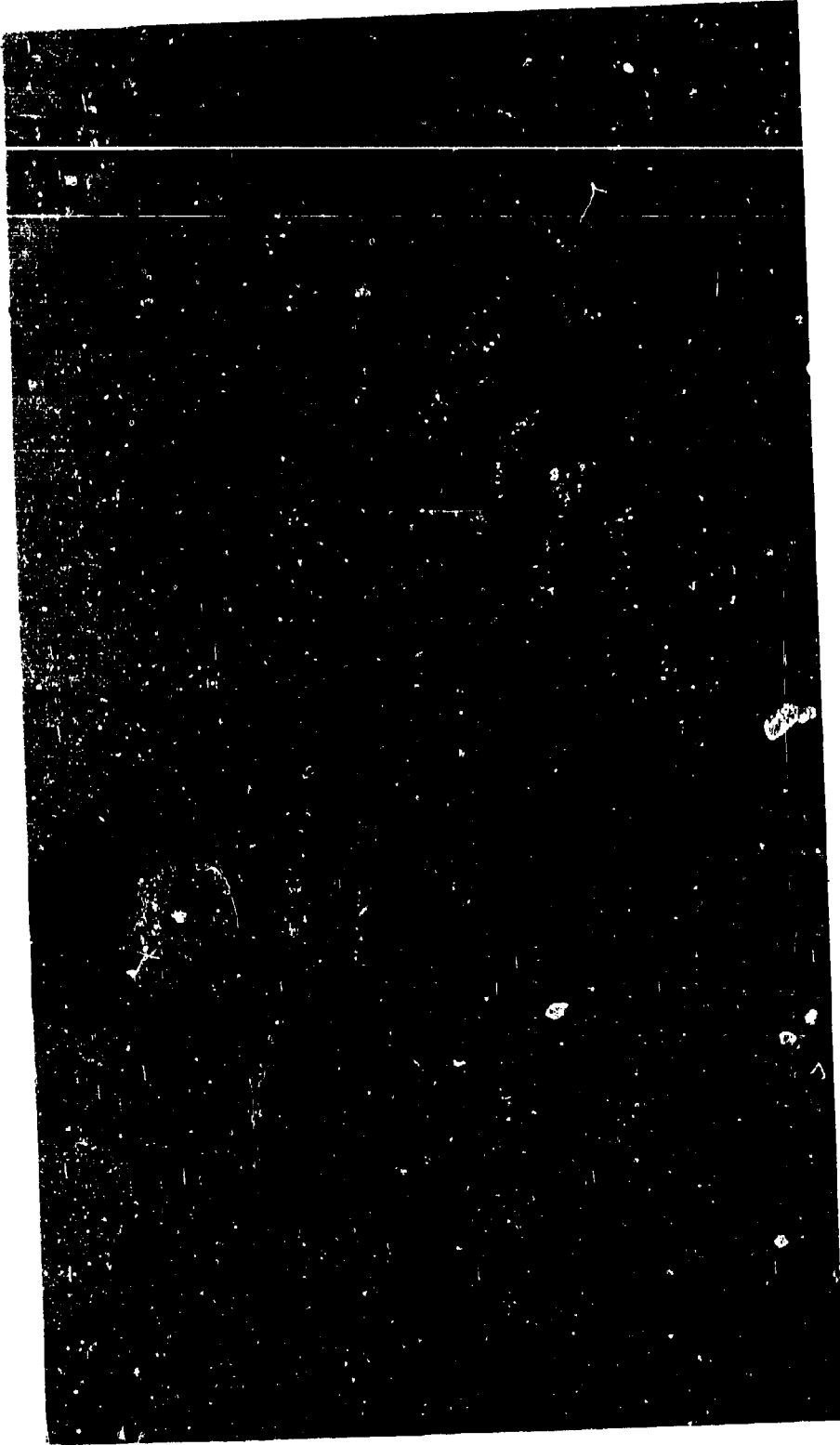
ARTIST'S CONCEPT OF THE AIR CUSHION
LANDING SYSTEM

FIGURE 1-3

SEPARATE AIR
SUPPLY MANIFOLD

INFLATED AIR CUSHION
SHOWING BRAKING PILLOWS
IN FLUSH POSITION

FORWARD

BRAKING
PILLOW

CROSS SECTION

SIDE SHOWING PILLOW CONTACT

FORWARD
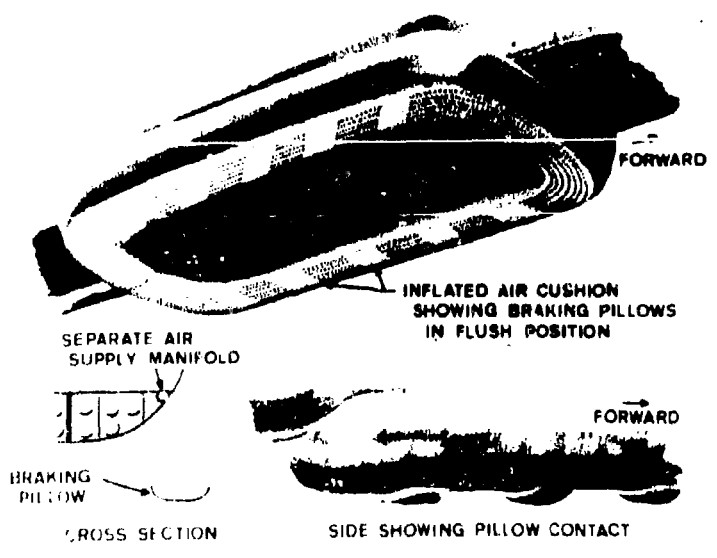
BRAKING SYSTEM FOR ACLS

FIGURE 1-4

NORMAL FOOTPRINT PRESSURE
DISTRIBUTION

(a)

FOOTPRINT PRESSURE DURING
ROLL

(b)
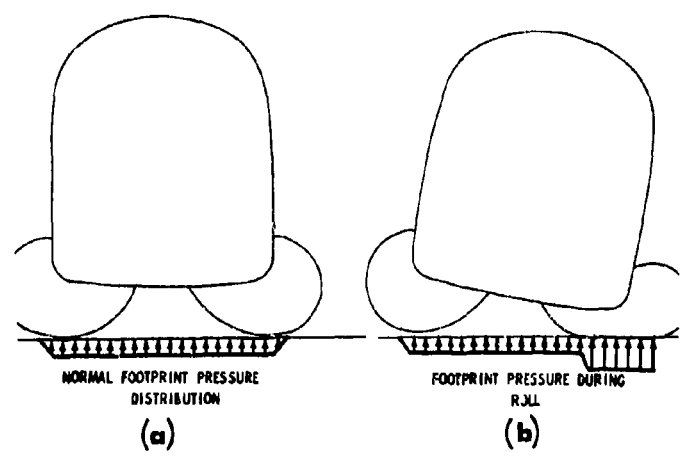
ACLS FOOTPRINT PRESSURE DISTRIBUTION

FIGURE 1-5

The mechanism by which roll angles are reacted is shown in Figure 1-5. The figure on the left shows the approximate footprint pressure of the ACLS under equilibrium conditions. The aircraft is totally supported by the cushion of air maintained under the fuselage. Under a large roll angle, the footprint pressure changes. The change is shown in the flight figure. In addition to the cushion of air, the trunk is supporting the aircraft. The pressure in the trunk is roughly twice the pressure in the cushion. The trunk pressure, acting over the area shown in Figure 1-5, develops a large restoring moment whenever the bag is flattened against the ground. Negligible scrubbing of the bag against the ground occurs due to the large flow of air between the bag and ground. Very low friction results. The phenomena by which pitch stiffness is obtained is identical to that by which roll stiffness is obtained.

This Air Cushion Landing System is an extension of the technology developed for air cushion vehicles. Figure 1-6(a) shows one such vehicle used by the U.S. Army in Vietnamm.[28] This vehicle weighs about eight tons. A larger vehicle built for the Navy by Bell Aerosystems is shown in Figure 1-6(b). This vehicle weighs about 30 tons — approximately equal to the C-119 and C-123.[7,28] The Britsh operate a vehicle which weighs 163 tons, or nearly twice the weight of the C-130.[7,28] This vehicle, shown in Figure 1-6(c), provides commercial ferry service across the English Channel.

An extensive amount of work has been published concerning the performance of Air Cushion Vehicles.[8] Much of this work can, and has been applied to predicting the static performance of the ACLS. However, the design of the trunks and the peripheral nozzles on the ACLS are considerably different from the design of the same items on Air Cushion Vehicles. A comparison of the three designs is shown in Figure 1-7. The left figure shows the cross section of a typical plenum chamber with a flexible skirt. The middle figure shows the cross section of a typical ACV peripheral jet trunk. The continuous peripheral nozzle directs the jet inward at a constant angle. In the ACLS trunk shown on the right, the jet is formed by many holes which direct the jet at various angles. Consequently, corrections will be necessary in applying existing flow theories developed for simple peripheral jets. These corrections are developed in Chapter 5.

(a) 8 TON ACV
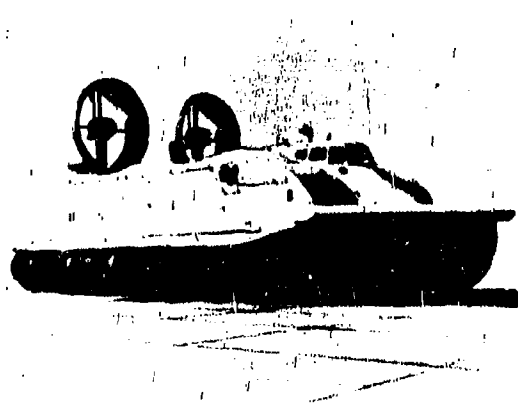
(b) 30 TON ACV
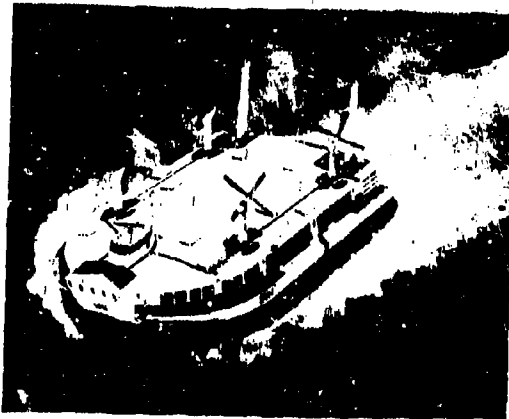
(c) 160 TON ACV

HISTORICAL AIR CUSHION VEHICLES

FIGURE 1-6
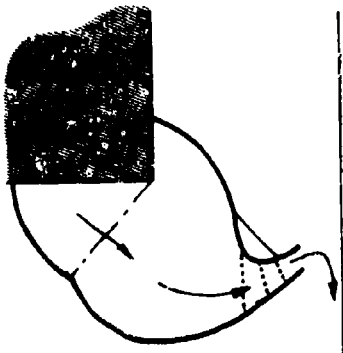
DISTRIBUTED JET

JETTED TRUNK
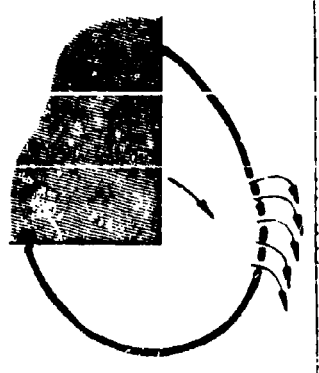
SIMPLE SKIRT

COMPARISON OF AIR CUSHION DESIGNS

FIGURE 1-7

2. PERIPHERAL JET FLOW RELATIONSHIPS

2.1 Method of Approach to Problem

It is desired to predict the interrelationship among load capacity, power and jet height for a peripheral jet air suspension system. This problem involves eight independent variables whose values are fixed by the environment, the design, or the mode of operation. There are also eight dependent variables of interest. Consequently, it is necessary to develop eight independent equations which relate the eight dependent variables.

The variables of interest and the laws which have been applied to develop the eight equations are summarized in Section 2.2. The development of the equations requires the assumption of a velocity profile across the jet. Several authors have made different assumptions regarding this velocity profile. These different assumptions lead to different theories on the performance of the peripheral jet. The basic relationships which are common to all the theories of interest are developed in Section 2.3. The relationships for specific theories are developed in Sections 2.4 through 2.9.

2.2 Background

The Air Cushion Landing System is generally similar in design to Air Cushion Vehicles shown in Figure 1-6. Both employ peripheral jets of the type shown in Figure 1-1(b). However, there are differences in the design of the trunk as shown in Figure 1-7. The ACLS uses a distributed jet as compared with a concentrated jet for the Air Cushion Vehicles. The single-peripheral jet system will be considered in this section. Distributed jet systems will be presented in Section 5.

13

A number of flow theories have been advanced to predict the plenum pressure which will result from a peripheral jet of a given design.[8] These flow theories fall into three general categories.

The first category involves the development of an exact solution of the Navier-Stokes equations of the jet flow. The viscous exact theory developed by Boehler[30] falls into this category. The resulting relationships are quite complicated and therefore only numerical evaluations will yield useful results.

The second category involves the conformal mapping of the hadograph plane for solving the annular jet flow. A number of authors including Chaplin and Stephenson,[31] Strand,[32] Ehrich,[33] Cohen,[34] Bligh,[35] and Roche[36] have developed solutions to the jet flow field, assuming two dimensional, nonviscous flow. These theories have the disadvantage of being overly complex without providing better agreement with experimental results than provided by the simpler theories of category three.[8,37]

The third category involves an approximation of the exact solution based upon simplifying assumptions to predict the jet momentum. These theories are known as momentum theories. They have the advantage of providing simple relationships and agreeing reasonably well with experimental results.[8,37] A momentum theory which included the effect of viscosity was advanced by Chaplin.[38] However, this analysis requires the assumption of an experimentally developed entrainment function. This approach is considered to have little merit over the application of an experimentally determined coefficient of discharge to a simple nonviscous momentum theory.

The nonviscous momentum theories differ principally in the assumption made for the velocity profile across the jet. The thin jet theory[39] assumes a velocity across the jet which is constant and independent of cushion pressure. It is applicable only for large jet heights or low cushion pressures. The exponential theory[40] assumes an exponential velocity profile across the jet. The Barratt Theory[41] assumes a velocity in the jet which is inversely proportional to the jet radius of curvature. Earl[1] developed a semi-empirical relationship between jet height and velocity so that the predicted flow would be zero at the end point where the jet height is zero.

Khanzhonkor[42] and Fujita [43] developed separate analyses for suspension systems which employ two peripheral jets to provide a "double seal" Khanzhonkor used the exponential theory and Fujita used the thin jet theory to predict the flow and pressure ratio across each jet.

A number of other authors[8,37] have used the nonviscous momentum theories to predict flow performance of peripheral jet air suspension systems. The momentum theories which have been reported to give the best agreement with test results are the Exponential Theory and the Barratt Theory.[40,37]

In the sections to follow, the most prevalent nonviscous momentum theories will be summarized. The development of relationships which are common to all of the peripheral jet theories are presented in Sections 2.3 and 2.4. The momentum theories developed are as follows:

The Thin Jet Theory — Section 2.5,

The Exponential Theory — Section 2.6,

The Barratt Theory — Section 2.7.

The Simple Plenum Theory is presented in Section 2.8. This theory is applicable to the type of air suspension system shown in Figure 1-1(a). The plenum chamber relies upon flow restriction rather than a momentum seal to maintain the overpressure in the plenum.

2.3   Development of Common Relationships

2.3.1   Approach

In this section, the variables associated with peripheral jet performance are listed, the laws which have been applied are stated, and the relationships which are common to all the peripheral jet theories have been developed.

The variables involved in the problem are shown on the idealized model of an air cushion landing system in Figure 2-1. These variables may be grouped as follows:

Independent Environmental Variables

P_a — Atmospheric pressure, psfa

ρ — Atmospheric air density lb/ft^3

Independent Design Variables

A_c — The effective horizontal area over which cushion pressure acts (cushion area), ft^2

S — Length of the peripheral jet nozzle, ft

t — Width of peripheral jet nozzle gap, ft

θ — Effective nozzle angle, radians

Independent Operating Variables

hp — Energy per unit time contained in air supplied to the jet, horsepower

W_A — Weight of aircraft, lb

Dependent Variables

d — Jet height, ft

J' — Magnitude of the reaction imparted by the jet (-lbs)

P_c (P_c) — Cushion pressure, psfg (psf)

P_j (P_j) — Trunk (jet) pressure, psfg (psf)

p (P) — Pressure at an arbitrary point inside the jet, psfg (psf)

Q_j — Flow rate of air from jet, ft^3/sec

R — Radius of curvature of the path of an infinitesimal element of gas in the jet, ft

v — Velocity of an infinitesimal element of gas inside the jet, ft/sec
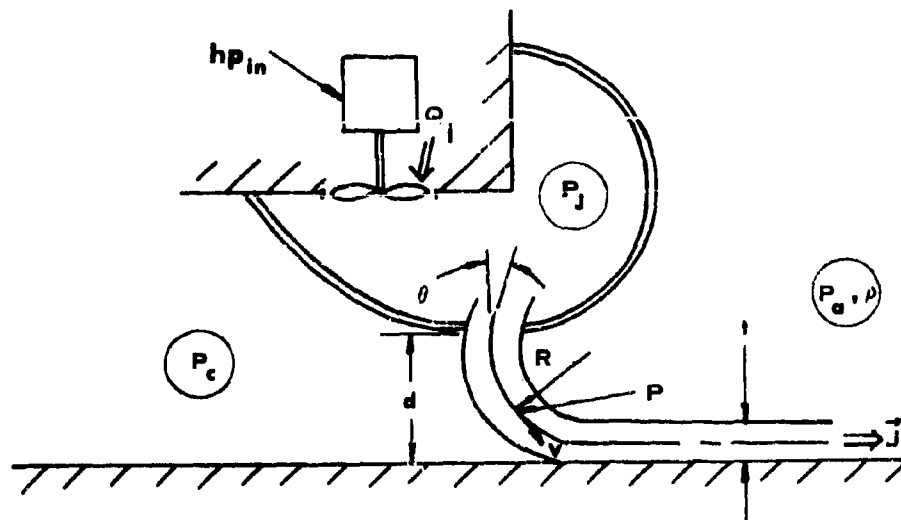
(a) TRUNK CROSS-SECTION
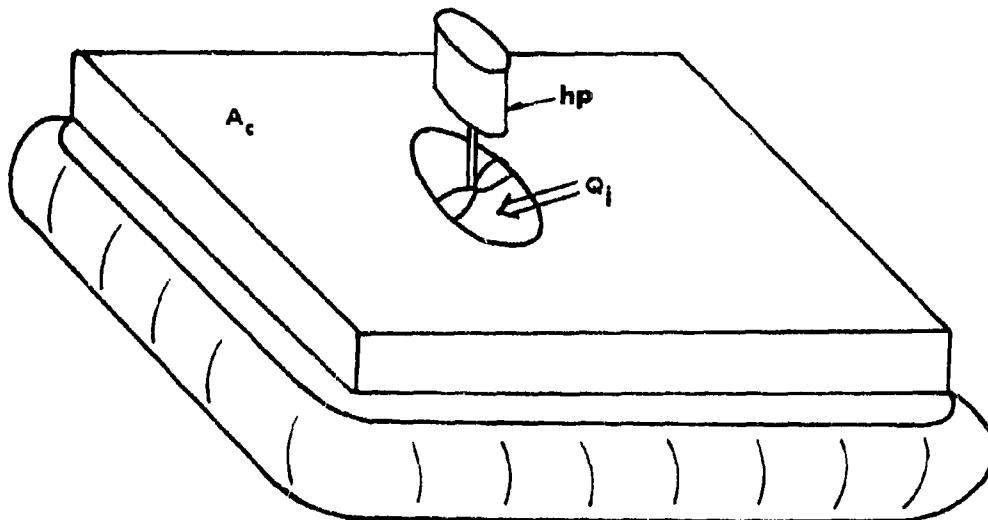
(b) 3 DIMENSIONAL DYNAMIC MODEL

ILLUSTRATION OF MAJOR VARIABLES
FIGURE 2-1

The independent environmental variables are considered constants. For a given design, the independent design variables are fixed. It is desired to develop relationships between the independent operating variables and the dependent variables for fixed values of the independent environmental and design variables. Such relationships would allow the prediction of the jet height as a function of power input and aircraft weight. The jet height is an index of the air cushion performance as is discussed in detail in Chapter 9.

If one applies basic laws and principles to a free body of the peripheral jet system, the necessary relationships may be developed. Since there are eight dependent variables, it will be necessary to develop eight independent relationships among the variables.

The relationships are as follows:

(a)   Force equilibrium applied at a cross section of the air cushion taken parallel to the ground and at ground level gives:

$$W_A = f(p_c, A_c) \tag{2-1}$$

(b)   Conservation of energy involving the energy source for the system gives:

$$hp = f(p_j, Q_j) \tag{2-2}$$

(c)   Geometric compatibility between the jet radius and the other dimensions gives:

$$R = f(d, \theta, t) \tag{2-3}$$

(d)   D'Alembert's principle applied to an element within the jet gives:

$$P = f(p, v, R) \tag{2-4}$$

(e)   Conservation of energy applied to the jet gives Bernoulli's equation

$$P_j = f(P, v, \rho) \tag{2-5}$$

(f)   Conservation of mass applied to the jet at its exit plane gives:

$$Q_j = f(v, t) \tag{2-6}$$

(g)   Force equilibrium applied to the cushion seal gives:

$$d = f(p_c, J', \theta) \tag{2-7}$$

(h)   The definition of momentum applied to the jet gives:

$$J' = f(S, p_j, t) \tag{2-8}$$

The first two equations (2-1 and 2-2) provide relationships among the two independent operating variables and three of the dependent variables. These equations do not involve assumptions concerning the flow in the jet. Consequently, they are applicable to all of the jet flow theories to be developed later. The approach taken here is to develop these two relationships first, then develop the remaining relationships based upon various theories of flow in the jet.

The development of the first two relationships, which are common to all flow theories for the peripheral jet, is presented in Sections 2.3.2 and 2.3.3.

2.3.2 . Force Equilibrium

Force equilibrium may be applied to the air cushion vehicle at the ground footprint as shown in Figure 1-5(a). The following assumptions are made:

2.3.2.1   The ACLS is symmetric and the opposite sides have identical flow, stiffness and geometric characteristics.

2.3.2.2   The center-of-gravity of the aircraft is directly above the center of the air cushion.

2.3.2.3   The pressure is equal to P_c inside the plenum and equal to P_a outside the plenum.

2.3.2.4   All flow into the trunk exhausts through the peripheral jet.

2.3.2.5   The net vertical thrust from the peripheral jet is negligible.

Force equilibrium applied at a cross section of the air cushion taken parallel to the ground and at ground level gives:

$$W_A = p_c A_c \qquad\qquad (2\text{-}9)$$

2.3.3   Conservation of Energy Involving the Power Source

The conservation of energy law may be applied to the energy supplied to the air. In order to apply this principle, the following assumptions are made:

2.3.3.1   The air is incompressible.

2.3.3.2   The air is inviscid.

2.3.3.3   Energy losses are negligible.

2.3.3.4   Flow is adiabatic.

2.3.3.5   The air velocity in the trunk may be neglected ($P_t = P_j$, where P_t = total pressure).

The work done on the air by the fan must produce an increase in the energy of the air.

$$\overline{W_f} = (P_j - P_a)V_f$$

where: $\overline{W_f}$ is the work done by the fan per revolution and

V_f is the air volume displaced per revolution.

The above equation may be differentiated with respect to time.

$$\frac{d\overline{W_f}}{dt} = p_j\frac{dV_f}{dt}$$

Written in terms of horsepower input to the air, the relationship becomes:

$$hp = \frac{p_j Q_j}{550} \tag{2-10}$$

2.4 General Technique for Developing Flow Relationships

2.4.1 Approach

In this section, the assumptions required to develop the flow equations are listed and the general flow equations are developed. All the assumptions stated in this section apply to all peripheral jet theories developed by this author in Sections 2.5 through 2.8. Each of the theories also has additional assumptions peculiar to the particular theory. The various laws will be applied in the same order as will be used in the sections to follow.

2.4.2 Geometric Compatibility

The various theories differ somewhat with respect to the assumptions made in the area of geometric compatibility. The particular assumption for the geometry of the jet will be considered separately for each of the theories to follow. It will be shown later that a convenient dimensionless ratio associated with the nozzle geometry can be defined and will

be referred to as the jet thickness parameter. This parameter is represented by the symbol X and is defined as follows:

$$X = \frac{t}{d} (1 + \sin \theta) \qquad (2\text{-}11)$$

2.4.3 D'Alembert's Principle Applied to the Jet

A relationship involving the pressure, the velocity and the radius of curvature of the jet may be obtained by applying d'Alembert's principle.

The following assumptions are applicable:

2.4.3.1 The viscosity is negligible.

2.4.3.2 The density of the gas is constant.

2.4.3.3 The pressure and velocity along any streamline is constant.

D'Alembert's principle may be applied in the R direction to the infinitesimal element of gas shown in Figure 2-2. The resulting equation is:

$$\frac{v^2}{R}dm = (P + dP)(R + \frac{dR}{2}) \quad d\eta - 2(P + \frac{dP}{2}) \sin \frac{d\eta}{2} dR - P(R - \frac{dR}{2}) d\eta$$

The above equation may be simplified by eliminating third order differentials and introducing the following substitutions:

$$\frac{d\eta}{2} \approx \sin \frac{d\eta}{2}.$$

$$R\left(\frac{\rho}{g_o}\right)dR \ d\eta = dm$$

$$\left(P+\frac{dP}{2}\right)\left(\sin\frac{d\eta}{2}\right)dR$$

$$\left(P+dP\right)\left(R+\frac{dR}{2}\right)d\eta$$

$$dR$$

$$\frac{v^2}{R}dm$$

$$P\left(R-\frac{dR}{2}\right)d\eta$$

$$d\eta$$

$$\left(P+\frac{dP}{2}\right)\left(\sin\frac{d\eta}{2}\right)dR$$
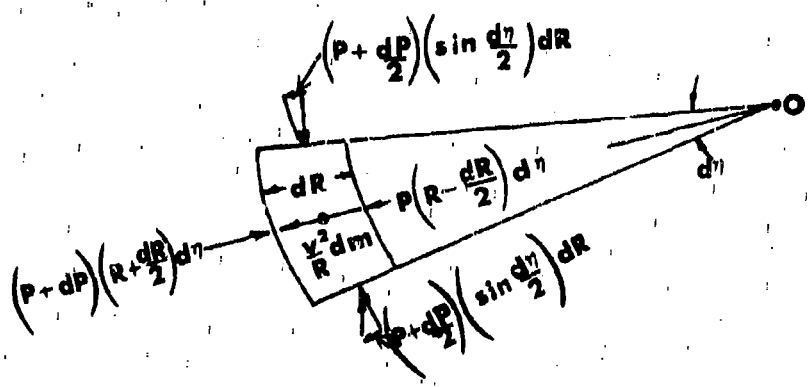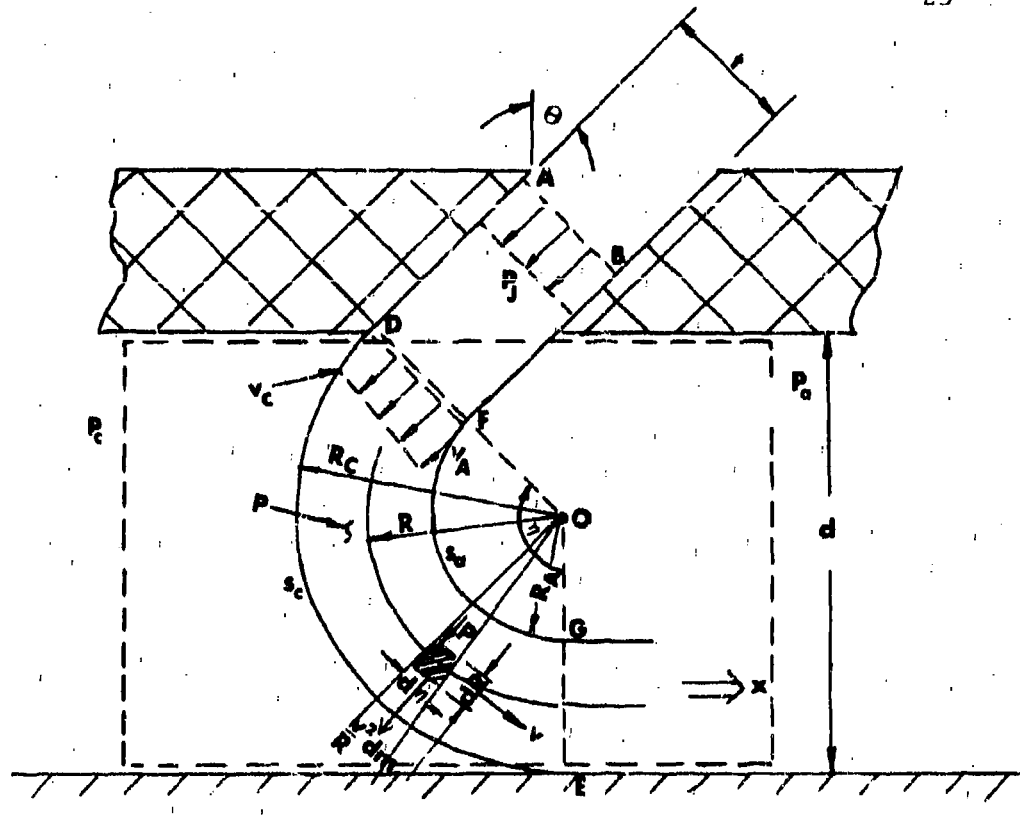
MODEL FOR GENERAL THEORY

FIGURE 2-2

The resulting equation becomes:

$$\frac{\rho v^2}{g_0 \hat{R}} \, dR \, d\eta = dP \, d\eta$$

Since $d\eta \neq 0$ it is possible to divide by $d\eta$ to give a simple differential equation which relates the pressure at any point in the jet to the velocity and the radius of curvature at that point. The equation is:

$$dP = \frac{\rho}{g_0} v^2 \frac{dR}{R} \tag{2-12}$$

2.4.4 Conservation-of-Energy Applied to Jet

A relationship between the pressure and velocity at any point in the jet may be obtained by applying conservation of energy.

The following assumptions are applicable:

2.4.4.1 The air is incompressible.

2.4.4.2 The air is inviscid.

2.4.4.3 Energy losses are negligible.

2.4.4.4 The flow is adiabatic.

2.4.4.5 The air velocity in the trunk may be neglected.

2.4.4.6 The total pressure is everywhere constant.

2.4.4.7 The air velocity in the trunk is equal to zero and the pressure $P_j = P_t$ (where P_t = total pressure).

2.4.4.8   The flow velocity is perpendicular to the exit plane DF.

2.4.4.9   The effect of change of height of the gas is negligible.

2.4.4.10   The energy along any streamline is constant.

The conservation of energy principle may be applied to an arbitrary streamline(s) in the jet shown in Figure 2-2. The energy of the gas at any point in the trunk must equal the energy of the gas at any point in the streamline. Since there is negligible heat transfer, work, frictional losses, gas compression, and change in height during the flow process, the energy balance becomes:

$$\frac{P_j}{\rho} + \frac{v_j^2}{2g_0} = \frac{P}{\rho} + \frac{v^2}{2g_0}$$

In the above equation, the j subscripts denote any point in the trunk and the variables which are not subscripted denote any point in the jet. Assumption 2.4.4.5 permits the elimination of the v_j^2 from the above equation. The resulting equation is:

$$\frac{P_j}{\rho} = \frac{P}{\rho} + \frac{v^2}{2g_0} \qquad (2\text{-}13)$$

Equation (2-13) gives a relationship between the trunk pressure and the pressure and velocity at any point in the jet.

2.4.5   Conservation of Mass

A relationship involving the flow may be obtained by summing the increments of flow across the jet. The assumptions in applying this principle are the same as those for the conservation-of-energy principle. These assumptions are listed in Section 2.4.4. A model for

the jet flow is shown in Figure 2-2. For an arbitrary value of η, the increments of flow across the jet may be summed in the radial direction. The resulting equation is:

$$Q_j = S \int_{R_a}^{R_c} v \, dR \qquad (2\text{-}14)$$

In the above equation, the integration is performed with η = constant. The variable S is the length of the jet curtain. Equation (2-14) gives the total flow from the jet, evaluated at any angle η. It is generally convenient to evaluate the flow at the exit plane where $\eta = 90^o + \theta$.

2.4.6 Force Equilibrium Applied to the Jet Seal

Force equilibrium may be applied to the peripheral jet seal shown in Figure 2-2. The assumptions from the previous sections are retained. The following assumptions are added:

2.4.6.1   The surfaces above and below the air cushion are rigid and impervicus.

2.4.6.2   The cushion is in static equilibrium (no air entering or leaving the cushion).

2.4.6.3   The cushion pressure is separated from the atmosphere by a peripheral jet.

2.4.6.4   The mixing between the jet and the surrounding environment is negligible and the velocity profile is constant along the length of the jet (two dimensional flow).

2.4.6.5 The total momentum of the jet at the nozzle exit plane (Section DF, Figure 2-2) is equal in magnitude to the total momentum of the jet at the cushion exit plane (Section EG, Fiaure 2-2)

Under equilibrium conditions, air neither enters nor leaves the cushion (plenum). The cushion pressure is maintained by the reaction which results from the momentum change in the peripheral jet. For force equilibrium in the air gap (d), the cushion pressure times the area over which it acts must equal the time rate of change of the total jet momentum. The equation expressing force equilibrium across the air gap in the direction perpendicular to the air gap (the x direction) is:

$$p_c \, S \, d \; = \; \frac{d}{dt} \, (\vec{J})_x \; \frac{1}{g_o} \tag{2-15}$$

The magnitude of the force in the x direction developed by the change in momentum of the gas may be determined by the momentum principle applied to the control volume. The momentum principle may be stated:

$$F_x \; = \; \frac{d}{dt} \, (J)_x \, \frac{1}{g_o} \; = \; \frac{1}{g_o} \left[\frac{d \, (wv_x)}{dt} \; + \; \sum_{out} wv_x \; - \; \sum_{in} wv_x \right]$$

If the velocity and flow rate are assumed constant, and the geometry of Figure 2-2 is applied, the resulting equation is

$$\frac{d}{dt} \, (J)_x \, \frac{1}{g_o} \; = \; J' \, (1 + \sin \theta) \tag{2-16}$$

where

$$J' \; \equiv \; \frac{wv}{g_o}$$

2.4.7 Pressure Variation Across the Jet

The principal difference between the various momentum theories is a difference in the pressure variation across the jet. All theories presented assume the pressure and velocity along any streamline is constant (Assumption 2.4.3.3). Consequently, jet pressure is independent of η in Figures 2-2, 2-3, and 2-4.

The pressure variation across the jet may be determined by combining the conservation-of-energy equation, Equation (2-13), and the D'Alembert's equation, Equation (2-12). The result is:

$$\frac{dP}{P - P_j} = -2\frac{dR}{R}$$

The resulting differential equation gives the pressure variation with radius. This equation may be integrated between the jet boundary and some arbitrary radius to give the pressure at any point inside the jet.

The pressure variations for the three momentum theories are presented in Sections 2.5.7, 2.6.7, and 2.7.7.

2.4.8 · Velocity Variation Across the Jet

The velocity variation across the jet may be found in a similar manner to the pressure variation. In this case, the pressure terms in the D'Alembert's Principle relationship, Equation (2-12), may be eliminated by substitution of the conservation-of-energy relationship, Equation (2-13). The result is:

$$\frac{dv}{v} = \frac{-dR}{R}$$

The resulting differential equation relates the velocity variation to the radius. The equation may be integrated between the jet boundary and some arbitrary radius vector with terminus inside the jet to give the velocity at any point inside the jet. As a consequence of Assumption 2.4.3.3 the velocitv in the jet is independent of η in Figures 2-2, 2-3, and 2-4.

The velocity variations for the three momentum theories are presented in Sections 2.5.8, 2.6.8, and 2.7.8.

2.4.9   Momentum

The magnitude of the total   reaction   of the jet at the nozzle exit plane (Section DF, Figure 2-2), may be determined by summing the total mass flow rate and velocity across Section DF. The mass flow rate is determined by summing all the flow across section DF. The result is

$$w = \rho S \int_{R_a}^{R_c} v \, dR$$

The integration is performed at Section DF. This section is specified by holding the angle η constant at $90^\circ + \theta$. By applying the definition of momentum, Equation (2-16), and by using the mass-flow-rate relationship developed above, an expression for the magnitude of the total jet   reaction   may be developed.

$$J' = \frac{\rho}{g_0} S \int_{R_a}^{R_c} v^2 \, dR \qquad (2\text{-}17)$$

The integration is performed with η = constant = $90 + \theta$.

Equation (2-17) gives the magnitude of the total   reaction   of all the air escaping from the jet at the bottom of the trunk, evaluated at the nozzle exit plane at the lower surface of the trunk.

2.4.10 Jet Flow

The different momentum theories predict different flows as a consequence of the different pressure distributions assumed to exist across the jet. The total jet flow, Q_j, may be found by integrating Equation (2-14). This integration has been performed in Sections 2.5.10, 2.6.10, and 2.7.10. In each section, the final result has been arranged so that the expressions for the different theories may be compared easily. In each case, the expression for flow has the following form:

$$Q_j = t\, S\sqrt{\frac{2g_0}{\rho}(p_j)} \quad f\left[(p_c/p_j),\, X\right]$$

The term in brackets, if any, signifies the difference between the flow predicted by the three theories. In later sections this term is treated as a flow coefficient and designated C_Q.

2.4.11 Recovery Pressure Ratio

The final relationship desired is the ratio of the cushion pressure to trunk pressure as a function of the jet thickness parameter. This relationship has the form

$$p_c/p_j = f(X)$$

where $X \cong t/d\,(1 + \sin\theta)$. A second relationship between p_c/p_j can be developed by combining Equations (2-9) and (2-10). The result is:

$$p_c/p_j = \left(\frac{W_A}{hp}\right)\left(\frac{Q_j}{A}\right)\frac{1}{550}$$

It is evident from the above relationships that p_c/p_j forms an important link in relating the independent variables W_A and hp to the resulting jet height d.

The $p_c/p_j = f(X)$ relationships for the three momentum theories have been developed in Sections 2.5.11, 2.6.11, and 2.7.11. The re.ationships involving aircraft weight (W_A), horsepower (hp) and jet height (d) have been developed in Chapter 3.

2.5   The Thin Jet Theory

2.5.1   Approach and Assumptions

In Section 2.3.2, Equation (2-9) was developed which relates aircraft weight to cushion pressure and area

$$W_A = p_c A_c \qquad (2-9)$$

In Section 2.3.3, Equation (2-10) was developed which relates input power to trunk pressure and flow.

$$hp = \frac{p_j Q_j}{550} \qquad (2-10)$$

It is evident that if a relationship between p_c and p_j could be determined, and if Q_j could be expressed in terms of p_c and p_j, then the aircraft weight and input horsepower could be directly related.

A number of theories have been presented in the literature for relating p_c and p_j. The simplest of these theories is the thin jet theory which is developed in this section. The objective is to determine the flow Q_j and the p_c/p_j relationship which can be used to link Equations (2-9) and (2-10).

The Thin Jet Theory advanced by Chaplin[39] assumes that the jet height is very much larger than the nozzle thickness (d ≫ t). Under these conditions, the jet is extremely thin and is considered as a single streamline (see Figure 2-3). In addition to the assumptions made in Section 2.1, the following restrictions are imposed:

THIN JET THEORY

$t \ll d$

$P_c \approx P_a$
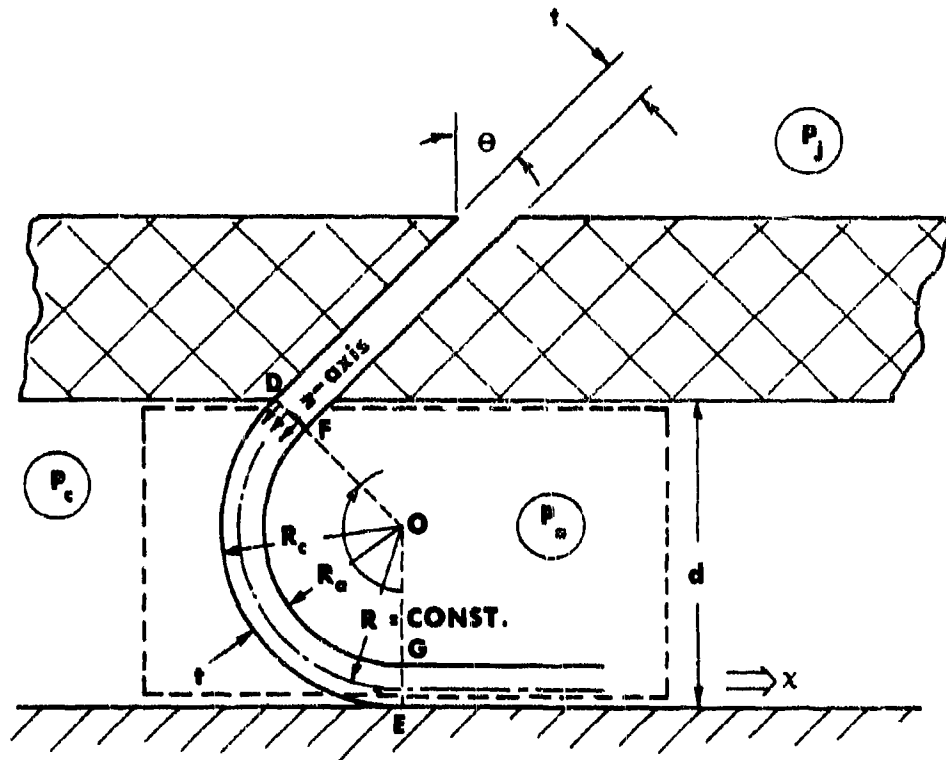
$$R \approx \frac{d}{1+\sin\theta}$$

MODEL FOR THIN JET AND EXPONENTIAL THEORIES
FIGURE 2-3

2.5.1.1   The radius R is constant in magnitude.

2.5.1.2   The velocity and pressure variations are linear across the jet.

2.5.1.3   The increments dP and dR in Equations (2-12), (2-14), and (2-17) may
be replaced by the finite quantities:

$$\Delta P = P_c - P_a \text{ and } \Delta R = t$$

2.5.1.4   The streamline is tangent to the ground at Section EG of Figure 2-3.

2.5.1.5   The thickness of the jet is sufficiently small such that $R_c = R = R_a$.

2.5.1.6   The pressure and velocity along the streamline from DF to EG is
constant (Figure 2-3).

2.5.1.7   The pressure variation across the jet is assumed to be linear and the
average pressure may be expressed by the relation:

$$P = P_a + f (P_c - P_a) \tag{2-18}$$

where $0 \leqslant f \leqslant 1$. Therefore, $P_c \geqslant P \geqslant P_a$. The value of f may be
determined experimentally. Chaplin [39] suggests the use of f = 0.
Stanton-Jones[40] and Gates[44]   have developed theories using a
value of f = 1. For the purposes of this development, f = 0 will be
considered.

2.5.2 Geometric Compatibility

From Figure 2-3 it may be seen that the following geometric relationship holds:

$$R = \frac{d}{1 + \sin \theta}$$

(2-19)

2.5.3 D'Alembert's Principle

Assumption 2.5.1.3 applied to the D'Alembert's equation, Equation (2-12), gives:

$$p_c = \left(\frac{\rho}{g_0}\right)\left(v^2\right)\left(\frac{t}{R}\right)$$

(2-20)

In the above equation, both p_c and v are unknown quantities. The calculation of p_c is dependent upon v. In turn, v is dependent upon P which is determined by the choice of f in Assumption 2.5.1.7.

2.5.4 Conservation of Energy

Conservation-of-energy applied as specified in Section 2.4.4 gives:

$$P_j = P + \frac{1}{2}\left(\frac{\rho v^2}{g_0}\right)$$

(2-21)

2.5.5 Conservation of Mass

Conservation-of-mass applied as specified in Section 2.4.5 together with Assumption 2.5.1.3 gives:

$$Q_j = S \, t \, v$$

(2-22)

2.5.6 Force Equilibrium

Force equilibrium applied as specified in Section 2.4.6, together with Assumptions 2.5.1.1, 2.5.1.4, 2.5.1.6, and the Geometric Compatibility Assumption, Equation (2-19), gives:

$$p_c d\,S = J'(1 + \sin \theta) \qquad (2\text{-}23)$$

2.5.7 Pressure Variation

The pressure variation across the jet is constant and equal to the value assumed in Assumption 2.5.1.7,

$$P = P_a \qquad (2\text{-}24)$$

2.5.8 Velocity in the Jet

The velocity in the jet may be determined by substituting the pressure in the jet, Equation (2-24), into the conservation-of-energy relationship, Equation (2-21). The result is:

$$v = \sqrt{\frac{2g_o}{\rho}(p_j)} \qquad (2\text{-}25)$$

2.5.9 Momentum

The reaction of the jet may be determined by combining Equations (2-16), (2-22), and (2-25). The result is:

$$J' = 2\,S\,p_j\,t \qquad (2\text{-}26)$$

2.5.10 Jet Flow

The flow may be determined by combining the energy and mass-conservation equations, Equations (2-21) and (2-22), and applying the pressure equation, Equation (2-24). The result is:

$$Q_j = St\sqrt{\left(\frac{2g_o}{\rho}\right)(p_j)} \qquad (2\text{-}27)$$

2.5.11 Pressure Ratio

The pressure ratio for the system may be obtained by combining the equilibrium and momentum equations, Equations (2-23) and (2-26), and applying the definition for jet thickness parameter, $X = (t/d)(1 + \sin \theta)$, Equation (2-11). The result is:

$$p_c/p_j = 2 X \tag{2-28}$$

2.6 The Exponential Theory

2.6.1 Approach and Assumptions

The simplest theory for relating p_c/p_j to jet geometry was presented in Section 2.5. In the present section, a more accurate theory has been developed. The development presented follows the overall approach outlined in Section 2.4. The objective of this section is to develop a more exact relationship between p_c and p_j so that input horsepower, Equation (2-9), and aircraft weight, Equation (2-10), can be directly related.

The exponential theory was advanced by Stanton-Jones.[40] In this theory, the pressure variation across the jet is exponential as shown in Equation (2-37). The additional assumptions are:

2.6.1.1 The radius R is constant and can be approximated by R_c.

2.6.1.2 The radius R_c is tangent to the ground at Section EG of Figure 2-3.

2.6.2 Geometric Compatibility

The geometric compatibility assumptions are based upon Figure 2-3. It may be seen that the following relationships hold:

$$R_c = \frac{d}{1 + \sin \theta} \tag{2-29}$$

$$R_c = R_a + t \tag{2-30}$$

2.6.3   D'Alembert's Principle

Assumption 2.3.3.1 applied to the D'Alembert equation (2-12) gives:

$$\int_{P_a}^{P_c} \frac{dP}{v^2} = \frac{\rho}{g_0 R_a} \int_{R_a}^{R_c} dR \tag{2-31}$$

The variables of integration in the above equation may be changed to eliminate the R_c and R_a variables. The integration is performed along the z axis (at Section DF in Figure 2-3) between z=o and z=t. By applying the new dummy variable, z, and using Equations (2-29) and (2-11), the R variable may be eliminated from Equation (2-31). The result is:

$$\int_{P_a}^{P_c} \frac{dP}{v^2} = \frac{\rho}{g_0} \frac{X}{t} \int_{0}^{t} dz \tag{2-32}$$

2.6.4   Conservation of Energy

Conservation of energy applied as specified in Section 2.4.4 gives:

$$v^2 = \frac{2g_0}{\rho} (P_j - P) \tag{2-33}$$

2.6.5   Conservation of Mass

Conservation of mass may be applied by integrating the velocity across the z-axis between z=o and z=t as shown in Figure 2-3.

$$Q_j = S \int_{0}^{t} v\,dz \tag{2-34}$$

2.6.6 Force Equilibrium

Force equilibrium applied as specified in Section 2.4.6, combined with Assumptions 2.6.1.1 and 2.6.1.2, gives:

$$p_c \, S \, d \; = \; J'(1 + \sin \theta) \tag{2-35}$$

2.6.7 Pressure Variation

The velocity relationship, Equation (2-33), substituted into the D'Alembert equation (2-32) between the outer boundary and some arbitrary point (z) inside the jet gives:

$$p \; = \; p_j \, (1 - e^{-2X \, z/t}) \tag{2-36}$$

where X is defined by Equation (2-11).

2.6.8 Velocity in the Jet

The velocity in the jet may be determined by solving the pressure variation, Equation (2-36), with the energy equation, Equation (2-33). The result is:

$$v \; = \; \sqrt{\frac{2g_0}{\rho} \, p_j} \; (e^{[-X \, z/t]}) \tag{2-37}$$

2.6.9 Momentum

The total reaction of the jet may be determined by Equation (2-17).

$$J' = \rho \frac{S}{g_0} \int_0^t v^2 \, dz$$

Substituting in Equation (2-37) and integrating gives:

$$J' = 2t\, S\, p_j \left[\frac{1}{2X} (1 - e^{-2X}) \right]$$

(2-38)

2.6.10 Jet Flow

The jet flow may be determined by combining the velocity relationship, Equation (2-37), with the conservation of mass equation, Equation (2-34), and integrating. The result is:

$$Q = t\, S \sqrt{\frac{2g_0}{\rho} (p_j)} \; \frac{1}{X} [(1 - e^{-X})]$$

(2-39)

2.6.11 Pressure Ratio

The pressure ratio may be determined from the force equilibrium relationship, Equation (2-35), combined with the momentum relationship, Equations (2-38) and (2-11). The result is:

$$p_c/p_j = 1 - e^{-2X}$$

(2-40)

2.7 The Barratt Theory

2.7.1 Approach and Assumptions

The Barratt theory has been reported to provide quite accurate predictions of the performance of a peripheral jet.[40,37] In this section, the jet flow and recovery pressure ratio predicted by the Barratt theory have been developed. These parameters are related to aircraft weight and horsepower in Chapter 3.
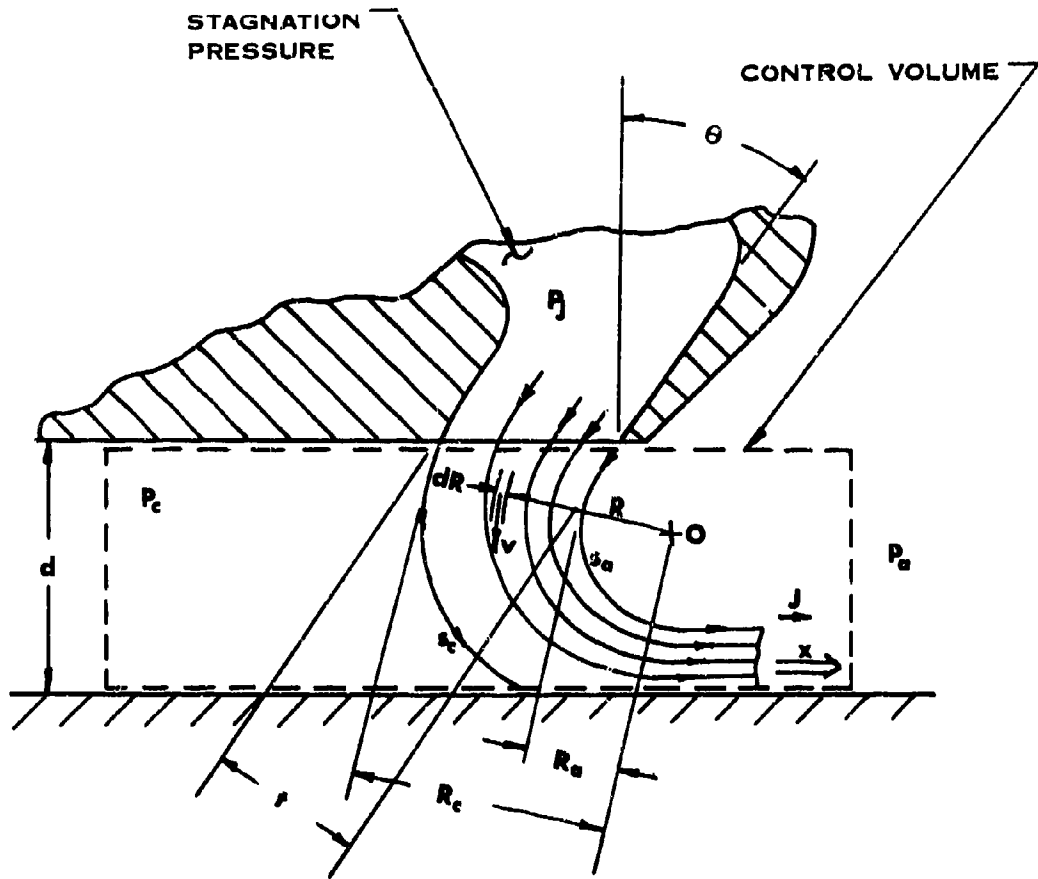
MODEL FOR BARRATT THEORY

FIGURE 2-4

Barratt's theory[41] differs from the previous theories in the geometry assumed for the jet. A cross section of the jet is shown in Figure 2-4. It should be noted that in this theory it is not necessary for the jet thickness to be constant and streamline s_c does not have to be tangent to the ground.

In addition to the assumptions made in Sections 2.3 and 2.4, the following assumptions are made:

2.7.1.1   At the jet exit plane all streamlines have a common center of curvature (shown as point M in Figure 2-4).

2.7.1.2   The total head or stagnation pressure is constant across the jet.

2.7.1.3   The total momentum J of the jet after the jet has been deflected is equal in magnitude to the exit plane jet momentum.

2.7.1.4   The pressure along any streamline is constant.

2.7.2   Geometric Compatibility

From the geometry in Figure 2-4 it may be seen that at Section DF

$$R_c = R_a + t \tag{2-41}$$

Based upon Assumption 2.7.1.3 it is possible to use geometric compatibility to calculate the charge in momentum of the jet. The angle through which the jet turns is $90^O + \theta$. The net change of the momentum vector may then be written:

$$\frac{d}{dt} (\vec{J})_x = J'(1 + \sin \theta) \, g_o \tag{2-42}$$

2.7.3 D'Alembert's Principle

D'Alembert's Principle applied as specified in Section 2.4.3 gives:

$$\frac{dP}{dR} = \frac{\rho v^2}{R\, g_o} \tag{2-43}$$

2.7.4 Conservation of Energy

The conservation-of-energy principle applied as specified in Section 2.4.4 gives:

$$P_j = P + \frac{\rho v^2}{2\, g_o} \tag{2-44}$$

In order to determine the velocity variation across the jet, it is desired to replace dP/dR in Equation (2-43) with an expression for d v/dR. The needed expression may be derived by differentiating the energy equation (2-44) with respect to R and applying Assumption 2.7.1.2.

$$\frac{dP}{dR} = -\frac{\rho}{g_o}\, v\, \frac{dv}{dR} \tag{2-45}$$

Equations (2-45) and (2-43) have been combined in Equation (2-51).

2.7.5 Conservation of Mass

The conservation-of-mass principle applied as specified in Section 2.4.5 gives:

$$Q_j = S \int_{R_a}^{R_c} v\, dR \tag{2-46}$$

2.7.6 Force Equilibrium

Force equilibrium applied as specified in Section 2.4.6 in conjunction with the geometric compatibility relationship developed in Equation (2-41) gives:

$$p_c \, S \, d = J'(1 + \sin \theta) \tag{2-47}$$

2.7.7 Pressure Variation

The pressure variation may be found by solving the D'Alembert equation (2-43) for v^2 and substituting it in the conservation of energy equation (2-44). The result is:

$$\int \frac{dP}{P - P_j} = -2 \int \frac{dR}{R} \tag{2-48}$$

At the inside to jet boundary (streamline s_c)

$$P = P_c$$

$$R = R_c$$

By integrating Equation (2-48) and applying the boundary condition to evaluate the constant the following equation is obtained:

$$P = P_j + \left(\frac{R_c}{R}\right)^2 (P_c - P_j) \tag{2-49}$$

At the outside of the jet boundary (streamline s_a),

$$P = P_a$$

$$R = R_a$$

$$v = v_a$$

Equation (2-49) evaluated at the outside boundary gives:

$$\frac{R_a}{R_c} = \sqrt{1 - P_c/P_j}$$

(2-50)

2.7.8 Velocity Variation

The velocity variation may be determined by equating the D'Alembert and the energy equations as formulated in Equations (2-43) and (2-45) respectively. The result is:

$$\int \frac{dv}{v} = -\int \frac{dR}{R}$$

(2-51)

At the outside jet boundary (streamline s_a)

$R = R_a$

$v = v_a$

$P = P_a$

By integrating Equation (2-51) and applying the boundary conditions, the following equation results:

$$v = \frac{R_a}{R} v_a$$

v_a may be expressed in terms of P_j by applying $v = v_a$ where $P = P_a$, in the conservation of energy equation (2-44). The result is:

$$v_a = \sqrt{\frac{2g_0}{\rho} P_j}$$

The last equation may be substituted into the general velocity equation to yield:

$$v = \frac{R_a}{R} \sqrt{\frac{2g_o}{\rho} \, p_j}$$

(2-52)

2.7.9 Momentum

The total reaction of the jet may be determined by substituting the value of v given by Equation (2-52) in the momentum equation, Equation (2-17), and integrating between the limits R_a and R_c. The resulting equation is:

$$J' = 2 S (R_a)^2 \, p_j \int_{R_a}^{R_c} \frac{dR}{R^2}$$

(2-53)

Integration gives:

$$J' = 2 S p_j \frac{R_a (R_c - R_a)}{R_c}$$

Equations (2-41) and (2-50) applied to the above relationship give:

$$J' = 2 S p_j t \sqrt{1 - p_c/p_j}$$

(2-54)

2.7.10 Jet Flow

Jet flow may be determined by substituting the velocity equation (2-52) in the conservation of mass equation (2-46). The resulting equation is:

$$Q_j = S R_a \sqrt{\frac{2g_o}{\rho} \, (p_j)} \int_{R_a}^{R_c} \frac{dR}{R}$$

(2-55)

Integrating and applying Equations (2-41) and (2-50) gives:

$$Q_j = tS \sqrt{\frac{2g_0}{\rho}\,(p_j)} \quad \frac{\sqrt{1 - p_c/p_j}}{1 - \sqrt{1 - p_c/p_j}} \quad \log_e (1 - p_c/p_j)^{-\frac{1}{2}} \tag{2-56}$$

2.7.11 Pressure Ratio

The pressure ratio may be determined by substituting the momentum equation, Equation (2-54), in the force equilibrium equation, Equation (2-47), and applying the definition for jet thickness parameter, Equation (2-11), to simplify. The result is:

$$p_c/p_j = 2X \left(\sqrt{X^2 + 1} - X \right) \tag{2-57}$$

2.8 Plenum Theory

2.8.1 Approach and Assumptions

The relationships developed in Sections 2.4, 2.5, 2.6, and 2.7 apply only to a peripheral jet and not to a plenum chamber. In this section, the equations for predicting the horsepower, flow and jet height for a plenum chamber have been developed.

The plenum chamber differs from the peripheral jet as may be observed by comparing Figures 1-1(a) and 1-1(b). In the plenum chamber design, the air is blown directly into the plenum (cushion) rather than into the trunk. Consequently, the plenum chamber has ro trunk pressure, no peripheral jet, and no momentum seal. The cushion pressure is maintained by the flow restriction imposed by the air gap between the vehicle skirt and the ground. The relationships for this system may be developed by conservation of energy applied to the exit and by conservation-of-mass applied to the air flowing from the power source. The assumptions made in Section 2.3 apply, but those made in Sections 2.4, 2.5, 2.6, and 2.7 do not apply.

The additional assumptions required are:

2.8.1.1 The air is incompressible.

2.8.1.2   The air is inviscid.

2.8.1.3   Energy losses are negligible.

2.8.1.4   The flow is adiabatic.

2.8.1.5   The air velocity in the cushion may be neglected ($p_t = p_c$, where $p_t =$ total pressure).

2.8.1.6   The total pressure is everywhere constant.

2.8.1.7   The flow velocity at the exit is two dimensional and perpendicular to the exit plane.

2.8.2   Conservation-of-Energy Applied to Exhaust Exit Plane

The conservation-of-energy equation may be written:

$$P_c = P_a + \frac{\rho}{2g_0} v^2 \qquad (2\text{-}58)$$

Equation (2-58) expresses the cushion pressure in terms of pressure and velocity of the exhaust air which has expanded to atmospheric pressure.

2.8.3   Conservation of Mass

Conservation-of-mass applied to the exhaust exit gives:

$$Q_p = v_p d_p S_p C_d \qquad (2\text{-}59)$$

where the subscript p refers to the plenum.

Equation (2-59) expresses the total flow from the plenum chamber in terms of the effective flow area and the velocity of the gas crossing the flow area.

2.8.4 Conservation-of-Energy Involving the Power System

Using a development similar to that given in Section 2.3.1, the horsepower delivered to the plenum is:

$$hp = \frac{p_c Q_p}{550} \qquad (2\text{-}60)$$

2.8.5 Determination of Flow

Flow from the plenum may be obtained by combining Equations (2-58) and (2-59). The result is:

$$Q_p = \sqrt{\frac{2g_o}{\rho}} \; (p_c) \; C_d \; S_p \; d_p \qquad (2\text{-}61)$$

Equation (2-61) gives the total flow from the plenum in terms of the cushion pressure and the effective flow area.

2.8.6 Horsepower Relationship

The horsepower input can be determined from Equations (2-61) and (2-60). The result is:

$$hp = \frac{(p_c)^{3/2} S_p \; d_p \; C_d}{550} \left(\frac{2g_o}{\rho} \right)^{1/2} \qquad (2\text{-}62)$$

Equation (2-62) gives the total horsepower which must be supplied to the air in terms of the cushion pressure and the effective flow area.

3. COMPARISON OF FLOW THEORIES

3.1   Introduction

In order to make a general comparison of the performance predicted by the flow theories developed in Chapter 2, it is necessary to develop six nondimensional parameters. Three of these parameters are widely used in the literature of Air Cushion Vehicles. These parameters include:

(1) A_I, the jet augmentation ratio is defined as follows:

$$A_I = \frac{\text{total vehicle lift force}}{\text{reference force}} \qquad (3\text{-}1)$$

A number of different reference forces are used in the literature.[8] In this chapter, the reference force is the thrust which could be generated if the exhaust were discharged vertically downward. The augmentation ratio is discussed in Section 3.7.

(2) p_c/p_j, the recovery pressure ratio is defined as follows:

$$p_c/p_j = \frac{\text{cushion pressure (gage)}}{\text{trunk pressure (gage)}} \qquad (3\text{-}2)$$

The recovery pressure ratio is discussed in Section 3.2.

(3)   X, the nozzle thickness parameter which was defined in Section 2.4.2 as follows:

$$X = \frac{t}{d} (1 + \sin \theta) \qquad (2\text{-}11)$$

49

The nozzle thickness parameter is discussed in Section 3.3.

Three additional parameters not found in the literature are also defined in this chapter. These parameters include:

(1) C_Q, the cushion pressure coefficient is a flow coefficient. This parameter is developed in Section 3.4.

(2) C_{ht}, the power-thickness parameter, is a dimensionless parameter useful in predicting power requirements for a peripheral jet. This parameter is developed in Section 3.5.

(3) C_{hd}, the power-height parameter, is a dimensionless parameter useful in determining the minimum power for a required jet height. This parameter is developed in Section 3.6.

3.2   Recovery Pressure Ratio

The ratio of cushion pressure to trunk pressure is known as the recovery pressure ratio. It has been shown previously (Section 2.3.2) that the value of p_c may be determined by the aircraft weight and the cushion area. The value of p_j is dependent upon the input power, the jet area, the jet height, and the jet angle. Consequently, the ratio of p_c/p_j gives an important dimensionless quantity which is dependent on all the major variables. In addition, it will be shown in Chapter 4 that the trunk shape and stiffness are strongly influenced by p_c/p_j.

Because of the features cited above, p_c/p_j was selected as the standard dependent variable against which other dimensionless parameters have been plotted.
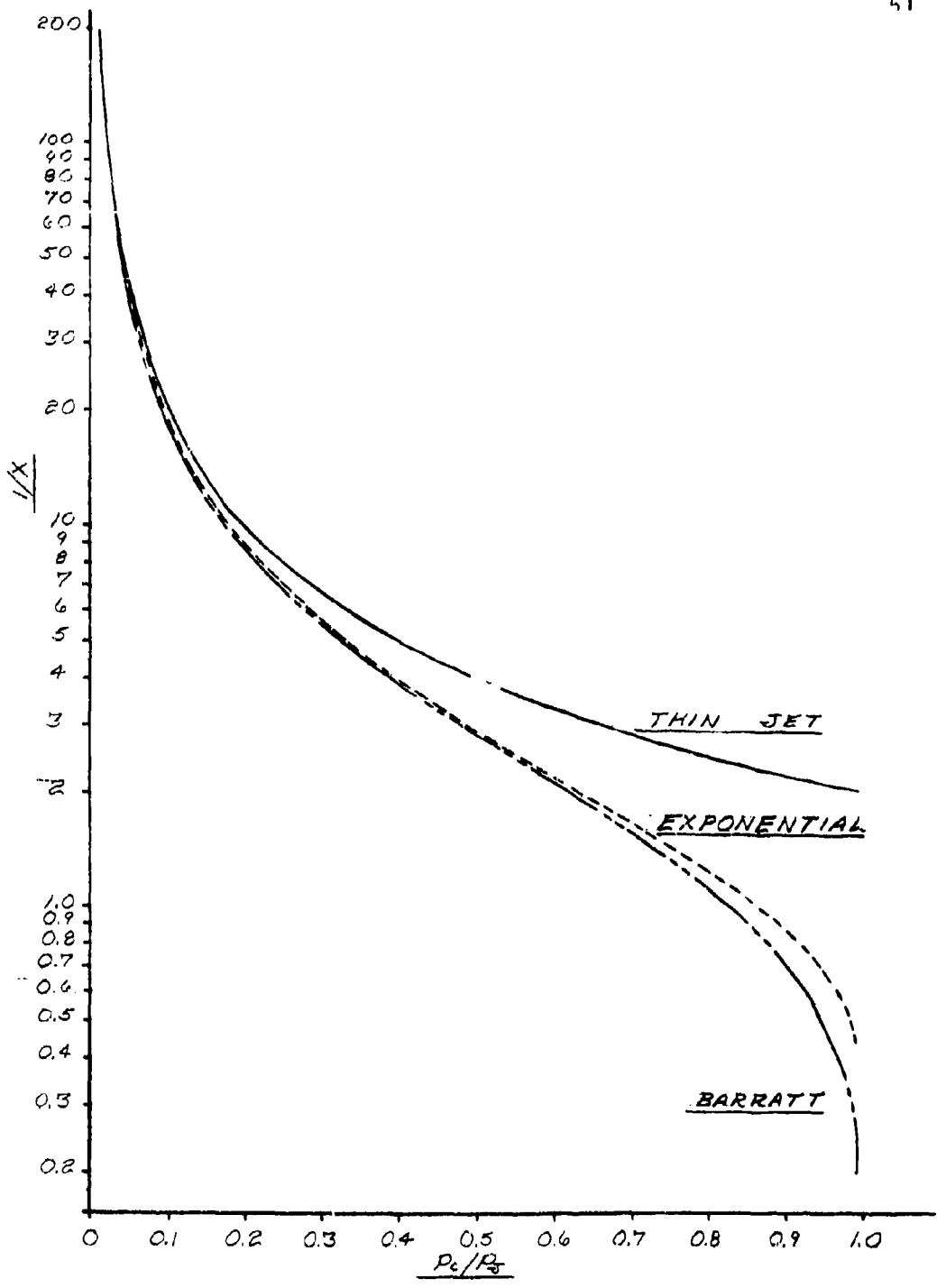
NOZZLE THICKNESS PARAMETER vs P_c/P_J

FIGURE 3-1

3.3 Nozzle Thickness Parameter

The nozzle thickness parametei was defined in Section 2.4.2 as follows:

$$X = \frac{t}{d} (1 + \sin \theta) \tag{2-11}$$

This parameter relates nozzle geometry to jet height. For a given design, the nozzle thickness (t) and the jet angle (θ) are relatively constant. Equation (2-11) shows that the jet height (d) and the parameter (X) are inversely related. Consequently, the nozzle thickness is valuable in showing the interrelationship between the independent variables and the jet height. This interrelationship has been shown by graphs of various nondimensional parameters plotted against the dependent variable p_c/p_j.

Graphs of $1/X$ versus p_c/p_j for the three flow theories are presented in Figure 3-1. The analytical relationships between (p_c/p_j) and X are shown in Table 3-I.

3.4 Pressure Coefficient

The pressure coefficient, C_Q, is, in fact, a flow coefficient which is dependent upon the recovery pressure ratio (p_c/p_j). This coefficient has been developed in this section.

Consider the total flow from the jet at the nozzle exit plane as shown by Section DF in Figure 2-2. The pressure on the cushion side of the jet is higher than the pressure on the atmospheric side of the jet. Consequently, a velocity and a flow gradient may exist across the thickness of the jet. It is the nature of the assumed pressure gradient across the jet thickness which gives rise to the differences between the three momentum theories. In Sections 2.5.10, 2.6.10, and 2.7.10, expressions have been developed for the total flow from the jet as predicted by the three momentum theories. The resulting equations are:

Thin jet theory

$$Q_j = t S \sqrt{\frac{2g_o}{\rho}} (p_j) \ [1] \tag{2-27}$$
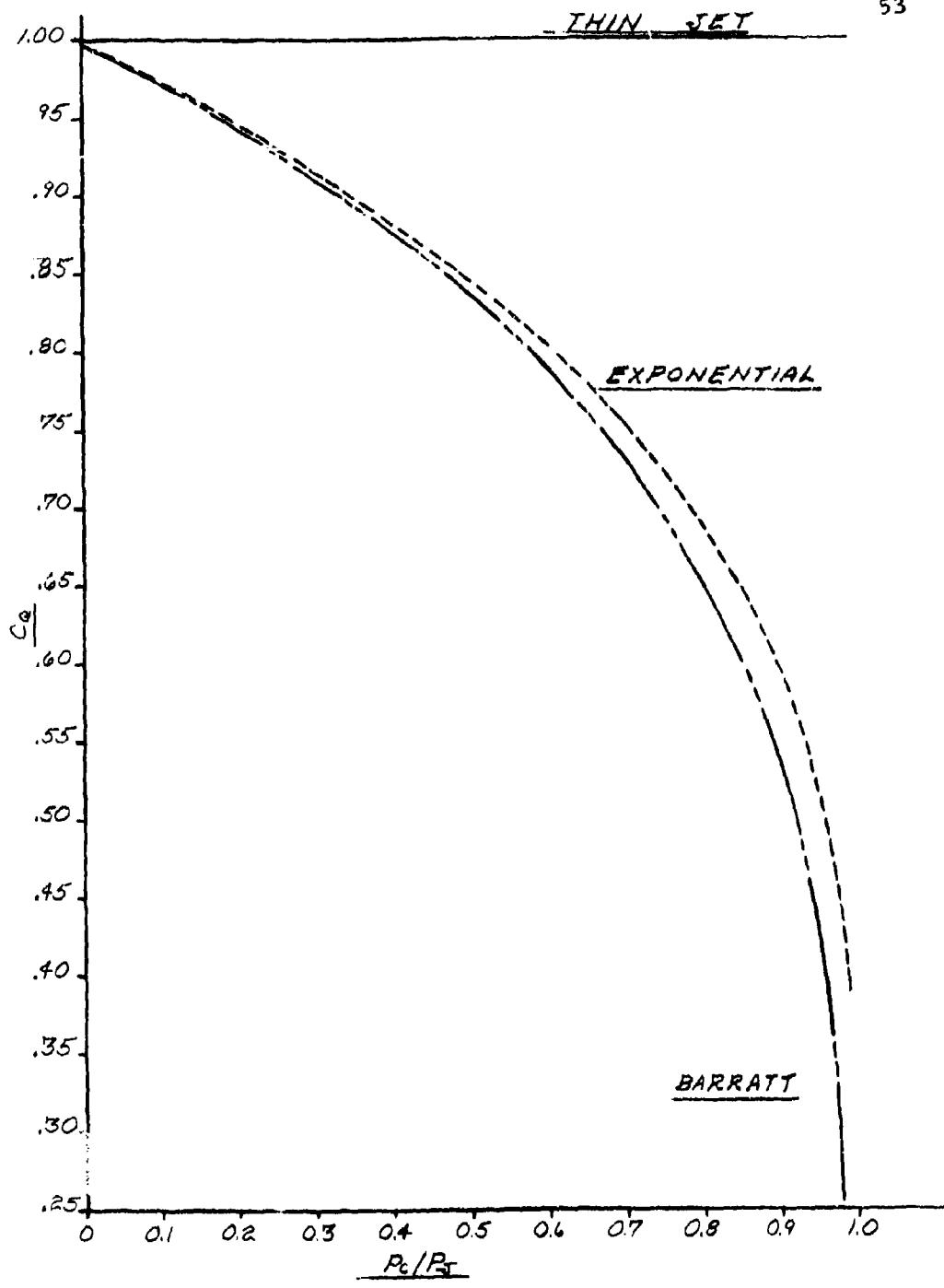
FLOW COEFFICIENT vs P_c/P_J

FIGURE 3-2

Exponential theory

$$Q_j = tS\sqrt{\frac{2g_o}{\rho}(p_j)}\left[\frac{1}{X}(1-e^{-X})\right] \qquad (2\text{-}39)$$

Barratt theory

$$Q_j = tS\sqrt{\frac{2g_o}{\rho}(p_j)}\left[\frac{\sqrt{1-p_c/p_j}}{1-\sqrt{1-p_c/p_j}}\log_e(1-p_c/p_j)^{-\frac{1}{2}}\right] \qquad (2\text{-}56)$$

Equations (2-28), (2-39), and (2-56) were constructed so that the flow is dependent upon a standard reference pressure (p_j) multiplied by a factor to compensate for the pressure gradient across the jet thickness. The factor in brackets defines pressure coefficient, C_Q.

The pressure coefficient, C_Q, is defined from Equations (2-28), (2-39), or (2-56) as follows:

$$C_Q \equiv \frac{Q_j}{tS\sqrt{\frac{2g_c}{\rho}(p_j)}} \qquad (3\text{-}3)$$

Graphs of C_Q versus p_c/p_j are shown in Figure 3-2. The expressions for C_Q are summarized in Table 3-1.

Using the pressure coefficient, it is possible to write a general flow equation for the total flow from an actual concentrated peripheral jet air suspension system. The relationship is:

$$Q_j = St\sqrt{\frac{2g_Q}{\rho}(p_j)}\, C_Q C_x \qquad (3\text{-}4)$$

where:

C_x = coefficient of discharge for jet nozzle with $p_c/p_j = 0$
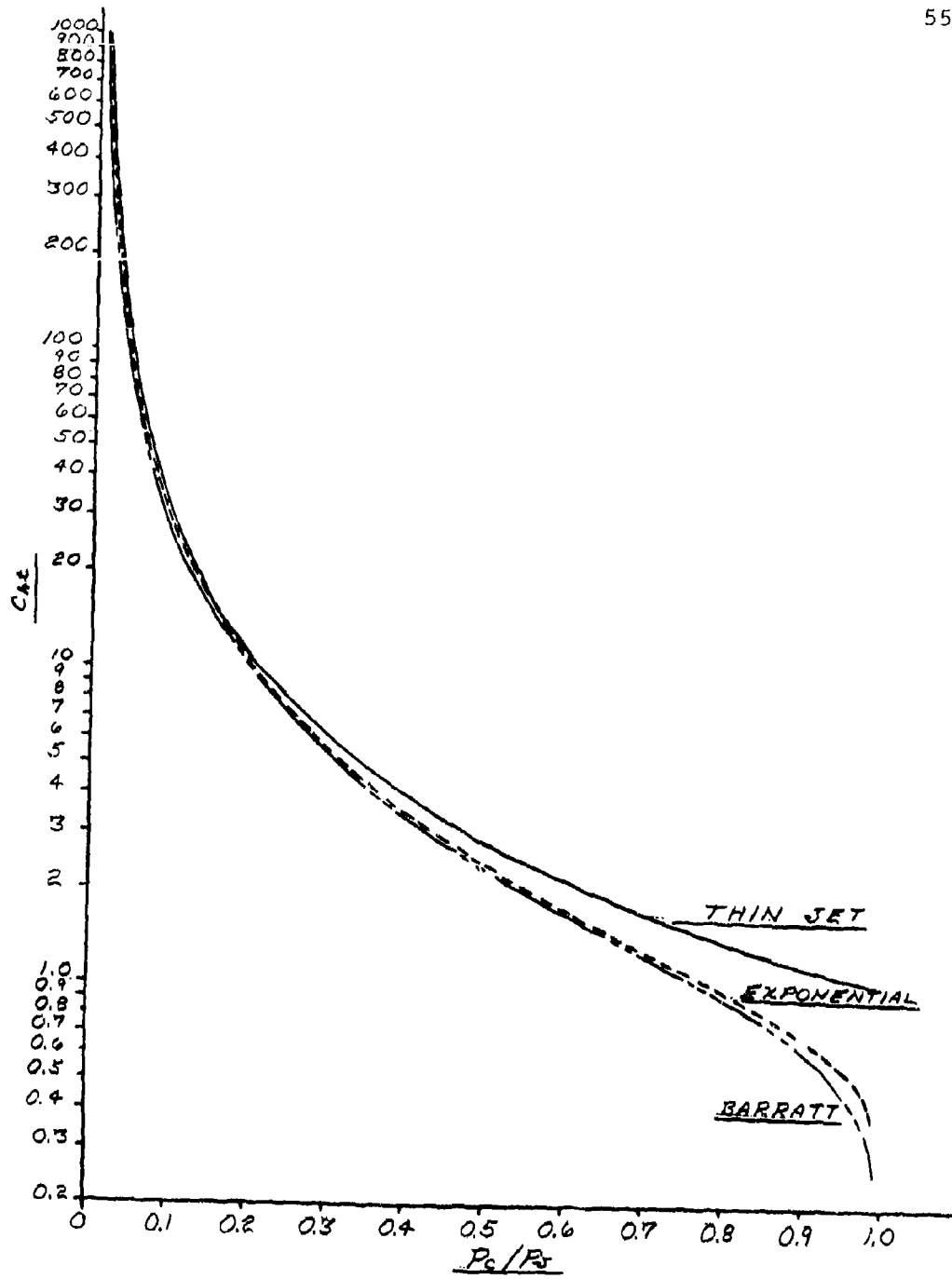
POWER-THICKNESS PARAMETER vs P_c/P_j

FIGURE 3-3

C_Q = pressure coefficient which compensates for pressure gradient across the jet.

3.5 Power Thickness Parameter

The power-thickness parameter, C_{ht}, is a dimensionless parameter useful in visualizing the effect of trunk pressure on power requirements. This parameter may be developed from the general horsepower equation (2-10) and the general flow equation (3-4). These equations are:

$$hp = \frac{p_j \, Q_j}{550} \qquad (2\text{-}10)$$

$$Q_j = S \, t \, \sqrt{\frac{2g_0}{\rho} (p_j)} \; C_Q \, C_x \qquad (3\text{-}4)$$

Equations (2-10) and (3-4) may be combined to yield:

$$hp = (p_j)^{3/2} \; S \, t \, \sqrt{\frac{2g_0}{\rho}} \; \frac{C_Q \, C_x}{550} \qquad (3\text{-}5)$$

A dimensionless relationship may be developed by rearranging Equation (3-5) and dividing both sides by $(p_c)^{3/2}$. The resulting relationship forms the basis for defining the power-thickness parameter, C_{ht}.

$$C_{ht} \equiv \frac{(hp)\,(550)}{S \, t \, \sqrt{\frac{2g_0}{\rho}} \, (p_c)^{3/2}} = \left(\frac{p_j}{p_c}\right)^{3/2} C_Q \, C_x \qquad (3\text{-}6)$$

For a given load, cushion area, cushion periphery and jet configuration, the parameter C_{ht} is directly proportional to horsepower. A plot of p_c/p_j versus C_{ht} (see

$$\theta = 0°$$
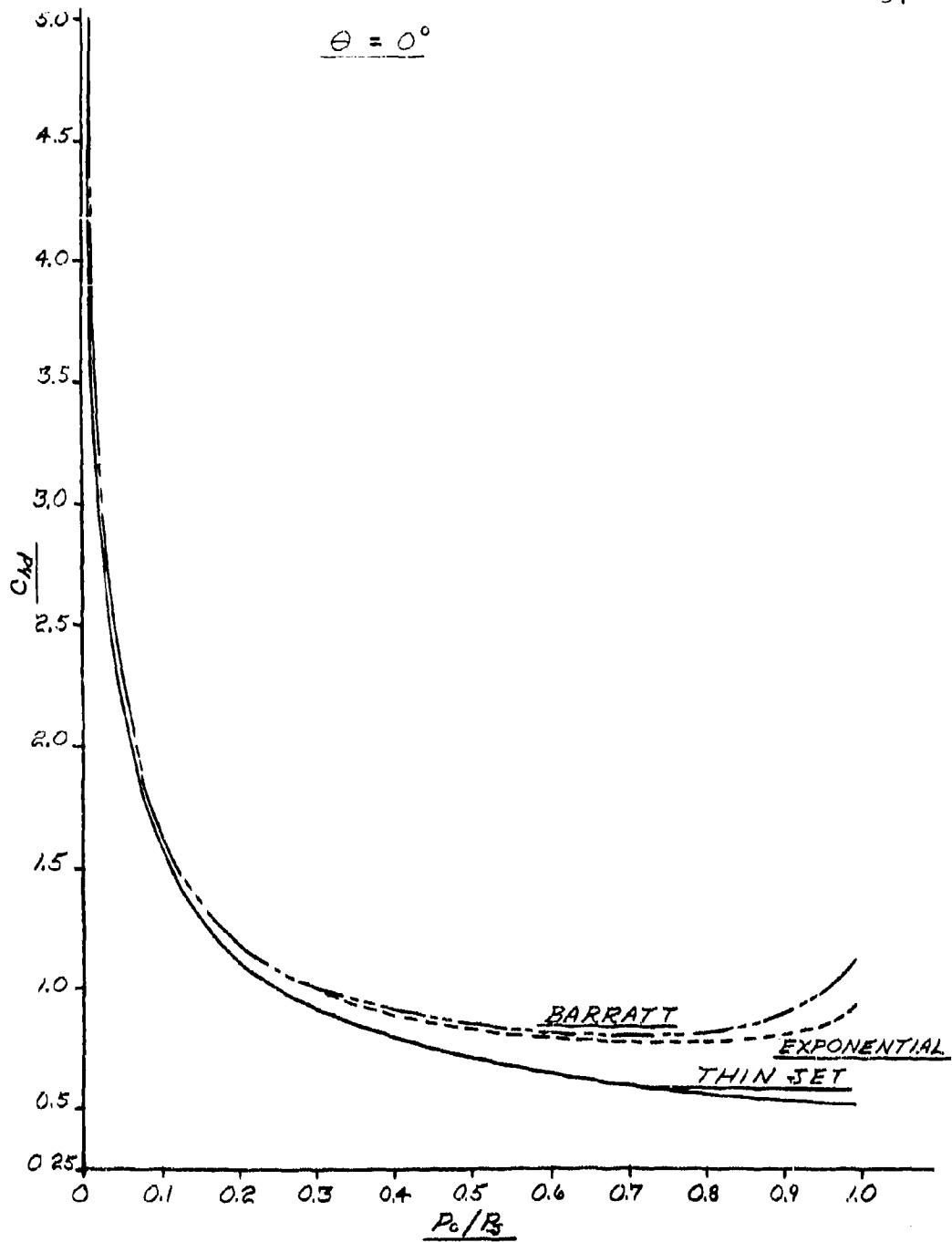
POWER-HEIGHT vs P_c / P_J, SIMPLE JET THEORY
FIGURE 3-4a
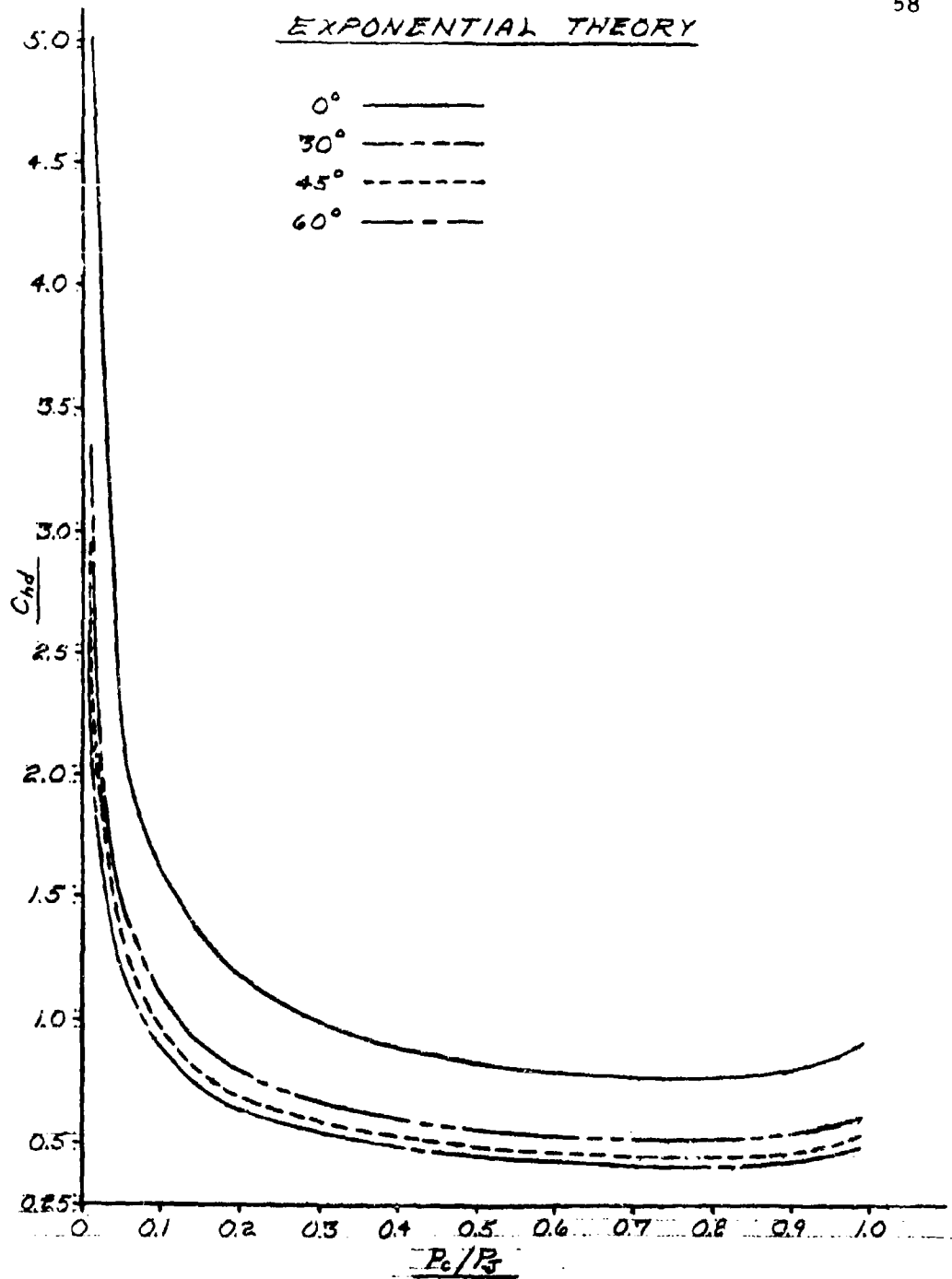
POWER-HEIGHT PARAMETER vs P_c/P_j, EXPONENTIAL THEORY
FIGURE 3-4b

BARRATT THEORY

0°	————
30°	— ·— ·—
45°	— — — —
60°	— — — —
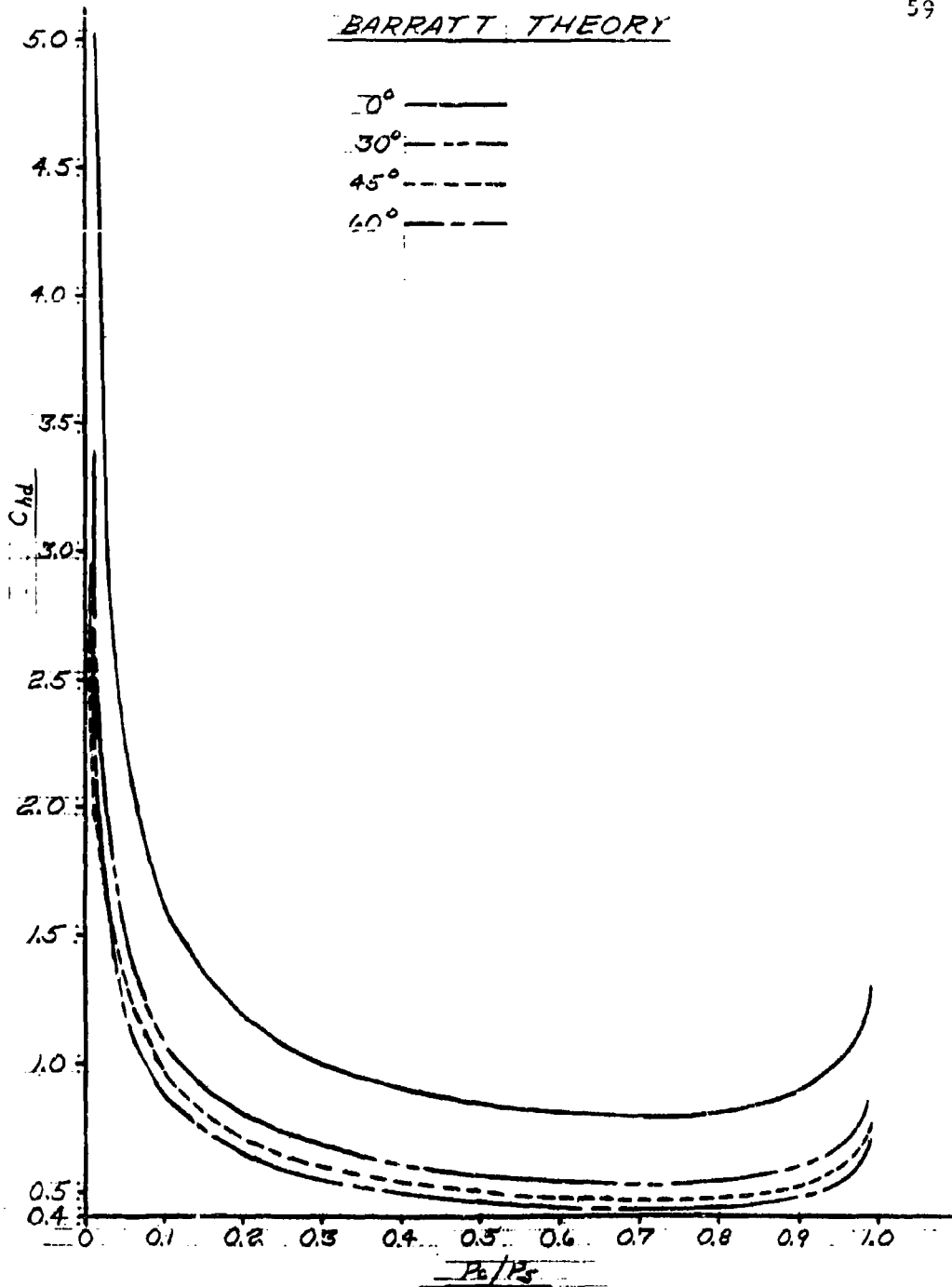
POWER-HEIGHT PARAMETER vs p_c/p_j, BARRETT THEORY

FIGURE 3-4c

Figure 3-3) shows how, other parameters being constant, increases in trunk pressure cause increases in horsepower.

3.6   Power-Height Parameter

The power-thickness parameter, developed in Section 3.5, does not include the jet height (d) in the relationship. In the design of a peripheral jet air cushion system, it is generally desirable to maximize jet height and minimize power. A dimensionless parameter which includes both horsepower and jet height may be developed by multiplying both sides of Equation (3-6) by the ratio (τ/d). The result is defined as C_{hd} the power-height parameter.

$$C_{hd} = \left(\frac{hp}{d}\right)\left(\frac{550}{S}\right)\frac{1}{\sqrt{\frac{2g_o}{\rho}}}\left(\frac{1}{(p_c)^{3/2}}\right) = \left(\frac{t}{d}\right)\left(\frac{p_j}{p_c}\right)^{3/2} C_Q C_x \qquad (3-7)$$

Equation (3-7) contains horsepower and jet height as a ratio. Since it is desirable to minimize power and maximize jet height, a minimum value of the parameter C_{hd} should be selected as a design point.

Graphs of C_{hd} versus p_c/p_j for $\theta = 0$ and $C_x = 1.0$ are shown in Figure 3-4(a). The effect of θ is shown in Figure 3-4(b and c). It is evident from Figure 3-4(a) that design points in the range of $p_c/p_j = 0.4$ to $p_c/p_j = 0.9$ are desirable from a maximum jet height, minimum power standpoint.

3.7   Augmentation Ratio

The augmentation ratio is, in fact, a lift coefficient for the vehicle. This parameter is defined at least seven different ways in the literature,[8] depending on the choice of the reference force in Equation (3-1). Only one definition will be considered here. The reference force assumed here is the maximum thrust which could be generated if the jet nozzle

exhaust were discharged vertically downward. This thrust has been designated F_j. The expression for the augmentation ratio is:

$$A_l = \frac{\text{pressure support} + \text{actual jet thrust in vertical direction}}{\text{ideal jet thrust}}$$

or

$$A_l = \frac{p_c A_c + F_j \cos\theta}{F_j} \qquad (3\text{-}8)$$

An expression for F_j may be developed by evaluating the total change of momentum in the vertical direction for the air as it flows from the trunk to the atmosphere. If the simple jet theory is assumed, the magnitude of the total momentum of the jet at the exhaust plane is given by Equation (2-26).

$$J' = 2 S t p_j \qquad (2\text{-}26)$$

The momentum of the gas in the trunk is assumed to be zero. The magnitude of the jet thrust may be written:

$$F_j = 2 S t p_j \qquad (3\text{-}9)$$

Equation (3-9) may be substituted into Equation (3-8) and the result rearranged to give an expression which relates A_l to p_c/p_j. The resulting equation is:

$$A_l = \cos\theta + (p_c/p_j)\left(\frac{A_c}{2 St}\right) \qquad (3\text{-}10)$$

Equation (3-10) may be further simplified by assuming the cushion is circular in shape. For a circular shaped cushion with a diameter, D ,
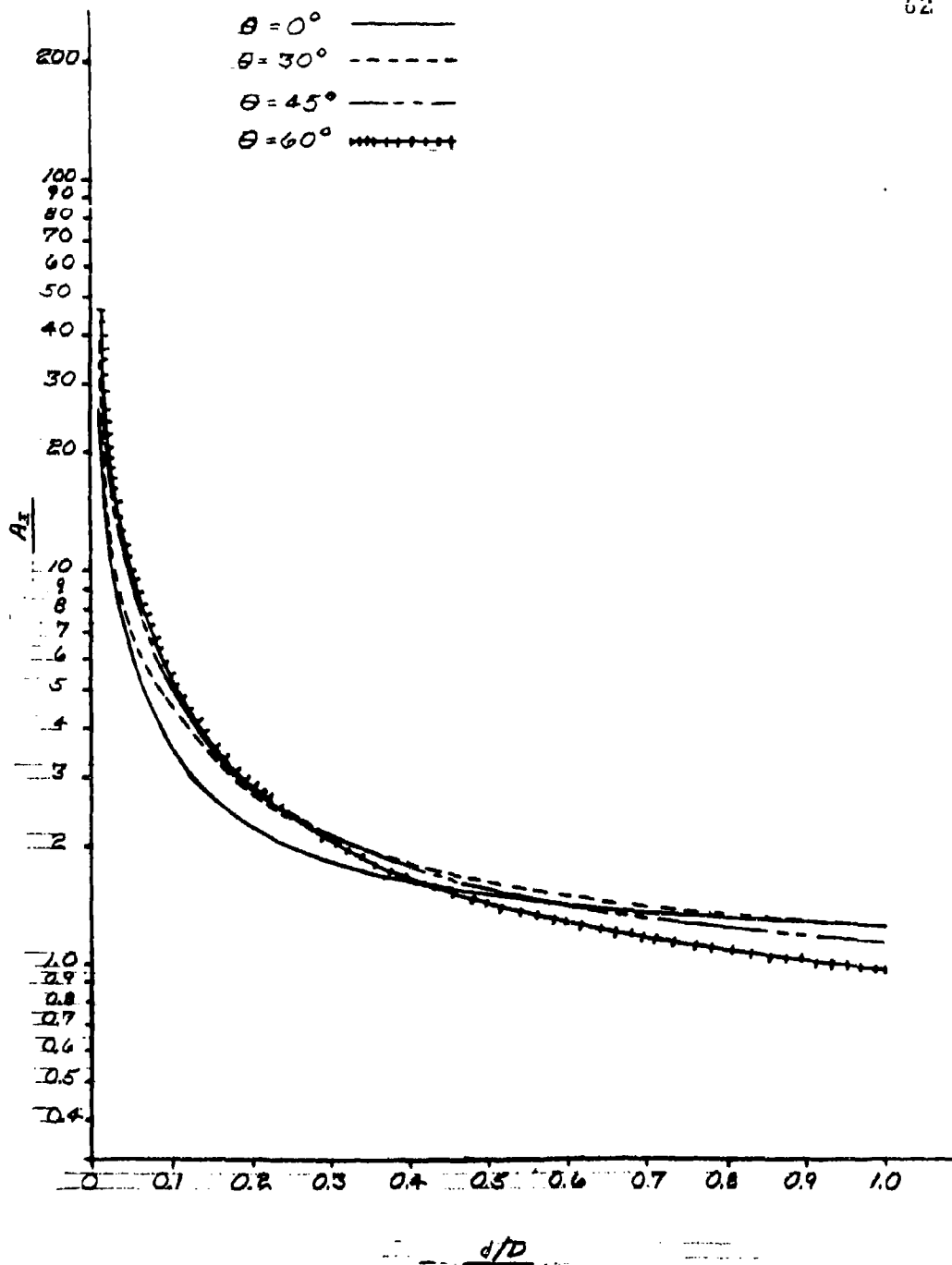
AUGMENTATION vs JET HEIGHT TO CUSHION DIAMETER RATIO

FIGURE 3-5

$$A_c = \frac{\pi D^2}{4}$$

$$S = \pi D$$

The recovery pressure (p_c/p_j) may be written:

$$p_c/p_j = 2\frac{t}{d}(1 + \sin \theta)$$

The above three relationships may be substituted into Equation (3-10) to give:

$$A_I = \cos \theta + \frac{1}{4\,d/D}(1 + \sin \theta) \tag{3-11}$$

Equation (3-11) expresses the augmentation ratio in terms of jet angle, cushion diameter and jet height. A circular cushion (plenum) area and the simple jet theory were assumed in developing Equation (3-11).

The influence of d/D on A_I for various values of jet angle θ is shown in Figure 3-5.

3.8   Summary of Results

The influence of p_c/p_j on the nozzle thickness parameter is shown in Figure 3-1. The inverse of the nozzle thickness parameter is directly proportional to jet height. Consequently, Figure 3-1 shows how the jet height varies with p_c/p_j for constant values of nozzle thickness (t) and jet angle (θ). This figure shows that jet height increases with decreasing p_c/p_j. It may be recognized that a decreasing p_c/p_j implies an increasing p_j, if p_c is held constant. The figure suggests that jet height increases witn increasing p_j. This result is intuitively appealing. The three theories shown give similar results for small values of p_c/p_j but diverge with increasing p_c/p_j. The Barratt theory has been shown (Reference 41) to give the closest agreement with experimental results. The exponential theory is useful because of

its relative simplicity and its close agreement with the more complicated Barratt theory. The simple jet theory (with f=o, Eq 2-18) is accurate only at low values of p_c/p_j and X (say p_c/p_j <0.4 and X <0.2). It is useful in developing simple preliminary relationships and trends.

The influence of p_c/p_j on the pressure coefficient (C_Q) is shown in Figure 3-2. For the theories presented, this relationship is independent of the jet angle, θ. The figure shows that a high value of p_c/p_j is desirable to minimize this coefficient.

The influence of p_c/p_j on the power-thickness parameter is shown in Figure 3-3. The parameter, C_{ht}, is directly proportional to input power. Figure 3-3 shows that, for constant values of nozzle area and cushion pressure (aircraft weight), high values o of p_c/p_j (low values of p_j) are desired for minimum power.

The influence of p_c/p_j on the power-height parameter (C_{hd}) is shown in Figure 3-4. It is generally desirable to minimize power and maximize jet height. For constant p_c (aircraft weight), and fuselage perimeter (S), a minimum C_{hd} would give a maximum jet height and minimum power input. Figure 3-4(a) shows that both the exponential and the Barratt theory give C_{hd} curves with minimum values around p_c/p_j = 0.7. Since the curve is flat in the region of p_c/p_j = 0.4 to p_c/p_j = 0.9 a considerable latitude exists in selecting an optimum p_c/p_j.

The influence of θ on the power-jet height parameter is shown in Figure 3-4(b and c). The curves show that a high value of θ is desirable. However, if θ becomes too large, the flow will attach to the underside of the aircraft and momentum seal will be lost. A value of θ = 60° is generally considered as the maximum practical.

The effect of the jet height to cushion diameter ratio on augmentation ratio for a circular cushion is shown in Figure 3-5. The figure shows that it is desirable to have small values of d/D for maximum augmentation. Large values of augmentation are desirable to minimize power. The value of jet height (d) is generally determined by the roughness of the terrain on which the vehicle is designed to operate. Consequently, d is largely independent of vehicle size. For maximum augmentation it is desirable to make the cushion diameter as

large as possible without violating structural weight and dynamic constraints.

In summary, Figure 3-3 shows that power decreases with increasing p_c/p_j if jet height is allowed to decrease. However, for a specified value of jet height it is desirable to select a value of p_c/p_j in the range of 0.4 to 0.7. Figures 3-4(b and c) show that it is desirable to employ a jet angle θ of at least 30°. Larger angles, up to 60°, give slight additional benefits in minimizing the power-height parameter. Finally, Figure 3-5 shows that it is desirable to make the vehicle diameter large and the jet clearance small for maximum augmentation.

TABLE 3-1

Expressions for p_c/p_j and C_Q for Momentum Flow Theories

PARAMETER \ THEORY	p_c/p_j	C_Q
SIMPLE JET	$2X$	1.0
EXPONENTIAL	$1 - e^{-2X}$	$\frac{1}{X}(1 - e^{-X})$
BARRATT	$2X\left(\sqrt{X^2 + 1} - X\right)$	$\left[\dfrac{\sqrt{1 - p_c/p_j}}{1 - \sqrt{1 - p_c/p_j}} \log_e(1 - p_c/p_j)\right]^{-\frac{1}{2}}$

4. PREDICTION OF THE SHAPE OF A TWO DIMENSIONAL AIR CUSHION TRUNK

4.1   Approach

Accurate predictions of the cross-sectional shape and area of the air cushion trunk are necessary in determining the flow rate, jet height, stiffness and dynamic response of the system. It is desired to predict the trunk shape when it is subjected to two types of loading.

The first type occurs when the aircraft is being supported totally by the air cushion. In this case, the trunk transmits none of the load directly to the ground. The trunk shape associated with this type of loading is illustrated by Figure 4-1. This case is called the Free Trunk Shape. It is developed in detail in Section 4.4.

The second type of loading occurs during dynamic loading of the air cushion. In this case, a portion of the trunk may be flattened against the ground and transmits loads to the ground through a thin layer of air. The trunk shape associated with this type of loading is illustrated in Figure 4-2. This case is called the Loaded Trunk Shape. It is developed in Section 4.5. Computer programs which predict these two shapes for an inelastic trunk material are presented in Appendices I and II respectively. Appendix III contains a computer program for predicting the Free Trunk Shape including the effects of trunk material which have non-linear elasticity.

4.2   Background

The configuration and loading of the trunk of the Air Cushion Landing System is considerably different from the trunk on Air Cushion Vehicles. Consequently, the literature associated with air cushion vehicle trunks is of little assistance in predicting the ACLS shape.

Esgar and Morgan[45] conducted an analysis of the energy absorptive characteristics of gas bags of various shapes and at various rates of gas bleed. The study
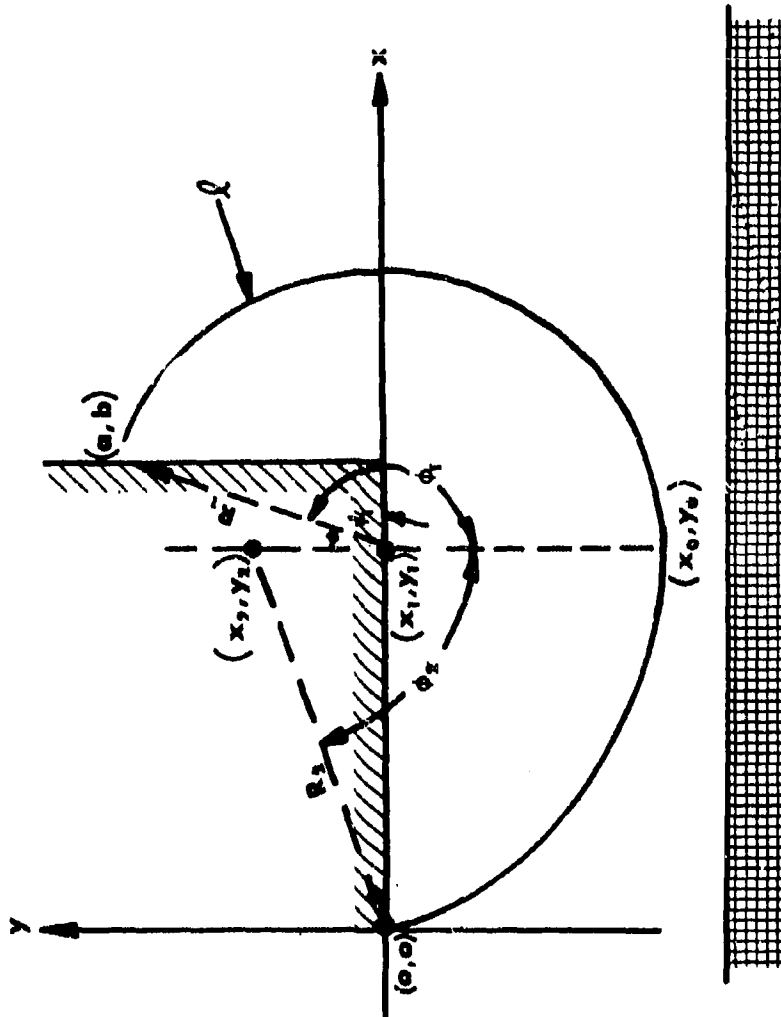
FREE TRUNK SHAPE

FIGURE 4-1
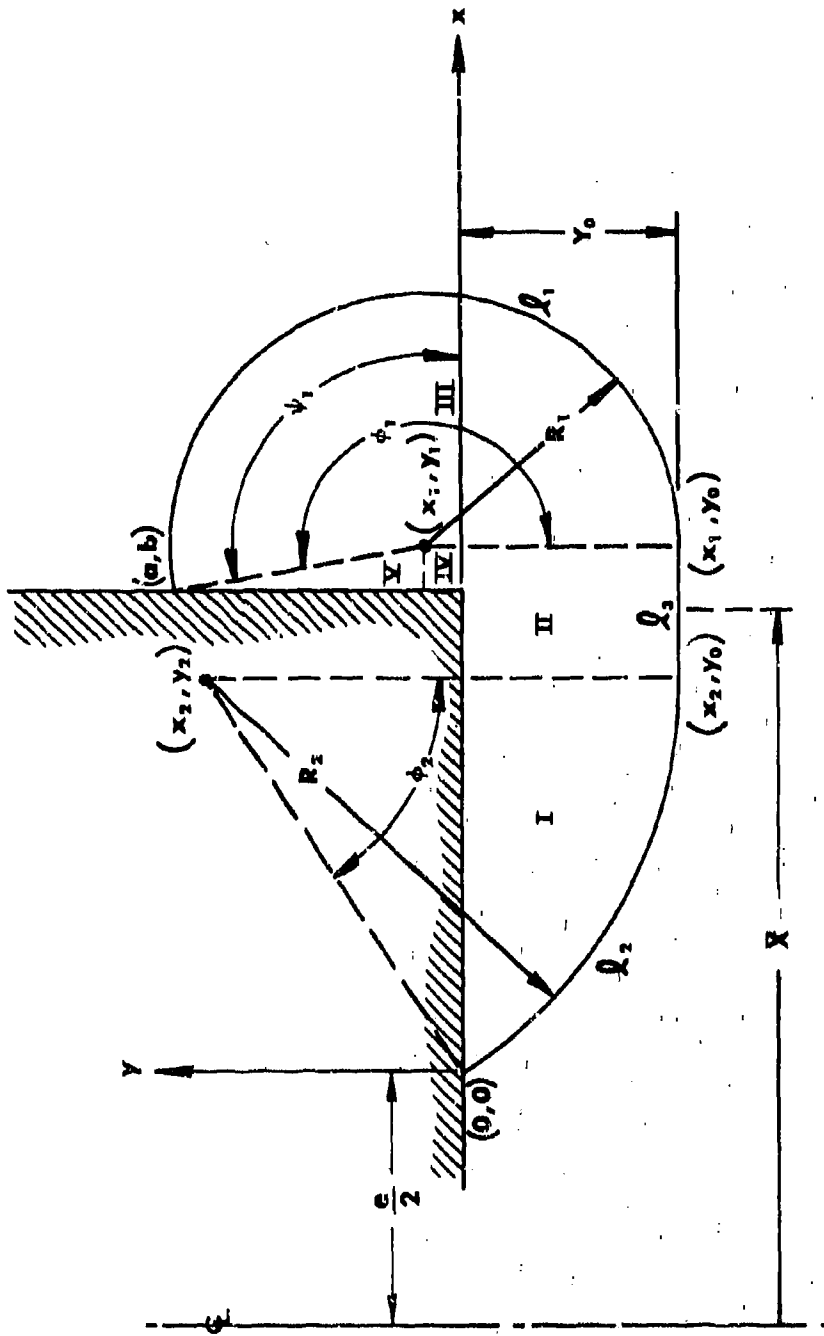
LOADED TRUNK SHAPE

FIGURE 4-2

included cylindrical shaped bags impacted on their sides. This case approaches the Loaded Trunk Shape problem. These authors found that the deflected cross-sectional shape approximated two circular arcs tangent to the ground surface and connected by a straight line at the ground contact. A similar condition is shown in Figure 4-2.

In the sections to follow, numerical solutions to predict the shape of the trunk under both free and loaded conditions are presented. Digital computer programs which evaluate the trunk shape for these conditions are presented in Appendix I and Appendix II.

The relationships which are common to both the free and the loaded trunk shape are presented in Section 4.3.

4.3   Development of Common Relationships

4.3.1   Approach

In this section, the variables associated with the trunk shape are listed, the laws which will be applied are stated, and the relationships which are common to both problems are developed.

The variables for this problem are illustrated in Figures 4-1 and 4-2. They may be grouped as follows:

Independent Design Variables

$a(\bar{a})$ x coordinate of (horizontal distance between) trunk attachment points, ft.

$b(\bar{b})$ y coordinate of (vertical distance between) trunk attachment points, ft.

e   distance between lower trunk attachment points, ft (see Figure 4-8).

ℓ cross-sectional length of trunk material, ft.

ℓ_c cross-sectional length of the trunk material at the design point, ft (see Figure 4-14).

E_t the unit elongation per pound of tension per foot-length in the axial direction for the trunk material, lb/ft (see Figure 4-14).

Independent Operating Variables for Free Trunk Shape

$p_c(P_c)$ = cushion pressure, psfg (psf).

$p_j(P_j)$ = trunk pressure, psfg (psf).

For the Loaded Trunk Shape, one additional independent variable is:

Y_o = vertical distance between the aircraft hard structure and bottom of the trunk (ft).

Dependent Variables

ℓ_1 length of trunk segment inscribed by angle ϕ_1, ft.

ℓ_2 length of trunk segment inscribed by angle ϕ_2, ft.

ℓ_3 length of trunk segment flattened against the ground, ft.

R_1 radius of curvature for segment ℓ_1, ft.

R_2 radius of curvature for segment ℓ_2, ft.

T_t tension in trunk material, pounds in tangential direction per foot-length in the axial direction, lb/ft.

$\bar{x}$ distance from aircraft center of gravity to center of pressure of the trunk footprint, ft.

x_i x coordinate of ith point, ft.

y_i y coordinate of ith point, ft.

ϕ_1 central angle formed by trunk segment ℓ_1, radians.

ϕ_2 central angle formed by trunk segment ℓ_2, radians.

The laws to be applied to this problem are:

(1)   Force equilibrium applied to the trunk.

(2)   Load-elongation of the trunk

(3)   Geometric compatibility of the trunk shape

The first two laws hold for both trunk shapes. The difference in the two problems lies in the geometric compatibility assumptions. Consequently, the first two relationships will be developed in Sections 4.3.2 and 4.3.3 to follow.

4.3.2   Force Equilibrium

Consider an elastic material of length ℓ attached to the structure at points (a,b) and (o,o) as shown in Figures 4-1 or 4-2. The trunk is subjected to an internal pressure P_j, to

a cushion pressure P_c and to atmospheric pressure P_a. The following assumptions are made:

4.3.2.1   The trunk behaves as a membrane. Thus it forms a segment of a circle when subjected to internal pressure loading.

4.3.2.2   Reactions from the nozzles are negligible.

4.3.2.3   The tension in the trunk is constant in the Sections ℓ_1 and ℓ_2.

Based upon the assumptions, a free body diagram of the loading on the two sections of the trunk is shown in Figure 4-3(a). The tension at any point in the trunk is calculated by a force balance (as shown in Figure 4-3(b) and found to be:

$$(P_j - P)\ 2\ R \sin\frac{\phi}{2}\ =\ 2\ T_t \sin\frac{\phi}{2}$$

Applying this force balance to the two trunk sections and simplifying gives:

$$T_t = p_j R_1 \tag{4-1}$$

and

$$T_t = (p_j - p_c)\ R_2 \tag{4-2}$$

4.3.3   Load-Elongation of the Trunk

The length of the trunk material is determined from the tension-elongation characteristics of the material. For a purely elastic material, the tension-elongation relationship is:

$$\ell = \ell_o + \frac{T_t}{E_t}\ \ell_o \tag{4-3}$$
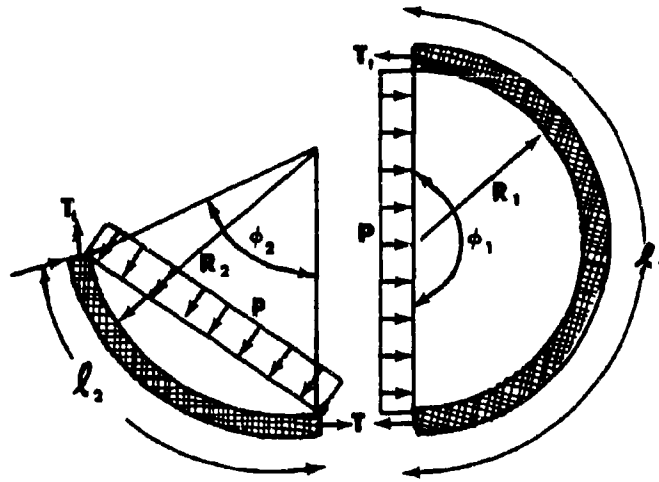
(a) DIAGRAM OF PRESSURE-TENSION EQUILIBRIUM
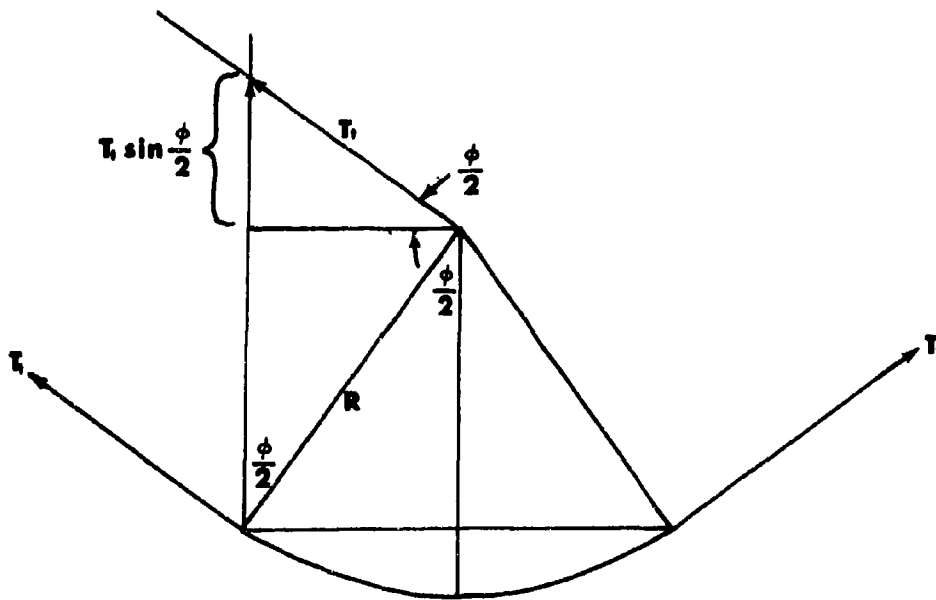
(b) DIAGRAM OF TENSION COMPONENT

FREE BODY DIAGRAM OF TRUNK LOADING

FIGURE 4-3

In general, the elasticity of trunk materials will be non-linear. Consequently, a more complicated relationship than Equation (4-3) must be used. A typical tension-elongation curve for a trunk material is shown in Figure 4-14.

4.3.4 Geometric Compatibility

The geometric compatibility conditions of the free trunk shape problem differ from the loaded trunk shape problem. The differences are shown in Figures 4-1 and 4-2, respectively. Separate development of the geometric compatibility conditions will be presented in Sections 4.4 and 4.5.

4.4 Free Trunk Shape

4.4.1 Assumptions

A cross section of the free trunk shape is shown in Figure 4-1. In addition to the assumptions listed in Section 4.3.2 the following restrictions are imposed:

4.4.1.1 The pressure change from P_c to P_a occurs over a short distance in the vicinity of point (x_0, y_0).

4.4.1.2 The trunk is assumed to be tangent to the ground at point (x_0, y_0). No flattening of the trunk around point (x_0, y_0) is allowed. This assumption requires that the centers of curvature for radii R_1 and R_2 have the same x coordinate.

4.4.2 Geometric Compatibility (Free Trunk Shape)

The assumed trunk geometry is shown in Figure 4-1.

In order for the trunk segments formed by ℓ_1 and ℓ_2 to both be tangent to the ground at (x_0, y_0) the centers of curvature must have the same x coordinate. Thus

$$x_1 = x_0 \tag{4-4}$$

$$x_2 = x_0 \tag{4-5}$$

The distance between (o, o) and (x_2, y_2) is R_2

$$(x_2 - o)^2 + (y_2 - o)^2 = R_2^2 \tag{4-6}$$

The distance between $(x_1\, y_1)$ and (a,b) is R_1

$$(x_1 - a)^2 + (y_1 - b)^2 = R_1^2 \tag{4-7}$$

The distance between (x_0, y_0) and (x_2, y_2) is R_2. Since $x_0 = x_2$ the distance is simply the y distance:

$$y_2 - y_0 = R_2 \tag{4-8}$$

Similarly, the distance between (x_0, y_0) and (x_1, y_1) is R_1.

$$y_1 - y_0 = R_1 \tag{4-9}$$

The arc formed by ℓ_2 is defined by ϕ_2. The angle ϕ_2 may be written in trigometric terms as:

$$\phi_2 = \arctan\frac{x_2 - o}{y_2 - o}; \qquad o \leqslant \phi_2 \leqslant \pi \text{ radians} \tag{4-10}$$

The arc formed by ℓ_1 is defined by ϕ_1. The angle ϕ_1 may be written in terms of the angle ψ_1 which is defined in Figure 4-1.

$$\phi_1 = \psi_1 + \frac{\pi}{2} \qquad o < \phi_1 < 2\pi \qquad\qquad (4\text{-}11)$$

The angle ψ_1 may be written in trigometric terms as:

$$\psi_1 = \arctan \frac{b - y_1}{a - x_0} \qquad \frac{-\pi}{2} < \psi_1 < 3\frac{\pi}{2} \qquad (4\text{-}12)$$

The total length of the trunk is equal to the sum of the two segments:

$$\ell = R_1 \phi_1 + R_2 \phi_2 \qquad\qquad (4\text{-}13)$$

4.4.3 Solution of Equations

In Equations (4-1) through (4-13) the following variables are known:

a, b, p_c/p_j, ℓ_0, E_t, P_j.

The following variables are unknown:

T_t, R_1, R_2, ℓ, x_0, x_1, x_2, y_0, y_1, y_2, ϕ_1, ϕ_2, ψ_1.

In principle, the thirteen equations can be solved simultaneously to predict the unique trunk shape for the given known quantities.

Equations (4-1) and (4-2) may be combined to solve for R_2:

$$R_2 = R_1 / 1 - (p_c/p_j) \qquad\qquad (4\text{-}14)$$

Equations (4-4) through (4-9) may be combined to solve for y_0. Combining Equations (4-4), (4-6) and (4-8) gives:

$$x_0^2 + (y_0 + R_2)^2 = R_2^2$$

or

$$x_0^2 = -y_0^2 - 2y_0 R_2 \qquad (4\text{-}15)$$

Combining Equations (4-5), (4-7), and (4-9) gives:

$$(x_0 - a)^2 + (y_0 + R_1 - b)^2 = R_1^2$$

or

$$x_0^2 = 2ax_0 - a^2 - y_0^2 - b^2 + 2R_1 b + 2y_0 b - 2R_1 y_0 \qquad (4\text{-}16)$$

Equating (4-15) and (4-16) to eliminate x_0^2 yields:

$$-y_0^2 - 2y_0 R_2 = 2ax_0 - a^2 - y_0^2 - b^2 + 2R_1 b + 2y_0 b - 2R_1 y_0$$

or

$$x_0 = \frac{y_0}{a}(R_1 - b - R_2) + \frac{a}{2} + \frac{b^2}{2a} - R_1 \frac{b}{a} \qquad (4\text{-}17)$$

Let

$$C_1 = \frac{R_1 - b - R_2}{a} \qquad (4\text{-}18)$$

$$C_2 = \frac{a}{2} + \frac{b^2}{2_a} - R_1 \frac{b}{a} \qquad (4\text{-}19)$$

Then Equation (4-17) becomes:

$$x_0 = C_1 y_0 + C_2 \qquad (4\text{-}20)$$

Combining Equations (4-20) and (4-1b) yields:

$$-y_0^2 - 2y_0 R_2 = (C_1 y_0 + C_2)^2$$

or

$$(C_1^2 + 1)y_0^2 + 2(R_2 + C_1 C_2)y_0 + C_2^2 = 0 \qquad (4\text{-}21)$$

Applying the quadratic formula to Equation (4-21)

$$y_0 = \frac{-2(R_2 + C_1 C_2) \pm \sqrt{(2R_2 + 2C_1 C_2)^2 - 4(C_1^2 + 1)C_2^2}}{2(C_1^2 + 1)} \qquad (4\text{-}22)$$

The choice of positive or negative square root is dependent on the quantities a, b, and ℓ. A physical representation of the two solutions is shown in Figure 4-4. The figure illustrates that for given values of a and b the negative square root requires a larger value of ℓ than the positive square root.

In order to develop criteria for selecting the sign of the square root, consider the case where $p_c = 0$. For this case, the trunk takes the shape of the arc of a circle of radius R_1. In order for the circle to pass through $(0,0)$ and (a,b) the radius R_1 must equal at least half the distance between the two points. The minimum value for R_1 would be $(\frac{1}{2})\sqrt{a^2 + b^2}$. The value of ℓ associated with the minimum value of R_1 is $(\pi/2)\sqrt{a^2 + b^2}$. Smaller values of ℓ would require larger values of R_1 but smaller values of Y_0. Consequently, the positive square root gives the desired solution for this case. Larger values of ℓ would require larger values of R_1 and larger values of Y_0. Consequently, the negative square root would give the desired solution for this case.

NOTE: DASHED LINE SHOWS ZERO VALUE FOR THE RADICAL IN EQUATION (4-22) $P_C/P_J = 0$
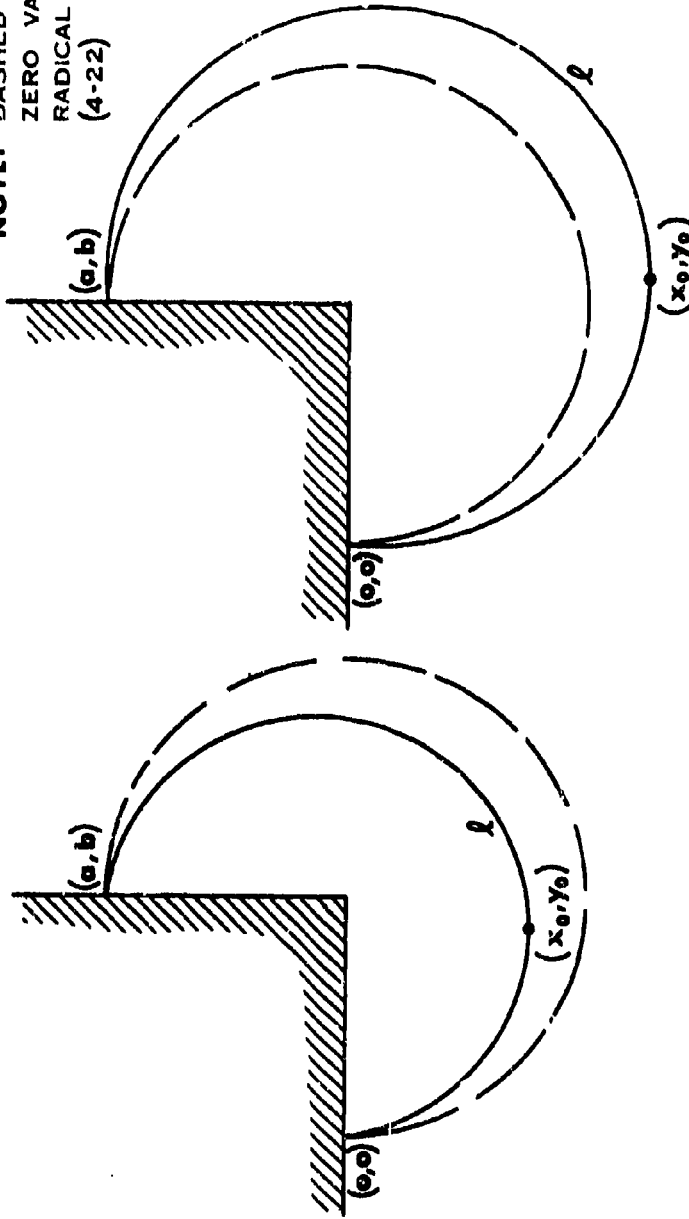
(a) POSITIVE SQUARE ROOT

(b) NEGATIVE SQUARE ROOT

PHYSICAL INTERPRETATION OF POSITIVE & NEGATIVE SQUARE ROOT

FIGURE 4-4

When $p_c/p_j \doteq o$, the criteria for the sign on the square root is as follows.

Take positive root when

$$\ell \leqslant \frac{\pi}{2} \cdot \sqrt{a^2 + b^2}$$

Take negative root when

$$\ell > \frac{\pi}{2} \sqrt{a^2 + b^2}$$

The problem may now be solved by an iterative process as follows.

The following information is given:

$a, b, \ell_o, p_c/p_j, p_j, E_t$

The iterative procedure is as follows:

(1) R_1 must be assumed for a trial solution. A trial guess is

$$R_1 = \tfrac{1}{2} \sqrt{a^2 + b^2}$$

(2) From Equation (4-1) compute T_t

$$T_t = p_j R_1 \qquad\qquad (4\text{-}1)$$

(3) From Equation (4-3) compute ℓ

$$\ell = \ell_o + \frac{T_t}{E_t} \ell_o \qquad\qquad (4\text{-}3)$$

(4) Calculate the other variables as follows:

$$R_2 = R_1/1 - (p_c/p_j) \tag{4-14}$$

$$C_1 = \frac{R_1 - b - R_2}{i} \tag{4-18}$$

$$C_2 = \frac{a}{2} + \frac{b^2}{2a} - R_1 \frac{b}{a} \tag{4-19}$$

$$y_0 = \frac{-2(R_2 + C_1 C_2) \pm \sqrt{(2R_2 + 2C_1 C_2)^2 - 4(C_1{}^2 + 1)C_2{}^2}}{2(C_1{}^2 + 1)} \tag{4-22}$$

$$x_0 = C_1 y_0 + C_2 \tag{4-20}$$

$$y_1 = y_0 + R_1 \tag{4-9}$$

$$y_2 = y_0 + R_2 \tag{4-8}$$

$$\phi_2 = \arctan \frac{x_2}{y_2} \qquad o \leqslant \phi_2 \leqslant \pi \text{ radians} \tag{4-10}$$

$$\psi_1 = \arctan \frac{b - y_1}{a - x_0} \qquad -\frac{\pi}{2} \leqslant \psi_1 \leqslant 3\frac{\pi}{2} \text{ radians} \tag{4-12}$$

$$\phi_1 = \psi_1 + \pi/2 \tag{4-11}$$

$$\overline{\ell} = R_1 \phi_1 + R_2 \phi_2 \tag{4-13}$$

where $\overline{\ell}$ is a trial value of ℓ.

(5) Check to see if $\bar{\ell}$ from Equation (4-13) agrees with ℓ from Equation (4-3). If not, iterate the process. A new guess for R_1 may be found using Newton's method, Mueller's method[46] or other numerical techniques.

(6) Continue the process until the desired accuracy is obtained in the $\bar{\ell}$ computed from Equation (4-13) and the ℓ computed from Equation (4-3).

4.5 Loaded Trunk Shape

4.5.1 Assumptions

The assumed shape of the trunk under an imposed P_c, P_j and Y_o is shown in Figure 4-2.

In addition to the assumptions listed in Section 4.3.2 the following restrictions are added:

4.5.1.1 The pressure on both sides of segment ℓ_3 is equal to p_j, and ℓ_3 is a straight line.

4.5.1.2 The pressure change from p_j to p_c and p_j to p_a occurs instantaneously at points (x_2, y_o) and (x_1, y_o) respectively.

4.5.1.3 The trunk is assumed to be tangent to the ground at points (x_1, y_o) and (x_2, y_o).

4.5.2 Geometric Compatibility (Loaded Shape)

Referring to Figure 4-2, the algebraic relationships for the assumed geometry may be developed as a consequence of Assumption 4.5.1.3:

The distance between (o,o) and (x_2, y_2) is R_2.

$$(x_2 - o)^2 + (y_2 - o)^2 = R_2^2 \tag{4-23}$$

The distance between (a,b) and (x_1, y_1) is R_1.

$$(x_1 - a)^2 + (y_1 - b)^2 = R_1^2 \tag{4-24}$$

The distance between (x_2, y_2) and (x_2, y_o) is R_2.

$$y_2 - y_o = R_2 \tag{4-25}$$

The distance between (x_1, y_1) and (x_1, y_o) is R_1.

$$y_1 - y_o = R_1 \tag{4-26}$$

The distance between (x_1, y_o) and (x_2, y_o) is ℓ_3.

$$x_1 - x_2 = \ell_3 \tag{4-27}$$

The arc formed by segment ℓ_2 is defined by ϕ_2.

The angle ϕ_2 may be written in trigometric terms as:

$$\phi_2 = \arc\tan\frac{x_2}{y_2} \qquad o \leqslant \phi_1 \leqslant \pi \tag{4-28}$$

The arc formed by segment ℓ_1 is defined by ϕ_1. The angle ϕ_1 may be written in terms of the angle ψ_1.

$$\phi_1 = \psi_1 + \frac{\pi}{2} \qquad\qquad 0 \leqslant \phi_1 \leqslant 2\pi \qquad\qquad (4\text{-}29)$$

The angle ψ_1 may be written in trigonometric terms as:

$$\psi_1 = \arctan\frac{b-y_1}{a-x_1} \qquad\qquad -\frac{\pi}{2} \leqslant \psi_1 \leqslant 3/2\,\pi \qquad\qquad (4\text{-}30)$$

The total length of the trunk must equal the sum of the length of the segments:

$$\bar{\ell} = \ell_1 + \ell_2 + \ell_3 \qquad\qquad (4\text{-}31)$$

where

$$\ell_1 = R_1\phi_1 \qquad\qquad (4\text{-}32)$$

$$\ell_2 = R_2\phi_2 \qquad\qquad (4\text{-}33)$$

$\bar{\ell}$ is a trial value of ℓ.

Using the coordinate system shown in Figure 4-2, we note that:

$$Y_0 = -y_0 \qquad\qquad (4\text{-}34)$$

4.5.3   Solution of Equations

In Equations (4-1), (4-2), (4-3), and (4-23) through (4-35), the following variables are known:

a, b, p_c/p_j, ℓ_0, E_t, p_j, Y_0

The following variables are unknown:

$$T_t, R_1, R_2, \ell, x_1, x_2, y_o, y_1, y_2, \phi_1, \phi_2, \psi_1, \ell_1, \ell_2, \ell_3$$

In principle, the fifteen equations can be solved simultaneously to predict the unique trunk shape for the given known quantities.

Equations (4-23) and (4-25) may be solved simultaneously for x_2. The result is:

$$x_2 = \sqrt{-y_o^2 - 2R_2 y_o} \qquad (4\text{-}35)$$

It may seem from geometry that x_2 should always be positive; consequently, only the positive sign of the squre root in Equation (4-35) was chosen.

Similarly, Equations (4-24) and (4-26) may be solved simultaneously for x_1. The result is:

$$x_1 = a + (\text{sign}) \sqrt{R_1^2 - (y_o + R_1 - b)^2} \qquad (4\text{-}36)$$

The choice of sign on the square root in Equation (4-36) will depend upon whether x_1 falls to the right or to the left of a. The criteria for this sign will be treated later.

The process for solving the equation will now be outlined. The known variables are:

$$a, b, \ell_o, E_t, p_c/p_j, Y_o$$

The iterative process requires the assumption of R_1 and a determination of the sign in Equation (4-36) to provide a trial solution. Criteria for R_1 selection and sign will be given later.

(1)   Assume R_1 value and determine sign.

(2)   From Equation (4-1) compute T_t.

$$T_t = n_j R_1 \tag{4-1}$$

(3) From Equation (4-3) compute ℓ.

$$\ell = \ell_o + \frac{T_t}{E_t} \, \ell_o \tag{4-3}$$

(4) Calculate the length of ℓ_2 as follows:

$$y_o = -Y_o \tag{4-34}$$

$$R_2 = \frac{R_1}{1 - p_c/p_j} \tag{4-14}$$

$$x_2 = \sqrt{-y_o{}^2 - 2R_2 y_o} \tag{4-35}$$

$$y_2 = R_2 + y_o \tag{4-25}$$

$$\phi_2 = \text{arc tan} \frac{x_2}{y_2} \tag{4-28}$$

$$\ell_2 = R_2 \phi_2 \tag{4-33}$$

(5) Calculate the length of ℓ_1 as follows:

$$x_1 = a + (\text{sign}) \sqrt{-(y_o + R_1 - b)^2 + R_1{}^2} \tag{4-36}$$

$$y_1 = R_1 + y_o \tag{4-26}$$

$$\psi_1 = \text{arc tan} \frac{b - y_1}{a - x_1} \qquad -\frac{\pi}{2} \leqslant \psi_1 \leqslant 3\frac{\pi}{2} \tag{4-30}$$

$$\phi_1 = \frac{\pi}{2} + \psi_1 \tag{4-29}$$

$$\ell_1 = R\phi_1 \tag{4-32}$$

(6) Calculate the length of ℓ_3 as follows:

$$\ell_3 = \left| x_1 - x_2 \right| \tag{4-27}$$

(7) Calculate the difference between the trial solution for $\overline{\ell}$ in Equation (4-31) and the value of ℓ from Equation (4-3). The results are:

$$\overline{\ell} = \ell_1 + \ell_2 + \ell_3 \tag{4-31}$$

$$\overline{\ell} - \ell \approx \epsilon \tag{4-37}$$

If ϵ approaches zero in Equation (4-37), the correct values of all the variables can be obtained. It should be noted that both $\overline{\ell}$ and ℓ are complicated functions of R_1.

(8) Iterate the procedure until ϵ in Equation (4-37) approaches zero to the accuracy desired.

In order to develop the desired solution to the system of equations, numerical methods using Mueller's algorithm (Appendix I) may be used. Mueller's algorithm converges on the root of a complicated function, such as those specified in Equation (4-37), by approximating the function with a second degree polynomial. In order to apply Mueller's algorithm, it is necessary to bracket the desired root of Equation (4-37).

Therefore, it is desired to determine two values of R_1 which will bracket the desired root in Equation (4-37). The value of R_1 which provides the upper bracket (makes

ϵ positive in Equation (4-37)) will be designated $(R_1)_U$. The value of R_1 which provides the lower bracket (makes ϵ negative) will be designated as $(R_1)_L$.

The technique for determining the lower bracket $(R_1)_L$ will now be considered.

For a given Y_0 and b, the minimum value which R_1 can assume (and yet be tangent to the ground line) is illustrated in Figure 4-5.

From Figure 4-5, it is evident that the minimum R_1 is:

$$(R_1)_{MIN} = \frac{b - Y_0}{2} \tag{4-38}$$

As a first trial, let $R_{1L} = (R_1)_{MIN}$.

A check to determine if $(R_1)_{MIN}$ provides a suitable lower bound can then be made. Steps 1 through 4 of the iteration process can be performed to calculate the value of ℓ_2. However, in order to calculate ℓ_1 the sign must be determined. The sign value is determined by comparing the actual trunk length with the trunk length associated with $(R_1)_{MIN}$.

The value of ℓ associated with $(R_1)_{MIN}$ is designated ℓ_4 and is calculated from geometry.

$$\ell_4 = \ell_1 + \ell_2 + \ell_3 = \frac{\pi (b - Y_0)}{2} + \phi_2 R_2 + \left| a - x_2 \right| \tag{4-39}$$

In Equation (4-39), ℓ_4 is the minimum trunk length associated with the condition $R_1 = (R_1)_{MIN}$ under the restrictions that $x_1 > x_2$ and $x_2 > 0$. It should be noted that ℓ_4 is not necessarily the minimum trunk length for all values of R_1.

The value of ℓ_4 is represented in Figure 4-5(a) (for $p_c/p_j = 0$). The fact that ℓ_4 is not the minimum trunk length for all values of R_1 is illustrated in Figure 4-5(b). It is evident from the figure that the trunk length (ℓ_4) associated with $(R_1)_{MIN}$ is greater than

$\ell_4 = \ell_1 + \ell_2 + \ell_3$

NOTE: (R_1)min DOES NOT ALWAYS CORRESPOND TO (ℓ)min

$\ell_A < \ell_B$
$\ell_B > \ell_A$

$(R_1)_A > (R_1)$min
$(R_1)_B > (R_1)$min
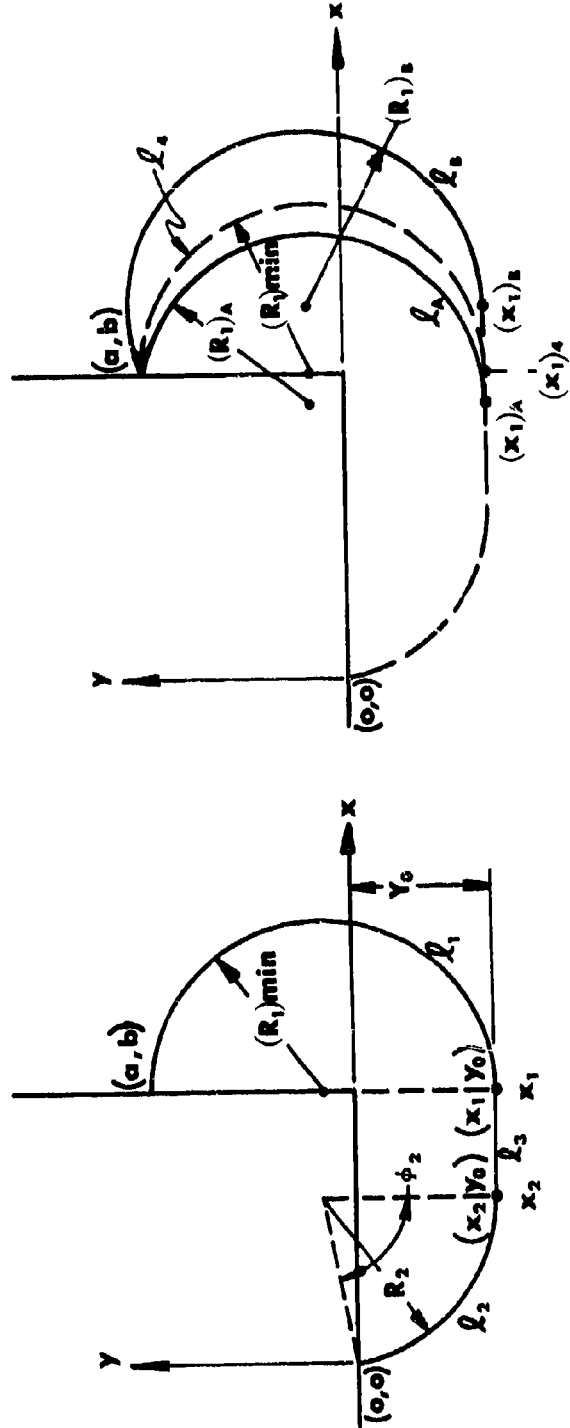
(a) PHYSICAL REPRESENTATION OF ℓ_4

(b) PHYSICAL REPRESENTATION OF VARIOUS VALUES OF R_1

ILLUSTRATION OF MINIMUM TRUNK LENGTH

FIGURE 4-5

the trunk length (ℓ_A) associated with $(R_1)_A$. Further, whenever $x_1 \geqslant a$, then $\ell > \ell_4$ for all values of $R_1 > (R_1)_{MIN}$. This condition is illustrated by the configuration with radius $(R_1)_B$ in Figure 4-5(b).

As illustrated above, the value of $(R_1)_{MIN}$ is a satisfactory lower bracket for the solution if $\ell > \ell_4$ and $x_1 > x_2$. In this case $x_1 \geqslant a$, and the sign in Equation (4-36) is plus.

The upper bracket for the condition $\ell > \ell_4$ may be found from the geometry of Figure 4-6. This figure shows the maximum value of R_1 possible for given values of a, b, and ℓ.

The length of the chord between coordinates (o,o) and (a,b) in Figure 4-6 may be written in terms of the radius and central angle or in terms of the rectangular coordinates. If the two expressions are equated, the result is:

$$\sqrt{a^2 + b^2} = 2 R_1 \sin \frac{\phi_1}{2}$$

Further, the radius, arc length and central angle are related as follows:

$$\phi_1 = \frac{\ell}{R_1}$$

These two relationships may be combined to give a relationship for R_1.

$$R_1 \sin \frac{\ell}{2R_1} = \sqrt{\frac{a^2 + b^2}{4}} \qquad (4\text{-}40)$$

Equation (4-40) may be solved numerically to give the upper bracket $(R_1)_U$ for the condition $\ell > \ell_4$.

It is now necessary to consider the upper and lower brackets for the condition $\ell < \ell_4$. Two cases are possible. The first is the condition $x_1 < x_2$. The second is the
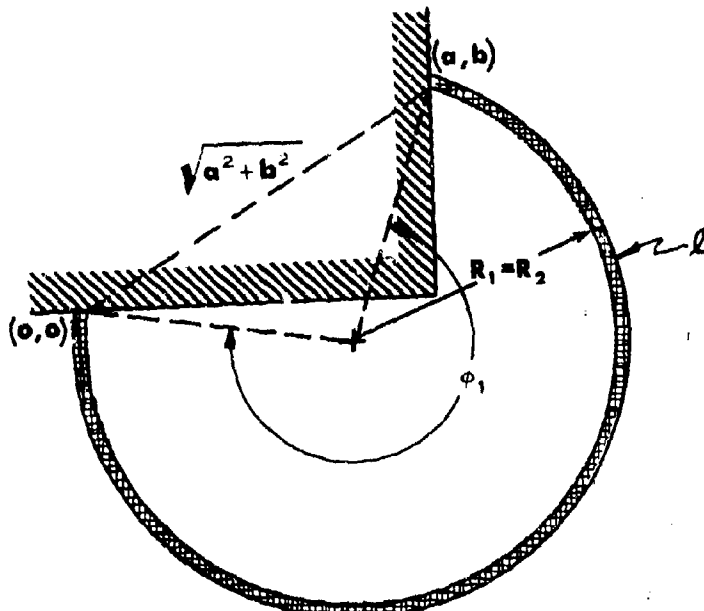
GEOMETRY FOR CALCULATING THE UPPER BOUND FOR R_1
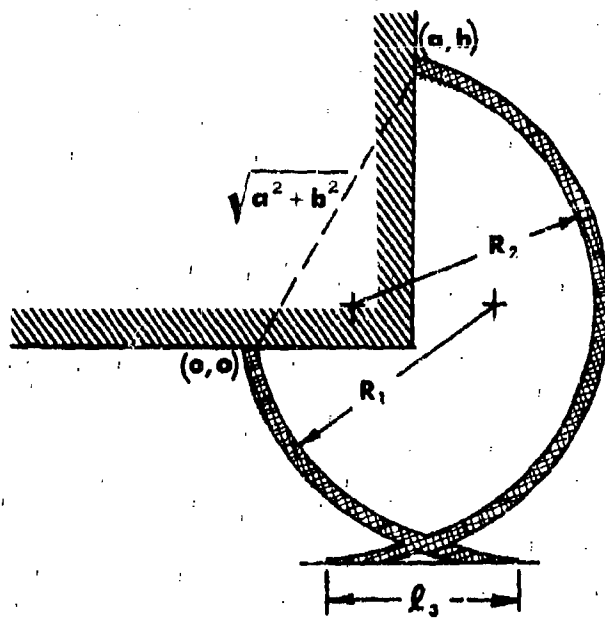
FIGURE 4-6

PHYSICALLY IMPOSSIBLE SOLUTION
FIGURE 4-7

condition $x_1 > x_2$. In the first case, the condition shown in Figure 4-7 exists. This case is of no practical interest and will not be considered.

If, on the other hand, $\ell < \ell_4$ and $x_1 > x_2$, then from the geometry of Figure 4-5(b) it is evident that $x_1 < a$. Therefore, in this case, the sign in Equation (4-36) is minus. Further, $(R_1)_{MIN}$ is not a satisfactory lower bracket for the solution of Equation (4-37). In this case, the correct value of ℓ lies between the configuration represented by $(R_1)_A$ and $(R_1)_{MIN}$ in Figure 4-5(b). Therefore, under these conditions, $(R_1)_{MIN} = (R_1)_U$ forms a satisfactory upper bound.

It is necessary to establish a different criteria for the lower bracket $(R_1)_L$ for the condition $\overline{\ell} < \ell_4$ and $x_1 > x_2$. The minimum value possible for ℓ for given values of a, b, p_c, p_j, and Y_0 is reached when $\ell_3 = o$ in Equation (4-31). This occurs when $x_1 = x_2$. The value of R_1 for the condition $x_1 = x_2$ establishes the lower bracket for the solution to Equation (4-36). This value occurs between the values of $x_1 = o$ and $x_1 = a$.

Numerically the upper bracket for $x_1 = x_2$ is:

$$(R_1)_U = \frac{b - Y_0}{2} \tag{4-41}$$

The lower bracket may be found by setting Equation (4-36) equal to zero and solving for R_1. The result is:

$$(R_1)_L = \frac{a^2 + b^2 + Y_0^2 - 2Y_0 b}{2(b - Y_0)} \tag{4-42}$$

Using iterative numerical techniques (Mueller's method) it is now possible to solve for the R_1 associated with $x_1 = x_2$. This R_1 is then taken as $(R_1)_U$ which is required to provide a solution to the system of equations which define the non-equilibrium trunk shape.

4.6 Trunk Cross-Sectional Area

The cross-sectional area of the free and loaded trunk shapes are shown in Figures 4-1 and 4-2 respectively. The cross-sectional area of the loaded trunk shape (Figure 4-2) has been divided into five regions which are designated by Roman numerals. The areas of each of these regions may be calculated as follows:

(1)   Region I is the area of the sector of the circle with radius R_2 and central angle ϕ_2 less the area of the triangle with vertices at coordinates (o,o), (x_2, y_2) and (x_2, o).

$$A_I = \frac{\phi_2}{2} R_2^2 - \frac{x_2 y_2}{2} \tag{4-43}$$

(2)   Region II is the area of the rectangle with corners at coordinates (x_2, o), (x_1, o), (x_1, y_o) and (x_2, y_o).

$$A_{II} = -\ell_3 y_o \tag{4-44}$$

(3)   Region III is the area of the sector of the circle with radius R_1 and central angle ϕ_1.

$$A_{III} = \frac{\phi_1}{2} R_1^2 \tag{4-45}$$

(4)   Region IV is the area of the rectangle with corners at coordinates (a, o), (x_1, o), (x_1, y_1) and (a, y_1).

$$A_{IV} = (x_1 - a) y_1 \tag{4-46}$$

(5)   Region V is the area of the triangle with vertices at coordinates (a, b), (x_1, y_1) and (a, y_1).

$$A_V = \frac{1}{2} (x_1 - a) (b - y_1) \tag{4-47}$$

The total cross-sectional area may be determined by summing the five areas given by Equations (3-43) through (3-47). The result for the Loaded Trunk Shape is:

$$(A_j)_{loaded} = \frac{\phi_2}{2} R_2{}^2 - \frac{x_2 y_2}{2} - \ell_3 y_0 + \frac{\phi_1}{2} R_1{}^2$$

$$+ (x_1 - a) y_1 + \frac{1}{2} (x_1 - a) (b - y_1) \tag{4-48}$$

For the Free Trunk Shape, the cross-sectional area may be derived by simplifying Equation (4-48). A comparison of Figures 4-1 and 4-2 shows that for the Free Trunk Shape the following simplifications are possible:

$$\ell_3 = 0$$

$$x_1 = x_2 = x_0$$

The above simplifications when applied to Equation (4-48) give an expression for the cross-sectional area of the Free Trunk Shape. The result is:

$$(A_j)_{free} = \frac{\phi_2}{2} R_2{}^2 - \frac{x_0 y_2}{2} + \frac{\phi_1 R_1{}^2}{2} + (x_0 - a) y_1$$

$$+ \frac{1}{2} (x_0 - a) (b - y_1) \tag{4-49}$$

4.7   Analytical Results

4.7.1   Approach

The trunk shape problems involve a large number of variables whose dimensions are length to the first power. A large number of nondimensional ratios result. Consequently, the use of nondimensional parameters is of little value in presenting the results of this problem. The approach will be to predict the shape for two trunk cross sections of a typical design and indicate how the general method could be applied to other designs.

The trunk dimensions may be scaled by holding two scale factors constant. These scale factors involve only the independent variables, and are defined as:

$$\pi_1 = \frac{a^2 + b^2}{\ell} \qquad \text{the trunk length parameter}$$

$$\pi_2 = \frac{b}{a^2 + b^2} \qquad \text{the trunk attachment parameter}$$

Provided these factors remain constant, the other dimensions may be scaled linearly with ℓ.

The design chosen for analysis is approximately 1/3 scale relative to the size required for a 60,000 pound aircraft such as the C-119. A drawing of the model is shown in Figure 4-8. This model is only 82 inches in length whereas the true 1/3 scale model should be around 150 inches in length. Except for the length dimension, all others are to the 1/3 scale.

The side and end trunk cross sections of the model shown in Figure 4-8 were selected for detailed analysis. The dimensions of these two sections are summarized in Table 4-I.

TABLE 4-1

Trunk Model Dimensions

QUANTITY	END TRUNK		SIDE TRUNK	
	MODEL	FULL SCALE	MODEL	FULL SCALE
a	2.35	7.06	1.44	4.33
b	0.00	0.00	1.00	3.00
ℓ	3.10	9.30	4.62	13.86
η_1	0.88	0.88	0.382	0.382
η_2	0.00	0.00	0.570	0.570
$\sqrt{a^2 + b^2}$	2.35	7.06	1.755	5.28
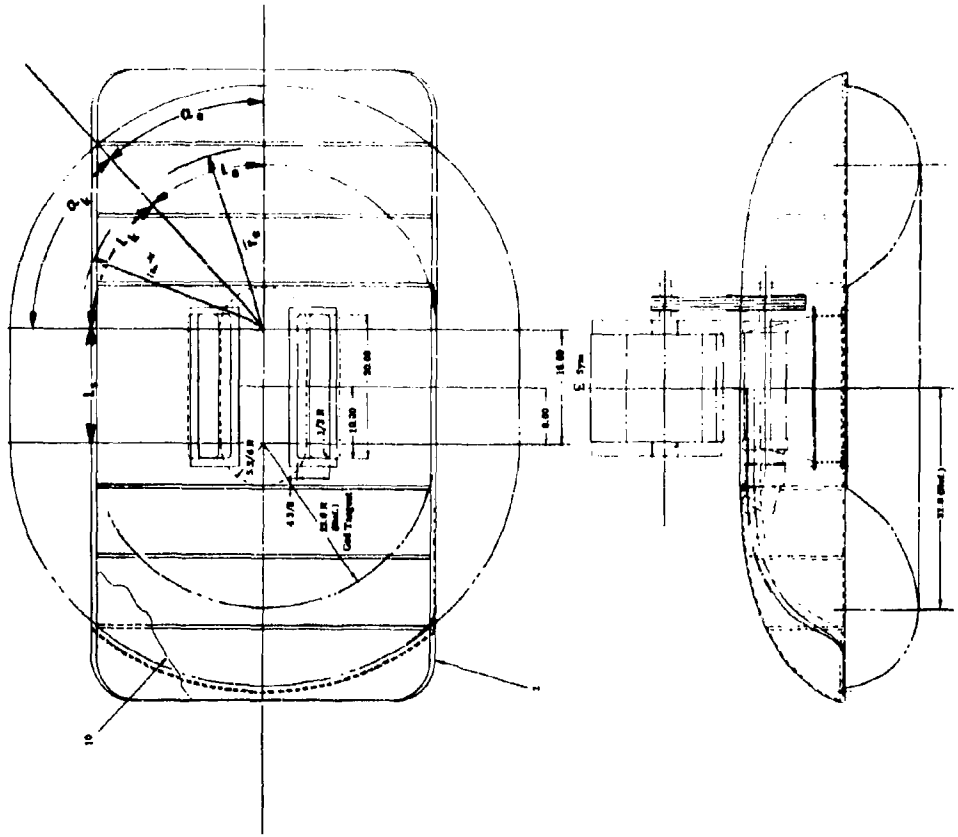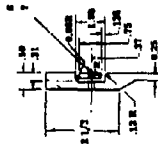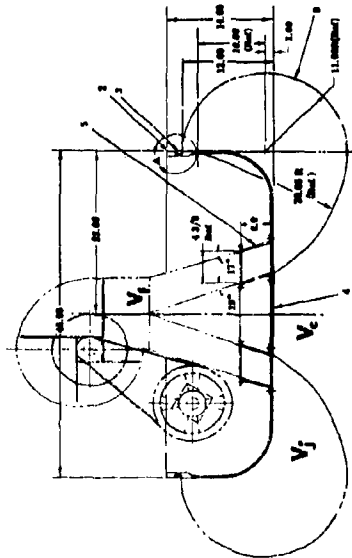
AIR CUSHION MODEL
FIGURE 4-8
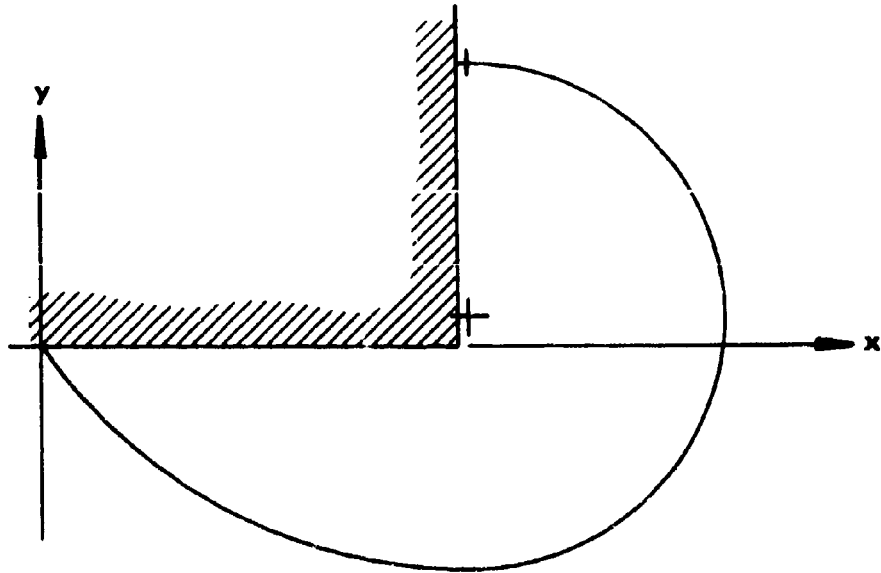
(a) SHAPE AT P_c/P_j = 0.5
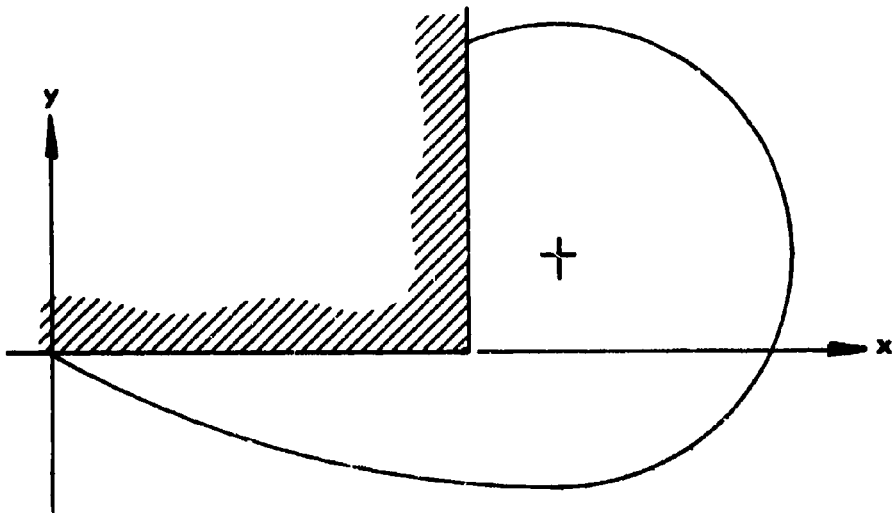
(b) SHAPE AT P_c/P_j = 0.8

SIDE TRUNK SHAPE
FIGURE 4-9
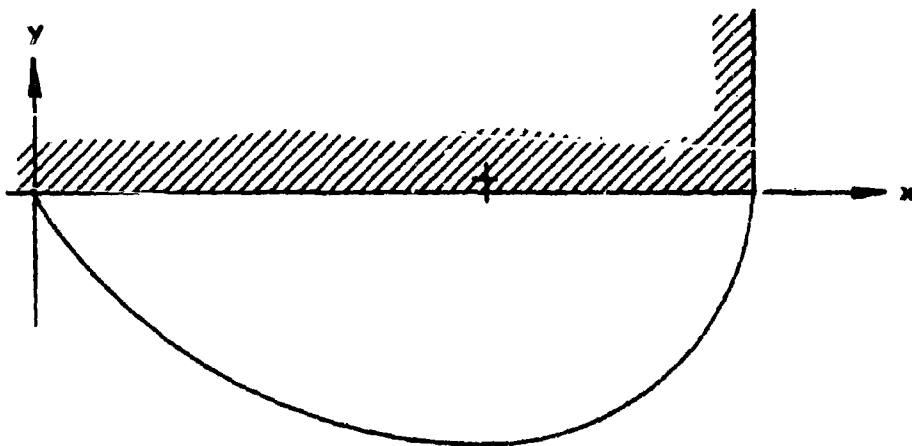
(a) SHAPE AT $P_c / P_j = 0.5$
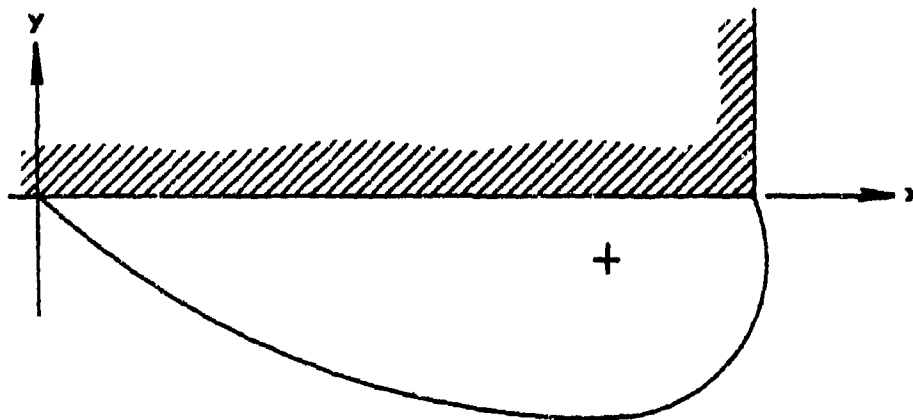
(b) SHAPE AT $P_c / P_j = 0.8$

END TRUNK SHAPE
FIGURE 4-10

The analysis applied to the trunk shapes is the two-dimensional analysis developed in Sections 4.1 through 4.5.

This analysis does not include the effect of loads and geometry changes perpendicular to the cross section shown in Figure 4-1.

It may be noted from the model drawing that the trunk cross-section at the sides is different from the cross section at the ends. This difference is caused by the necessity to pass the trunk under the fuselage to eliminate interference with the large cargo doors at the rear of the C-119. Most other military cargo aircraft also have a similar restriction.

4.7.2 Free Trunk Shape Results (Inelastic Trunk)

The cross-sectional shape of the trunk changes as p_c/p_j varies. The effect of this change is illustrated pictorially in Figures 4-9 and 4-10 and graphically in Figures 4-11, 4-12, and 4-13.

The cross sections of the side trunk at $p_c/p_j = 0.5$ and $p_c/p_j = 0.8$ are shown in Figure 4-9. Figure 4-10 shows a similar relationship for the side trunk. It may be seen from these figures that an increase in p_c/p_j results in a decrease in trunk height (Y_0), a decrease in cross-sectional area (A_j), and a shift to the outside for the ground tangent point (x_0, Y_0).

These qualitative effects are shown quantitatively in Figures 4-11, 4-12, and 4-13. These curves are developed from the computer program described in Appendix I.

Figure 4-11 shows the influence of p_c/p_j on trunk height (Y_0). The figure shows that there is a mismatch problem between the end trunk and the side trunk. The trunk was designed so that no mismatch would exist at $p_c/p_j = 0.45$. At p_c/p_j less than 0.45 the end trunk height is lower. At p_c/p_j greater than 0.45 the side trunk height is lower. In practice, the mismatch shown is reduced by the elasticity of the trunk material.

Figure 4-12 shows the outward movement of the ground tangent point with increasing p_c/p_j. For a two dimensional model of the type shown in Figure 6-1, the trunk
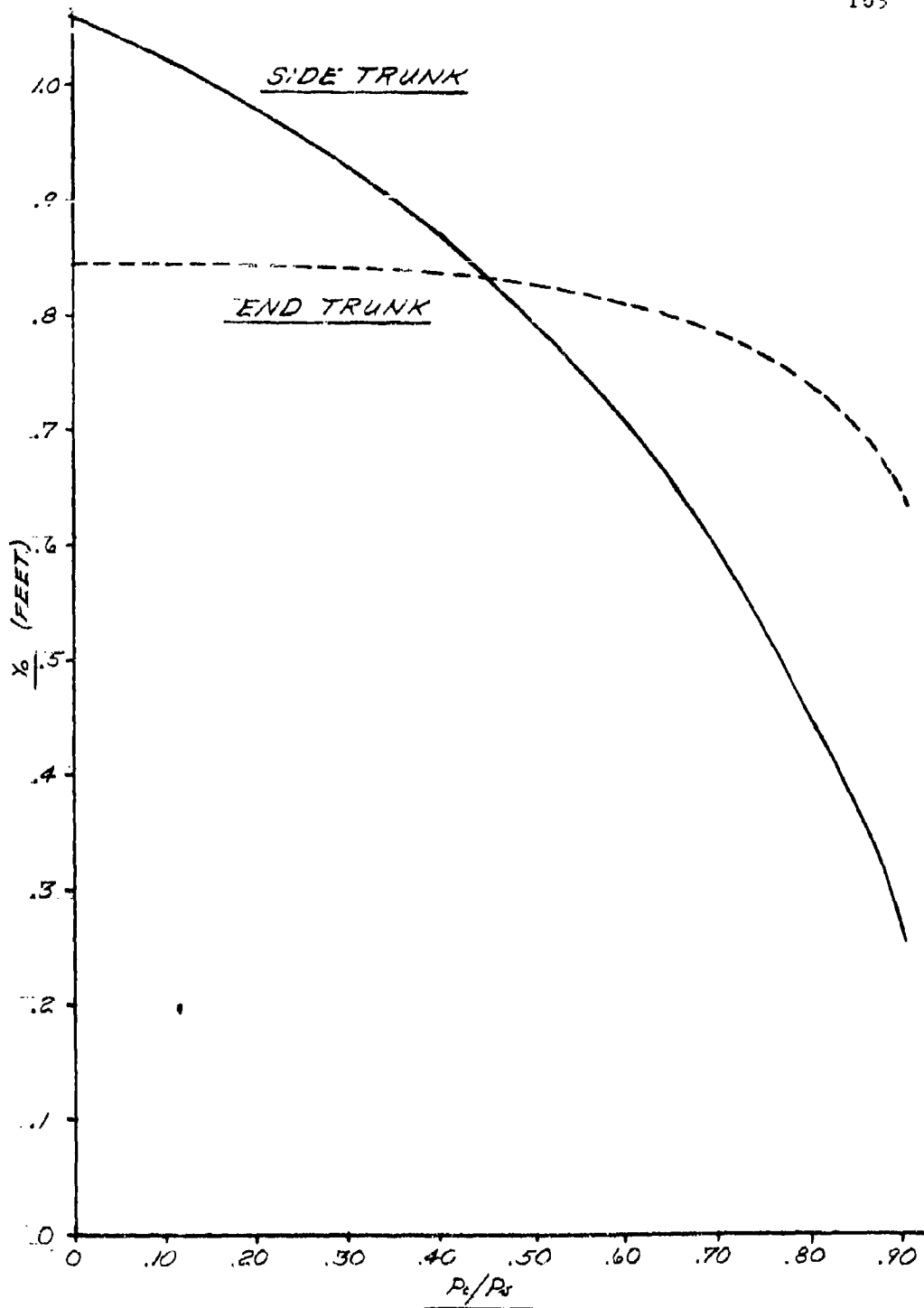
Y_O vs P_C/P_J , SIDE & END TRUNK

FIGURE 4-11
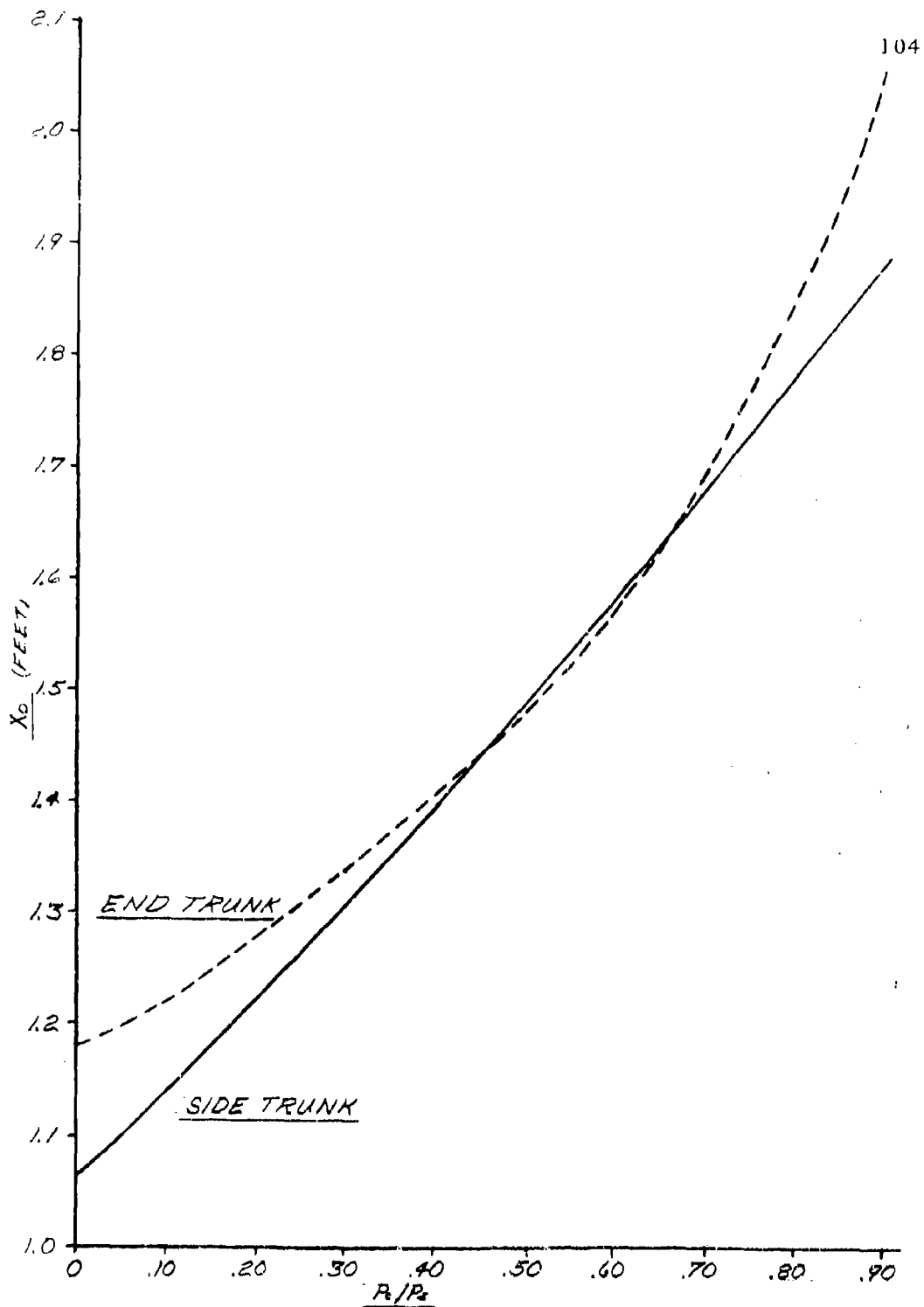
X_O vs P_c / P_j , SIDE & END TRUNK

FIGURE 4-12
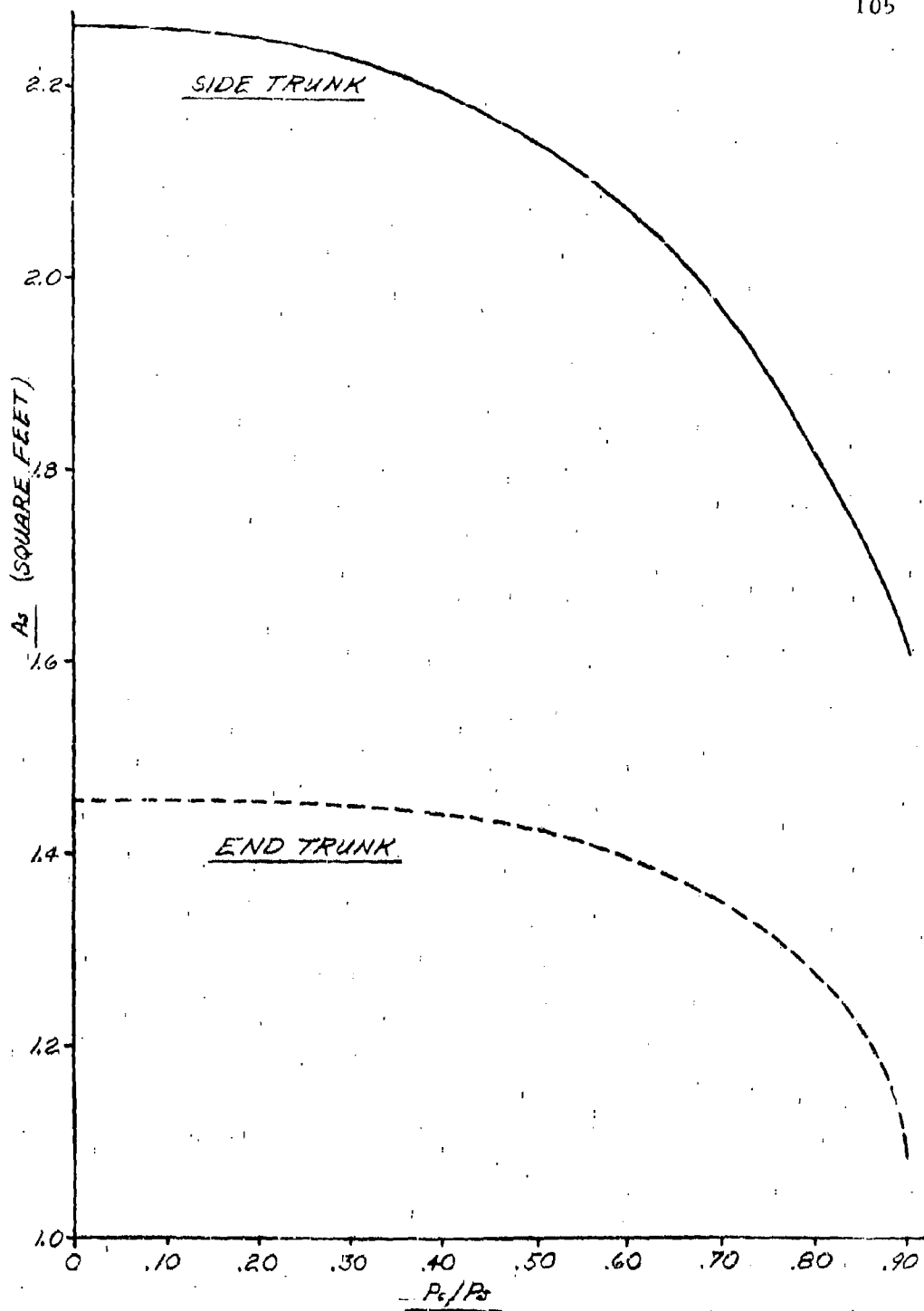
A_J vs P_c / P_J, SIDE & END TRUNK

FIGURE 4-13

ends are unconstrained and the tangent point is free to move outward. However, for a three dimensional model of the type shown in Figure 4-8, no free edges exist and the trunk material must stretch to permit outward movement of the ground tangent. The actual trunk material envisioned for use on an air cushion landing system would be highly elastic (300% stretch). Consequently, considerable movement of x_0 should be permitted, and the two dimensional predictions should be reasonable.

Figure 4-13 shows the variation in cross-sectional area with p_c/p_j as predicted by Equation (4-48). The curve shows relative small area variation below $p_c/p_j = 0.5$ and large variation above $p_c/p_j = 0.5$.

4.7.3   Free Trunk Shape Results (Elastic Trunk)

The effect of using an elastic material for the trunk was investigated using the computer program described in Appendix III. The trunk material envisioned is a rubber and nylon laminate. The nylon is laminated in a slack condition so that it does not carry load until the rubber has extended by at least 100%. A typical elastic curve for such a material is shown in Figure 4-14. The material was selected so that at the design point ($\epsilon = 0$, $p_c/p_j = 0.5$, $p_j = 80$ psfg) the length of the elastic side trunk was equal to the length of the inelastic side trunk and the resulting shapes were identical. The effects of changing p_c/p_j and p_j on the shape of the side trunk and the end trunk constructed from the elastic material described by Figure 4-14 were evaluated. The results are presented in Figures 4-15 through 4-20.

Figure 4-15 shows the effect of p_c/p_j on the trunk length. The effect of a 50% increase or decrease in the design pressure is also shown. The figure shows that the trunk length decreases with increasing p_c/p_j. The figure also shows that the trunk pressure has a large influence on the trunk length. The trunk material has a slack length of about 1.4 feet. At $p_j = 80$ psfg, the length has extended to around 4.9 feet. This large length change allows the trunk to elastically retract after take off to reduce aerodynamic drag.
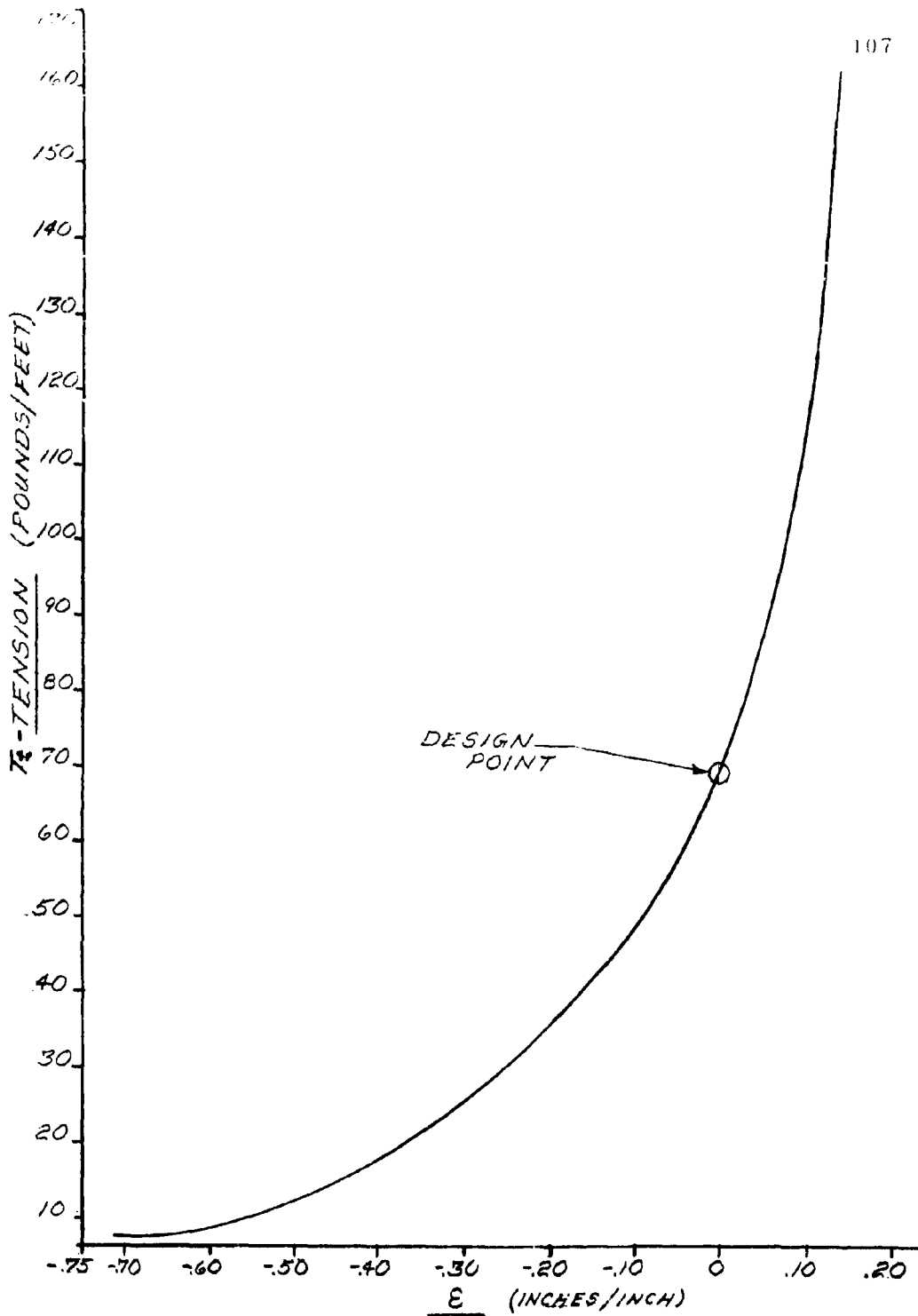
ELASTIC CURVE FOR TRUNK MATERIAL

FIGURE 4-14
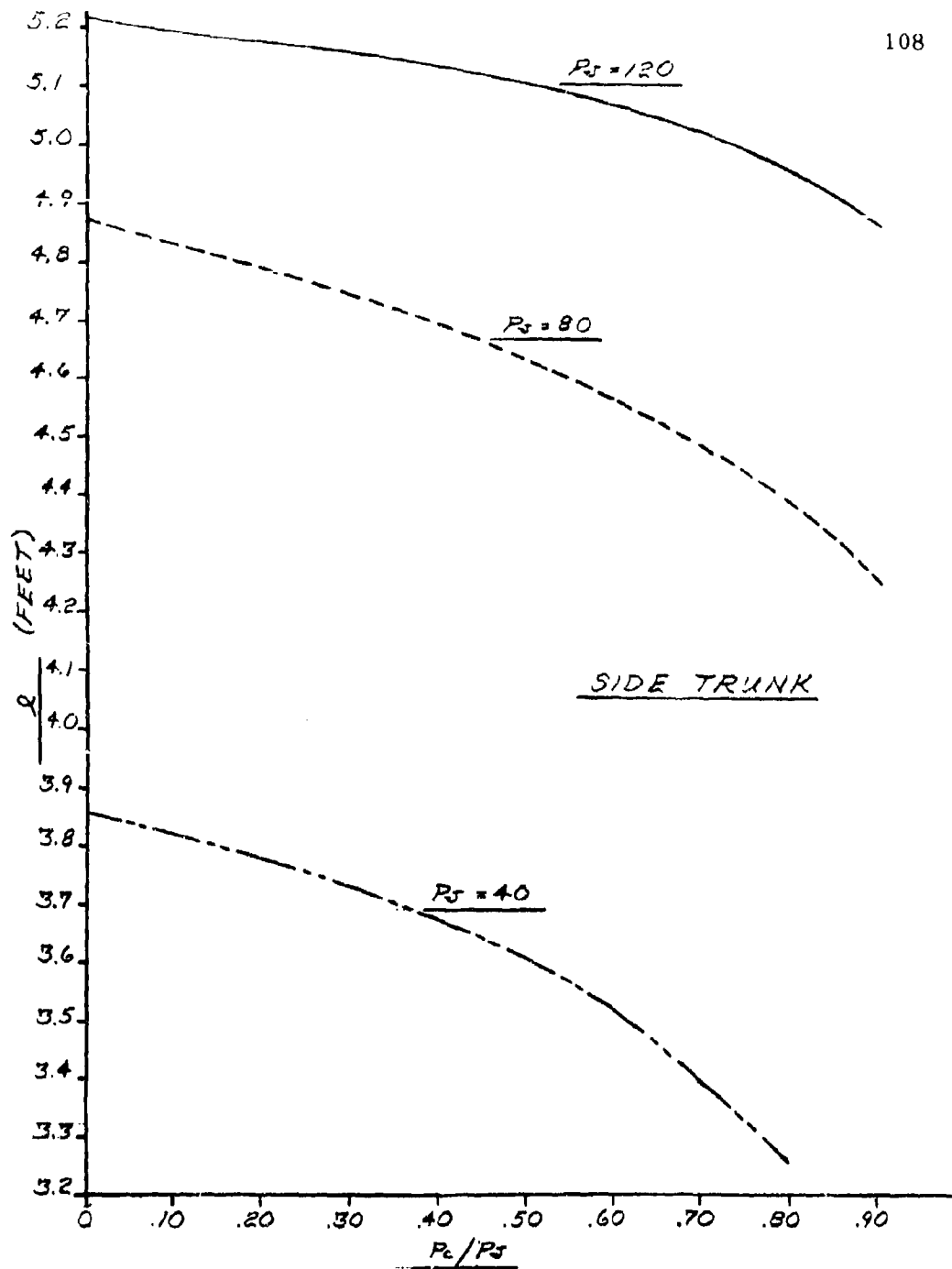
TRUNK LENGTH vs P_c/P_j , ELASTIC SIDE TRUNK
FIGURE 4-15

Figures 4-16 and 4-17 show the trunk height for the side and end trunks, respectively. A comparison of the curves shows that the elastic trunk tends to reduce the mismatch problem. A comparison of Y_o versus p_c/p_j for the design trunk pressure ($p_j = 80$ psfg) is shown in Figure 4-18. A comparison of Figure 4-16 and Figure 4-17 shows that the end and side trunk heights more nearly match for the elastic case than for the inelastic case.

The relationships between cross-sectional area (A_j) and p_c/p_j for the side and end elastic trunks are shown in Figures 4-18 and 4-19 respectively. The curves show that the cross-sectional area and consequently the trunk volume is very sensitive to changes in pressure below the design pressure (80 psfg). The sensitivity to changes in pressure above the design pressure is not as great. The curve points out the necessity of carefully tailoring the material, design pressure combination to achieve the desired cross section. Errors in providing an excessively stiff material or insufficient p_j could cause large degradation in the performance due to the large change in the trunk shape which would result.

A comparison of the trunk height for the elastic and inelastic side trunk is shown in Figure 4-20.

4.7.4 Loaded Trunk Shape (Inelastic Trunk)

The load support offered by the trunk is dependent upon the degree to which the trunk is flattened against the ground. This flattening is illustrated in Figure 4-2. The flattened length is characterized by ℓ_3. Since this segment of the trunk membrane forms a straight line, the pressure on both sides of the membrane is assumed to be equal. The load support offered by the trunk is proportional to ℓ_3, p_j and the trunk depth(s).

The flattened length ℓ_3 is dependent upon both p_c/p_j and Y_0. For any value of p_c/p_j there exists a value of Y_0 at which $\ell_3 = 0$. This value is the Y_∞ for the equilibrium trunk shape case and is shown in Figure 4-11. When Y_0 is less than the Y_∞ shown in Figure 4-11, trunk flattening occurs and ℓ_3 has a positive value. The shape of the flattened trunk was evaluated using the computer program described in Appendix II. Some of the results are presented in Figures 4-21 through 4-24.

Y_o vs P_c/P_j, ELASTIC SIDE TRUNK
FIGURE 4-16

$P_J = 120$

$P_J = 80$

$P_J = 40$

Y_O (FEET)
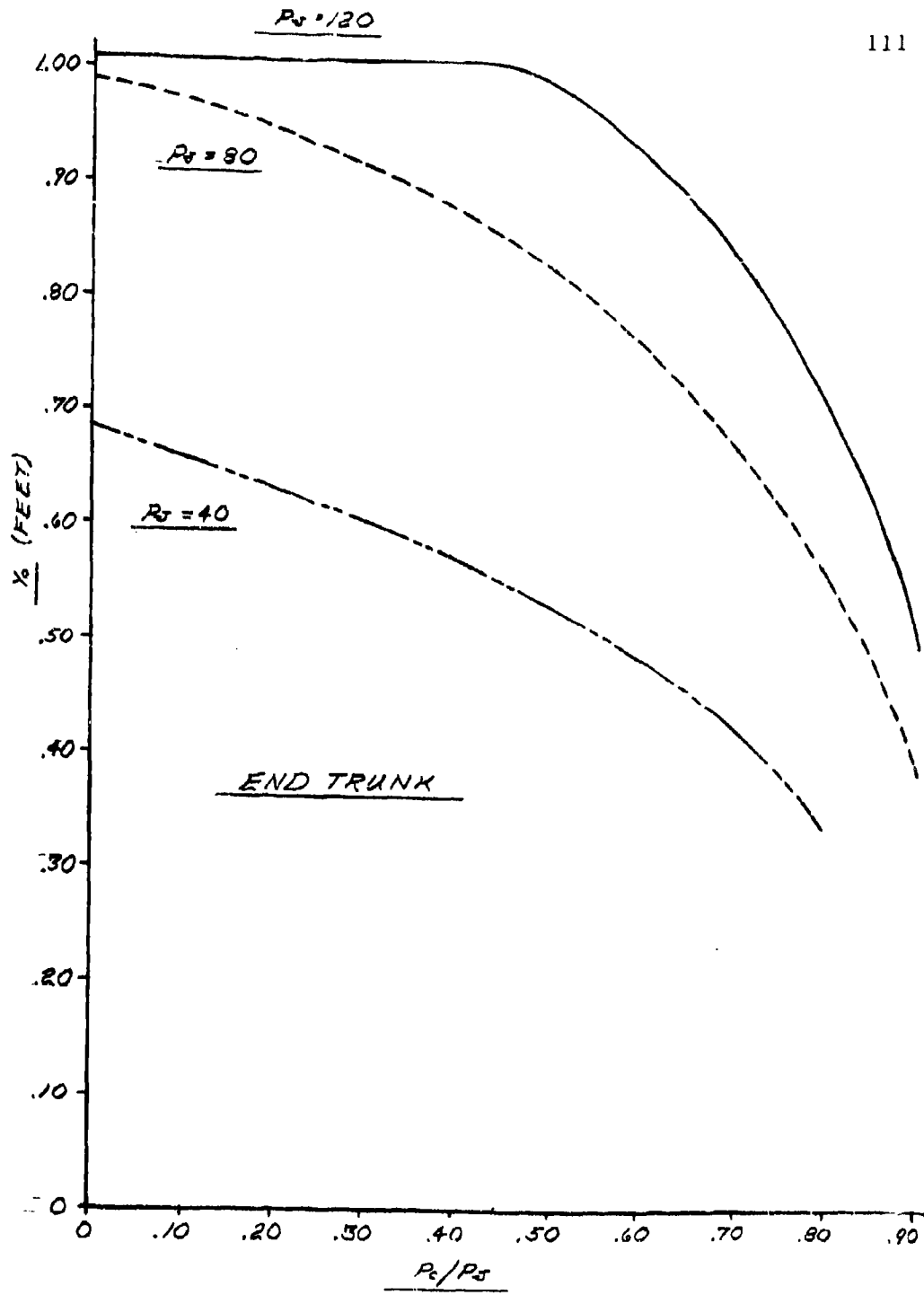
END TRUNK

P_c/P_J

Y_O vs P_c/P_J, ELASTIC END TRUNK
FIGURE 4-17
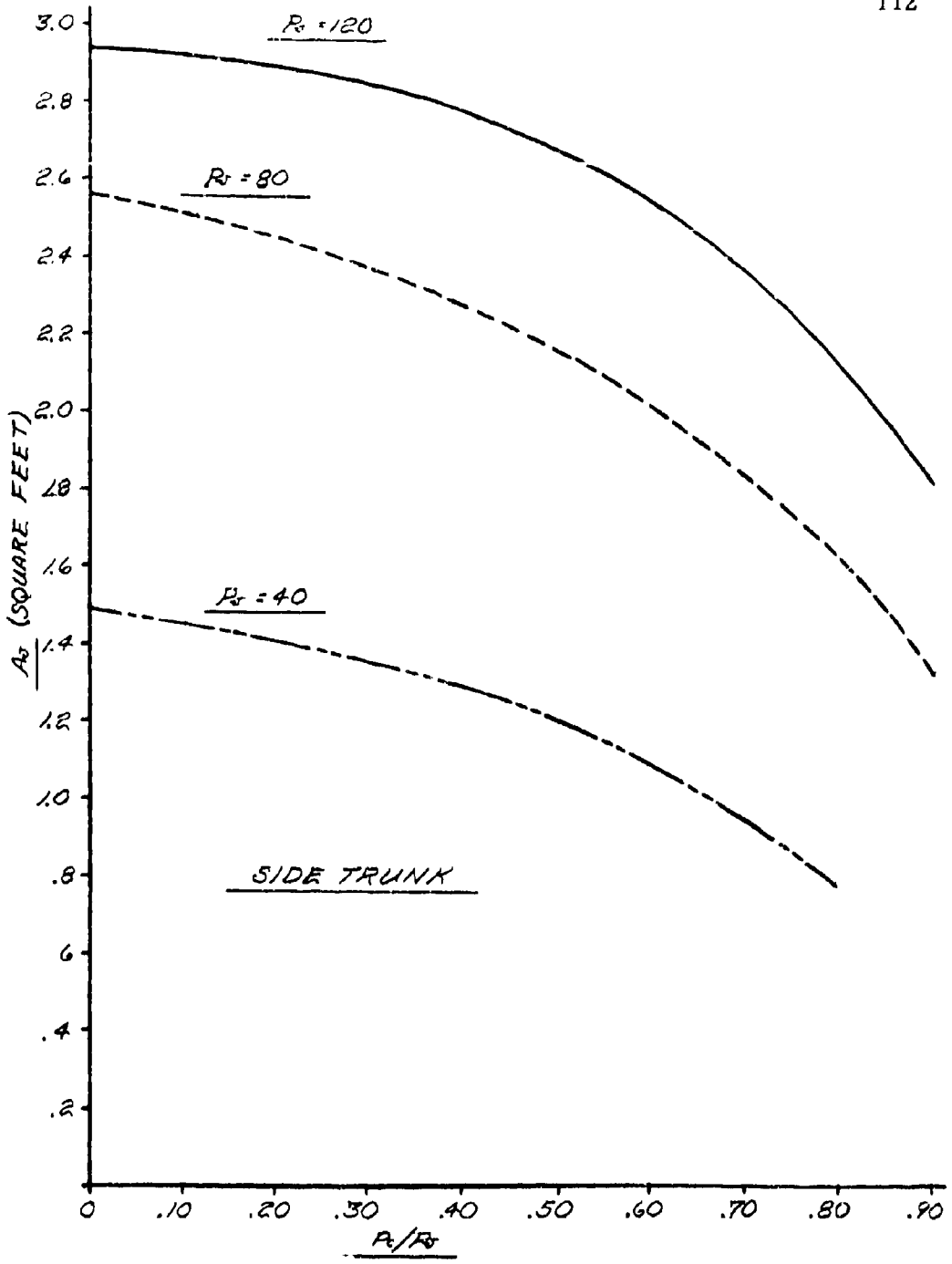
A_J vs P_c/P_J, ELASTIC SIDE TRUNK
FIGURE 4-18
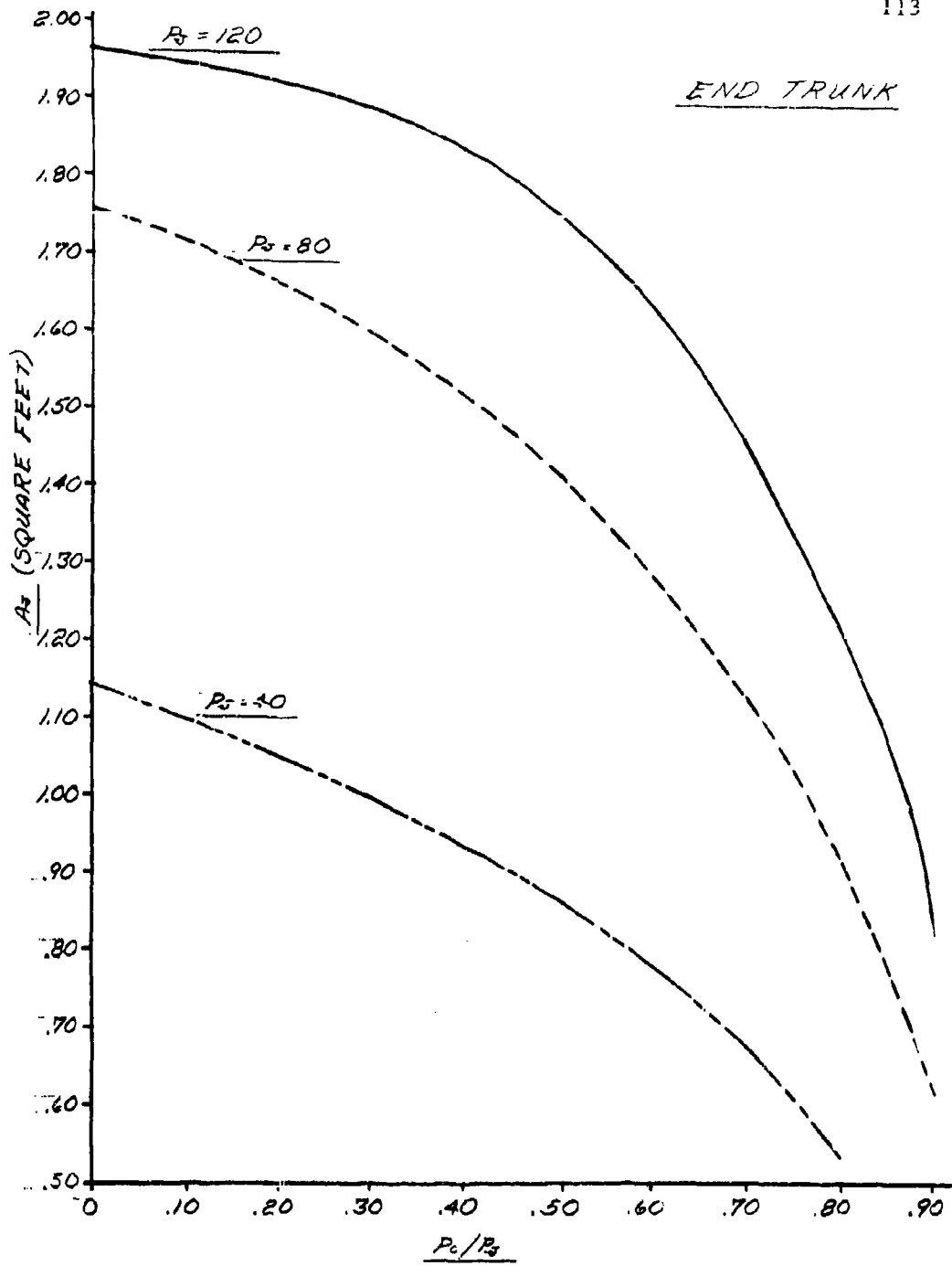
A_J vs P_c/P_J, ELASTIC END TRUNK
FIGURE 4-19
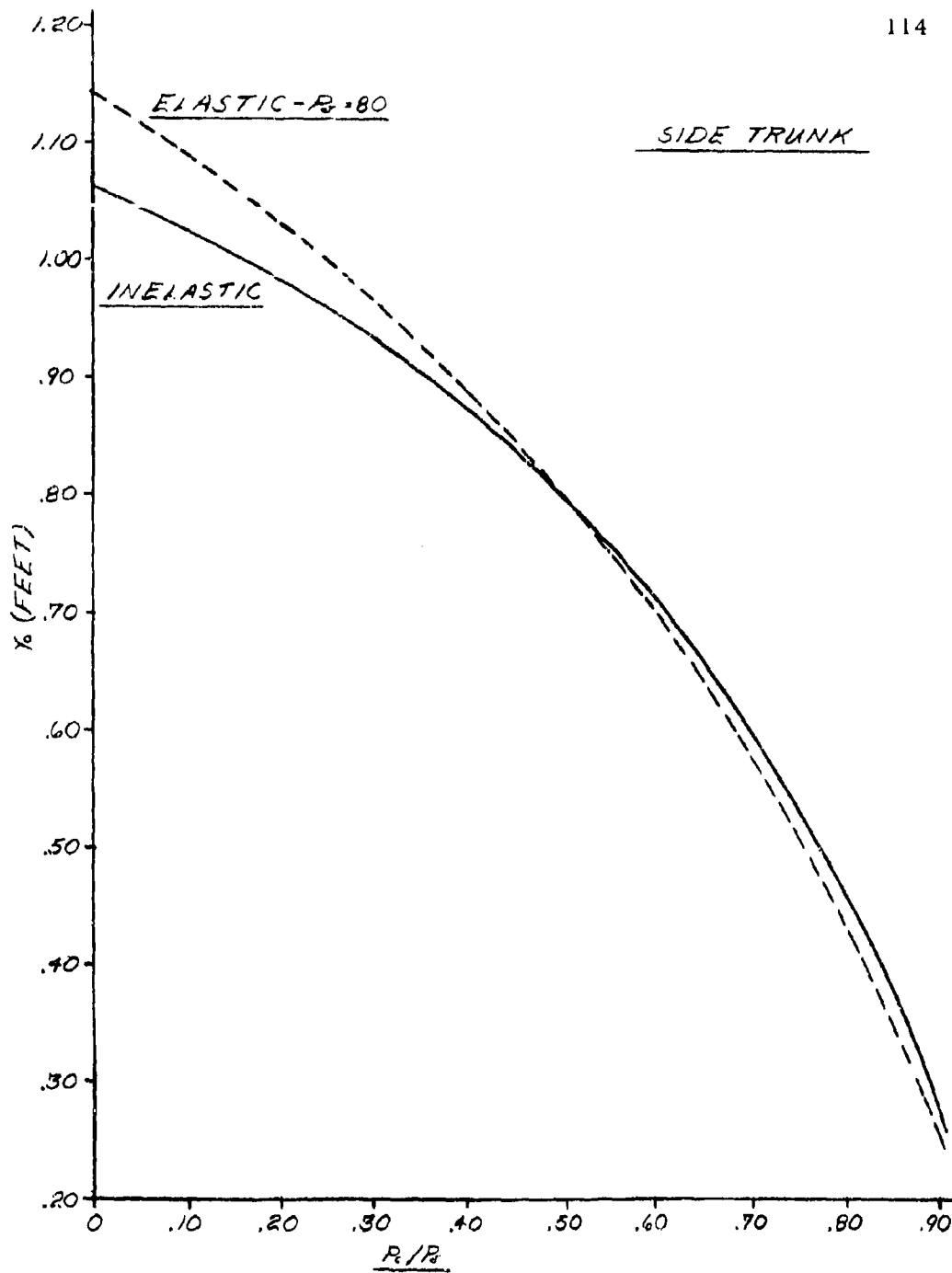
Y_0 vs P_c/P_J, **COMPARISON OF RESULTS**
FIGURE 4-20

Figure 4-21 shows the relationship between ℓ_3 and Y_0/Y_∞ at various p_c/p_j values for the side trunk. Figure 4-22 shows the same relationships for the end trunk. The slope of the ℓ_3 versus Y_0/Y_∞ curve is proportional to the stiffness. The curves show that the stiffness of both trunk shapes is nearly linear for deflections up to 50% of the free trunk height (Y_∞).

Figures 4-23 and 4-24 show the relationship between A_j and Y_0/Y_∞ for the side and end trunk respectively. The values of A_j were predicted by Equation (4-48).

SIDE TRUNK

ℓ_3 vs Y_o/Y_∞ , SIDE TRUNK
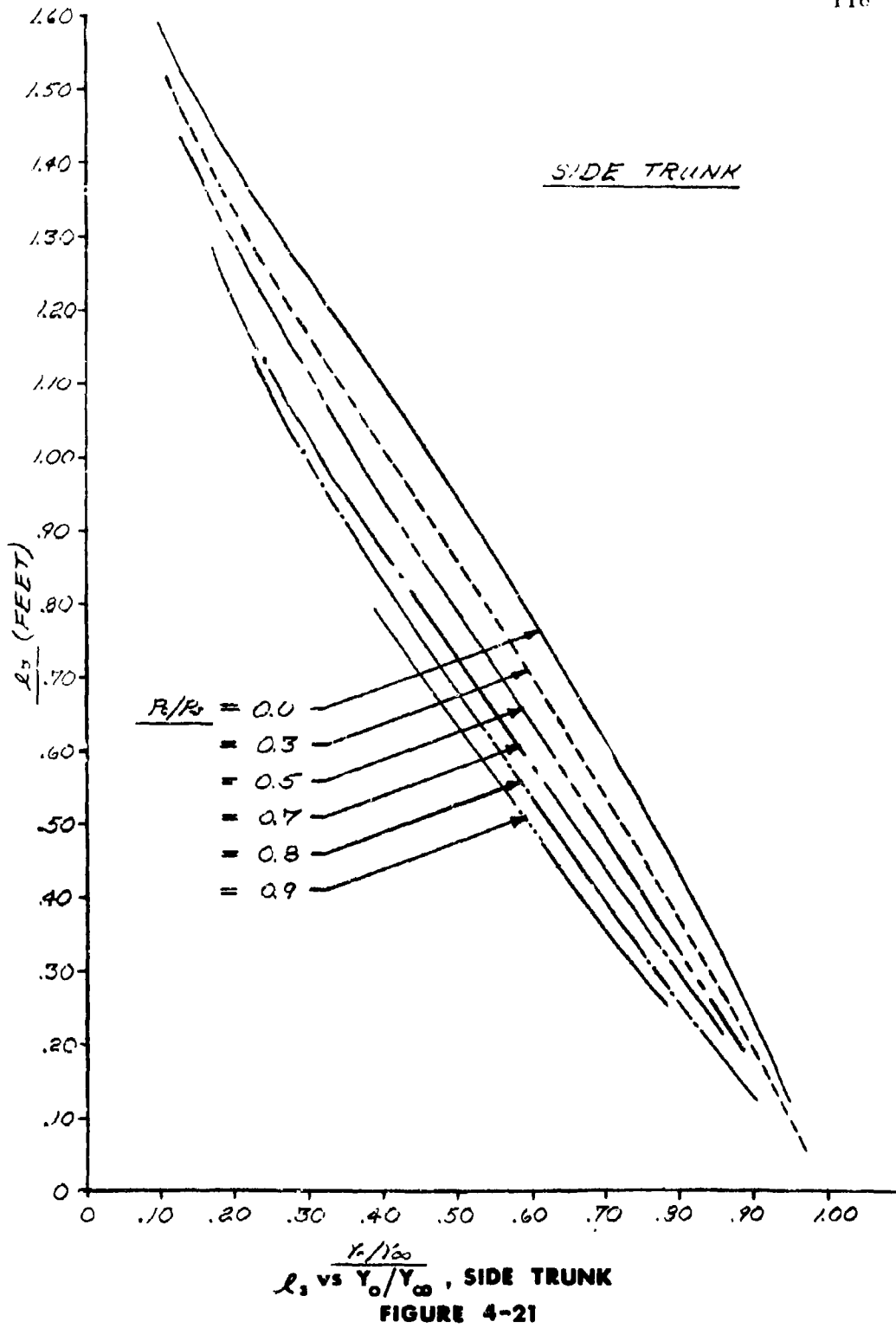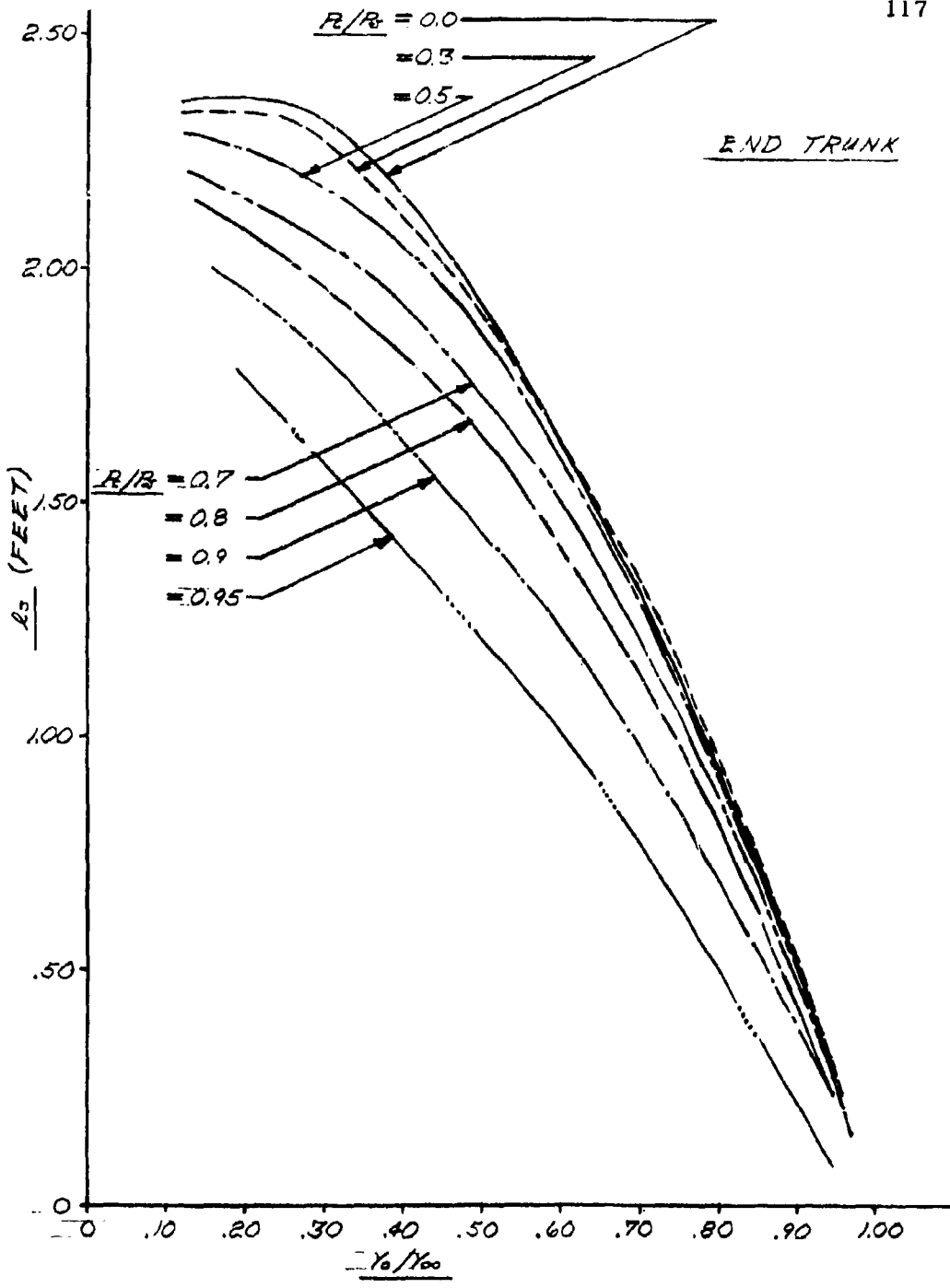
FIGURE 4-21

ℓ_3 vs Y_o/Y_∞ , **END TRUNK**
FIGURE 4-22
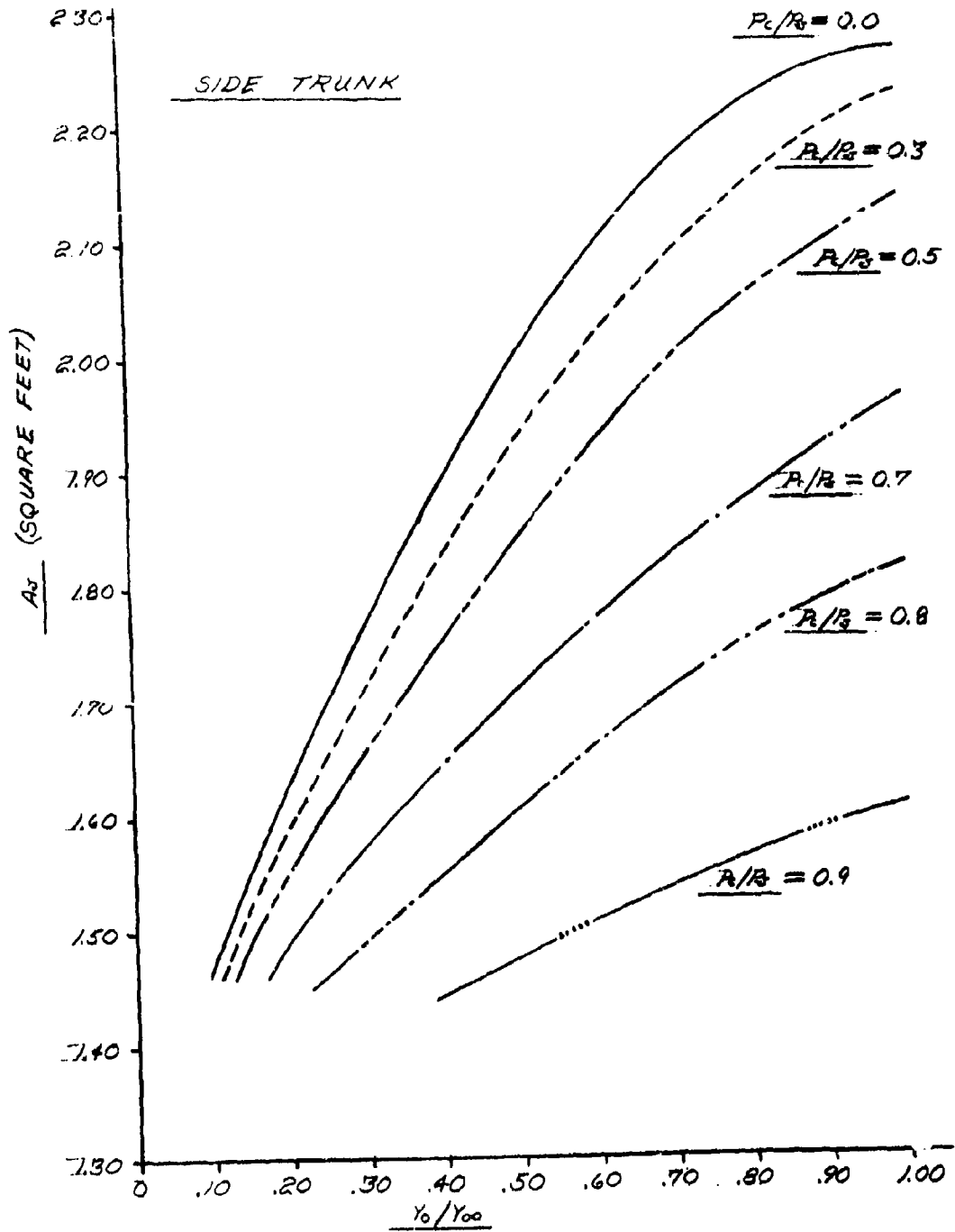
A_J vs Y_o/Y_∞ , SIDE TRUNK
FIGURE 4-23
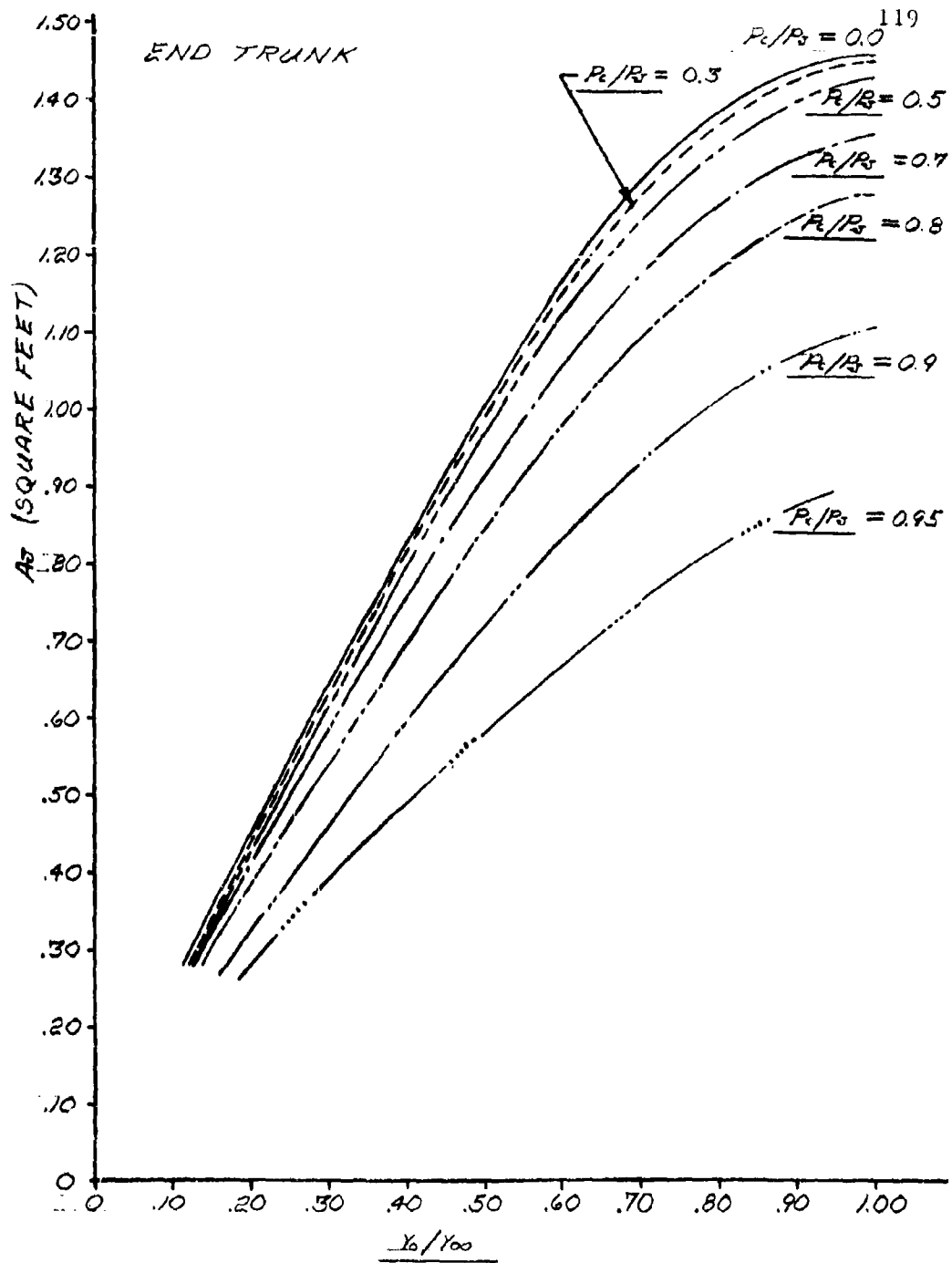
A_J vs Y_0/Y_∞ , END TRUNK

FIGURE 4-24

5. ANALYSIS OF DISTRIBUTED JET FLOW

5.1   Introduction

The Air Cushion Landing System introduces air throughout a large area of the bottom of the trunk in order to provide "air lubrication" to the trunk. This "air lubrication" is necessary to prevent excessive wear of the trunk during takeoff rotation and landing flare. During these maneuvers, the cushion pressure approaches atmospheric pressure and the trunk must carry a portion of the load.

For the ACLS, the peripheral jets are formed by a large number of slots or holes which are distributed over the bottom of the trunk. The Air Cushion Vehicle, on the other hand, normally employs a one continuous nozzle which concentrates the single jet at the point of minimum daylight clearance. Because of these differences, modifications of the concentrated jet theories are necessary when applying them to the distributed jet system.

In this Chapter, modifications to the concentrated jet theories presented in Chapter 2 have been developed. These modifications allow the concentrated jet theories to more closely conform to the actual Air Cushion Landing System distributed jet design.

Two cases have been considered: The Distributed Jet Momentum Theory and the Flow Restrictor Theory.

The Distributed Jet Momentum Theory applies the momentum theories developed in Chapter 2 to a number of jets in series. This theory assumes the cushion pressure is maintained by the change in momentum of the peripheral jet. The momentum theory is developed in Section 5.2.

The Flow Restrictor Theory applies the plenum theory to the trunk configuration for the Air Cushion Landing System. This theory assumes the cushion pressure is maintained by a flow restriction at the cushion periphery. The Flow Restrictor Theory is developed in Section 5.3.

120

The symbols are as follows:

a	x coordinate of the upper trunk attachment point, ft
a_j	total area of the orifices in the trunk, ft^2
a_n	total area of the orifices in the nth row, ft^2
b	y coordinate of upper trunk attachment point, ft
C_D	cushion exhaust nozzle shape coefficient
C_d	total coefficient of discharge for cushion chamber ($C_d = C_D C_T$)
$(C_Q)_n$	flow coefficient for pressure distribution at the nth row of trunk orifices
C_T	effective flow area reduction in the cushion exhaust nozzle caused by the flow from the trunk orifices
$(C_x)_n$	coefficient of discharge for the nth row of trunk orifices
D_q	trunk orifice diameter, ft
d	jet height or trunk daylight clearance, ft
d_n	jet height for the nth row of trunk nozzles, ft
g_0	gravitational constant, ft/sec^2
H	aircraft clearance, the distance between the aircraft hard structure and the ground, ft
$J_n^{'}$	the total reaction from the nth row of jet orifices, lbs
ℓ_1	partial trunk length (see Figure 5-3), ft
ℓ_2	partial trunk length (see Figure 5-3), ft
ℓ_3	trunk footprint length (see Figure 5-3), ft
N	number of jet orifices per row
n'	effective number of rows of jets which contribute to cushion nozzle area flow reduction
P_a	atmospheric pressure, psf
P_c	cushion pressure, psf

P_j trunk pressure, psf

$P_{\bar{n}}$ static pressure in the cushion exhaust nozzle at the nth row of trunk orifices, psf

p_c/p_j cushion to trunk pressure ratio

Q_n flow from the nth row of trunk orifices, ft^3/sec

Q_p flow from the plenum chamber, ft^3/sec

Q_j total flow from the trunk, ft^3/sec

$(Q_t)_n$ total flow from all trunk orifices from the mth row up to and including the nth row, ft^3/sec

R_1 radius of curvature for the trunk segment ℓ_1, ft

R_2 radius of curvature for the trunk segment ℓ_2, ft

S total length of the trunk, ft

S' effective flow length of the trunk, ft

t total effective jet thickness, ft

t_n effective jet thickness for the nth row of orifices, ft

v_n average velocity of the gas from the nth row of orifices, ft/sec

$(v_t)_n$ average velocity of the gas in the cushion exhaust nozzle at the nth row of trunk orifices, ft/sec

X jet thickness parameter for concentrated jet

X_n jet thickness parameter for n^{th} jet

X_0 horizontal distance from lower trunk attachment point (o,o) to trunk low point (x_0, y_0), ft

x_0 x coordinate of minimum jet height point

Y_0 vertical distance from lower trunk attachment point (o,o) to trunk low point (x_0, y_0), ft

y_0 y coordinate of minimum jet height point

Y_∞ value of Y_0 at which trunk flattening begins ($\ell_3 = 0$), ft

Z_n momentum parameter defined by Equation (5-7)

Greek symbols

β_n angular position of nth row of orifices relative to the vertical, radians

γ_n angle of nth orifice row relative to the trunk, radians

δ_n height of nth orifice row above minimum ground clearance of the trunk, ft

θ_n effective jet angle, radians

λ_n distance along the trunk from attachment point (a,b) to the nth row of orifices, ft

ρ density of the gas, lb/ft^3

Subscripts

ℓ first row of orifices inside the cushion

m   last row of orifices inside the cushion

n   arbitrary row of orifices

5.2   Distributed Jet Momentum Theory

5.2.1   Approach and Assumptions

In Chapter 2, several theories for predicting the performance of a peripheral jet air cushion were developed. These theories assumed that the peripheral jet was formed by a single concentrated slot or nozzle around the periphery of the cushion. The nozzle configuration for the Air Cushion Landing System may be considerably different from the assumed concentrated jet. In particular, the ACLS utilizes a large number of slots or nozzles distributed over the bottom portion of the trunk. Consequently, it was desirable to modify

TABLE 5-1

Values of Trunk Design Variables

VARIABLE	SYMBOL	VALUE
Trunk Length	1	4.803 ft.
Trunk Width	s	2.667 ft.
Equivalent jet thickness	t	.03832 ft.
Upper trunk attachment	a	1.44 ft.
Lower trunk attachment	b	1.00 ft.
Number of rows of orifices	M	8
Diameter of orifices	D	.026 ft.
Total number of orifices	- -	192
Porosity	ξ	.049

ORIFICE DETAILS			
ROW NUMBER n	ROW DISTANCE λ_n ft.	JET THICKNESS t_n ft.	JET ANGLE γ_n Radians
1	2.599	.00479	0
2	2.703	.00479	0
3	2.807	.00479	0
4	2.912	.00479	0
5	3.016	.00479	0
6	3.120	.00479	0
7	3.224	.00479	0
8	3.328	.00479	0

the theories to more closely approximate the ACLS configuration. In this section, the jet configuration was assumed to be represented by a series of continuous slots along the bottom portion of the trunk. This configuration is illustrated in Figure 5-1.

The general approach to the problem was to assume a trunk clearance (d) for given values of trunk pressure (p_j) and recovery pressure ratio (p_c/p_j). The jet height for each of the trunk nozzles was determined from the trunk shape programs developed in Chapter 4. Starting on the atmospheric side of the trunk, the pressure increment across each jet was calculated in succession until the pressure in the cushion was determined. If the calculated and assumed value of cushion pressure did not agree, the jet height was adjusted until agreement was achieved.

The pressure increment across each jet is dependent upon the momentum theory assumed. However, when the pressure increment is small, all of the momentum theories developed in Chapter 2 give similar results. In view of the small pressure increments associated with a series of distributed jets, only two theories — the thin jet theory and the exponential theory — were selected for further development.

The development of the distributed jet momentum theory is similar to the concentrated jet theories presented in Chapter 2. The assumptions made in Section 2.4 apply to the distributed jet system. Moreover, the assumptions made in Sections 2.5 and 2.6 are applicable when the thin jet or the exponential theories are applied to the distributed jet system. Two additional assumptions are necessary. These assumptions are as follows.

5.2.1.1   The jets are formed by a series of continuous slots along the bottom of the trunk.

5.2.1.2   The flow from any given jet is related only to the static pressure difference across the nozzle. The effect of flow from other jets is neglected.
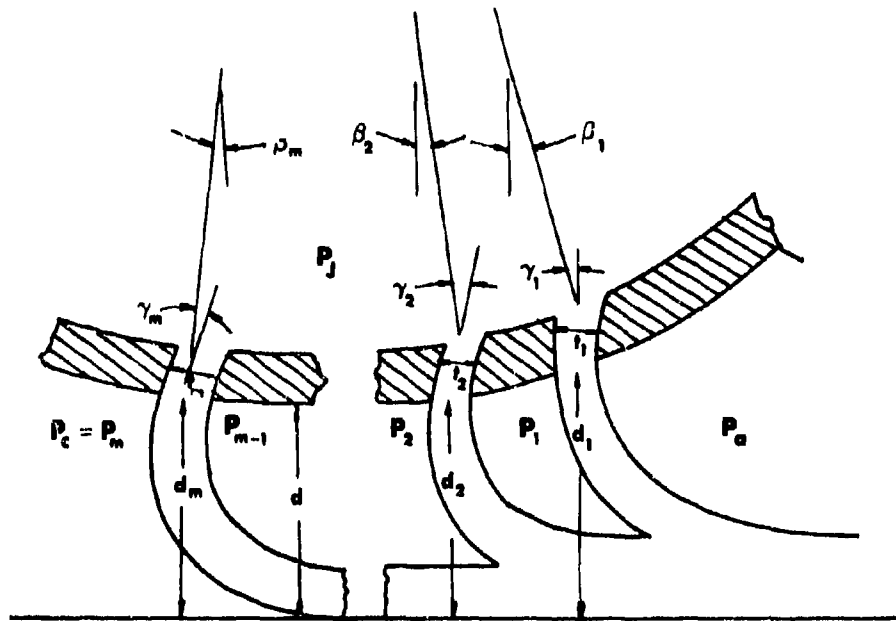
DISTRIBUTED JET GEOMETRY

FIGURE 5-1

5.2.2 Force Equilibrium Across the Jets

In Sections 2.4.6, 2.5.6, and 2.6.6 force equilibrium was applied in the x direction to a control volume containing the peripheral jet. The resulting expression equated the product of the jet height and the pressure increment across the jet to the change of momentum of the jet in the x direction. A similar expression may be developed for each jet in the series shown in Figure 5-1.

Force equilibrium applied to the first jet in Figure 5-1 gives:

$$d_1(P_1 - P_a) = \frac{J_1'}{S} (1 + \sin \theta_1) \qquad (5\text{-}1a)$$

where $\theta_1 = \gamma_1 + \phi_1$

Similarly, force equilibrim applied to the second jet is:

$$d_2(P_2 - P_1) = \frac{J_2'}{S} (1 + \sin \theta_2) \qquad (5\text{-}1b)$$

Across the nth jet, force equilibrim gives:

$$d_n(P_n - P_{n-1}) = \frac{J_n'}{S} (1 + \sin \theta_n) \qquad (5\text{-}1c)$$

where $\theta_n = \gamma_n + \phi_n$

In general, the pressure at any point P_n may be found by rearranging Equation (5-1c).

$$P_n = \frac{J_n'}{d_n S} (1 + \sin \theta_n) + P_{n-1} \qquad (5\text{-}2)$$

The value of J'_n is dependent upon the flow theory selected. The simple jet theory and the exponential theory are considered most appropriate for the distributed jet case. Both of these theories are applicable to thin jets, and the distributed jet configuration involves a series of thin jets.

The expressions for J'_n given by the two thin jet theories were developed in Sections 2.5 and 2.6 respectively. When applied to the nth jet in the series, the momentum expressions become:

Thin jet theory

$$J'_n = 2 S t_n (P_j - P_{n-1})$$

(5-3a)

Exponential theory

$$J'_n = 2 S t_n (P_j - P_{n-1}) \left[\frac{1}{2X_n} (1 - e^{-2X_n}) \right]$$

(5-3b)

where $X_n = \frac{t_n}{d_n} (1 + \sin \theta_n)$

(5-4)

The momentum expressions, Equations (5-3a) for (5-3b), may now be combined with Equations (5-2) and (5-4) to provide an expression for the pressure across the nth jet. The results are:

Thin jet theory

$$P_n = 2(P_j - P_{n-1}) X_n + P_{n-1}$$

(5-5a)

Exponential theory

$$P_n = (P_j - P_{n-1}) (1 - e^{-2X_n}) + P_{n-1}$$

(5-5b)

A general expression for the pressure across the jet may be written as follows:

$$P_n = 2 (P_j - P_{n-1}) Z_n + P_{n-1} \qquad (5\text{-}6)$$

where:

for thin jet theory

$$Z_n = X_n \qquad (5\text{-}7a)$$

for exponential theory

$$Z_n = \frac{1}{2} (1 - e^{-2X_n}) \qquad (5\text{-}7b)$$

5.2.3   Geometric Compatibility

In order to determine X_n for each of the jets, it is necessary to determine the trunk shape and the location of each jet. This problem may be solved by using the trunk shape solutions given in Sections 4.4 or 4.5. For a given a, b, ℓ and p_c/p_j, the trunk shape may be determined by the method derived in Section 4.4. It is necessary, in addition, to specify the location of the jets and their angle relative to the trunk membrane. These two variables are specified by γ_n and λ_n which are defined geometrically in Figures 5-1 and 5-2 respectively.

The trunk shape analysis presented in Section 4.4 predicts the lowest point on the trunk (x_0, y_0). This is the coordinate point at which the minimum jet height (trunk clearance) is measured. This height is specified as d and is shown in Figure 5-2. All other jet heights may be measured relative to the minimum d in terms of δ_n as shown in Figure 5-2. Consequently, it is possible to write the jet height of any nozzle as·

$$d_n = d + \delta_n \qquad (5\text{-}8)$$
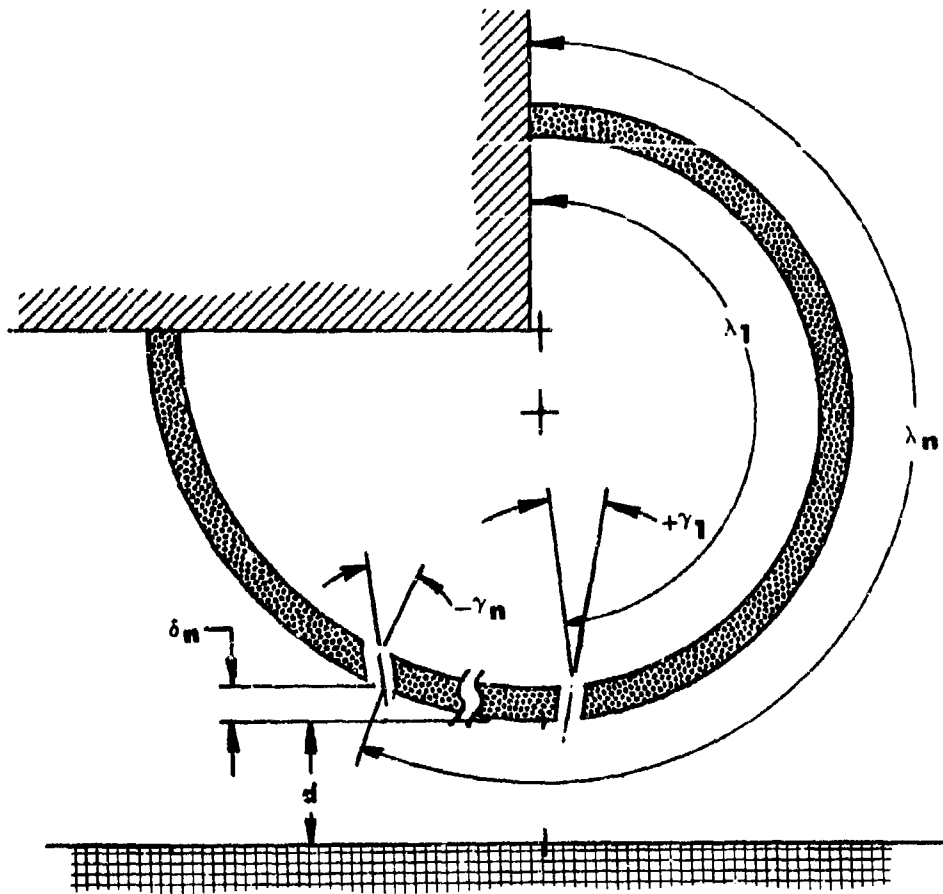
TRUNK GEOMETRY FOR DISTRIBUTED JET

FIGURE 5-2

It is now possible to calculate δ_n and θ_n from trunk geometry. These values, in turn, allow the calculation of X_n and P_n.

It is possible for the nth jet nozzle to be located on any one of the three trunk segments shown in Figure 5-3. Each of these locations constitutes a different case. The three cases are listed as follows:

Case 1

The nth jet is on the atmospheric side of the low point.

Case 2

The nth jet is at the low point.

Case 3

The nth jet is on the cushion side of the low point.

Case 1 may be recognized by the following condition:

$$\ell_1 - \lambda_n > 0 \tag{5-9a}$$

For Case 1, the remaining geometric relationships may be derived from the geometry shown in Figure 5-3(a). These relationships are:

$$\beta_n = \frac{\ell_1 - \lambda_1}{R_1} \tag{5-10a}$$

$$\delta_n = R_1 (1 - \cos \beta_n) \tag{5-11a}$$

$$\theta_n = -\beta_n + \gamma_n \tag{5-12a}$$

Case 2 may be recognized by the following condition:

$$\ell_1 + \ell_3 - \lambda_n > 0 > \ell_1 - \lambda_n \tag{5-9b}$$

The remaining geometric relationships as shown in Figure 5-3(b) are:

$$\beta_n = 0 \tag{5-10b}$$

$$\delta_n = 0 \tag{5-11b}$$

$$\theta_n = \gamma_n \tag{5-12b}$$

Case 3 may be recognized by the following condition:

$$\ell_1 + \ell_3 - \lambda_n < 0 \tag{5-9c}$$

The remaining geometric relationships as shown in Figure 5-3(c) are:

$$\beta_n = \frac{\lambda_n - \ell_1 - \ell_3}{R_2} \tag{5-10c}$$

$$\delta_n = R_2(1 - \cos\beta_n) \tag{5-11c}$$

$$\theta_n = \beta_n + \gamma_n \tag{5-12c}$$

5.2.4 Solution of Equations

The distributed jet momentum theory may now be solved on an iterative basis as follows.

(a) CASE I

(b) CASE II

(c) CASE III
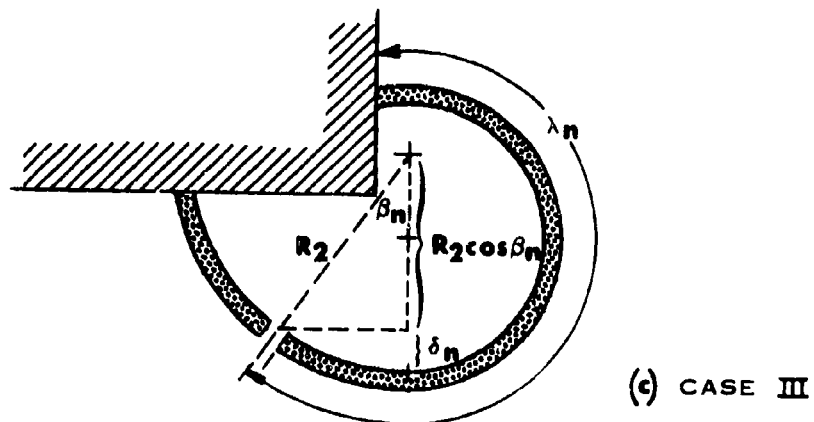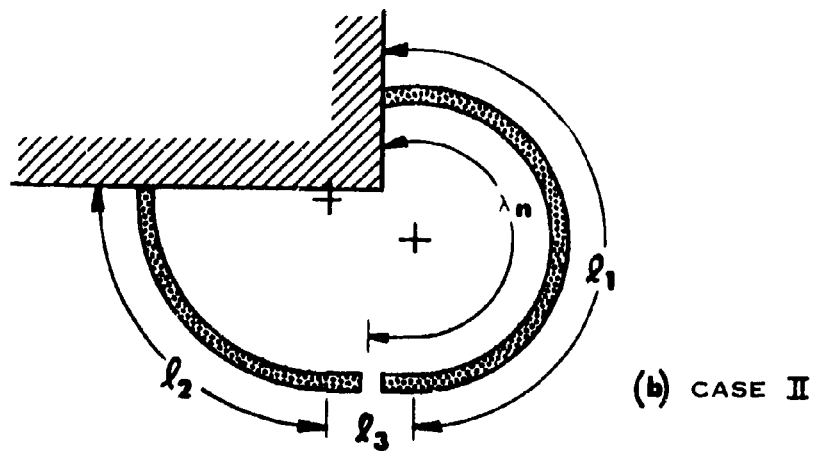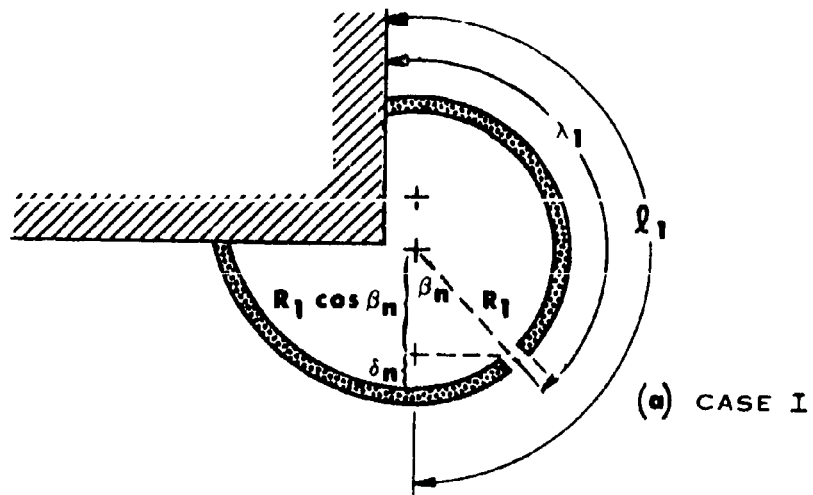
THREE CASES FOR JET LOCATIONS
FIGURE 5-3

(1) Given a, b, ℓ and p_c/p_j the trunk shape may be found using the procedure of Sections 4.4 or 4.5. This procedure gives R_1, R_2, ℓ_1, ℓ_2, and ℓ_3

(2) Assume a maximum value of d. This value may be determined from the simple jet pressure relationship given in Section 2.5.11.

$$p_c/p_j = 2X = 2\frac{t}{d} (1 + \sin \theta) \tag{2-28}$$

Rearranging:

$$d = \frac{2\,t\,(1 + \sin \theta)}{p_c/p_j}$$

and

$$d_{max} = \frac{4t}{p_c/p_j} \tag{5-13}$$

(3) The other known variables are:

$$\lambda_{1,2,\ldots m};\ \gamma_{1,2,\ldots m};\ t_{1,2,3,\ldots m};\ P_a, P_j, S \text{ and } \rho.$$

With the assumed value of d, it is possible to calculate X_n from Equation (5-4). Equations (5-8), (5-11), and (5-12) provide the values of d_n and θ_n which are required in the calculation of X_n.

(4)   It is now possible to solve for the pressure distribution across the jets. This solution is achieved by applying Equation (5-6) to each jet in turn, starting at the first jet (Figure 5-2) and proceeding inward.

$$P_1 = 2 (P_j - P_o) Z_1 + P_a$$

$$P_2 = 2 (P_j - P_1) Z_2 + P_1$$

$$\qquad . \qquad . \quad . \qquad . \quad . \qquad .$$
$$\qquad . \qquad . \quad . \qquad . \quad . \qquad .$$
$$\qquad . \qquad . \quad . \qquad . \quad . \qquad .$$

$$P_m = 2 (P_j - P_{m-1}) Z_m + P_{m-1}$$

(5)   The assumed value of d is correct when

$$\frac{P_m - P_a}{P_j - P_a} = p_c/p_j \qquad\qquad (5\text{-}14)$$

If p_c/p_j is greater than $(P_m - P_a)/(P_j - P_a)$, decrease d and repeat the procedure until agreement is reached.

(6)   Once Equation (5-14) is satisfied, it is possible to calculate the flow. The flow equations developed in Sections 2.5 and 2.6 applied to each jet give the following relationship:

$$Q_j = \sum_{n=1}^{m} S\, t_n \sqrt{\frac{2g_o}{\rho} (P_j - P_{n-1})}\; (C_Q)_n \qquad\qquad (5\text{-}15)$$

where:

$$(C_Q)_n = 1 \quad \text{for thin jet theory}$$

$$(C_Q)_n = \left[\frac{1}{X_n} (1 - e^{-X_n}) \right] \quad \text{for exponential theory}$$

5.3   Flow Restrictor Theory

5.3.1   Approach and Assumptions

The general configuration of distributed jets is shown in Figure 5-1. In the flow restrictor theory, it is assumed that the jets are formed by rows of circular holes rather than by continuous slots. As a result of the spacing between the holes, passages for air flow from the cushion exist. A continuous momentum seal does not exist, and the flow may approach that of a plenum chamber. The plenum chamber assumptions developed in Section 2.8 are applicable to this case. The additional assumptions for this case are as follows:

5.3.1.1   The lowest point of the trunk is specified by (x_o, y_o). The distance between (x_o, y_o) and the ground is d, the minimum jet height (trunk clearance).

5.3.1.2   The jets on the cushion side of (x_o, y_o) supply all the flow into the cushion which maintains the height d. The momentum seal effect of these jets is neglected.

5.3.1.3   The jets on the outside of (x_o, y_o) act to reduce the flow area. A flow coefficient (C_T) is used to account for this area reduction.

5.3.1.4   The flow from the cushion is dependent on the shape of the cushion
exhaust nozzle (which is formed between the trunk and the ground). A
flow coefficient (C_D) is used to account for this effect.

The jet height (trunk clearance) may be estimated by assuming that the pressure
on the cushion side of (x_o, y_o) is uniform and equal to the cushion pressure. The trunk
pressure is known. Since the total orifice area on the cushion side of (x_o, y_o) is also known,
the flow into the cushion may be calculated. Assuming the plenum theory is applicable, the
jet height will rise until the flow from the plenum equals the flow into the plenum. The jet
height may be determined by finding the value of d which equates the flow out to the flow
in. The expression for flow from the plenum is developed in Section 5.3.2. The flow to the
plenum is developed in Section 5.3.3. The jet height is then determined in Section 5.3.4.

A more exact determination of flow and jet height based upon a sequential
analysis of the flow and pressure increment associated with each row of orifices is presented
in Section 5.3.5.

5.3.2   Determination of Flow from Plenum

It was shown in Section 2.8 that the flow from a plenum chamber is given by:

$$Q_p = \sqrt{\frac{2g_o}{\rho}(P_c - P_a)}\ S\ d\ C_d \qquad (2\text{-}61)$$

The coefficient of discharge C_d is dependent upon a large number of variables.
For the purpose of this analysis, the dependence on nozzle pressure ratio, exhaust nozzle
shape and jet configuration will be considered.

The coefficient C_d may be considered as the product of two coefficients:

$$C_d = (C_T)(C_D) \tag{5-16}$$

where:

C_D = nozzle shape coefficient

C_T = flow area reduction coefficient

From Figure 5-4 it is evident that the nozzle shape for the plenum chamber exhaust approaches that of a convergent-divergent nozzle. Consequently, C_D should approach the coefficient of discharge for a nozzle.

The value of C_T is dependent on the flow area reduction caused by the jets outside of point (x_o, y_o) (see Assumption 5.3.1.3). Figure 5-5 shows a typical orifice pattern. Adjacent rows of orifices are generally not aligned in the direction of flow. Consequently, the cushion flow must follow circuitous paths between the orifices. As a result, the effective flow area is reduced and friction is increased.

The value of C_T may be approximated from an estimate of the effective flow area reduction caused by the nozzles. The effective flow area is proportional to the effective flow width:

$$S' = S - (N)(D_q)(n') \tag{5-17}$$

where:

S' = effective flow width

S = actual flow width

n' = effective number of rows of orifices which contribute to flow area reduction

D_q = diameter of orifices

N = number of orifices per row

The coefficient (C_T) may now be estimated as follows:

$$C_T \approx \frac{S'}{S} \tag{5-18}$$

The actual value of C_T requires experimental determination.
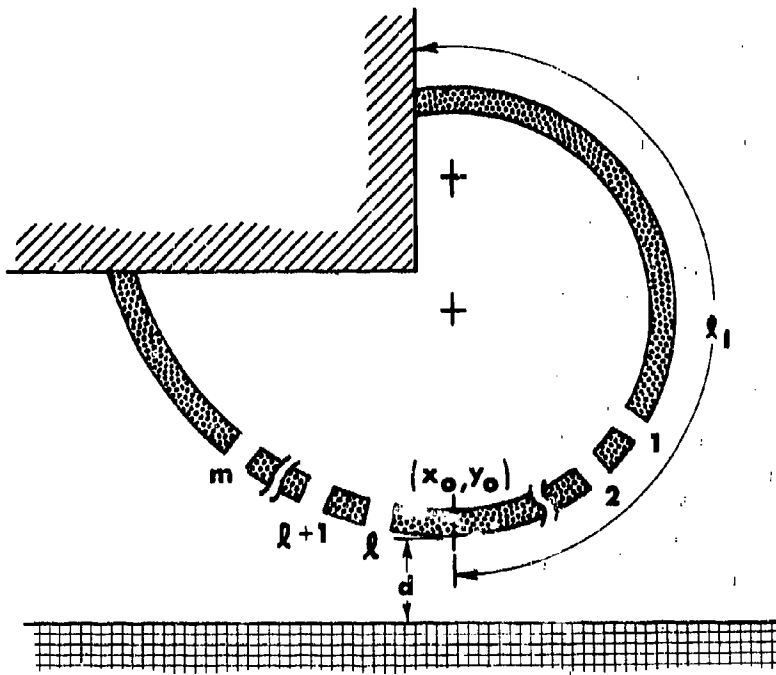
LOCATION OF JETS RELATIVE TO LOW POINT

FIGURE 5-4
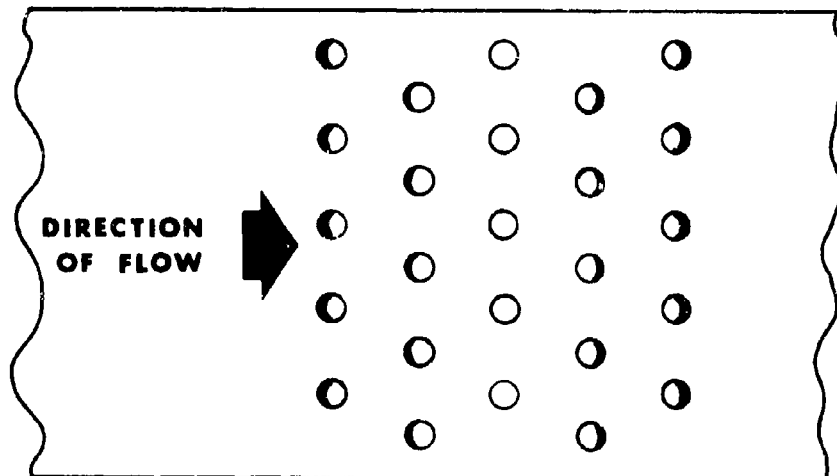
TYPICAL JET SPACING
FIGURE 5-5

5.3.3 Determination of Flow to Plenum

The flow to the plenum chamber, based on Assumption 5.3.1.1, is the sum of the flow from the jets on the cushion side of point (x_o, y_n). The first jet on the cushion side is represented by the ℓth row in Figure 5-4. The last jet is represented by the mth row. The flow may be written:

$$Q_P = \sum_{n=\ell}^{m} a_n \sqrt{\frac{2g_o}{\rho} (P_j - P_n)} \; (C_x)_n \qquad (5\text{-}19)$$

where:

Q_P = flow to plenum chamber

a_n = area of orifices in n^{th} row

P_n = exhaust pressure for holes in n^{th} row

$(C_x)_n$ = discharge coefficient for holes in n^{th} row

The total jet flow is:

$$Q_j = \sum_{n=1}^{m} a_n \sqrt{\frac{2g_o}{\rho} (P_j - P_n)} \; (C_x)_n \qquad (5\text{-}20)$$

The flow may be approximated by letting $P_n = P_c$ for $n > \ell$ and $P_n = P_a$ for $n \leqslant \ell$.

5.3.4 Determination of Jet Height

The jet height may be determined by equating the flow into the plenum, Equation (5-19), to the flow from the plenum, Equation (5-20), and rearranging. The result is:

$$d = \frac{\sum\limits_{n=\ell}^{m} a_n \sqrt{(P_j - P_n)} \; (C_x)_n}{S \sqrt{(P_c - P_a)} \; (C_T) \; (C_D)} \qquad (5\text{-}21)$$

As an approximation, P_n can be taken equal to P_c. The result then becomes:

$$d \approx \sqrt{\frac{p_j}{p_c} - 1} \quad \frac{\sum\limits_{n=\ell}^{m} a_n}{S} \quad \frac{(C_x)}{(C_T)(C_D)} \tag{5-22}$$

Equation (5-22) shows that for the flow restrictor theory, the jet height is dependent upon the ratio of p_c/p_j. Consequently, the parameter p_c/p_j continues to be a valuable dimensionless quantity for relating the independent and dependent variables associated with the system performance.

5.3.5 Determination of Pressure Distribution

A more exact prediction of flow and jet height is dependent upon a more exact prediction of the pressure distribution across the jets. Such a prediction has been developed in this section by a sequential analysis of the flow from each row of orifices. The flow is assumed to be governed by flow restriction as in the plenum theory.

The assumptions associated with the plenum theory (Section 2.9) and the flow restrictor theory (Section 5.3.1) apply to this analysis. In addition, the following assumptions apply.

5.3.5.1 Flow is adiabatic, incompressible and frictionless.

5.3.5.2 Flow from the jets impinges on the ground and is directed in all directions. The total pressure of the plenum exhaust is equal to the static cushion pressure.

5.3.5.3 The net flow from the cushion cavity is zero.

5.3.5.4   The total pressure of gas in the trunk and cushion are equal to P_j and P_c, respectively.

The general approach to the problem was to assume a trunk clearance (d) for given values of trunk pressure (p_j) and recovery pressure ratio (p_c/p_j). The jet height for each row of the trunk nozzles was determined from the trunk shape programs developed in Chapter 4. Starting on the cushion side of the trunk, the flow from the mth row of jets (see Figure 5-4) was determined. The flow out of the cushion at the $(m-1)^{th}$ row of jets was assumed to equal the flow into the cushion from the mth row of jets. Since the jet height at the $(m-1)^{th}$ row of jets was known, the velocity and static pressure in the cushion exhaust nozzle at the $(m-1)^{th}$ row could be calculated. The resulting static pressure was used to determine the flow from the $(m-1)^{th}$ row of trunk orifices. The flow and pressure at subsequent rows of orifices were determined sequentially in a similar manner until the pressure at the cushion nozzle exhaust (the ℓth row of trunk orifices) was found. If the calculated and assumed value of pressure at the cushion nozzle exhaust did not agree, the trunk clearance (d) was adjusted until agreement was achieved.

The equations for predicting the pressure distribution across the distributed jets for the restrictor theory are summarized in the following paragraphs.

The jet velocity from the mth row of jets (see Figure 5-4) may be calculated from Bernoulli's equation.

$$(v_t)_m = \sqrt{P_j - P_c}\sqrt{\frac{2g_0}{\rho}} \qquad (5\text{-}23)$$

Equation (5-23) gives the jet velocity for the mth row of orifices in terms of the known pressure difference across these orifices. The velocity of the gas in the trunk was assumed to be zero and Assumptions 5.3.5.1 and 5.3.5.2 were applied in the development of Equation (5-23).

The total flow from the mth row of orifices may be determined by applying the continuity equation.

$$(Q_t)_m = (v_t)_m (t)_m (C_x)_m (S)$$ (5-24)

The entire flow from the mth jet is assumed to exhaust through the plenum exhaust nozzle formed between the trunk and the ground. The velocity of the gas in the plenum exhaust nozzle at a section just to the left of the $(m-1)^{th}$ row of jets (see Figure 5-4) may be computed from the continuity equation. The resulting relationship is:

$$(v)_{m-1} = \frac{(Q_t)_m}{(d + \delta_{m-1})(S)(C_t)}$$ (5-25)

Equation (5-25) predicts the velocity of the gas in the plenum exhaust nozzle at a section just to the left of the $(m-1)^{th}$ row of trunk orifices. The values of S and C_t are known and constant for a particular trunk design. The value of $(Q_t)_m$ was predicted by Equation (5-24). The value of δ_{m-1} may be determined from the trunk shape program developed in Section 4.4. Only the value of d on the right hand side of Equation (5-25) is unknown. The correct value of d is the value which will predict atmospheric pressure at plenum nozzle exhaust plane. At this point it is necessary to assume a trial value of d.

The pressure at the $(m-1)^{th}$ row of trunk orifices may be computed from the total pressure and the gas velocity. Based on Assumption 5.3.5.2, the total pressure at any point in the plenum exhaust nozzle is P_c. The resulting static pressure at the $(m-1)^{th}$ jet row is

$$(P)_{m-1} = P_c - \frac{(v_{m-1})^2}{2g_o}$$ (5-26)

Equation (5-26) predicts the static pressure at the $(m-1)^{th}$ row of trunk orifices. Since the static pressure at the $(m-1)^{th}$ row is known, velocity and flow from the $(m-1)^{th}$ row of jets may be calculated. In a similar manner to the procedure developed by Equations (5-23) through (5-26), the pressure distribution for all the remaining jets may be calculated in sequence.

The general equations for the pressure distribution calculation are:

$$(v_t)_{m-n} = \sqrt{\frac{2g_o}{\rho} (P_j - P_{m-n})} \tag{5-27}$$

$$(Q_t)_{m-n} = (v)_{m-n} (t)_{m-n} (C_x)_{m-n} (S) \tag{5-28}$$

$$(Q)_{m-n} = \sum_{n=o}^{m=\ell} (Q_t)_{m-n} \tag{5-29}$$

$$(v)_{m-n} = \frac{(Q)_{m-n}}{(d + \delta_{m-n}) (S) (C_T)} \tag{5-30}$$

$$(P)_{m-n-1} = P_c - \frac{(v)_{m-n}^2 (\rho)}{2g_o} \tag{5-31}$$

The pressure at each jet may be calculated in sequence until the minimum pressure and maximum exhaust velocity is reached. The maximum velocity in the exhaust nozzle is determined by the expansion of the exhaust flow from the total cushion pressure to atmospheric pressure (Assumptions 5.3.5.1, 5.3.5.2, and 5.3.5.4). The resulting maximum exhaust velocity is:

$$(v)_{max} = \sqrt{\frac{2g_o}{\rho}} \sqrt{P_c - P_a} (C_D) \tag{5-32}$$

In Equation (5-32), the coefficient C_D was introduced to compensate for the convergent divergent shape of the plenum exhaust nozzle.

The pressure distribution problem may now be solved on an iterative basis by varying the jet height (d) until the maximum predicted plenum exhaust velocity agrees with the velocity predicted by Equation (5-32).

The procedure is basically the same as outlined in Section 5.2.4. Total jet flow and jet height may be predicted from Equations (5-20) and (5-21) respectively, once the pressure distribution for the distributed jet is known.

5.4   Analytical Results

The distributed jet theories require the specification of more design parameters than the concentrated jet theories. In particular, the distributed jet theories require the specification of the trunk shape and the nozzle size, location, spacing, and number. The concentrated jet theories are useful in visualizing general trends. The distributed jet theories are useful in predicting actual performance of a particular distributed jet design.

Because of the large number of variables involved, the analytical results will be presented for one single design. The design selected was the side trunk discussed in Section 4.6 and shown in Figure 4-8. The trunk material is assumed to be inelastic. The nozzles are formed by 8 rows of 5/16″ diameter orifices. The spacing between the rows is 1-14″. The spacing orifices in a given row is 2-1/2″. The location of the rows of orifices on the trunk is determined by specifying λ_n as shown in Figure 5-2. The values for λ_n and the other specified variables are shown in Table 5-1.

The jet height predicted by the distributed jet theories may be compared with the concentrated jet predictions if an equivalent jet thickness is assumed for the distributed jet. The equivalent jet thickness (t) is defined as follows:

$$t = \sum_{n=1}^{m} \frac{a_{ri}}{S} \tag{5-33}$$

where:

a_n is the total area per row of jets. S is the length of the jet row (trunk section length).

Using the above definition of t, the ratio d/t for the distributed jet case becomes equivalent to d/t for the concentrated jet case. It may be noted that:

$$1/X = \frac{d}{t(1 + \sin \theta)}$$

Consequently, 1/x and d/t are equal when $\theta = 0^\circ$.

Figure 5-6 gives a comparison of the predicted d/t versus p_c/p_j for the distributed and concentrated jet theories. For the concentrated jet theories, it was assumed that $\theta = 0$. It is evident from the figure that the jet height predicted by the flow restrictor theory is considerably lower than that predicted by the various momentum theories.

The relationship between C_Q and p_c/p_j is shown in Figure 5-7. The definition of C_Q was given by Equation (3-4).

$$C_Q = \frac{Q_j}{t S \sqrt{\frac{2g_0}{\rho} p_j}} C_x \qquad (3-4)$$

The parameter C_Q is a flow coefficient which compensates for the pressure variation across the jet. The physical significance of this parameter was discussed in detail in Section 3.4.

In computing C_Q, all other flow coefficients were assumed to be unity. The results shown in Figure 5-7 indicate that all distributed jet momentum theories give nearly the same value of C_Q. The corresponding values of C_Q are slightly higher for the distributed jet theories than for the Barratt theory for a concentrated peripheral jet.
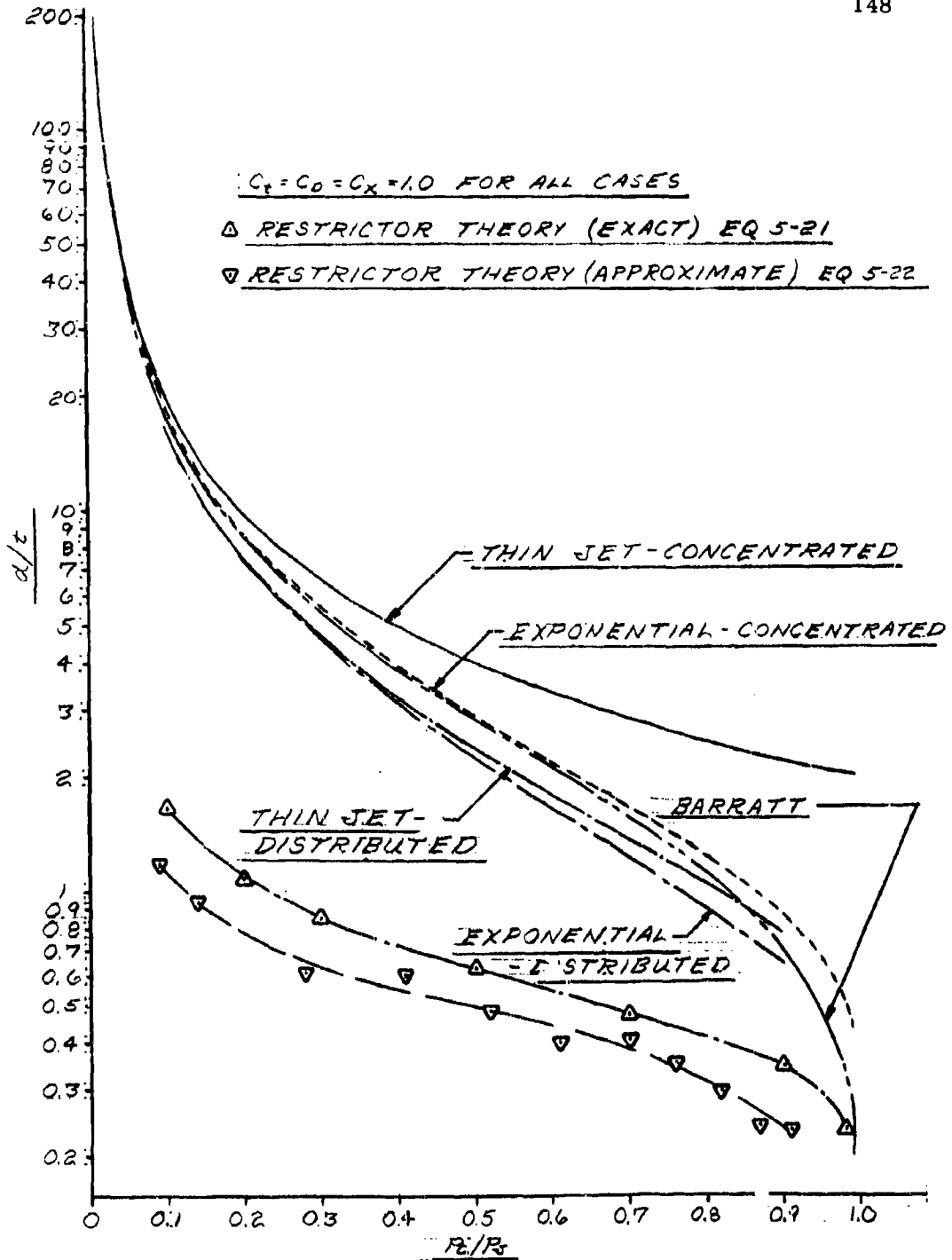
ANALYTICAL PREDICTIONS OF d/t vs P_c/P_j –MODEL SIDE TRUNK

FIGURE 5-6

Legend:
- O THIN JET
- ▽ THIN JET-DISTRIBUTED, $C_x = 1.0$
- ⊘ EXPONENTIAL-DISTRIBUTED, $C_x = 1.0$
- ◌ RESTRICTOR, $C_o = C_x = C_t = 1.0$
- ☐ EXPONENTIAL
- △ BARRATT

Vertical axis: C_Q

Horizontal axis: P_c / P_J
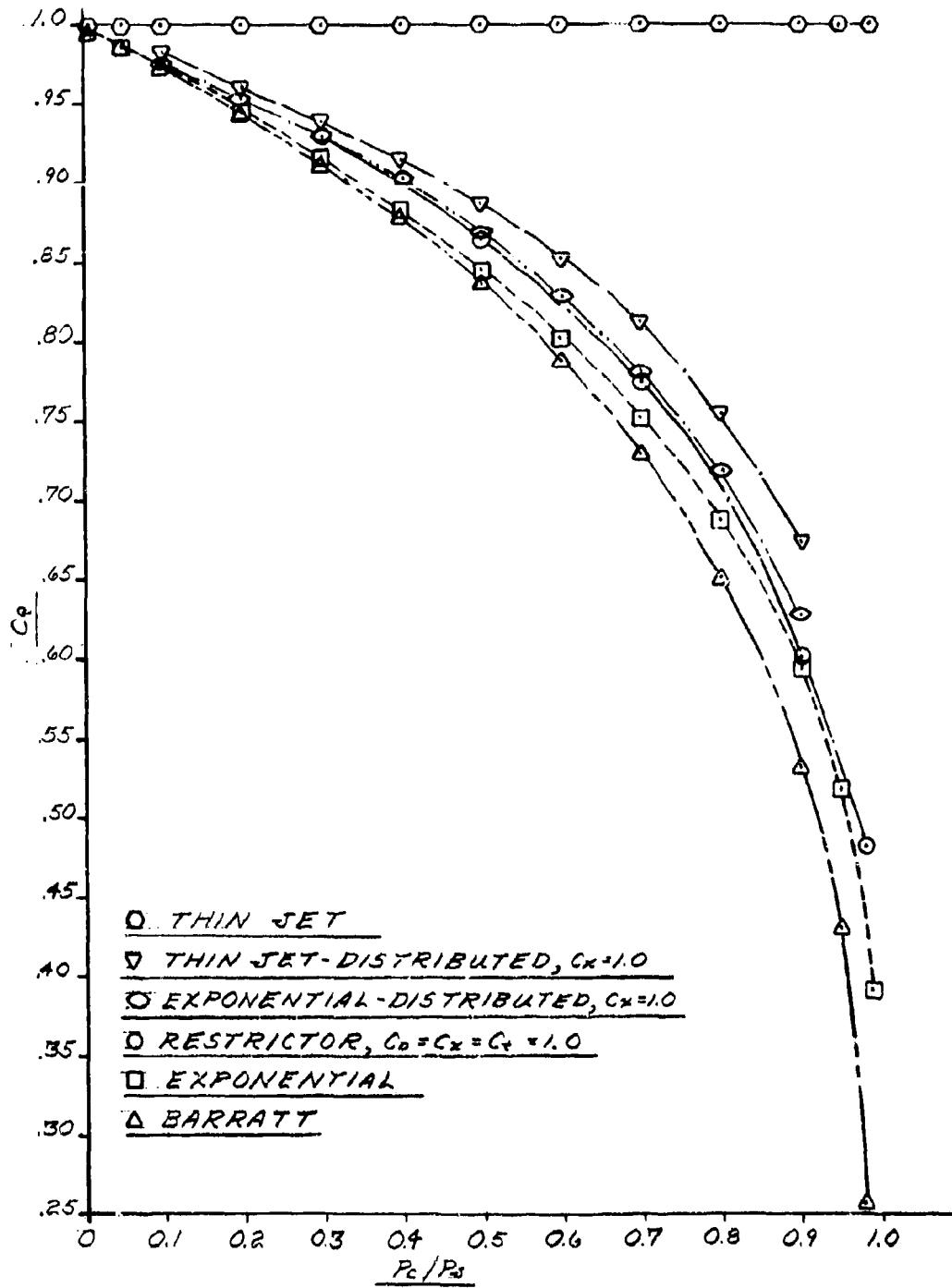
ANALYTICAL PREDICTIONS OF C_Q vs P_c/P_J—MODEL SIDE TRUNK

FIGURE 5-7

The distributed jet curves presented in Figures 5-6 and 5-7 were based on an assumed trunk pressure of 120 psfg. Computations were also made for trunk pressures of 80 psfg and 160 psfg. The resulting values of C_Q and d/t were within a few percent of those predicted at 120 psfg. It was concluded that the curves presented in Figures 5-6 and 5-7 are dependent only on p_c/p_j and independent of the magnitude of p_j.

6. EXPERIMENTAL PROGRAM – STATIC MODEL

6.1 Experimental Apparatus – Static Tests

Figure 6-1 shows the test apparatus used for verification of the trunk shape, flow, distribution, and jet height which were predicted by the analysis developed in Chapters 4 and 5. The plexiglas side in the test rig allowed the inspection of the two-dimensional shape of the trunk cross section. For this reason, the apparatus was generally referred to as the 2D test rig. The total test apparatus consisted of three units: an air supply, a test section, and a trunk specimen.

Airflow was supplied by a Spenser Gas Booster capable of delivering 3,000 cfm at 1.65 psig. Air was ducted to the test section through 16 feet of 12-inch diameter galvanized ducting. Trunk pressure was controlled by adjusting a butterfly valve located in the blower housing ahead of the ducting. A flow straightener was positioned in the ducting in accordance with standards set forth in Reference (47). Flow was determined by measuring the differential head across an orifice plate meeting ASME specifications[48], using a micromanometer with a 20-inch range. Air temperature upstream was measured by a 0-120 F mercury thermometer.

The test section consisted of a box approximately 32" wide by 42" long by 52" high. The box was constructed from plywood and plexiglas. The front of the box was open to allow air to exhaust and the floor was movable to enable the model to simulate varying vehicle heights. Sixteen static pressure taps, spaced two inches apart, were installed along the centerline of the test section floor.

The trunk specimen under test was made of a nylon-hypalon material which was fastened in the test section by wooden stringers. Six static pressure taps spaced 2-1/2 inches apart were installed along the centerline of the trunk in the jet region. The trunk section was

151
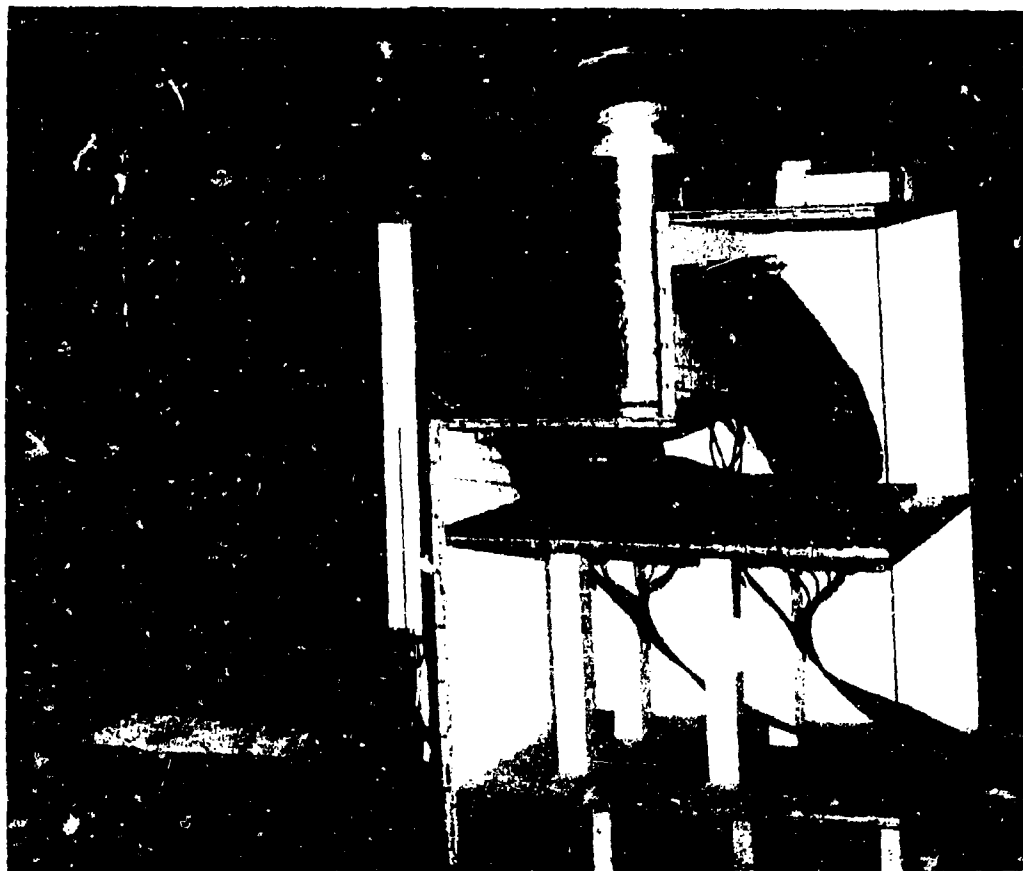
STATIC (2 D) TEST RIG
FIGURE 6-1

32" wide and 57" long. A flap was installed on the edge of the trunk to seal leakage between the trunk and the test section edges. Details of the jet configuration and the trunk elastic properties are given in Appendix IV. The trunk dimensions were the same as those listed in Table 5-I. Consequently, the trunk test specimen represented the side trunk whose shape was analyzed in Chapter 4 and whose flow, pressure distribution, and jet height was analyzed in Chapter 5.

Airflow was ducted into the trunk through the top of the test section. The air flowed through the trunk, out of the jets, and exhausted through the front of the test section. The flow caused a static pressure to build up between the trunk and the rear of the box when the floor was in place. This pressure was equivalent to the cushion pressure (p_c). Both cushion pressure (p_c) and trunk pressure (p_j) were measured by pressure taps installed in the top and rear of the test section. All pressure taps were connected to a 100-tube well type manometer bank. Water was used as the manometer fluid.

A grid was marked on the plexiglas side of the test section to facilitate observation and measurement of the trunk shape. Trunk shape and low points were measured with a scale.

6.2 Experimental Procedures — Static Test

It was necessary to determine the magnitude of leakage flow and the coefficient of discharge for the jets prior to conducting the flow verification tests. The leakage flow was measured by installing in the test section a trunk specimen without jets and measuring the flow for various values of p_j but with $p_c = 0$. The results of the leakage flow test are summarized in Appendix V. The flow coefficient for the jets was measured by repeating the leakage flow procedure after the jets had been installed in the trunk specimen. The results of the coefficient of discharge test are summarized in Appendix VI.

In order to verify the predictions of trunk shape, jet height (d) and pressure coefficient (C_Q), tests were conducted on a trunk specimen of the configuration specified in

Table 5-I. This configuration was identical to the side trunk shape analyzed in Chapter 4 and Chapter 5.

The independent variables in the tests were trunk pressure (p_j) and vehicle height (H). The vehicle height was set at 10 positions in 1-inch increments between 4.5 and 13.5 inches. For each vehicle height, the trunk pressure was set at nominal pressures of 40, 60, 80, 100, 120, and 140 psfg. A tolerance of ± 2 psf was allowed in the pressure setting. At the beginning of each run, the ambient pressure and temperature were recorded. The micromanometer which measured the differential pressure across the ASME flow orifice was leveled and zeroed. The vehicle height was set by adjusting the supports for the movable floor. The desired trunk pressure was obtained by adjusting the butterfly valve in the blower housing.

The following data was collected and recorded.

(1)   The location of the low point on the trunk was determined by visual sighting and its coordinates were measured from a coordinate system grid with a steel rule.

(2)   The jet height was measured by means of calibrated steel rods; the rod was placed on the floor of the model so that its longitudinal axis was parallel to the direction of flow from under the trunk. The rod was then slid under the trunk until it was positioned below the low point of the trunk. Clearance, or the lack of it, between the rod and the trunk was visually detected and a larger, or smaller, rod was tested for equality of rod diameter and jet height. The rods were calibrated to 0.001 inch in increments of approximately 0.01 inch between 0.03 and 1.00 inch.

(3)   The pressure distributions on the floor and trunk were indicated on the micromanometer bank, as were the cushion and trunk region pressures.

(4)   The micromanometer, thermometer, and upstream pressure readings were recorded.

Photographs of the trunk shape were made for a run with p_j = 80 and the vehicle height varied in 1.0 inch increments between 13.5 and 4.5 inches.

The results of the tests are summarized in Section 6.3. The variables used in this chapter are summarized in Chapter 5.

6.3   Summary of Results — Static Tests

6.3.1   Introduction

Experiments were conducted on a trunk specimen which simulated the side trunk configuration shown in Figure 4-9. This configuration was similar to the side trunk of the model shown in Figure 4-8 whose shape was analyzed in Chapter 4. The verification of the trunk shape predictions are presented in Section 6.3.2.

The side trunk specimen was also similar to the model analyzed for jet height, pressure distribution and flow in Chapter 5. The details for this configuration were summarized in Table 5-I. The verifications of the trunk flow characteristics are presented in Section 6.3.3.

6.3.2   Trunk Shape

The predicted and experimental values of ℓ_1, x_0 and y_0 for the free trunk shape are shown in Figures 6-2, 6-3, and 6-4 respectively.
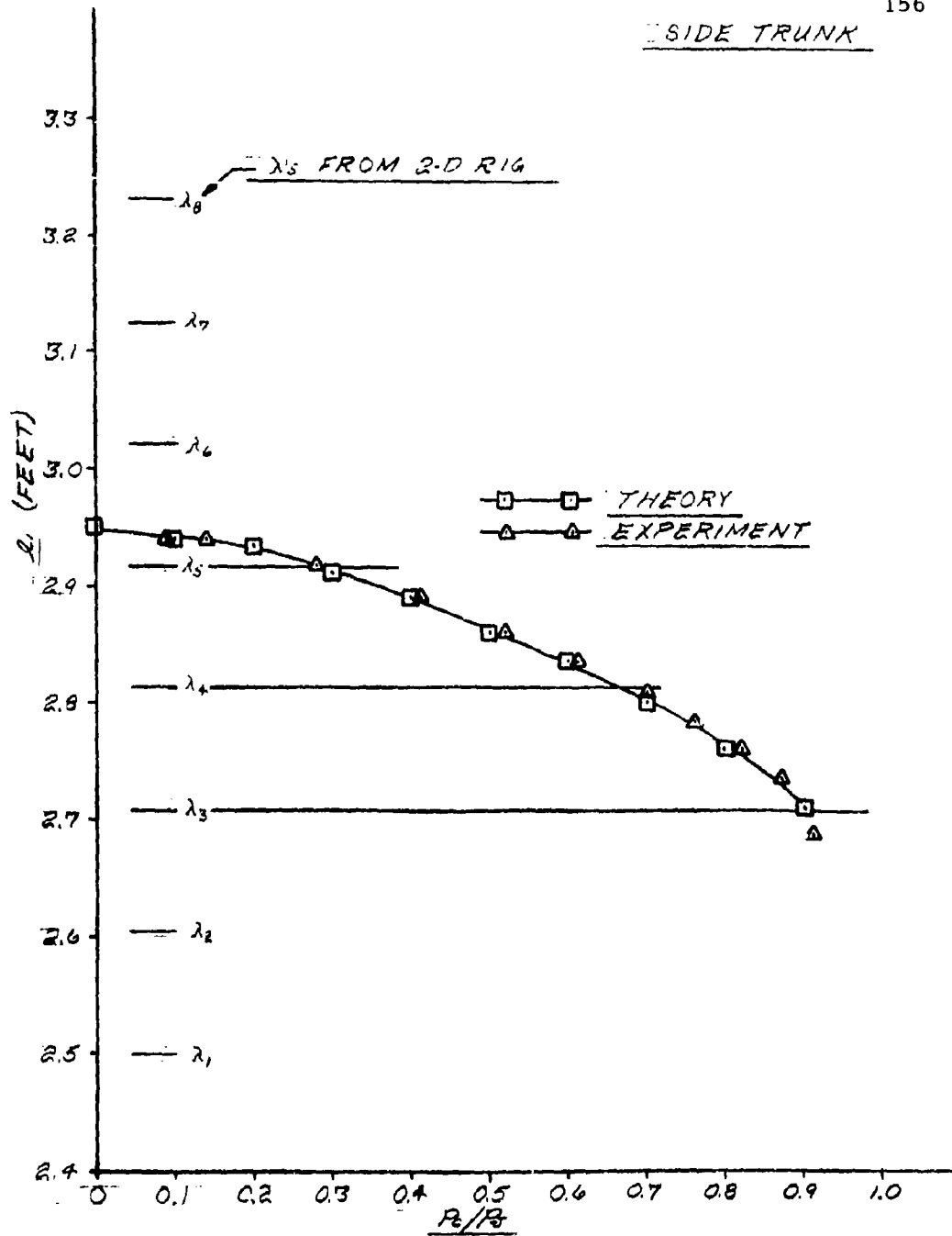
ℓ_1 vs P_c/P_j RESULTS
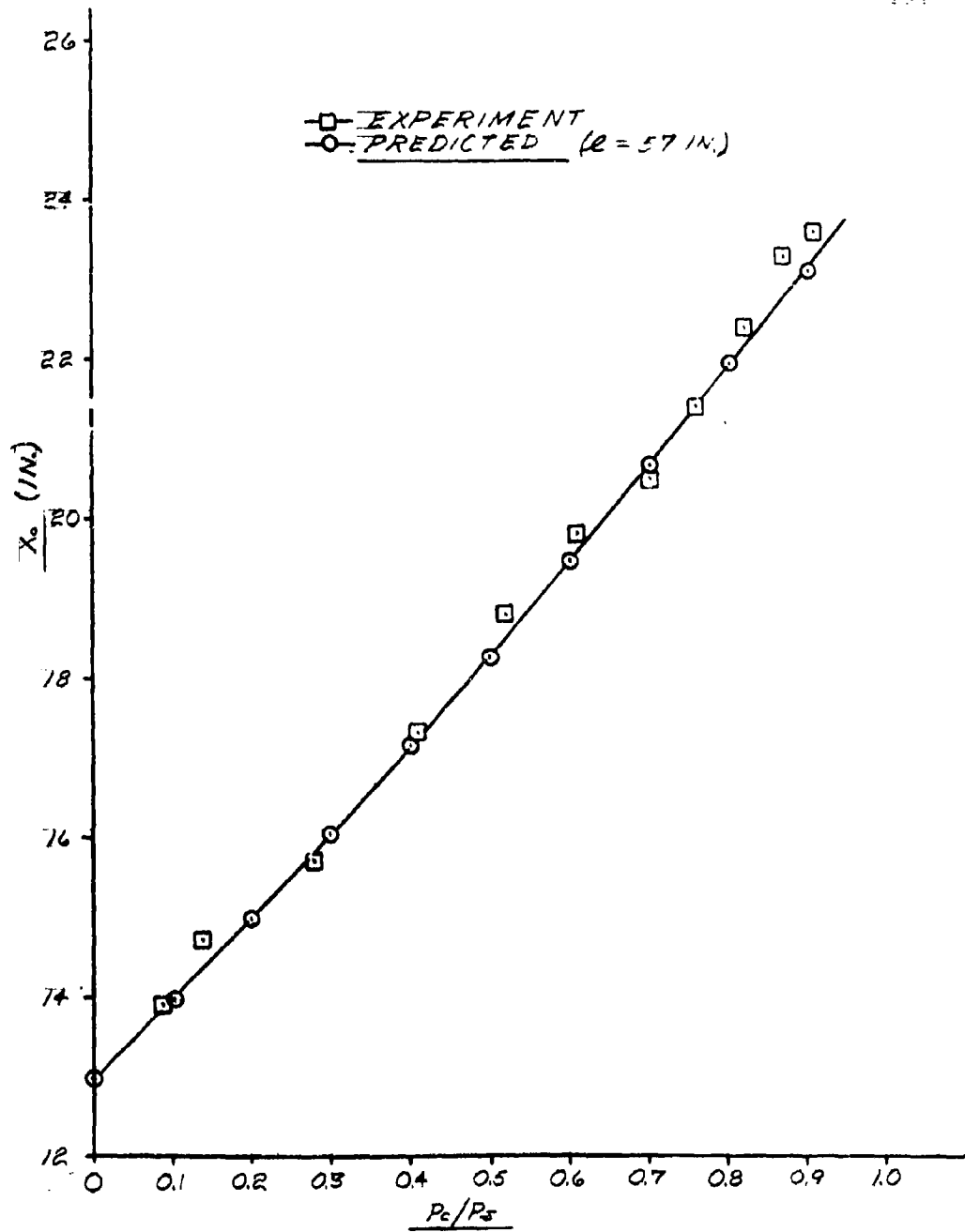
FIGURE 6-2

X_0 vs P_C/P_J RESULTS
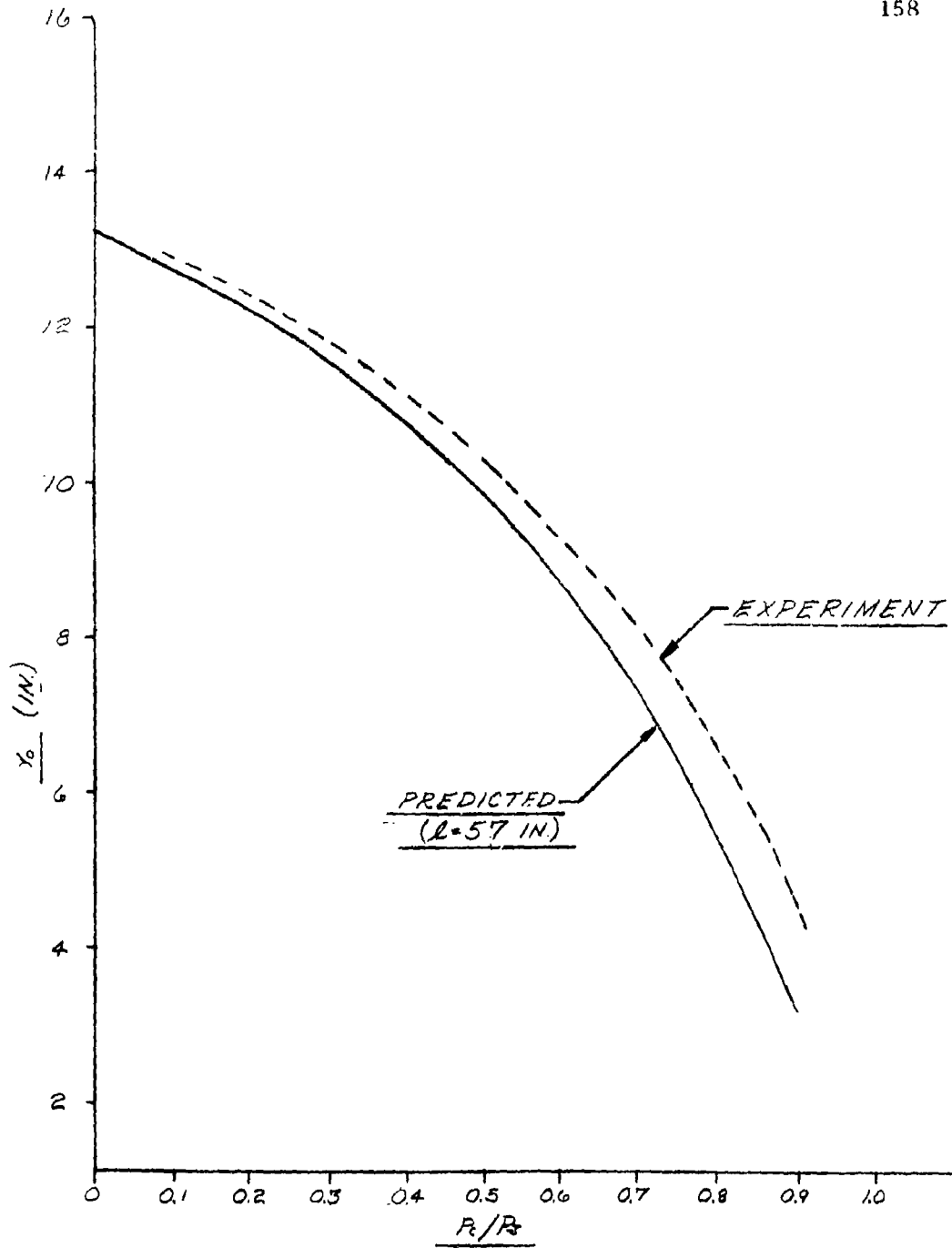
FIGURE 6-3

Y_0 vs P_c/P_J RESULTS
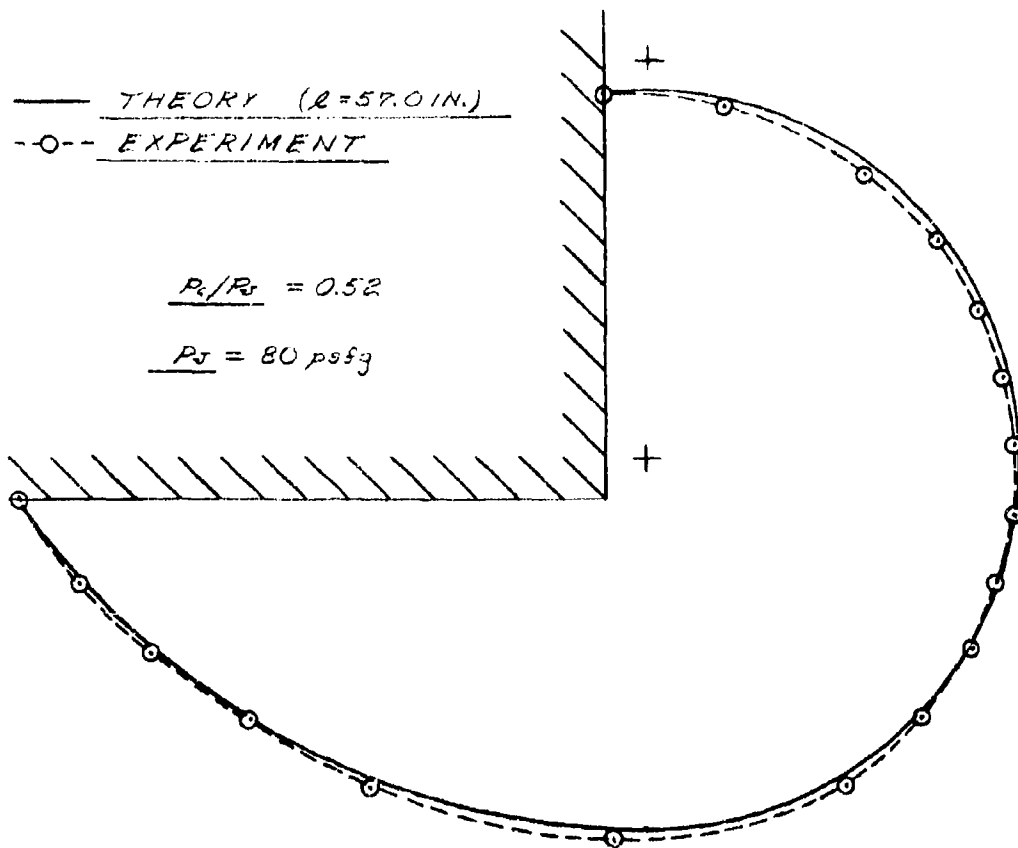
FIGURE 6-4

TRUNK SHAPE RESULTS

FIGURE 6-5

The trunk segment length (ℓ_1) is defined as the length of the trunk segment between the attachment point (a, b) and the low point (x_o, y_o). This segment is illustrated in Figure 5-4. The length of ℓ_1 is important in determining the location of the orifices relative to the low point (x_o, y_o). The distance from the attachment point (a, b) to the nth row of orifices is defined by λ_n. For an inelastic trunk, the value of λ_n is independent of p_c/p_j while the value of ℓ_1 is not. The values of the λ_n's and ℓ_1 are plotted versus p_c/p_j in Figure 6-2. A value of λ_n greater than ℓ_1 indicates that the nth row of orifices is on the cushion side of the low point (x_o, y_o). Figure 6-2 shows that the number of rows of orifices on the cushion side of the low point varies from 3 at p_c/p_j = 1.0 to 6 at p_c/p_j = 0.9. Close agreement between theory and experiment is shown by the curve.

Figure 6-3 shows the variation of the horizontal position of the trunk low point (X_o) with p_c/p_j. It is evident from the curve that the agreement between theory and experiment is excellent.

Figure 6-4 shows the variation of the vertical position of the trunk low point (Y_o) with p_c/p_j. It is evident from the curve that the agreement decreases as p_c/p_j increases. The slight difference between predicted and measured values of Y_o was probably due to a vacuum produced just to the atmospheric side of the trunk low point. This phenomena would tend to force the trunk down. The phenomena is discussed in more detail in Section 6.3.2.

Figure 6-5 shows a comparison of the predicted and measured trunk shape for p_c/p_j = 0.5. It is evident that the agreement between theory and experiment for the free trunk shape is excellent.

In order to determine the validity of the ground loaded trunk shape prediction, a second series of tests was conducted. In this series of tests, the cushion area was vented to the atmosphere. The trunk clearance (Y_o) was varied and the resulting footprint length ℓ_3 was measured with a scale. The resulting values of ℓ_3 versus Y_o/Y_∞ are compared with the

ℓ_3 vs Y_0/Y_∞ RESULTS, $P_c/P_j = 0$
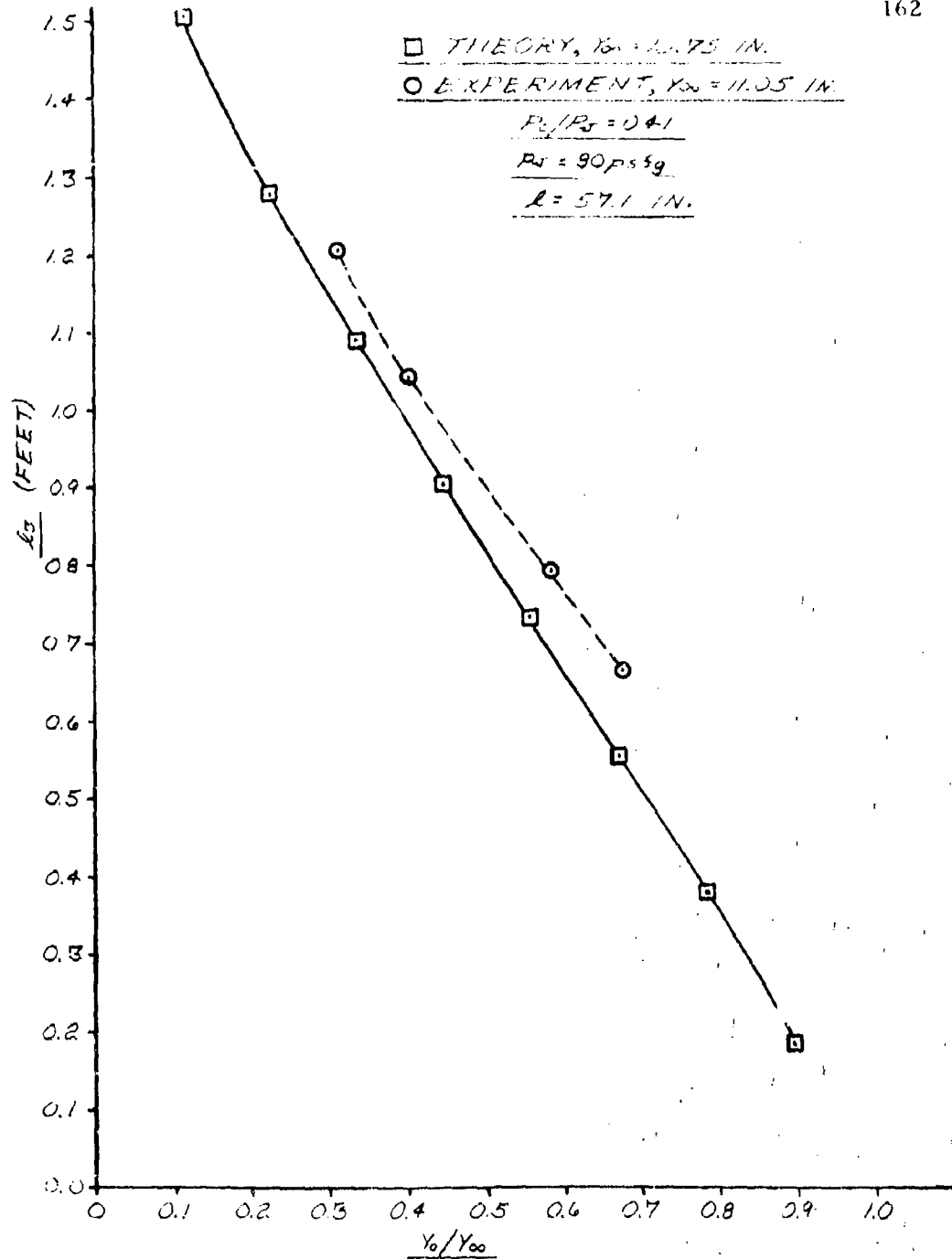
FIGURE 6-6

ℓ_3 vs Y_0/Y_∞ RESULTS, $P_c/P_J = .41$

FIGURE 6-7

analytically predicted values in Figure 6-6. The figure shows that the agreement between theory and experiment is good for $p_c/p_j = 0$.

A second run was made with $p_c/p_j = 0.41$. During this run, the cushion pressure was maintained by introducing flow into the cushion area from a separate air source and venting the resulting cushion flow through the floor of the test section. The resulting values of ℓ_3 versus Y_0/Y_∞ are compared with the analytically predicted values in Figure 6-7. The figure shows good agreement between theory and experiment.

The trunk shape experiments have demonstrated the accuracy of the analytical models developed in Chapter 4 for predicting the trunk low point, the location of the nozzles, trunk shape, the cross-sectional area, and the footprint length.

6.3.2 Flow Characteristics

The results of the tests for leakage flow are shown in Appendix V. The experimentally determined flow coefficient for the trunk orifices (C_X) is given in Appendix VI.

The influence of vehicle (floor) height (H) on p_c/p_j is shown in Table 6-I. This table shows that the pressure ratio (p_c/p_j) is largely independent of the trunk pressure (p_j).

The influence of vehicle height (H) on the jet height-thickness ratio (d/t) is shown in Table 6-II. The results show that the jet height-thickness ratio (d/t) is not strongly dependent on trunk pressure (p_j).

The influence of vehicle height (H) on the pressure coefficient (C_Q) is shown in Table 6-III. The results show that C_Q is largely independent of trunk pressure (p_j). The method by which C_Q was calculated is given in Appendix VII. Since the jet height (d) and pressure coefficient (C_Q) are largely independent of p_j, the presentation of experimental results can be greatly simplified. Table 6-IV shows the average values of the data collected at the various floor heights. These values are assumed to be independent of p_j.

TABLE 6-I

Pressure Ratio (p_c/p_j) vs Vehicle Height (H)
and Trunk Pressure (p_j)

p_j (psig) H (in)	40	60	80	100	120	140	Ave
4.44	.91	.91	.91	.91	.91	.91	.91
5.44	.88	.88	.87	.87	.87	.87	.87
6.44	.82	.82	.82	.82	.82	.82	.82
7.44	.76	.76	.76	.76	.77	.76	.76
8.44	.70	.70	.70	.70	.70	.70	.70
9.44	.60	.61	.60	.61	.61	.61	.61
10.44	.52	.52	.52	.53	.53	.53	.52
11.44	.41	.41	.41	.41	.41	.41	.41
12.44	.28	.28	.28	.28	.29	.29	.28
13.44	.13	.14	.14	.14	.15	.15	.14
13.94	.08	.08	.09	.09	.09	.09	.09

TABLE 6-II

Flow Theory Coefficient (C_Q) vs
Vehicle Height (H) and Trunk Pressure (p_j)

p_j (psfg) H (in)	40	60	80	100	120	140	Ave
4.44	.570	.581	.589	.581	.580	.580	.58
5.44	.670	.665	.675	.672	.667	.673	.67
6.44	.727	.730	.735	.740	.736	.735	.735
7.44	.784	.791	.804	.792	.797	.795	.794
8.44	.824	.830	.830	.825	.828	.825	.828
9.44	.975	.875	.870	.873	.870	.870	.872
10.44	.920	.924	.915	.920	.918	.923	.920
11.44	.942	.950	.950	.948	.953	.953	.950
12.44	.974	.990	.978	.974	.974	.975	.977
13.44	.940	.980	.980	.973	.980	.975	.971
13.94	.975	.985	.982	.983	.981	.978	.982

TABLE 6-III

Jet Height - Thickness Ratio (d/t) vs

Vehicle Height (H) and Trunk Pressure (p_j)

p_j (psig) H (in)	40	50	80	100	120	140	Ave
4.44	.37	.37	.37	.37	.39	.39	.37
5.44	.415	.415	.435	.435	.435	.435	.43
6.44	.46	.47	.48	.50	.50	.50	.48
7.44	.50	.52	.52	.52	.545	.545	.53
8.44	.58	.58	.58	.59	.59	.60	.59
9.44	.62	.62	.63	.64	.64	.64	.63
10.44	.71	.71	.72	.72	.72	.72	.72
11.44	.85	.85	.85	.85	.86	.87	.85
12.44	1.02	1.02	1.03	1.04	1.04	1.04	1.03
13.44	1.59	1.57	1.57	1.57	1.57	1.59	1.58
13.94	2.19	2.17	2.10	2.08	2.08	2.10	2.12

TABLE 6-IV

Calculated Data vs Vehicle Height (H)

H (in)	P_c/P_j	C_Q	d (in)	$\frac{d}{t}$	X_o (in)	y_o (in)
4.44	0.91	0.58	0.17	0.37	23.6	-4.27
5.44	0.87	0.67	0.19	0.43	23.3	-5.24
6.44	0.82	0.73	0.22	0.48	22.4	-6.22
7.44	0.76	0.79	0.24	0.53	21.4	-7.20
8.44	0.70	0.83	0.27	0.59	21.0	-8.17
9.44	0.61	0.87	0.29	0.63	19.8	-9.15
10.44	0.52	0.92	0.33	0.72	18.8	-10.11
11.44	0.41	0.95	0.39	0.85	17.3	-11.05
12.44	0.28	0.98	0.48	1.03	15.7	-11.97
13.44	0.14	0.97	0.72	1.58	14.7	-12.72
13.94	0.09	0.98	0.98	2.12	13.9	-12.97

NOTE:

The above data exhibited slight variations with p_j.

The values shown are mean values over the range of p_j's.
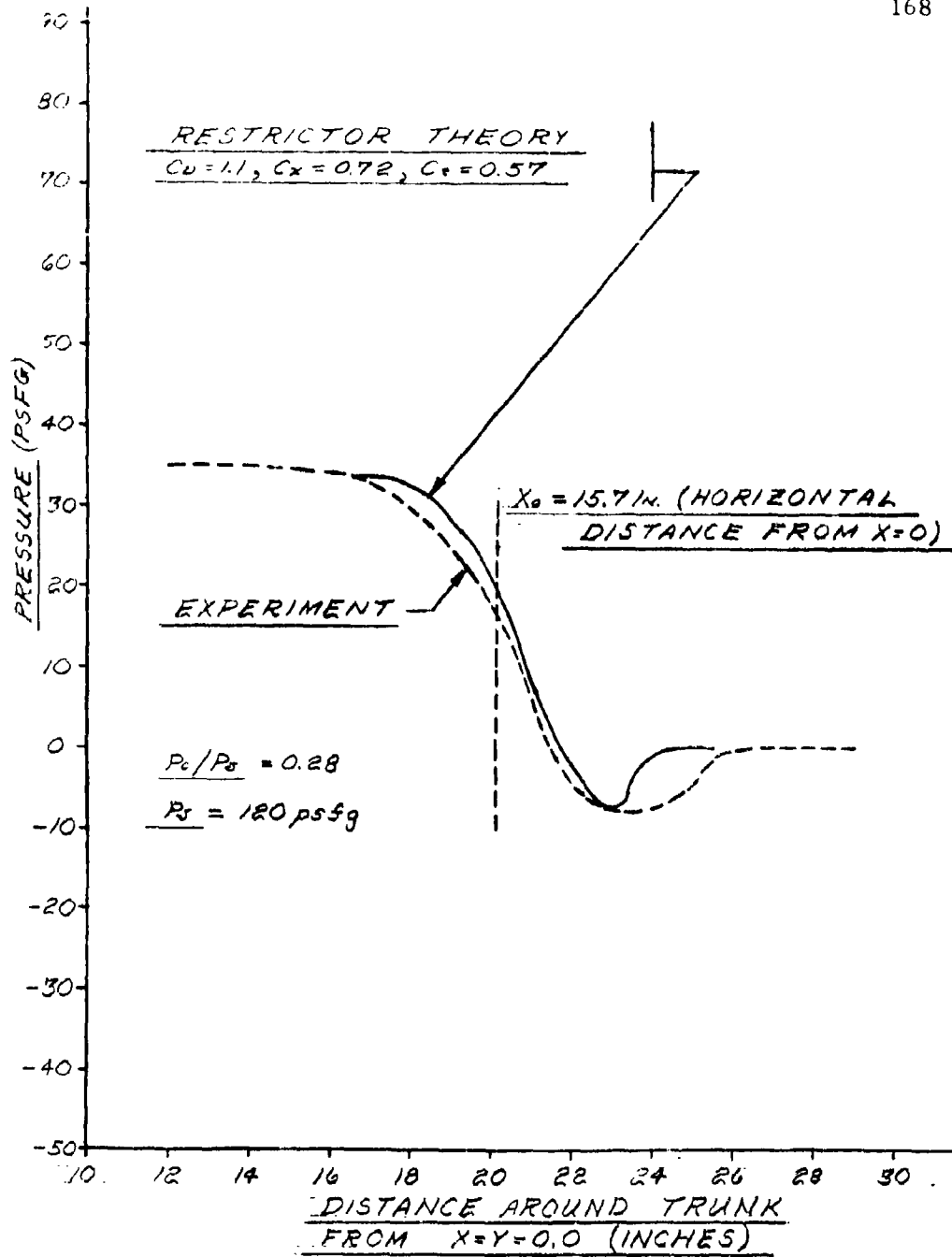
CUSHION EXHAUST PRESSURE DISTRIBUTION, $P_c/P_J = .28$
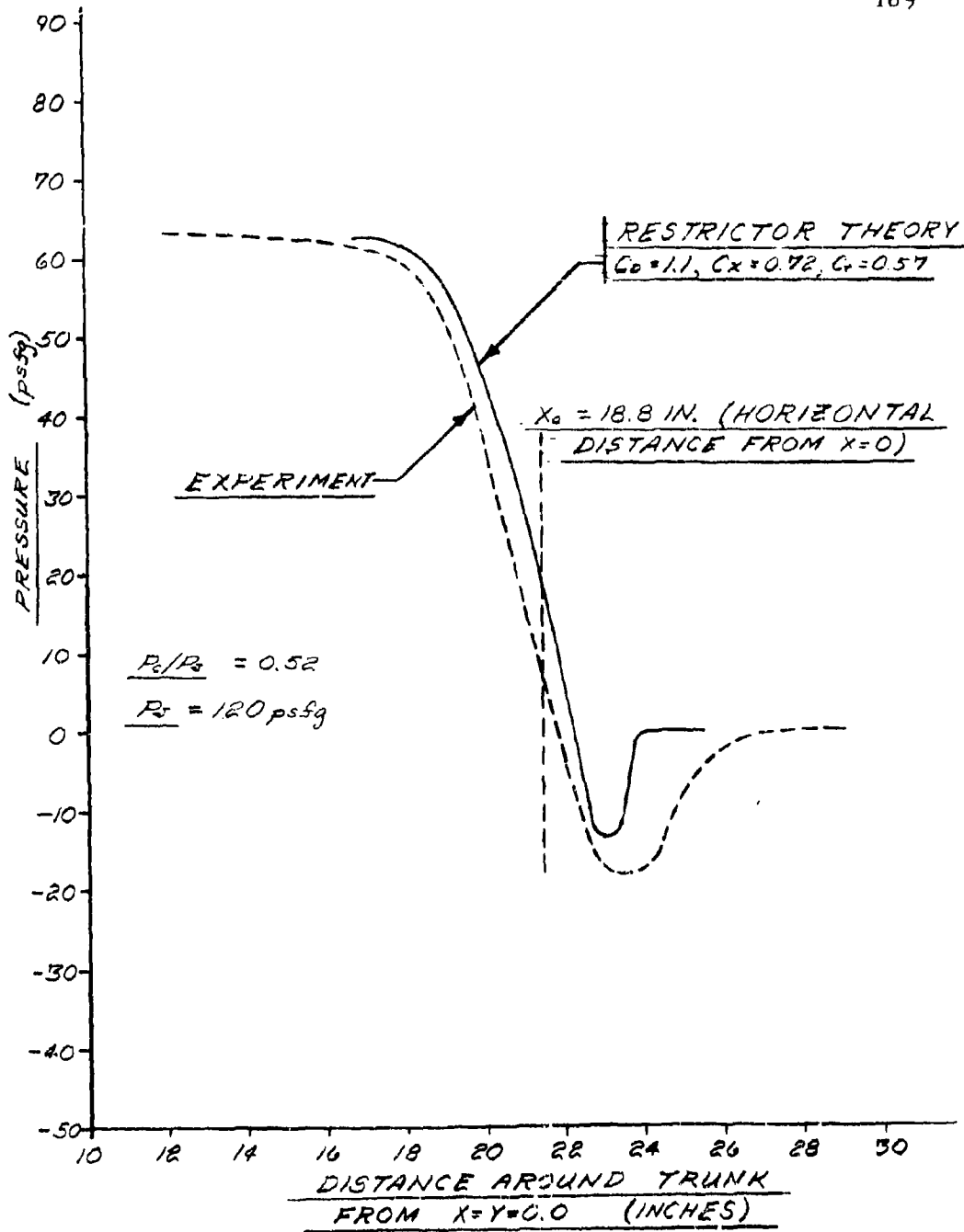
FIGURE 6-8

CUSHION EXHAUST PRESSURE DISTRIBUTION, P_c/P_J = .52
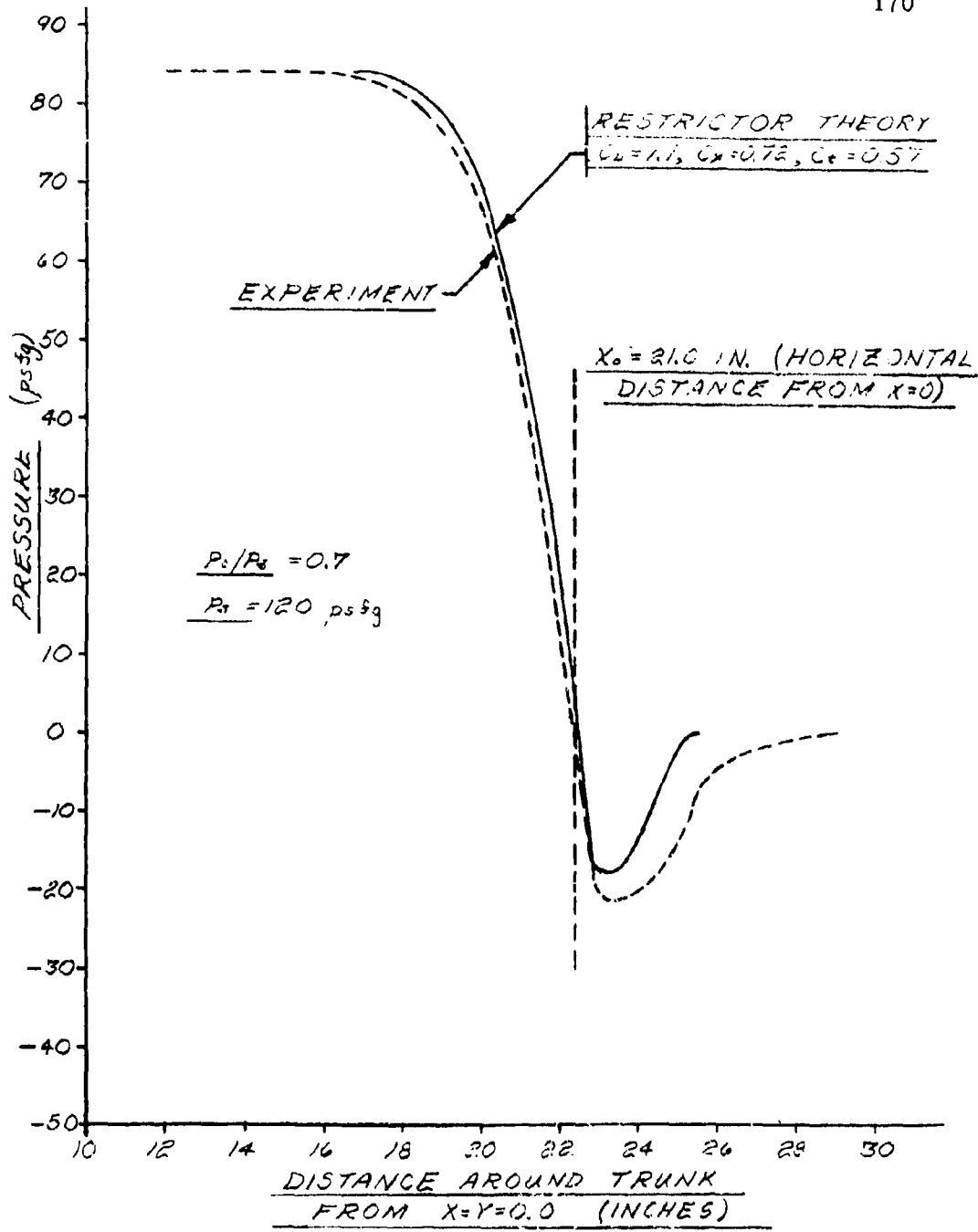
FIGURE 6-9

CUSHION EXHAUST PRESSURE DISTRIBUTION, $P_c/P_j = .7$

FIGURE 6-10

Experimentally measured static pressure distributions along the cushion exhaust nozzle at the trunk surface for the 120 psfg trunk pressure run are shown in Figures 6-8, 6-9, and 6-10. These figures show the pressure distributions for pressure ratios (p_c/p_j) of 0.28, 0.5, and 0.72 respectively.

Values of d/t and C_Q calculated from experimental measurements in the p_j = 120 psfg run are shown in Figures 6-11 and 6-12 respectively.

It was found that the value of C_Q predicted by the distributed jet momentum theories was in reasonable agreement with the experimental results. However, the jet height predicted by the momentum theories was an order of magnitude higher than that observed.

The flow restrictor theory was found to give much better agreement with experimental results. In applying the flow restrictor theory to the experimental model, it was necessary to select values for the three flow coefficients. These coefficients are C_X, C_D, and C_T.

The coefficient C_X is the trunk orifice coefficient. The measurement of this coefficient is discussed in Appendix VI. The values of C_X versus the pressure ratio across the trunk (P_X/P_j) are shown in Figure VI -1 (appendix). When cushion pressure is present, the value of P_X/P_j varies around the trunk. However, since this variation is not large, a constant value of C_X = 0.72 was assumed.

The coefficient C_D is intended to evaluate the efficiency of the convergent-divergent nozzle formed between the trunk and the ground in expanding the flow from the plenum chamber to atmospheric pressure. It may be observed from the pressure distribution curves (Figures 6-8, 6-9, and 6-10) that the pressure at the nozzle exhaust is below atmospheric. The flow in this area is highly complex and beyond reasonable analytical analysis. For the shape tested, the vacuum produced in the nozzle exhaust caused the exhaust velocity to be approximately 10% higher than would have occurred had the minimum pressure been atmospheric. On the basis of these observed results a C_D = 1.1 was selected.

The nozzle area reduction coefficient (C_T) represents the effective reduction in plenum nozzle area caused by the momentum seal formed by the jets from the trunk orifices. The high velocity flow from the trunk orifices results in forcing the plenum flow to follow a circuitous path between the jets. The net result is to reduce the effective plenum exhaust nozzle area.

The value of C_T should be less than 0.76 based upon constant width jets. The width is assumed to be equal to orifice daimeter (5/16") and the minimum distance between jets is 0.965". The value of 0.76 probably represents an upper bound since the effective area reduction is expected to be greater than the projected width of the orifices. A selection of $C_T = 0.57$ gave the best agreement with experimental data.

The computed pressure distributions for the flow restrictor theory using the selected discharge coefficients are shown in Figures 6-8 through 6-10. It may be seen from Figures 6-8, 6-9, and 6-10 that the agreement between experimental and calculated pressure distribution around the trunk is quite good.

The experimental and calculated values for C_Q are shown in Figure 6-11. The flow restrictor theory is shown to give the closest agreement with experiment.

The resulting jet height to thickness ratio (d/t) is shown in. Figure 6-12. Again, agreement between calculated results and experimental data is excellent. Figure 6-12 also shows the predicted values of d/t using the approximate formula (Equation 5-22). The approximate formula gives the correct trend but predicts a lower jet height than is actually observed.

The trunk flow experiments have demonstrated the accuracy of the flow restrictor theory developed in Chapter 5 for predicting the pressure distribution, jet height and flow coefficient of the trunk design under test. The distributed jet momentum theories were unsatisfactory for predicting the jet height for the tested jet configuration.

EXPERIMENT

RESTRICTOR THEORY
$C_D = 1.1, C_x = 0.72, C_t = 0.57$

THIN JET THEORY-
DISTRIBUTED

EXPONENTIAL THEORY-
DISTRIBUTED

DISTRIBUTED JET
SIDE TRUNK
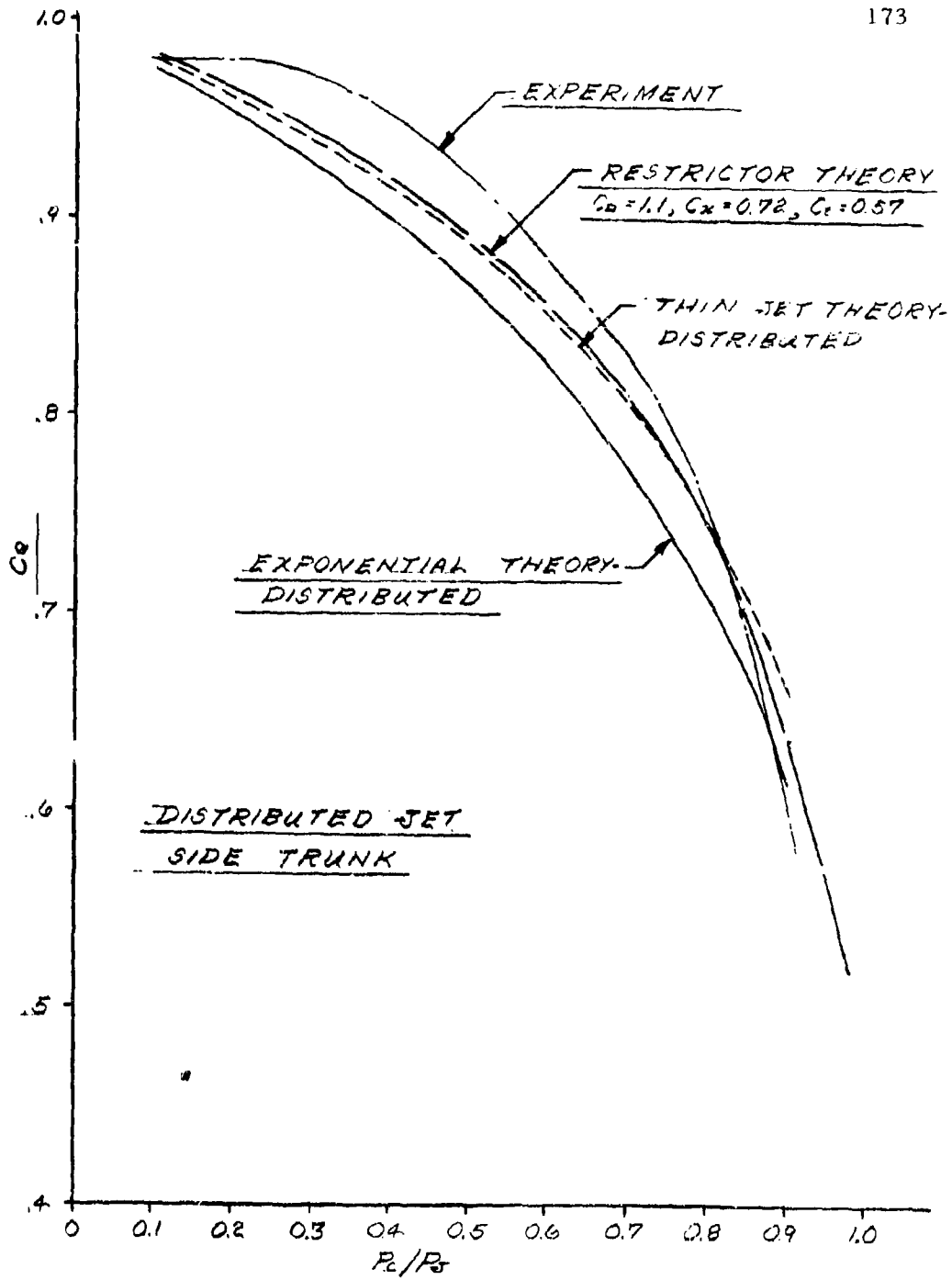
P_c/P_J

C_Q vs P_c/P_J RESULTS
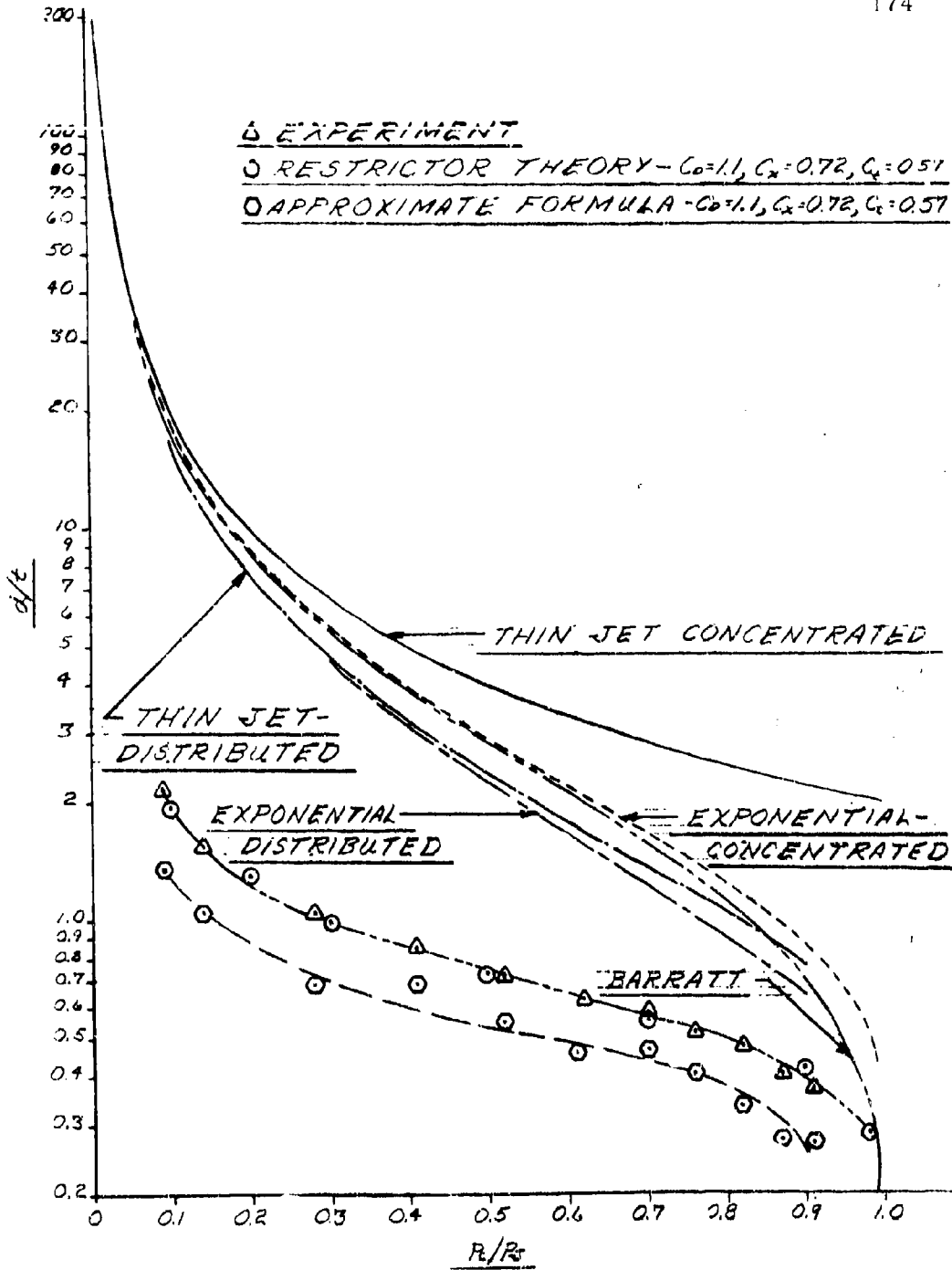
FIGURE 6-11

d/t vs Pc/Pj RESULTS

FIGURE 6-12

7.1 Introduction

The landing gear of an aircraft must have the capacity to absorb the vertical landing energy of the aircraft without overloading the aircraft structure. Two critical parameters in designing the gear are the maximum "g" load and maximum stroke which results from landing at a given weight and sink speed. Consequently, it is desired to predict the load stroke characteristics of the Air Cushion Landing System as functions of aircraft weight and vertical velocity.

The aircraft attitude and forward velocity at touchdown also exert an appreciable influence on the load stroke characteristics of conventional landing gear. For the purposes of the analysis presented in this chapter, these two influences are neglected. The pitch and roll angles at touchdown are assumed to be zero, and the forward velocity is assumed to be negligible.

The system of equations which describe the dynamic response of the ACLS is developed in the following sections. Section 7.2 presents a simplified model of the trunk portion of the system. Section 7.3 presents a more complete model of the trunk, but neglects the effect of pressure build-up in the plenum beneath the aircraft. Section 7.4 presents a model of the combined trunk plenum system.

The variables involved in the analysis are as follows:

A piston area, ft^2

A_g cushion area under the trunk, ft^2

A_h cushion area under the aircraft hard structure, ft^2

A_3 truck footprint area, ft^2

a_D	total exhaust area of nozzles in fan calibration test, ft^2
a_j	total area of orifices in the trunk, ft^2
a_n	area of orifices in the ℓn^{th} segment of the trunk, ft^2
a_3'	effective flow area for the ℓ_3 segment of the trunk, ft^2
C_D	flow coefficient for the cushion exhaust nozzle
C_p	specific heat at constant pressure for air, Btu/lb ^oF
C_Q	flow coefficient for pressure distribution
C_v	specific heat at constant volume for air, Btu/lb ^oF
C_x	flow coefficient for orifices in the trunk
C_y	flow coefficient for jet height
C_z	flow coefficient for jet height
d	jet height, ft
e	distance between lower trunk attachment points, ft
F_j	total vertical thrust from jet exhaust, lb
F_3	total force developed by the trunk footprint, lb
g	acceleration due to gravity, ft/sec^2
g_0	gravitational constant,(lbm/lbf)(ft/sec^2)
h	specific enthalpy, Btu/lb
K_n	effective length for calculating volume of the nth trunk segment from the cross-sectional area A_j, ft
k	ratio of specific heats
L_n	effective length for calculating the footprint area of the nth trunk segment from the footprint length ℓ_3, ft
L_s	length of trunk side segment, ft
M_n	number of rows of holes in the nth trunk segment
$\dot{m}$	mass flow rate, slug/sec
P	pressure in the control volume, lb/ft^2 absolute
P_c	cushion pressure, psfa

p_c	cushion pressure, psfg
P_j	trunk pressure, psfa
p_j	trunk pressure, psfg
Q_c	total flow from cushion, ft^3/sec
Q_i	total flow from fan, ft^3/sec
Q_n	total flow from orifices in the ℓ n^{th} trunk segment, ft^3/sec
Q_r	total fan flow at stall pressure, ft^3/sec
$\overline{R}$	gas constant, Btu/lb $^\circ F$
R_1	radius of curvature for trunk segment ℓ_1, ft
$\overline{r}_n$	radius from center of rotation to centroid of area A_j for n^{th} trunk segment, ft
S_g	effective length for calculating cushion area A_g from length X_o, ft
$S_g{}'$	effective length for calculating the volume V_g from area A_g, ft
S_j	effective length for calculating the trunk volume V_j from area A_j, ft
S_n	effective length of nth trunk segment, ft
S_3	peripheral distance around the trunk at cushion nozzle exhaust, ft
s_n	peripheral distance around the trunk at n^{th} row of orifices, ft
t	effective width of all rows of orifices, ft
t_n	effective width of nth row of orifices, ft
T	absolute temperature, $^\circ R$
T_t	trunk tension per unit length, lb/ft
U	total internal energy of the gas in the control volume, Btu
u	specific internal energy of the gas in the control volume, Btu/lb
V	volume of gas control volume, ft^3
V_c	total cushion volume, ft^3
V_f	volume of ducting between fan and trunk, ft^3
V_n	total volume of the nth trunk segment, ft^3

V_g portion of cushion volume under the trunk, ft

V_h portion of cushion volume under the hard structure, ft

V_j total trunk volume, ft^3

v velocity of the gas, ft/sec

W mass   of gas in control volume, lb

W_A mass   of aircraft, lb

w_i mass   flow into the control volume, lb/sec

w_n mass   flow from the ℓn^{th} segment of the trunk, lb/sec

w_o mass   flow from the control volume, lb/sec

X_o horizontal distance from inside attachment point to inside of the trunk footprint, ft

Y_o vertical distance between the aircraft hard structure and the ground, ft

Y_∞ vertical distance at which no footprint exists ($\ell_3 = 0$), ft

y vertical coordinate, ft

$\dot{y}$ vertical velocity, ft

$\ddot{y}$ vertical acceleration, ft

Greek letters:

α_n angle of revolution for trunk cross-section to form trunk volume segment n, radians

ξ trunk porosity

ρ density of gas, lb/ft^3

ψ_t angle between trunk and ground at edge of footprint, radians

Subscripts:

c   refers to the cushion

e   refers to the end trunk segment

i   refers to flow into the control volume
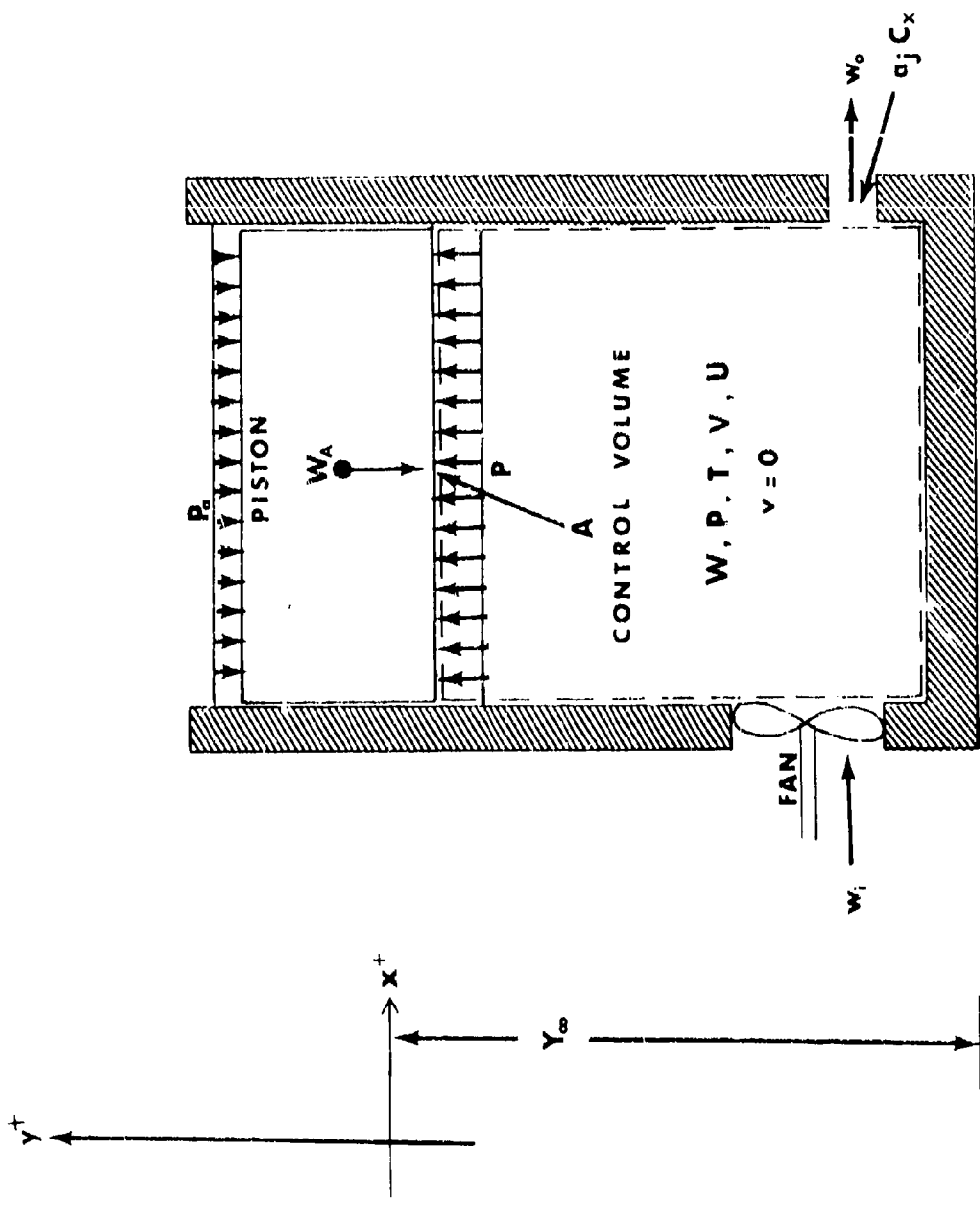
SIMPLE MODEL FOR DYNAMIC ANALYSIS

FIGURE 7-1

j	refers to the trunk
k	refers to the corner trunk segment
n	arbitrary
o	refers to flow out of the control volume
r	refers to stall condition of the fan
s	refers to the side trunk segment
1	refers to the segment ℓ_1
2	refers to the segment ℓ_2
3	refers to the segment ℓ_3

7.2   Simple Dynamic Model

7.2.1   Approach and Assumptions

A greatly simplified model of the air cushion trunk is shown in Figure 7-1. The figure shows an insulated cylinder of gas. The gas is being compressed by a piston falling under the action of gravity. During the compression process, air may enter the control volume from a fan and may leave the volume through an orifice.

The assumptions for the analysis are as follows:

7.2.1.1   Thrust from the exhaust gas is neglected.

7.2.1.2   Adiabatic expansion or compression occurs in the control volume.

7.2.1.3   The change in height of the gas flowing through the control volume is neglected.

7.2.1.4   The enthalpy of the input air equals the enthalpy of the exhaust air.

7.2.1.5   The gas obeys the perfect gas law.

7.2.1.6   The flow through the exhaust orifice is assumed to be adiabatic and incompressible.

7.2.1.7   The velocity of the gas in the control volume is negligible. The static and total pressure are equal.

7.2.1.8   The flow in, Q_i is constant.

The variables involved in this model may be grouped as follows:

Independent environmental variables

g	acceleration due to gravity, ft/sec^2
P_a	atmospheric pressure, lb/ft^2
ρ	atmospheric density, lb/ft^3
k	ratio of specific heats for gas

Independent design variables

A	piston area, ft^2
a_j	orifice area, ft^2
C_x	coefficient of discharge of orifice
Y_∞	distance of origin of coordinate system above ground, ft

Independent operating variables

Q_i	flow from the fan into cylinder, ft^3/sec
W_A	piston weight, lb

Time dependent variables.

$P(t)$	control volume pressure, lb/ft^2
$T(t)$	control volume gas temperature, $^\circ R$
$V(t)$	control volume, ft^3
$W(t)$	control volume gas weight, lb
$y(t)$	piston position, ft
$\dot{y}(t)$	piston velocity, ft/sec

In order to determine the variation of the dependent variables with the time parameter, six independent equations are necessary. These equations may be developed by applying the following laws and principles:

(1) Newton's second law applied to the free piston body in the vertical direction gives:

$$\ddot{y}(t) = f[P(t)]$$

(2) Geometric compatibility applied to the control volume gives:

$$y(t) = f[V(t)]$$

(3) An energy balance applied to the control volume gives:

$$T(t) = f[W(t), V(t), P(t)]$$

(4) The perfect gas law gives:

$$T(t) = f[W(t), V(t), P(t)]$$

(5) The continuity and energy principles applied to flow through the orifice and fan gives:

$$W(t) = f[P(t)]$$

It may be noted that the equation resulting from principles (3) and (4) may be combined to eliminate $\bar{T}(t)$. An additional equation defining $\dot{y}(t) = f[y(t)]$ may be introduced to eliminate $\ddot{y}(t)$ from the relationship in principle (1).

7.2.2   Newton's Second Law

Newton's second law may be applied to the piston shown in Figure 7-1. The result is:

$$\frac{W_A}{g_o} \frac{d^2 y}{dt^2} = -W_A \frac{g}{g_o} + A (P - P_a) \tag{7-1}$$

Equation (7-1) equates the vertical external forces acting on the piston to the product of the mass and acceleration in the vertical direction. The thrust force is neglected (Assumption 7.2.1.1).

7.2.3   Geometric Compatibility

Since the piston area is constant, the relationship between the piston height and the control volume is linear. It is evident from the geometry of Figure 7-1 that:

$$V = A (Y_\infty + y) \tag{7-2}$$

7.2.4   Energy Balance Applied to the Control Volume

To complete the problem, a force (pressure) versus deflection relationship must be derived from thermodynamic considerations. The first law of thermodynamics may be applied to the control volume shown in Figure 7-1 as follows:

change in stored energy = energy in -- energy out + work in + heat in

Based upon Assumptions 7.2.1.2 and 7.2.1.3 the heat in is zero and the change in potential energy of the gas flowing through the cylinder is zero. The energy balance then becomes:

$$\frac{dU}{dt} - (h_i w_i - h_o w_o) + P\frac{dV}{dt} = 0 \tag{7-3}$$

The conservation-of-mass law may be applied to the control volume. The resulting equation equates the change of mass of the gas in the control volume to the difference between in flow and out flow. The results are:

$$\frac{dW}{dt} = w_i - w_o \tag{7-4}$$

The application of Assumption 7.2.1.4 gives:

$$h_i = h_o \tag{7-5}$$

For a perfect gas (Assumption 7.2.1.5), internal energy (u) and enthalpy (h) can be represented as:

$$U = W u \tag{7-6}$$

$$du = C_v dT \tag{7-7}$$

$$h = u + \frac{PV}{W} \tag{7-8}$$

Substituting Equations (7-4) through (7-8) in Equation (7-3) and dividing the resulting equation by $C_v WT$, gives the following results:

$$\frac{dT}{T} = \frac{PV}{C_vWT} \frac{dW}{W} - \frac{P}{C_vWT} dV \qquad (7-9)$$

The perfect gas law and the specific heat definition gives the following relationships:

$$\frac{PV}{WT} = \bar{R} \qquad (7-10)$$

$$\frac{\bar{R}}{C_v} = k - 1 \qquad (7-11)$$

Combining Equations (7-10) and (7-11) yields:

$$\frac{PV}{WTC_v} = k - 1 \qquad (7-12)$$

The substitution of Equations (7-10), (7-11), and (7-12) in Equation (7-9) yields:

$$\frac{dT}{T} = (k-1)\frac{dW}{W} - (k-1)\frac{dV}{V} \qquad (7-13)$$

7.2.5 Perfect Gas Law Applied to the Control Volume

The temperature variable in Equation (7-13) may be eliminated by introducing the perfect gas law. Written in logarithmic form, the perfect gas law is:

$$\ell n\, P + \ell n\, V = \ell n\, W + \ell n\, \bar{R} + \ell n\, T \qquad (7-14)$$

Differentiation of Equation (7 14) gives:

$$\frac{dP}{P} + \frac{dV}{V} = \frac{dW}{W} + \frac{dT}{T}$$

(7-15)

The combination of Equations (7-13) and (7 15) allows the elimination of the temperature variable. The result is:

$$\frac{dP}{P} = k\frac{dW}{W} - k\frac{dV}{V}$$

(7-16)

Expressing Equation (7-16) as a time rate equation gives:

$$\frac{dP}{dt} = P\left(\frac{k}{W}\frac{dW}{dt} - \frac{k}{V}\frac{dV}{dt}\right)$$

(7-17)

Equation (7-17) predicts the time rate of change of the pressure within the control volume as a function of the weight and volume change.

7.2.6   Continuity and Energy Principles Involving
        Gas Flow from the Control Volume

The first law equation (7-17) introduced a new variable: W. A flow equation is needed to express the mass change in the control volume with respect to time. Such a relationship was derived in Section 7.2.4. The resulting equation was:

$$\frac{dW}{dt} = w_i - w_o$$

(7-4)

The exhaust flow through the orifice may be found by applying the continuity principle to the exhaust plane of the nozzle. The result is:

$$w_o = \rho_o \, v_o \, a_j \, C_x \tag{7-18}$$

The velocity v_o and density ρ_o of the exhaust gas at the nozzle throat may be determined from isentropic flow relationships. The results are:

$$v_o = \sqrt{\frac{2PV}{W} \, g_o \left[1 - \left(\frac{P_a}{P}\right)^{\frac{k-1}{k}} \right] \left(\frac{k}{k-1}\right)}$$

$$\rho_o = \rho \, (P_a/P)^{1/k}$$

These results may be substituted into Equation (7-19) to predict the exhaust flow from the orifice. However, for small pressure differences across the exhaust nozzle, the compressibility of the gas may be neglected. In the present investigation, pressure differences of less than two pounds per square inch are involved. Consequently, the Assumption (7.2.1.6) of incompressible subsonic flow in the exhaust nozzle was made. The static pressure and total pressure of the gas in the control volume were assumed to be equal (Assumption 7.2.1.7).

For incompressible flow, the velocity at the exhaust exit plane is:

$$v_o = \sqrt{\frac{2g_o}{\rho} \, (P - P_a)} \tag{7-19}$$

Combining Equations (7-18) and (7-19) gives:

$$w_o = \sqrt{2g_o \, \frac{W}{V} \, (P - P_a)} \; a_j \, C_x \tag{7-20}$$

Equation (7-20) predicts the flow from an exhaust nozzle for small pressure differences across the nozzle. For large pressure difference ratios (pressure ratios less than 0.9), Equation (7-20) should be modified to account for compressibility.

The weight flow into the control volume was assumed to be constant. The resulting relationship is:

$$w_i = \rho Q_i \tag{7-21}$$

Combining Equations (7-4), (7-20) and (7-21) gives:

$$\frac{dW}{dt} = Q_i \rho - \sqrt{2g_o \frac{W}{V} (P-P_a)} \; a_j \; C_x \tag{7-22}$$

7.2.7 Summary of Equations

The system of equations which describes the simple dynamic model may be summarized as follows:

Definition of velocity

$$\frac{dy}{dt} = \dot{y} \tag{7-23}$$

Newton's second law:

$$\frac{d\dot{y}}{dt} = -g \; + \frac{A}{W_A} \; g_o (P-P_a) \tag{7-1}$$

First law of thermodynamics:

$$\frac{dP}{dt} = P \left(\frac{k}{W} \frac{dW}{dt} - \frac{k}{V} \frac{dV}{dt} \right) \tag{7-17}$$

Conservation of mass:

$$\frac{dW}{dt} = \rho Q_i - \sqrt{2g_o \frac{W}{V} (P - P_a)} \; a_j \, C_x \qquad (7\text{ }22)$$

Geometric compatibility:

$$V = A \, (Y_\infty + y) \qquad (7\text{-}2)$$

The above set of linear, first order, differential equations may be solved by numerical procedures using the Runge and Kutta algorithm.[47]

7.3   Air Cushion Trunk Dynamic Analysis

7.3.1   Approach and Assumptions

The simplified analysis developed in Section 7.2 may be applied to the Air Cushion Landing System by the introduction of a few complications. The performance of the trunk alone is considered in this section. Under this condition, cushion pressure is not allowed to build up beneath the fuselage. The configuration for the analysis is shown in Figure 7-2. The assumptions made in Section 7.2.1 are modified as follows:

7.3.1.1 $p_c/p_j = 0$

7.3.1.2   Only vertical motion is considered.

7.3.1.3   Thrust from the exhaust gas is included.

7.3.1.4   Elasticity of the trunk material is neglected.
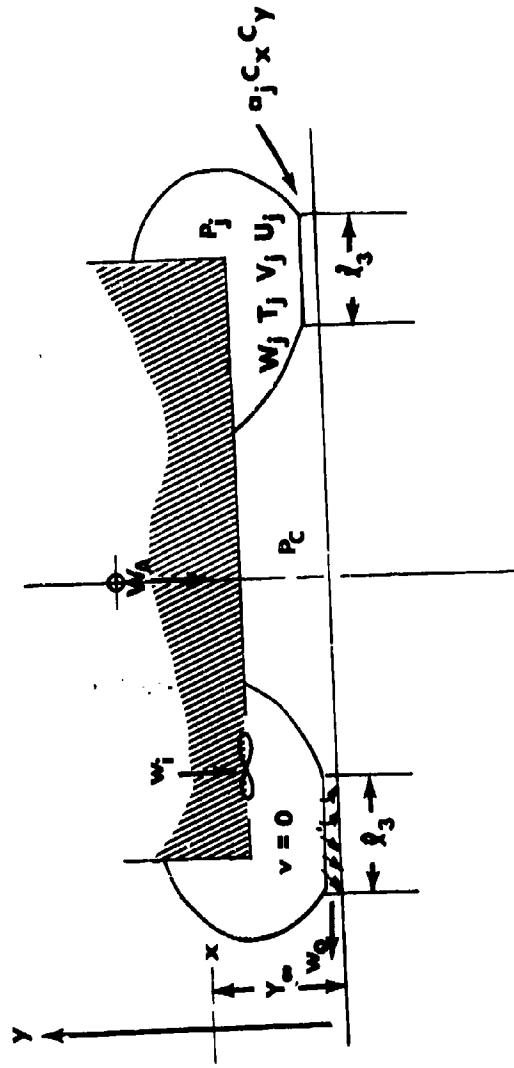
MODEL FOR TRUNK DYNAMIC ANALYSIS

FIGURE 7-2

7.3.1.5   The flow in, Q_i, is a known function of P_j.

7.3.1.6   The distance above the ground at which the trunk begins to influence the dynamic response of the aircraft is designated Y . More precisely, Y_∞ is the point above the ground at which A_3 = 0.

7.3.1.7   The coordinate system is selected as shown in Figure 7-2 such that y = 0 at distance Y_∞ above the ground. With this selection, the following relationship holds: Y_o = −y for all y ⩽ 0.

7.3.1.8   The fan speed is assumed to be constant.

It may be noted that there are five major differences between the simple model of Section 7.2 and that of the air cushion trunk. These differences are as follows:

(1)   The trunk model has a thrust force acting upward due to the change in momentum of the exhaust gas.

(2)   The footprint (piston) area (A_3) is not a constant, but is a function of y.

(3)   The control volume is a nonlinear function of Y rather than a simple linear function.

(4)   The effective area of discharge of the orifice is not a constant, but is a function of y.

(5)   The flow from the fan (Q_i) is not a constant, but rather a function of trunk pressure (p_j).

Corrections have been incorporated in the simple model analysis to compensate for the differences listed above. These corrections are summarized in the discussion to follow.

7.3.2 Correction for Thrust

The thrust may be included by applying Newton's second law to the free body shown in Figure 7-2. The result is:

$$\frac{W_A}{g_0} \frac{d^2 y}{dt^2} = -W_A \frac{g}{g_0} + A_3 (P_j - P_a) + F_j \tag{7-24}$$

The vertical thrust is equal to the rate of change in momentum in the y direction. By assuming the velocity of the gas in the trunk is negligible it is possible to write:

$$F_j = \left| \dot{m} v \right|_y = \frac{\rho}{g_0} Q_j v_j C_z = \frac{\rho}{g_0} v_j^2 a_j C_x C_y C_z \tag{7-25}$$

where:

C_x = coefficient of discharge for the trunk orifices

C_y = coefficient to compensate for the dependence of the discharge coefficient on y, and

C_z = coefficient to compensate for the various orifice angles.
(Not all of the exhaust velocity is in the vertical direction.)

Values of these coefficients are determined in Sections 8.2, 8.4, and 8.3, respectively. The expression for velocity, Equation (7-19), may be substituted into Equation (7-25) to give:

$$F_j = 2 (P_j - P_a) a_j C_x C_y C_z \tag{7-26}$$

Equation (7-26) may be substituted into Equation (7-24) to give:

$$\frac{W_A}{g_0} \frac{d^2 y}{dt^2} = -W_A \frac{g}{g_0} + A_3 (P_j - P_a) + 2 (P_j - P_a) a_j C_x C_y C_z \tag{7-27}$$

Equation (7-27) equates the sum of the vertical forces on the aircraft (weight, footprint pressure and thrust) to the product of the aircraft mass and the vertical acceleration. This equation provides the required correction for jet thrust.

7.3.3   Correction for Footprint Area

The footprint area (A_3) may be determined analytically from the values of footprint length (ℓ_3) predicted by the computer program developed in Section 4.5. It was noted in Section 4.5 that ℓ_3 is dependent on the trunk length ℓ, the attachment points (a,b) and on p_c/p_j and Y_0. It is evident from Figure 4-8 that different sections of the trunk on an actual model have different attachment points and trunk lengths. However, it is possible to separate the trunk into a number of segments which have approximately the same trunk length and attachment points. If the effective length of the nth segment is L_n and there are a total of m segments, the total footprint area is:

$$A_3 = \sum (\ell_3)_n L_n \tag{7-28}$$

Equation (7-28) predicts the total footprint area of the trunk as the sum of the footprint areas of all the trunk segments. The footprint length ℓ_3 is a known function of Y_0 and p_c/p_j. For the case considered in this section, $p_c/p_j = 0$. The variation of ℓ_3 with

Y_o for $p_c/p_j = 0$ was shown in Figures 4·21 and 4·22. The former figure is for a side trunk segment and the latter is for an end trunk segment.

The value of l_n is a constant for straight trunk segments such as the side segment shown in Figure 4·8. However, for curved segments such as the end segment shown in Figure 4·8, L_n is dependent on p_c/p_j and Y_o. This dependence may be calculated from the computer program given in Appendix III. Using the above procedure, it is possible to determine A_3 as a function of Y_o for the trunk on a given model.

7.3.4   Correction for Trunk Volume Change

The trunk volume (V_j) may be determined analytically from the values of cross-section area (A_j) predicted by the computer program developed in Sections 4.5 and 4.6 The trunk may be divided into a number of segments in a manner similar to that described in Section 7.3.3. If the effective length of the nth segment is K_n and there are a total of m segments, the total trunk volume is:

$$V_j = \sum (A_j)_n K_n \qquad (7·29)$$

The trunk segment cross-sectional area (A_j) is a known function of Y_o and p_c/p_j. The variation of A_j with Y_o for $p_c/p_j = 0$ was shown in Figures 4·23 and 4·24. The former figure is for a side trunk segment and the latter is for an end trunk segment.

The value of K_n is constant for straight trunk segments such as the side trunk segment shown in Figure 4·8. However, the end trunk segment is a volume of revolution. For a volume of revolution, the effect length may be defined as follows:

$$K_n = \bar{r}_n a_n \qquad (7·30)$$

where

$\bar{r}_n$ = radius from the center of revolution to the centroid of the area A_j for the nth trunk segment

a_n = angle of revolution for the volume of the nth trunk segment

The values of $\bar{r}_n$ and a_n may be calculated from the geometry of the particular model and trunk segment.

Using the above procedure it is possible to determine A_j as a function of Y_0 for the trunk on a given model.

7.3.5   Correction for Variable Discharge Area

As the trunk is pressed against the ground, the flow from trunk exhaust orifices in the footprint area is reduced. A discharge coefficient, C_y, has been introduced to account for the resulting dependence of the trunk exhaust flow on the vehicle height (Y_0).

The resulting flow relationship is:

$$Q_j = \sqrt{\frac{2g_0}{\rho} (p_j)} \; a_j C_x C_y \tag{7-31}$$

where C_y is a function of Y_0.

The value of C_y is determined by computing the flow from the various trunk segments ℓ_1, ℓ_2, and ℓ_3 shown in Figure 4-2. The resulting flows are designated Q_1, Q_2, and Q_3, and may be computed as follows:

$$Q_1 = \sqrt{\frac{2g_0}{\rho} (p_j)} \; a_1 C_x \tag{7-32}$$

$$Q_2 = \sqrt{\frac{2g_0}{\rho}(p_j)} \; a_2 \, C_x$$

(7-33)

$$Q_3 = \sqrt{\frac{2g_0}{\rho}(p_j)} \; a_3' \, C_x$$

(7-34)

$$Q_j = Q_1 + Q_2 + Q_3$$

(7-35)

The values of a_1 and a_2 are determined by the total trunk orifice area in segments ℓ_1 and ℓ_2 respectively. The value of a_3' is determined by the area which controls the flow from trunk segment ℓ_3.

If the area between the trunk and the ground is less than the trunk orifice area a_3, then flow is controlled by the ground clearance rather than by the trunk area. Consequently, the effective flow area for segment ℓ_3 may be written:

$$a_3' = \left\{ \begin{array}{c} a_3 \\[2ex] 2S_3 \, d \dfrac{C_D}{C_x} \end{array} \right\} \qquad \text{whichever is smaller}$$

(7-36)

The value of a_3 may be approximated by the product of the footprint area (A_3) and the porosity of the trunk ξ in the footprint area. The result is:

$$a_3 = A_3 \xi$$

(7-37)

The porosity of the trunk ξ is defined as the ratio of orifice area to total area in the section of the trunk containing the orifices.

The total jet area of the trunk is the sum of the area in the three segments.

$$a_j = a_1 + a_2 + a_3 \tag{7-38}$$

An expression for C_y is obtained by combining Equations (7-31), (7-32), (7-33), (7-34), and (7-35). The result is:

$$C_y = \frac{a_1 + a_2 + a_3'}{a_j} \tag{7-39}$$

It is evident from Equation (7-39) that $C_y = 1.0$ whenever $a_3' = a_3$.

The equation for C_y may be further simplified by substituting Equations (7-37) and (7-38) into (7-39). The result is:

$$C_y = \frac{a_j - A_3 \xi + a_3'}{a_j} \tag{7-40}$$

In Equation (7-40), a_j and ξ are constants. A_3 is a known function of Y_o as developed in Section 7.3.3. The value of a_3' was defined as follows:

$$a_3' = \left\{ \begin{array}{c} A_3 \xi \\ \\ 2 S_3 d\, C_D / C_x \end{array} \right\} \quad \text{whichever is less} \tag{7-36}$$

The values of S_3, C_x, and C_D are constants. The value of d is dependent on a number of variables including Y_o. An assessment of the value of d is presented in the remainder of this section.

An estimate of the jet height d variation with Y_0 has been made based upon an analysis conducted by Han[49], of idealized flow in a channel with injection from a porous wall. In his analysis, Han determined the pressure distribution in a channel of the configuration shown in Figure 7-3. The independent variables for this analysis were d, ℓ_3, P_j, and ξ. The latter quantity is the effective wall porosity and may be expressed by the ratio a_3/A_3. The total vertical force per unit length which is developed in the footprint area can be determined by integrating the pressure over the footprint length. Using a trunk pressure of 80 psf and the porosity value for the model side trunk given in Table 5-I, the footprint force was determined as a function of jet height and footprint length. The results are plotted in Figure 7-4.

Figure 7-4 presents the load-deflection characteristics of the jet for various footprint lengths. The actual jet height is determined by the load which the jet must support for a given trunk configuration.

A free body diagram of a trunk configuration is shown in Figure 7-5. Force equilibrium applied in the y direction gives:

$$p_j \ell_3 - F_3 - 2 T_t \sin \psi_t = 0 \tag{7-41}$$

The value of T_t was given by Equation (4-1).

$$T_t = R_1 p_j \tag{4-1}$$

Combining Equations (7-41) and (4-1) gives:

$$F_3 = p_j (\ell_3 - 2 R_1 \sin \psi_t) \tag{7-42}$$
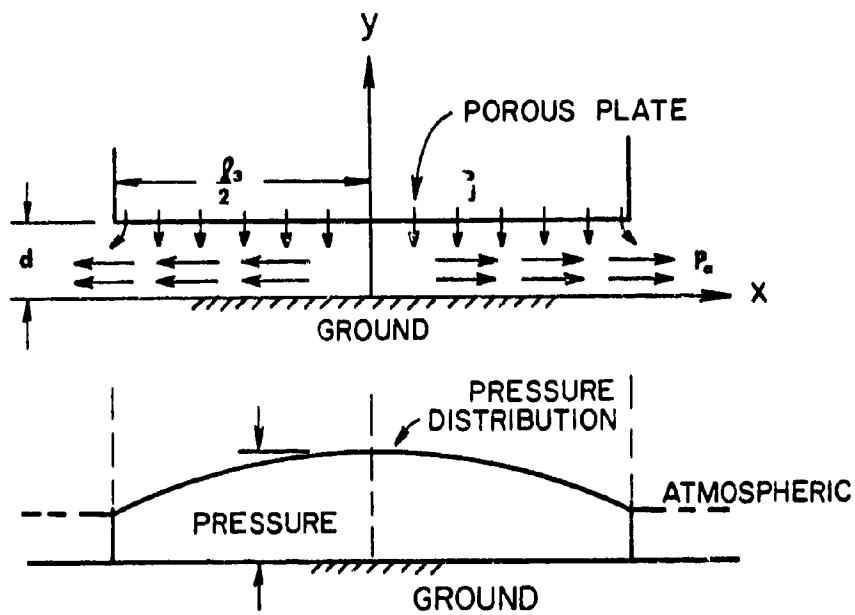
MODEL FOR PRESSURE DISTRIBUTION
ACROSS THE FOOTPRINT

FIGURE 7-3
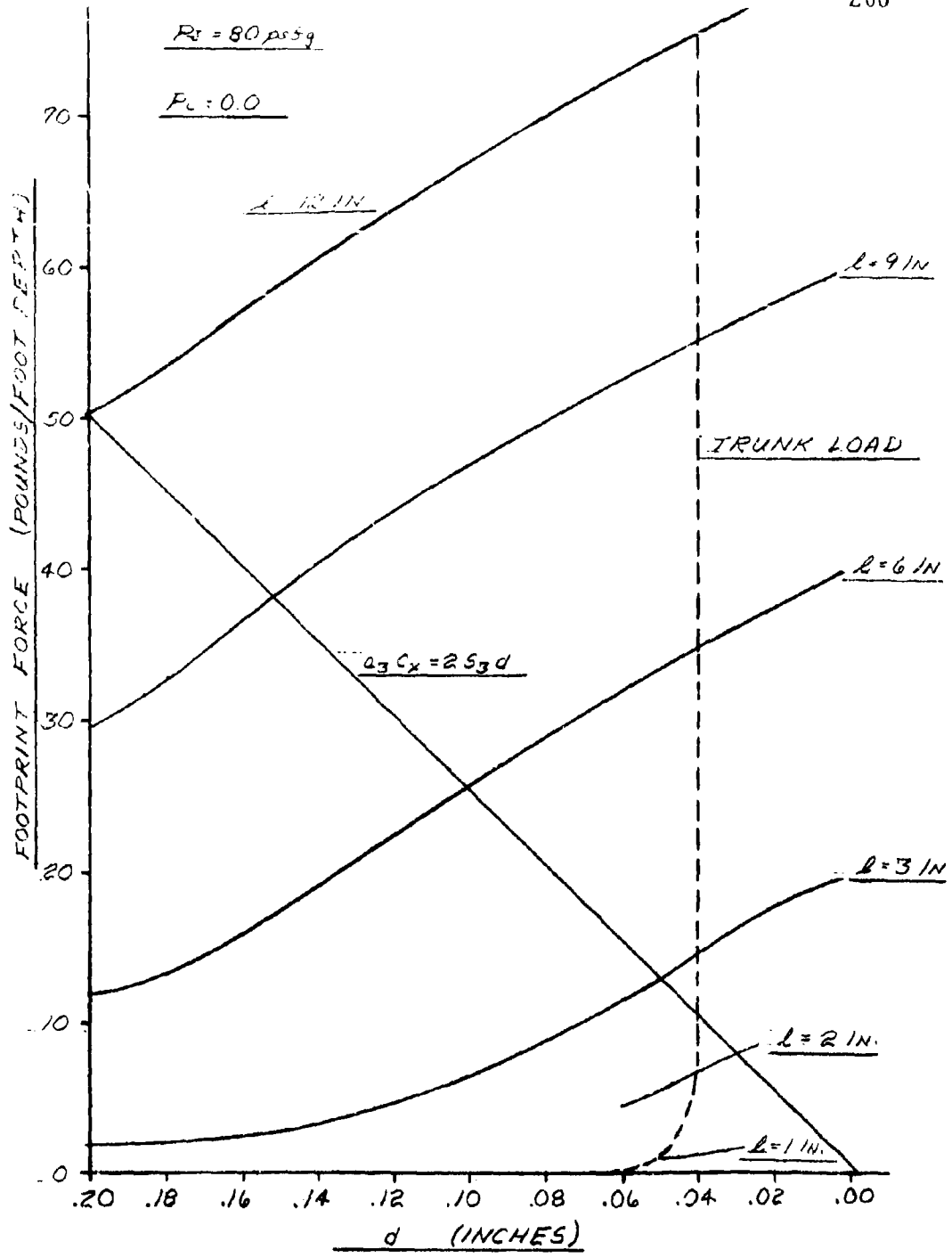
LOAD-DEFLECTION CHARACTERISTICS
OF THE CUSHION EXHAUST GAP

FIGURE 7-4
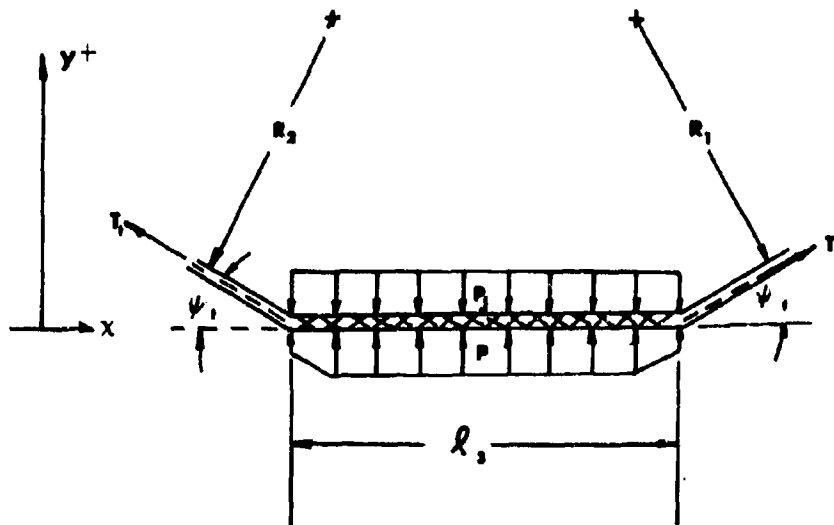
$$F_3 = S \int P \, dx$$

FREE BODY DIAGRAM FOR TRUNK FOOTPRINT
FIGURE 7-5

For the analysis of the trunk shape presented in Section 4.5, ψ_t was assumed to be zero. However, this analysis was made for a trunk section with free edges. A trunk on a three-dimensional model is constrained by the curvature of the trunk in the peripheral direction. Consequently, it is possible for a finite angle to exist at the edge of the footprint. Such an angle has been observed on a three-dimensional model. A value of $\psi_t = 4^O$ constant gives reasonable agreement with observed results on the dynamic model. Using the assumed value of ψ_t, the values of F_3 computed from Equation (7-42) are shown as the load line on Figure 7-4.

The jet heights at which $a_3 = 2S_3d$ are also shown on the curve. From the results presented in Figure 7-4, it is assumed that d = constant for values of ℓ_3 greater than about 2 inches.

7.3.6 Correction for Flow from the Fan

The flow from the fan is dependent upon the fan speed and the exhaust pressure. This variation may be determined by standard fan calibration tests. Such a test is described in Section 8.6 and the test results are shown in Figure 8-3.

For the purposes of this analysis, the fan speed is assumed to be constant during landing impact (Assumption 7.3.1.7).

7.3.7 Summary of Equations

The changes required to apply the system of equations developed in Section 7.2 to the air cushion trunk system have been developed in Sections 7.3.1 through 7.3.6. The resulting equations may be summarized as follows:

Definition of velocity

$$\frac{dy}{dt} = \dot{y}$$

<div align="right">(7-23)</div>

Newton's second law

$$\frac{d\dot{y}}{dt} = \frac{g_o}{W_A}\left[-W_A\ \frac{g}{g_o} + A_3\ (P_j - P_a) + 2\ (P_j - P_a)\ a_j\ C_x\ C_y\ C_z \right]$$ (7-27)

First law of thermodynamics

$$\frac{dP_j}{dt} = P_j\left(\frac{k}{W_j}\ \frac{dW_j}{dt}\ -\ \frac{k}{V_j}\ \frac{dV_j}{dt} \right)$$ (7-43)

Conservation of mass

$$\frac{dW_j}{dt} = \rho\ Q_j\ -\ \sqrt{2g_o\ \frac{W_j}{V_j}\ (P_j - P_a)}\ \ a_j\ C_x\ C_y$$ (7-44)

Geometric compatibility

$$V_j\ =\ \sum\ (A_j)_n\ K_n$$ (7-29)

In the system of equations, there are five dependent variables: $\dot{y}$, y, P_j, V_j, and W_j. The following variables are known and constant: W_A, g_o, P_a, a_j, C_x, C_z, k, ρ, K_n, g. The following variables are known functions of the dependent variables:

$A_3\ =\ f(Y_o)$ as developed in Section 7.3.3.

$A_j\ =\ f(Y_o)$ as developed in Section 7.3.4.

$C_y\ =\ f(Y_o)$ as developed in Section 7.3.5.

$Q_j\ =\ f(P_j)$ as developed in Section 7.3.6.
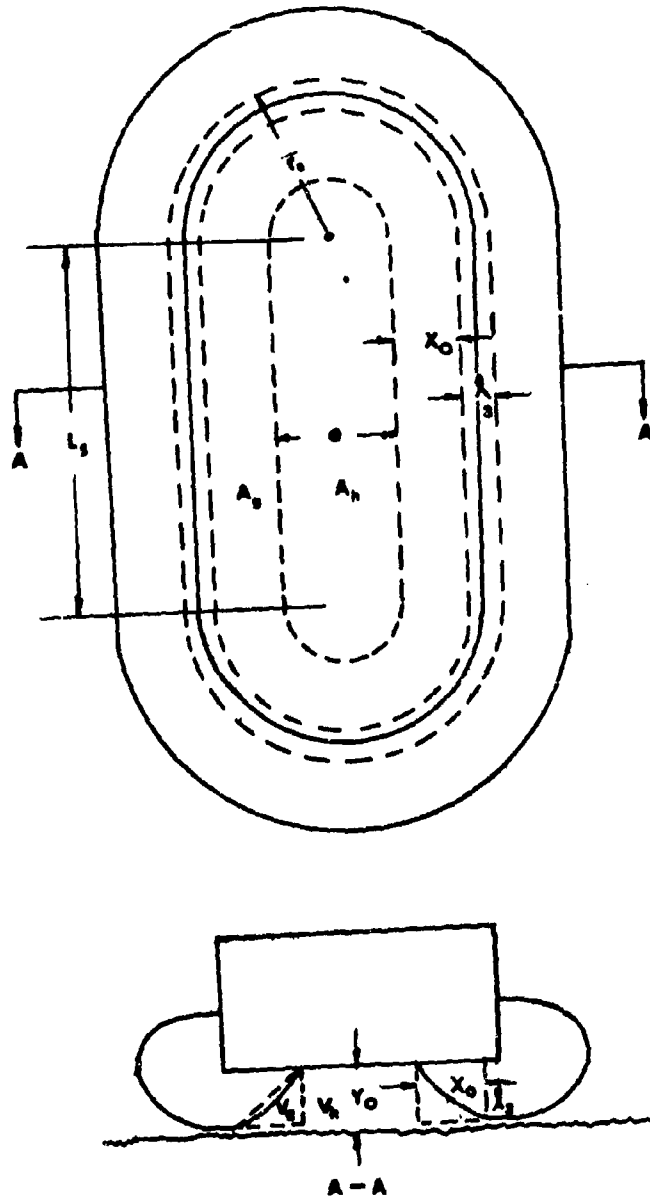
MODEL FOR AIR CUSHION SYSTEM DYNAMIC ANALYSIS

FIGURE 7-6

The system of equations and functions described in this section has been programmed and solved on a digital computer using the Runge and Kutta algorithm.[47] The computer results have been compared with experimental results in Chapter 8.

7.4   Complete Air Cushion System Dynamic Analysis

7.4.1   Approach and Assumptions

The analysis developed in Sections 7.2 and 7.3 may be applied to the complete air cushion system by introducing relationships to account for the effect of cushion pressure on the system response. The configuration for the analysis is shown in Figure 7-6. The assumptions made in Section 7.3.1 are modified as follows:

7.4.1.1   The cushion pressure is allowed to build up so that $p_c/p_j \neq 0$.

7.4.1.2   The model is of the type shown in Figure 7-6. The trunk cross section is the same at any section.

7.4.1.3   The trunk configuration is identical to the side trunk whose properties were listed in Table 5 I.

A number of additional simplifying assumptions are included in the sections to follow.

The equations of motion developed in Section 7.3 may be applied to a complete cushion-trunk system by the introduction of corrections for cushion pressure.

The necessary corrections are as follows:

(1)   Correction of the second law equation for the reaction force from the cushion pressure.

(2)   Prediction of the area over which the cushion pressure acts.

(3)   Prediction of the cushion pressure.

(4)   Prediction of the cushion volume.

(5)   Prediction of the cushion flow.

(6)   Prediction of the influence of cushion pressure on trunk flow.

(7)   Prediction of the influence of cushion pressure on trunk footprint area.

(8)   Prediction of the influence of cushion pressure on trunk volume.

(9)   Prediction of the influence of cushion pressure on vertical thrust.

These corrections have been developed in the sections to follow.

7.4.2   Cushion Reaction

The cushion pressure reaction may be included in the second law equation, Equation (7-27), by the introduction of an additional force term. The resulting equation is:

$$\frac{W_A}{g_o} \frac{d^2 y}{dt^2} = -W_A \frac{g}{g_o} + A_3 (P_j - P_a) + A_c (P_c - P_a) + F_j \qquad (7\text{-}45)$$

Equation (7-45) equates the sum of the vertical forces on the aircraft (weight, footprint force, cushion force and thrust) to the product of the mass and the vertical acceleration.

7.4.3   Cushion Support Area

The cushion support area (A_c) is a function of both Y_0 and p_c/p_j. Figure 7-6 shows that the cushion area may be divided into two parts -- A_h and A_g. The A_h part is the area under the hard structure which is enclosed by the inner trunk attachment. This area is constant. The A_g part is the area between the inner trunk attachment and the inner ground tangent. This area is dependent on the width X_0 and the effective length S_g. The total cushion area may be written as the sum of the parts as follows:

$$A_c = A_h + S_g X_0 \qquad\qquad (7\text{-}46)$$

The value of A_h is constant, and S_g may be considered constant for small changes in X_0. The value of X_0 is dependent on Y_0 and p_c/p_j. The relationship between these variables has been determined for a straight section of trunk with unconstrained edges using the computer program described in Appendix III. The results for the side trunk section are shown in Figure 7-7. The carpet plot in Figure 7-7 shows constant lines of p_c/p_j and ℓ_3.

It is evident from Figure 7-7 that for a given ℓ_3, the trunk low point X_0 moves outward with increasing (p_c/p_j) thereby increasing the cushion support area. On the other hand, it is evident that decreasing Y_0 at constant p_c/p_j causes an increase in the footprint length (ℓ_3). The increase in footprint length, in turn, results in a decrease in X_0 and an attendant decrease in cushion support area.

During a landing impact, the energy absorption process starts at the point defined by $\ell_3 = 0$ and $p_c/p_j = 0$. For the case when $p_c = 0$, the process proceeds along the $p_c/p_j = 0$
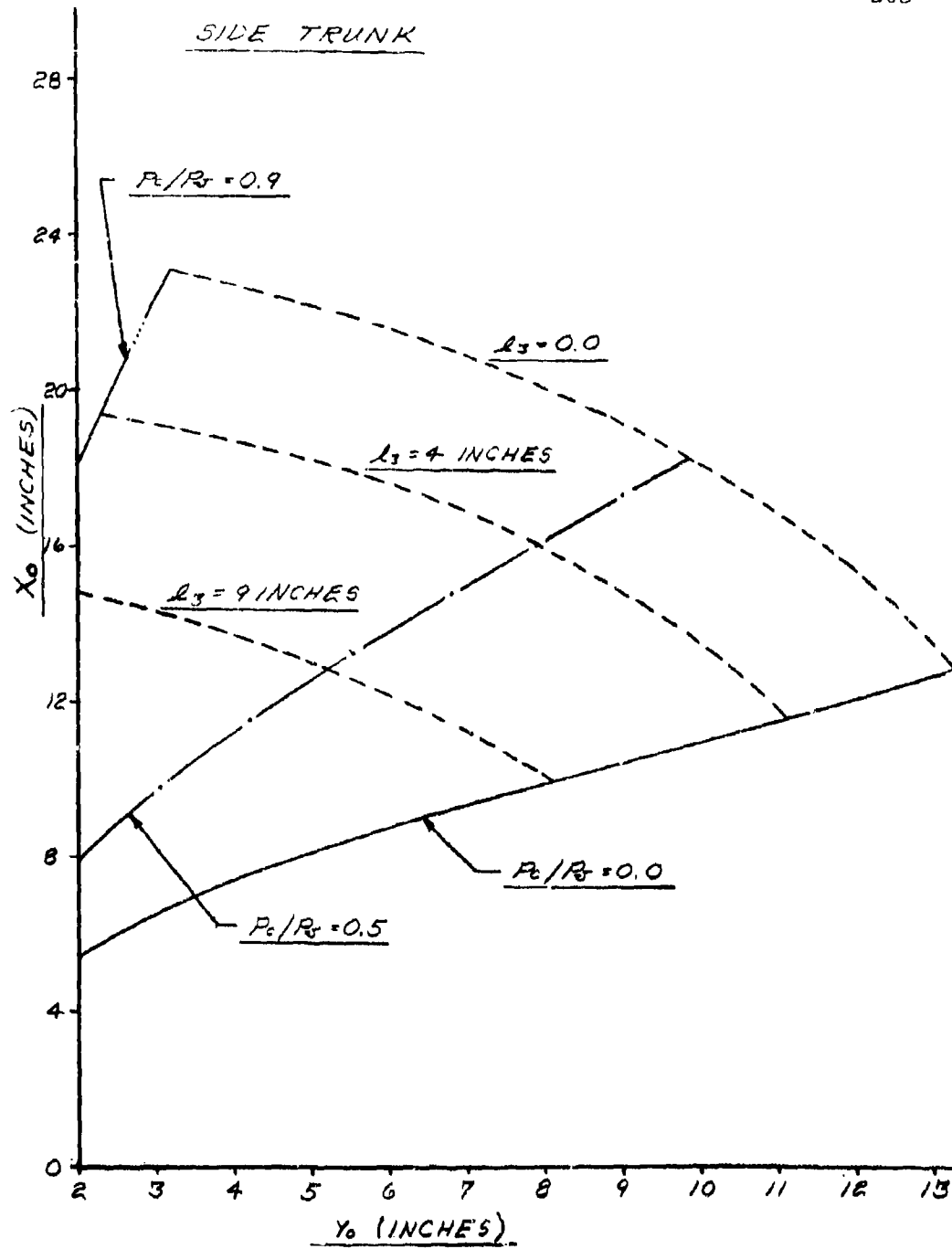
X_0 vs Y_0 FOR MODEL TRUNK

FIGURE 7-7

lines. On the other hand, for the case when the change in Y_0 is slow and the weight is supported only by the cushion pressure, the process follows the $\ell_3 = 0$ line. An actual impact process follows a path somewhere between these two extremes.

It should be noted that Figure 7-5 is for a trunk section with free ends. For a trunk on an actual model, there are no free ends. The trunk closes on itself as shown in Figure 7-6. In order for X_0 to increase with increasing p_c/p_j, the trunk must stretch along circumferential length S_q. The degree of constraint which results depends upon the elasticity of the material and the shape of the model. As a consequence, caution should be exercised in applying the free shape curves to an actual model. However, such curves are valuable in making approximations for the relationships among the variables.

In view of the offsetting influences of p_c/p_j and ℓ_3 on the value of X_0, a first approximation of $X_0 =$ constant is reasonable for the trunk shape shown in Figure 7-6.

7.4.4   Cushion Pressure Prediction

The cushion pressure equation may be developed in a manner identical to that presented in Sections 7.2.4 and 7.2.5. The resulting equation is:

$$\frac{dP_c}{dt} = P_c \left(\frac{k}{W_c} \frac{dW_c}{dt} - \frac{k}{V_c} \frac{dV_c}{dt} \right) \tag{7-47}$$

Equation (7-47) predicts the cushion pressure change with time as a function of the change of volume and change in weight of the gas in the cushion. In order to predict the cushion pressure, it is necessary to predict the volume and weight change of the cushion air.

7.4.5   Cushion Volume Prediction

The cushion volume is a function of Y_0, ℓ_3, and p_c/p_j. However, as in the case of the cushion support area, the influence of p_c/p_j and ℓ_3 tend to offset each other.

The cushion volume on the air cushion model shown in Figure 7-6 is considered to be composed of two parts — the portion directly under the hard structure (V_h) and the portion directly under the flexible trunk (V_g).

The volume under the hard structure (V_h) is a linear function of Y_o and is independent of p_c/p_j. The equation for this portion of the volume is:

$$V_h = \Lambda_h Y_o \tag{7-48}$$

The volume under the trunk is more difficult to calculate. For the purposes of simplification, a triangular cross section of V_g is assumed. Figure 7-6 shows that the altitude and base of the triangle have lengths of Y_o and X_o respectively. If the triangular area is assumed to be constant around the trunk, the portion of the cushion volume under the trunk is computed as follows:

$$V_g = \frac{1}{2} X_o Y_o S_g' \tag{7-49}$$

The variable S_g' is defined as the effective length for calculating the volume from the cross-sectional area. Figure 7-6 shows that the volume V_g consists of straight sections along the sides. However, the two ends, taken together, form a volume of revolution. The effective length for the two side volumes is $2L_s$. The effective length for the end volumes is the distance from the center of rotation to the centroid of the triangular area times the angle of revolution. The resulting equation for S_g' is:

$$S_g' = 2L_s + 2\pi \left(\frac{e}{2} + \frac{X_o}{3} \right) \tag{7-50}$$

The relationship between X_o and Y_o was shown in Figure 7-5 and discussed in Section 7.4.3. As a first approximation, X_o = constant is a reasonable assumption.

Combining Equations (7-48), (7-49), and (7-50) gives the following equation for the cushion volume:

$$V_c = \left\{ A_h + X_o \left[L_s + \pi \left(\frac{e}{2} + \frac{X_o}{3} \right) \right] \right\} Y_o \tag{7-51}$$

In Equation (7-51) the variables A_h, L_s, and e are assumed constant. A relationship of the type given in Figure 7-7 may be used to relate X_o to Y_o. However, as a first approximation, X_o = constant is assumed.

7.4.6 Cushion Flow Prediction

In a manner similar to the analysis developed in Section 7.2.6, the conservation of mass law may be written for the cushion:

$$\frac{dW_c}{dt} = (w_c)_i - (w_c)_o \tag{7-52}$$

All flow into the cushion cavity comes from the orifices in segment ℓ_2 of the trunk. This segment is shown in Figure 4-2. The total area of orifices in segment ℓ_2 is a_2. The flow into the cushion from the trunk may be written:

$$(w_c)_i = (sign) \sqrt{2g_o \rho \left| (P_j - P_c) \right|} \; a_2 C_x = w_2 \tag{7-53}$$

The sign on the radical in Equation (7-53) takes the same sense as the quantity (P_j-P_c). This convention is necessary because it is possible during dynamic impact for P_c to exceed P_j. The direction of flow is, of course, from the higher pressure to the lower pressure.

The value of a_2 may be determined by summing the area of all the orifices in segment ℓ_2. The total number of rows of orifices in segment ℓ_2 is designated as M_2. Each row has an effective thickness t_n and a length s_n. The total area a_2 is written:

$$a_2 = \sum t_n s_n \tag{7-54}$$

In Equation (7-54) the values of s_n and t_n are known constants. The value of M_2 is dependent on p_c/p_j and Y_o. This dependence has been determined using the computer program listed in Appendix III. The results are presented in Figure 7-8.

The flow out of the cushion is through the cushion exhaust nozzle. This flow may be expressed:

$$(w_c)_o = \sqrt{2g_o \rho (P_c - P_a)} \; S_3 \, d \, C_D \tag{7-55}$$

In Equation (7-55), g_o, ρ, S_3 and C_D are assumed constant. The variation of d is determined as discussed in Section 7.3.5.

An expression for the cushion flow may be written by combining Equations (7-52), (7-53), and (7-55). The result is:

$$\frac{dW_c}{dt} = w_2 - \sqrt{2g_o \rho (P_c - P_a)} \; S_3 \, d \, C_D \tag{7-56}$$

7.4.7 Influence of Cushion Pressure on Trunk Flow

The flow into the trunk is dependent only on trunk pressure and fan speed. No modification to the fan flow relationship is necessary to correct for the effect of cushion pressure.

SIDE TRUNK

FREE TRUNK SHAPE

$P_c/P_t = 0.7$ $P_c/P_t = 0.5$ $P_c/P_t = 0.0$

M_2

Y_0 (FEET)
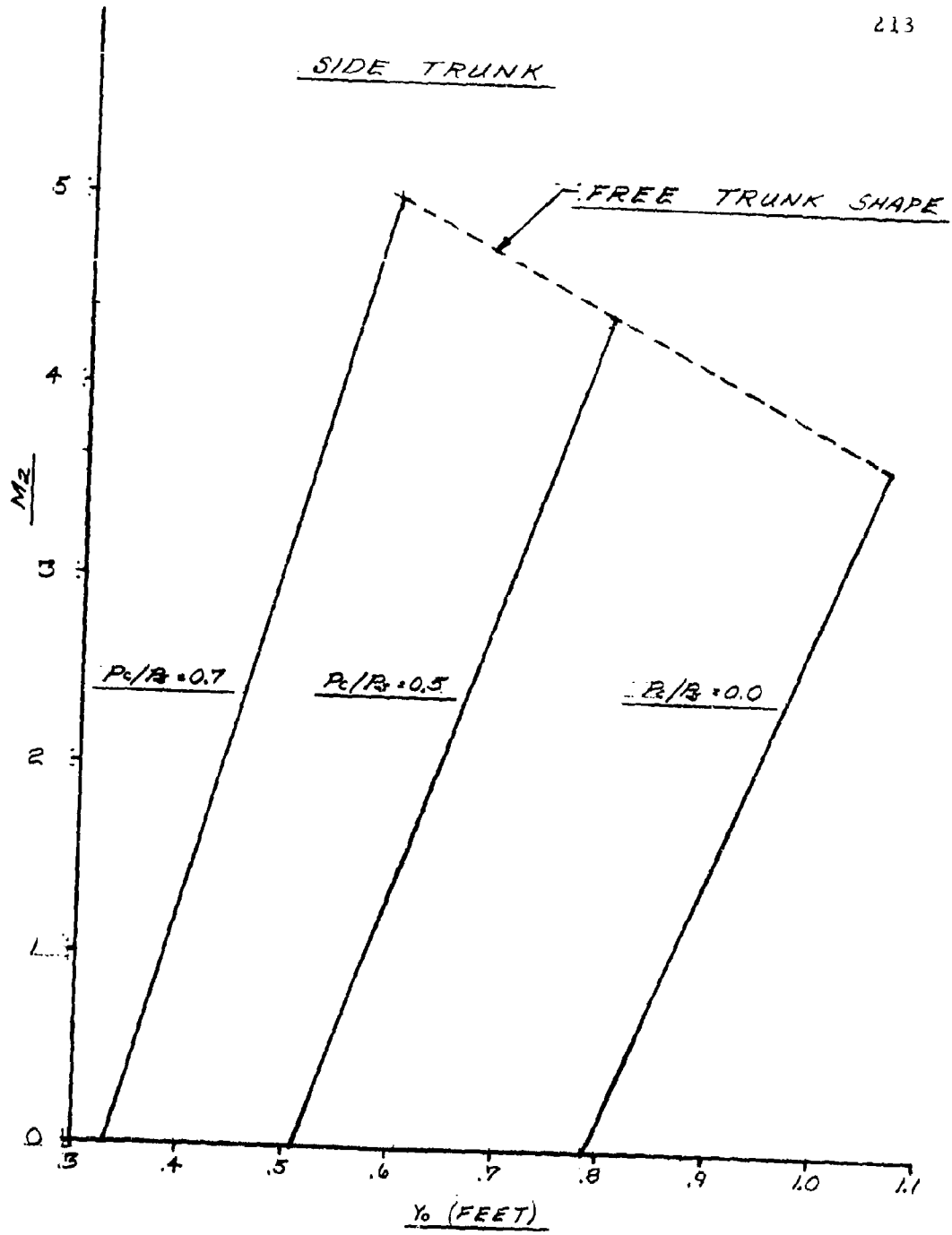
M_2 vs Y_0 FOR MODEL TRUNK

FIGURE 7-8

The flow from the trunk is influenced by the cushion pressure. The nozzle in trunk segment ℓ_2 exhausts to cushion pressure rather than atmospheric. The exhaust from the trunk segment ℓ_3 expands to P_c on the inside and P_a on the outside.

The flow from the trunk may be written as the sum of the flow from the three segments.

$$(w_j)_o = w_1 + w_2 + w_3 \qquad (7\text{-}57)$$

The flow from segment ℓ_1 exhausts to atmospheric pressure.

$$w_1 = \sqrt{2g_0\, \rho\, (P_j - P_a)}\ \ a_1\, C_x \qquad (7\text{-}58)$$

The flow from segment ℓ_2 exhausts to cushion pressure.

$$w_2 = \sqrt{2g_0\, \rho\ \left| (P_j - P_a) \right|}\ \ a_2\, C_x \qquad (7\text{-}59)$$

The sign for w_2 is positive when $p_j > p_c$ and negative when $p_c < p_j$.

The flow from segment ℓ_3 is assumed to exhaust to atmospheric pressure.

$$w_3 = \sqrt{2g_0\, \rho\, (P_j - P_a)}\ \ a_3{'}\, C_x \qquad (7\text{-}60)$$

The value of $a_3{'}$ is determined by the area which controls the flow from the trunk segment ℓ_3. The area $a_3{'}$ may be expressed:

$$a_3{'} = \left\{ \begin{array}{c} A_3\, \xi \\[2mm] S_3\, d\dfrac{C_D}{C_x} \end{array} \right\} \qquad \text{whichever is less} \qquad (7\text{-}61)$$

In Equations (7-58) through (7-60) the independent variables are P_j and P_c. The variables a_1, a_2, and a_3 are dependent on Y_o and p_c/p_j. The value a_1 may be determined by rearranging Equation (7-38).

$$a_1 = a_j - a_2 - a_3 \qquad (7\text{-}38)$$

where a_j is constant.

The values of a_2 and a_3 were determined in Sections 7.4.6 and 7.3.5 by Equations (7-54) and (7-37), respectively.

The value of a_3' is determined by the same method discussed in Section 7.3.5.

7.4.8 Influence of Cushion Pressure on Trunk Footprint Area

The influence of p_c/p_j on trunk footprint length for a side trunk section with free edges is shown in Figure 4-21. For the $p_c = 0$ case, the relationship between ℓ_3 and Y_o is given by the $p_c/p_j = 0$ curve. Higher values of p_c/p_j tend to decrease ℓ_3 for a given Y_o.

The total footprint area of the model shown in Figure 7-6 may be computed as the sum of the area of the side sections and the area of the end sections. The resulting equation is:

$$A_3 = L_s \ell_3 + \pi \left[\left(\frac{e}{2} + X_o + \ell_3 \right)^2 - \left(\frac{e}{2} + X_o \right)^2 \right] \qquad (7\text{-}62)$$

In Equation (7-62), L_s and e are constants. As a first approximation, X_o is assumed constant. The variation of ℓ_3 with Y_o and p_c/p_j is given in Figure 4-21.
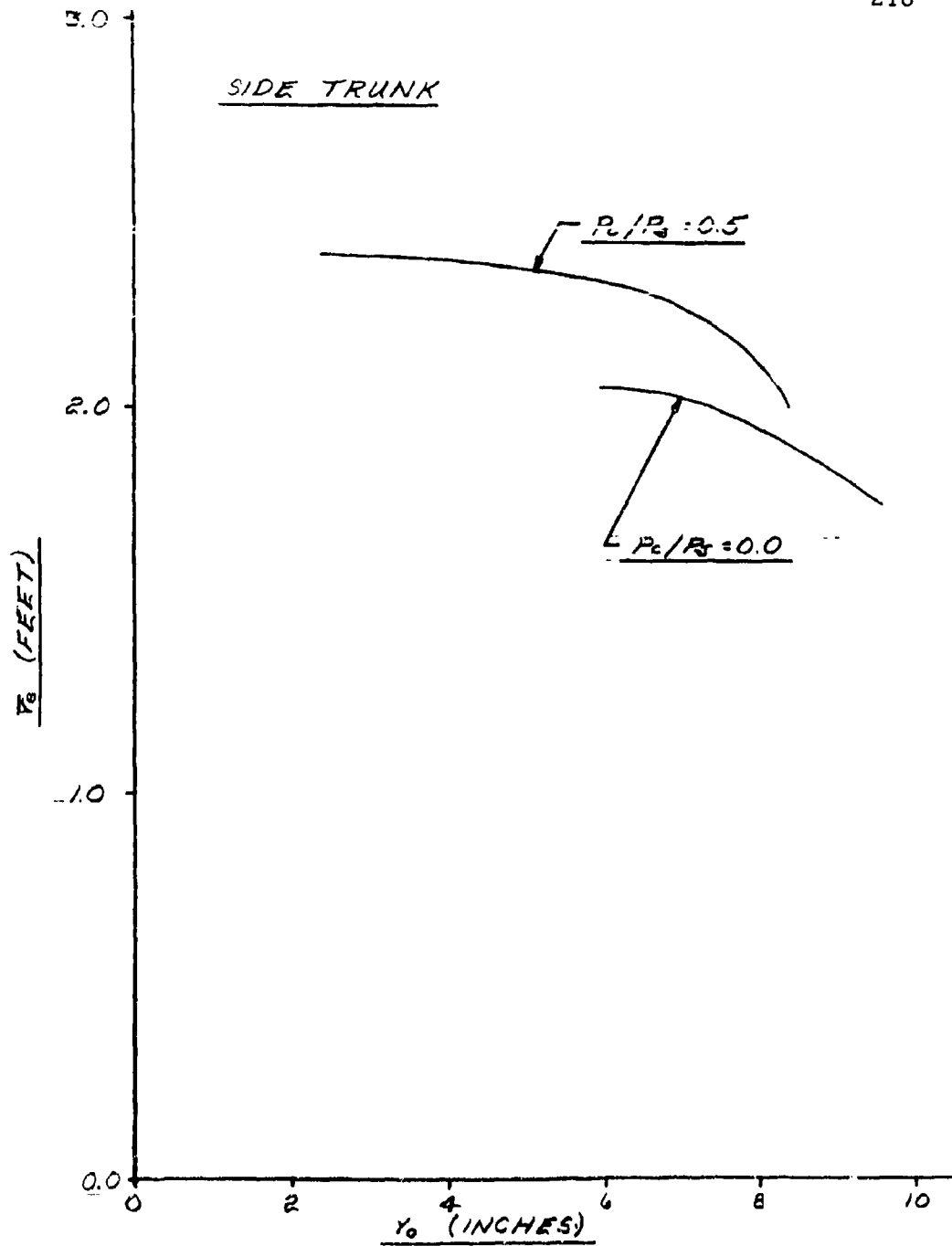
CENTROIDAL RADIUS vs TRUNK
HEIGHT FOR MODEL TRUNK
FIGURE 7-9

7.4.9 Influence of Cushion Pressure on Trunk Volume

The influence of p_c/p_j on trunk cross-sectional area for a side trunk section with free edges is shown in Figure 4-23. For the $p_c = 0$ case, the relationship between A_j and Y_0 is given by the $p_c/p_j = 0$ curve. Higher values of p_c/p_j tend to decrease ℓ_3 for a given Y_0.

The total trunk volume is the product of the trunk cross-sectional area (A_j) and the effective trunk length (S_j).

The effective length for the two sides is $2L_s$. The effective length for the two ends is the product of the distance from the center of revolution to the area centroid and the angle of revolution. The resulting equation for the trunk volume is:

$$V_j = (2L_s + 2\pi \, \bar{r}_e) \, A_j \qquad (7\text{-}63)$$

In Equation (7-63), L_s is constant. The centroidal distance $\bar{r}_e$ and the cross-sectional area A_j are dependent on both p_c/p_j and Y_0. The dependence of these variables has been shown in Figures 7-9 and 4-23, respectively.

7.4.10 Influence of Cushion Pressure on Thrust

The presence of cushion pressure reduces the exhaust velocity from the rows of orifices in the ℓ_2 segment of the trunk. The effect of this reduction may be approximated by adjusting Equation (7-26) to account for the cushion pressure across the ℓ_2 segment. The resulting equation is:

$$F_j = [(P_j - P_c) \, a_2 + (P_j - P_a) \, (a_j - a_2) \, C_y] \, C_x \, C_z \qquad (7\text{-}64)$$

7.4.11 Summary of Equations

The changes required to apply the system of equations developed in Section 7.3 to the complete air cushion system have been developed in this section. The resulting

equations may be summarized as follows:

Definition of velocity

$$\frac{dy}{dt} = \dot{y} \qquad (7\text{-}23)$$

Newton's second law

$$\frac{d\dot{y}}{dt} = \frac{g_0}{W_A} \left[-W_A \frac{g}{g_0} + A_3 (P_j - P_a) + A_c (P_c - P_a) + F_j \right] \qquad (7\text{-}45)$$

First law of thermodynamics

$$\frac{dP_j}{dt} = P_j \left(\frac{k}{W_j} \frac{dW_j}{dt} - \frac{k}{V_j} \frac{dV_j}{dt} \right) \qquad (7\text{-}43)$$

$$\frac{dP_c}{dt} = P_c \left(\frac{k}{W_c} \frac{dW_c}{dt} - \frac{k}{V_c} \frac{dV_c}{dt} \right) \qquad (7\text{-}47)$$

Conservation of mass law

$$\frac{dW_j}{dt} = \rho \, Q_i - [w_1 + w_2 + w_3] \qquad (7\text{-}44)$$

$$\frac{dW_c}{dt} = w_2 - \sqrt{2g_0 \frac{W_c}{V_c} (P_c - P_a)} \; S_3 d \, C_D \qquad (7\text{-}56)$$

Geometric compatibility

$$V_j = (2L_s + 2\pi \bar{r}_e) A_j \qquad (7\text{-}63)$$

$$V_c = \left\{ A_h + X_0 \left[L_s + \pi \left(\frac{e}{2} + \frac{X_0}{3} \right) \right] \right\} Y_0 \tag{7-51}$$

In the system of equations there are eight dependent variables: y, $\dot{y}$, P_j, P_c, W_j, W_c, V_j, and V_c. The following variables are known and constant: W_A, g_0, P_a, k, S_3, C_D, L_s, A_h, X_0, e, C_x, and C_z.

The following variables are known functions of the dependent variables:

$$F_j = \left[(P_j - P_c) a_2 + (P_j - P_a)(a_j - a_2) \right] C_y C_x C_z \tag{7-64}$$

$$Y_0 = -y \quad \text{for } y < 0 \quad \text{Assumption 7.3.1.7}$$

$$A_c = A_h + S_g X_0 \tag{7-46}$$

$$A_3 = 2L_s \ell_3 + \left[\left(\frac{e}{2} + X_0 + \ell_3 \right)^2 - \left(\frac{e}{2} + X_0 \right)^2 \right] \pi \tag{7-62}$$

$$w_1 = \sqrt{2g_0 \, W_j/V_j \, (P_j - P_a)} \quad a_1 C_x \tag{7-58}$$

$$w_2 = (\text{sign}) \sqrt{2g_0 \frac{W_j}{V_j} (P_j - P_c)} \quad a_2 C_x \tag{7-59}$$

where the sign takes the same sense as the quantity $(P_j - P_c)$.

$$w_3 = \sqrt{2g_0 \frac{W_j}{V_j} (P_j - P_a)} \quad a_3' \, C_x \tag{7-60}$$

Ω_i $\quad = f(P_j)$ as developed in Section 7.4.7.

C_y $\quad = f(Y_o)$ as developed in Section 7.3.5.

a_1 $\quad = f(Y_o, p_c/p_j)$ as developed in Section 7.4.7.

a_2 $\quad = f(Y_o, p_c/p_j)$ as developed in Section 7.4.7.

a_3' $\quad = f(Y_o, p_c/p_j)$ as developed in Section 7.4.7.

d $\quad = f(Y_o)$ as developed in Section 7.4.7.

$\bar{r}_e$ $\quad = f(Y_o, p_c/p_j)$ as developed in Section 7.4.9.

A sufficient amount of information has been developed in this section to allow the prediction of the dynamic response of the complete air cushion landing system. Such a solution would require development of the functional relationships described above for a particular model. These relationships can be developed from analytical predictions by a procedure similar to that described in Chapter 8.

8. EXPERIMENTAL PROGRAM — DYNAMIC MODEL

8.1   Experimental Apparatus - Dynamic Tests

Figure 8-1 shows the test apparatus used for verification of the dynamic model developed in Cahpter 7. The apparatus consisted of three units — a hydraulic power supply, a dynamic model, and a test platform.

Hydraulic power was supplied by a Sun Electric MK-3 Aircraft Hydraulic System Test Stand capable of delivering 0 to 30 gpm at variable pressures up to 5,000 psig. The hydraulic power delivered to the dynamic model was regulated by controlling the flow rate pressure of the hydraulic fluid which was piped by flexible hoses to the model.

A drawing of the dynamic model is shown in Gifure 4-8 and its dimensions are summarized in Table 8-1. The air source for the model was a centrifugal fan powered by a hydraulic motor. The fan and motor were connected by v-belts. The fan speed was 3.17 times the motor speed. The motor characteristics are shown in Figure 8-2. The fan characteristics are shown in Figure 8-3. Air was ducted from the fan into the trunk and exhausted from the trunk through 1093 holes located in the vicinty of the ground plane. The model structure was fiberglass and the trunk was a nylon-hypalon material. The trunk material was "inelastic" in that it did not possess the 200% to 300% elongation which would be required for complete retraction of the trunk. The elastic curve shown in Figure IV-3, Appendix IV, is typical for the trunk material.

The test platform was constructed of wood and was 10 feet in length by 8 feet in width. One section of the plywood surface was replaced with plexiglas in order to allow inspection of the underside of the test mode. The center of the platform contained by a 2' by 3' hole which could be covered with plywood and sealed. The hole in the center allowed the cushion pressure to escape and, consequently, the performance of the trunk could be

221
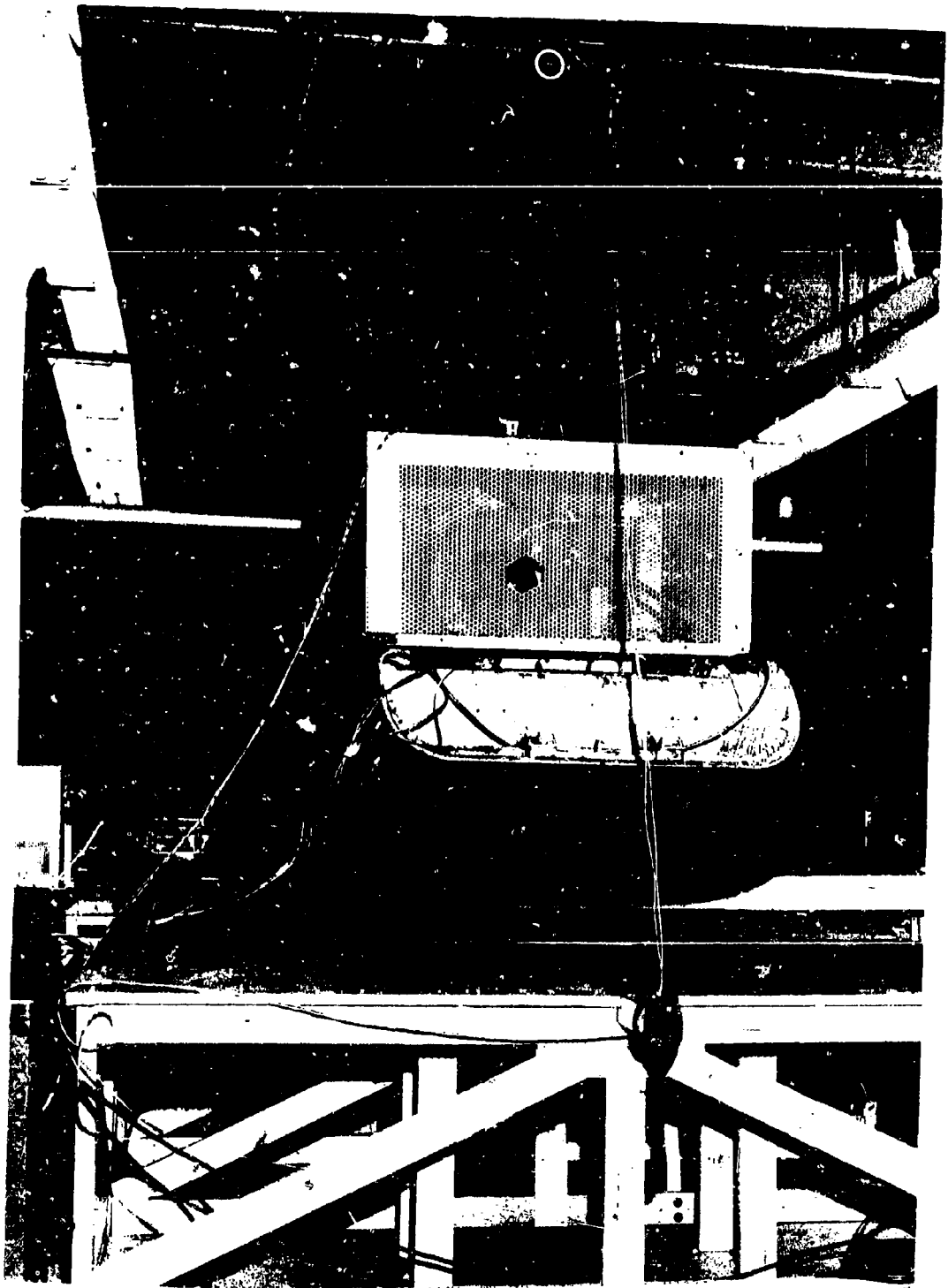
DYNAMIC MODEL AND TEST PLATFORM
FIGURE 8-1

TABLE 8-1

Dynamic Model Trunk Design Variables

VARIABLE	SYMBOL	VALUE
Total orifice area	a_j	104.16 in^2
Number of orifices	M	1093
Porosity	ξ	0.049
Cushion nozzle length	$(S_3)_\infty$	14.7 ft.

Trunk Section Properties

VARIABLE	SYMBOL	SIDE SECTION	CORNER SECTION	END SECTION
Cross-sectional area, in^2	$(A_j)_\infty$	326.1	235.6	202
Effective section length, in	L_N	16.0	17.1	14.6
Section angle of rotation, degrees	α_n	0	48	42
Centroidal radius, in	γ_n	20.9	20.4	19.9

224
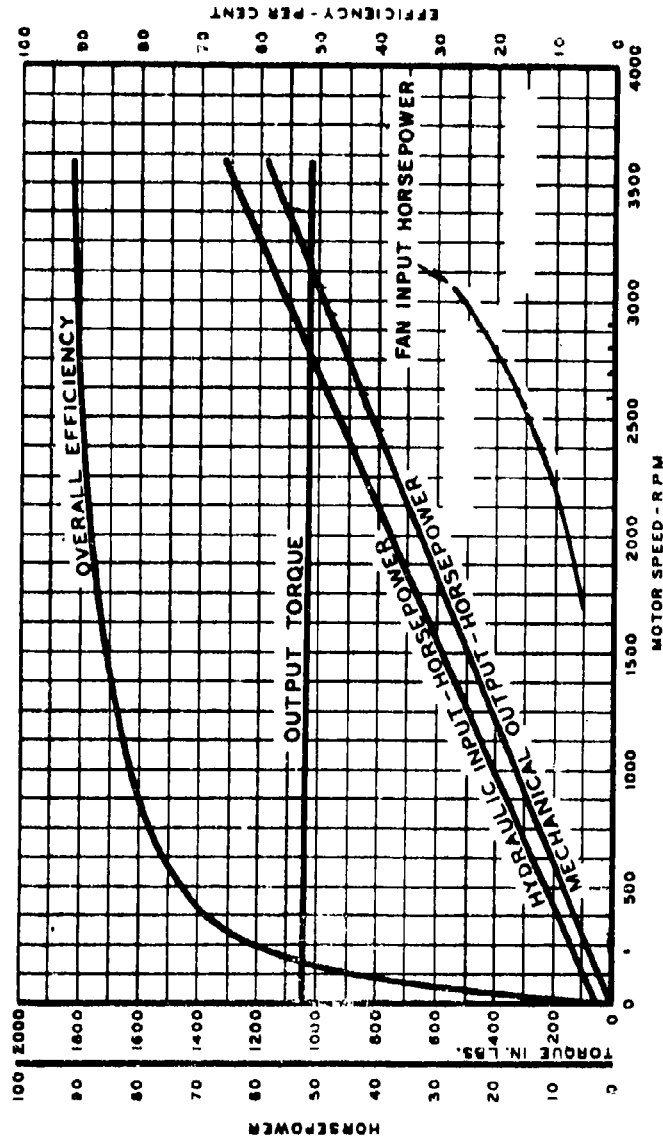
HYDRAULIC MOTOR CHARACTERISTICS

FIGURE 8-2
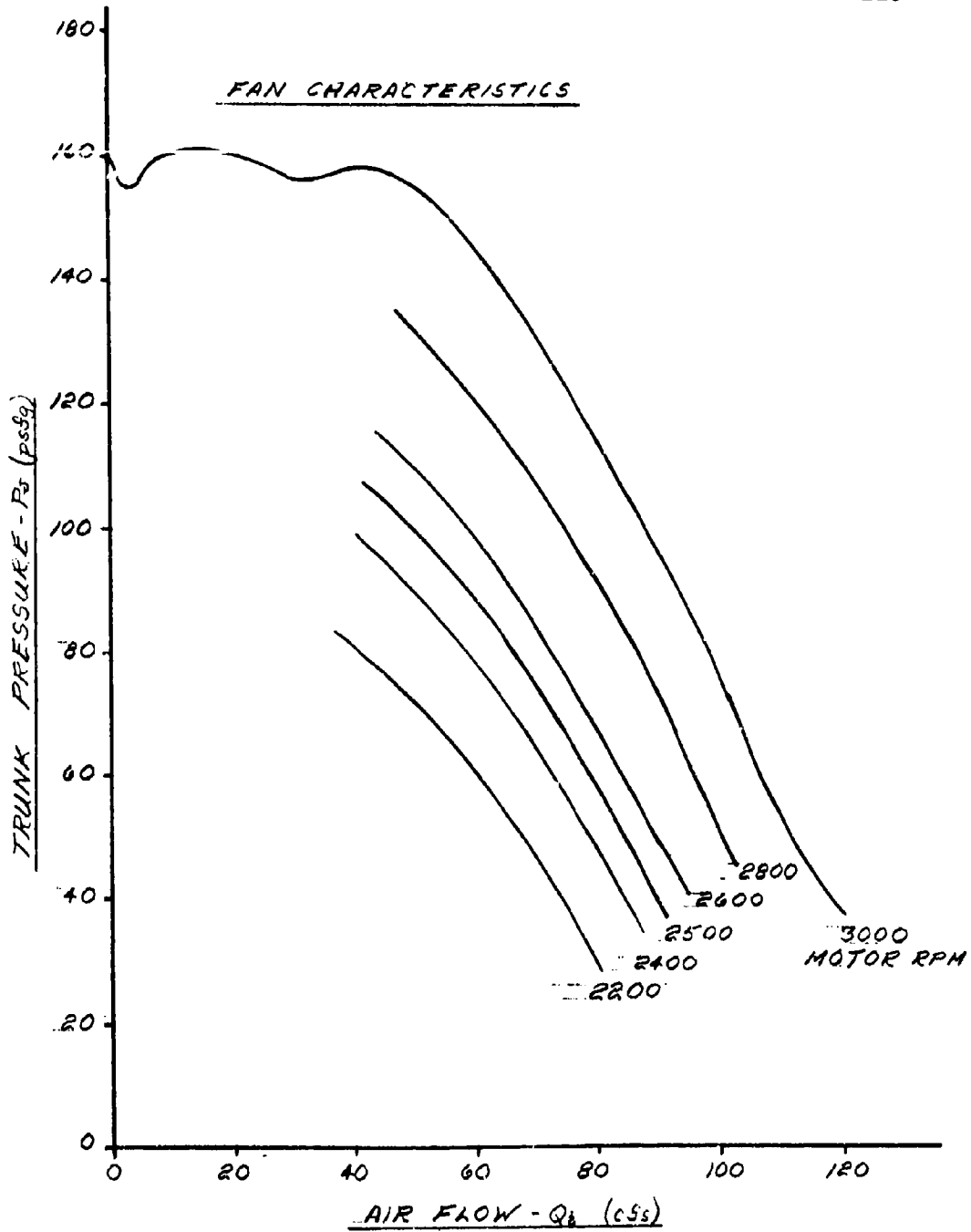
FAN CHARACTERISTICS

FIGURE 8-3

measured independently from the cushion. The performance of the combined trunk-cushion system could be measured when the hole was closed and sealed.

Two types of tests were conducted. The first was a series of static tests to determine the static performance of the model and to compare the results with the analysis presented in Sections 7.3.2 through 7.3.6. During these tests the values of the following variables were determined: C_x, F_j, C_z, A_3, C_y, d, A_j, and Q_j. The results of these tests are reported in Sections 8.2 through 8.6.

The second test was a dynamic drop test of the model to determine the dynamic response and compare the results with the analysis presented in Section 7.3.7. In all tests reported, the value of p_c was zero. The dynamic test is described in Section 8.7.

The variables used in this chapter are summarized in Chapter 7.

8.2   Determination of Discharge Coefficient C_x

A test was conducted to determine the discharge coefficient for the orifices in the trunk of the dynamic model. This test was conducted with the model suspended two feet above the test platform. At this distance, no cushion pressure existed and the influence of the ground plane on flow from the trunk was negligible.

By varying the hydraulic flow rate to the motor, the fan speed was varied to produce a trunk pressure which ranged from 25 to 65 psfg. For each data point, the rpm of the fan (N) was determined with a strobe light and the trunk pressure (p_j) was determined by a water filled manometer. The total air flow from the trunk was determined by entering p_j and N in Figure 8-3 and reading Q_j. The coefficient of discharge was determined from Equation (VI-2), Appendix VI.

$$C_x = \frac{Q_j}{\sqrt{\dfrac{2g_o}{\rho}\, p_j}\ a_j} \qquad\qquad \text{(see Appendix VI)} \quad \text{(VI-2)}$$
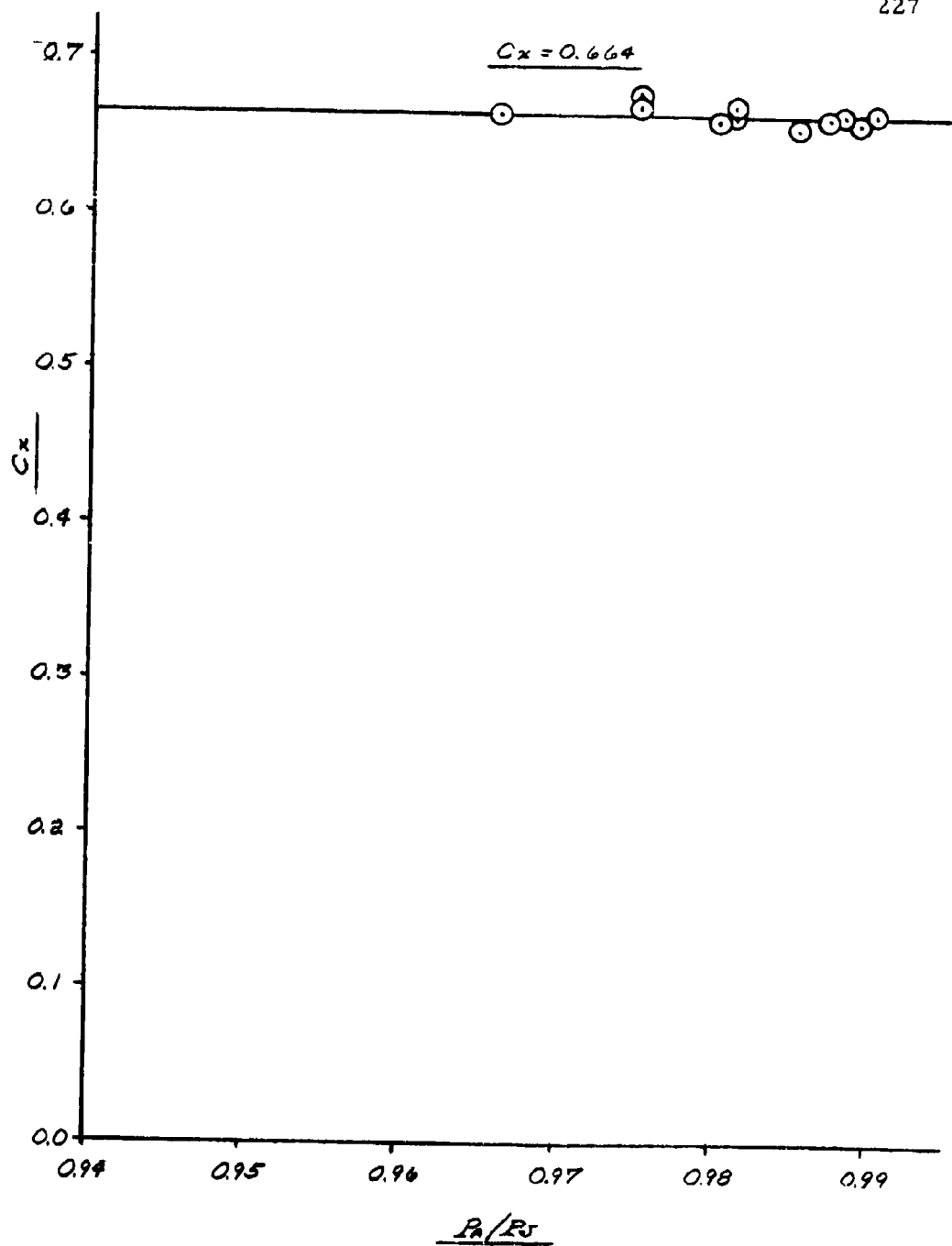
TRUNK DISCHARGE COEFFICIENT vs P_A/P_J

FIGURE 8-4
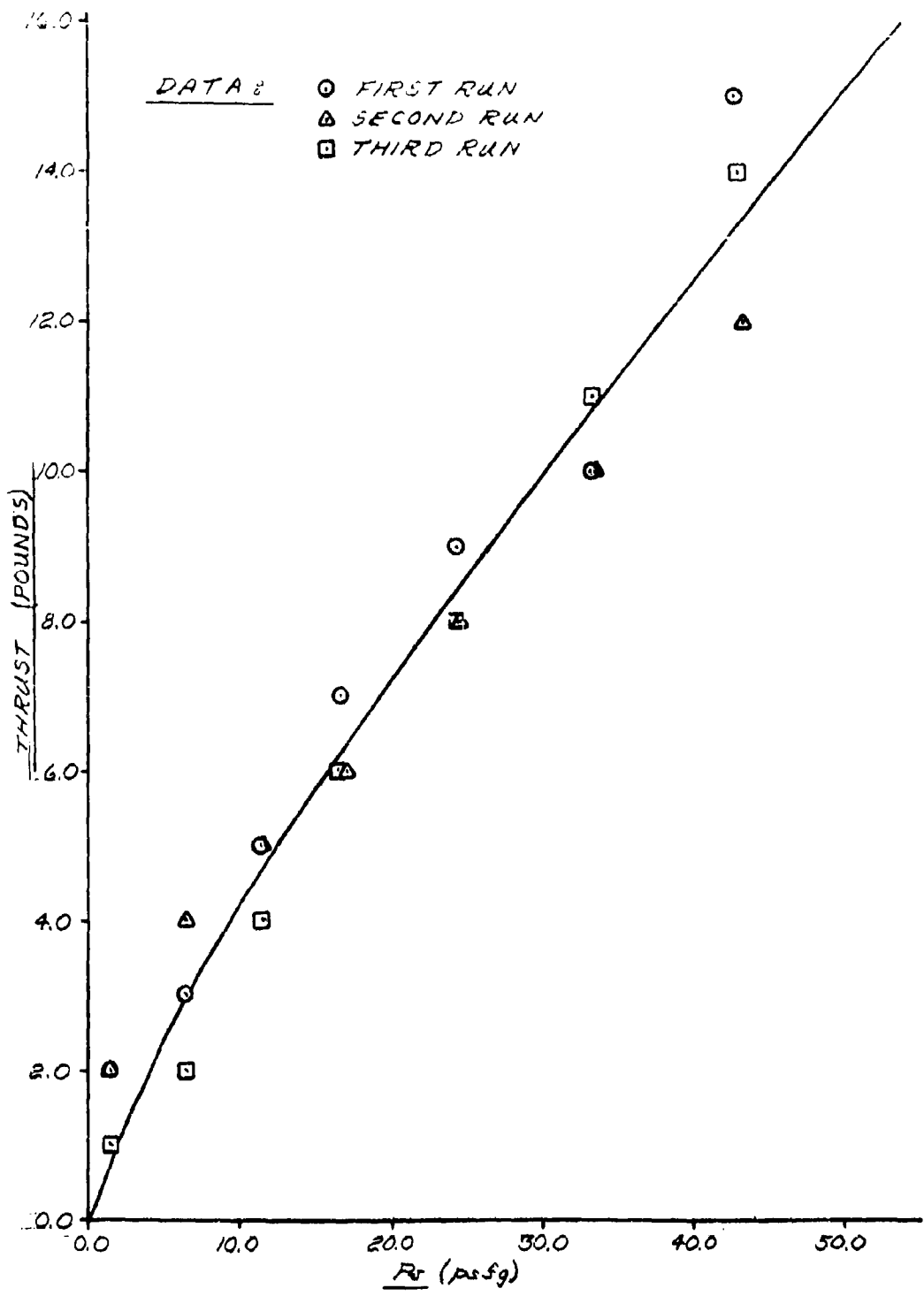
THRUST vs TRUNK PRESSURE

FIGURE 8-5

The resulting graph of P_a/P_j versus C_x is shown in Figure 8-4. From Figure 8-4 it is evident that $C_x = 0.66$ for the pressure range investigated.

8.3   Determination of Jet Thrust and C_z

In the test to measure vertical jet thrust, the model was suspended from a load cell. The model height was in excess of two feet so that the influence of the ground plane was negligible. The trunk pressure was varied from 0 to 45 psfg and the loss of weight registered by the load cell was recorded. The vertical thrust was equated to the difference between the static weight and the weight recorded at a given trunk pressure. The resulting thrust versus p_j was plotted in Figure 8-5.

The thrust coefficient (C_z) was calculated from Equation (7-26).

$$C_z = \frac{F_j}{2(P_j - P_a) a_j \, C_x \, C_y} \tag{8-1}$$

For the test conducted:

$C_x = 0.66$ (from Section 8.2)

$C_y = 1.00$ (from Section 7.3.5, Equation (7-39))

The resulting value of C_z was found to be

$C_z = 0.33$

8.4   Determination of A_3 and C_y

The variation of A_3 and C_y with model height was determined from a test series which statically loaded the model against the test platform. The center section of the test platform was uncovered so that no cushion pressure existed.
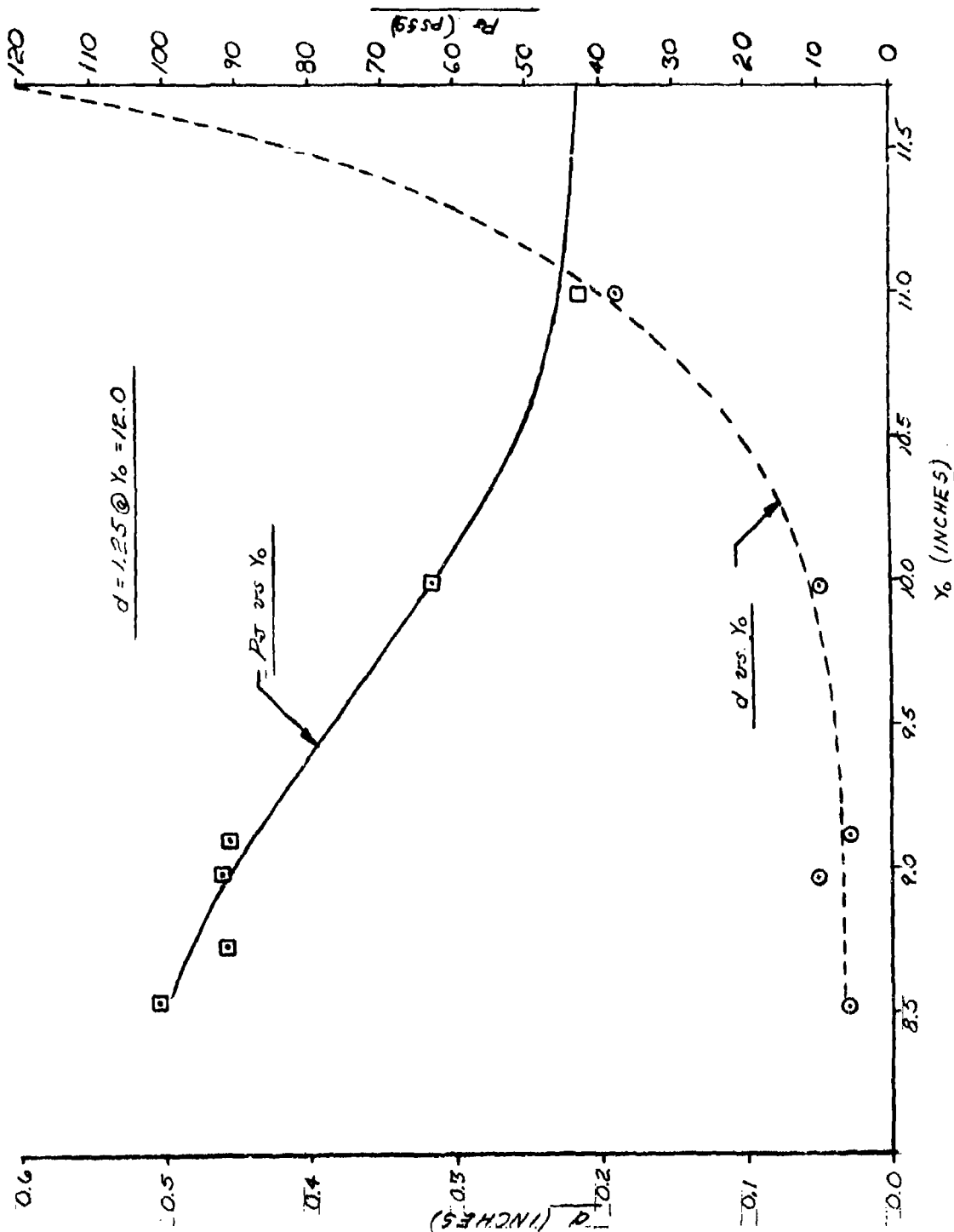
**TRUNK PRESSURE AND JET HEIGHT VARIATION
WITH VEHICLE HEIGHT**

FIGURE 8-6
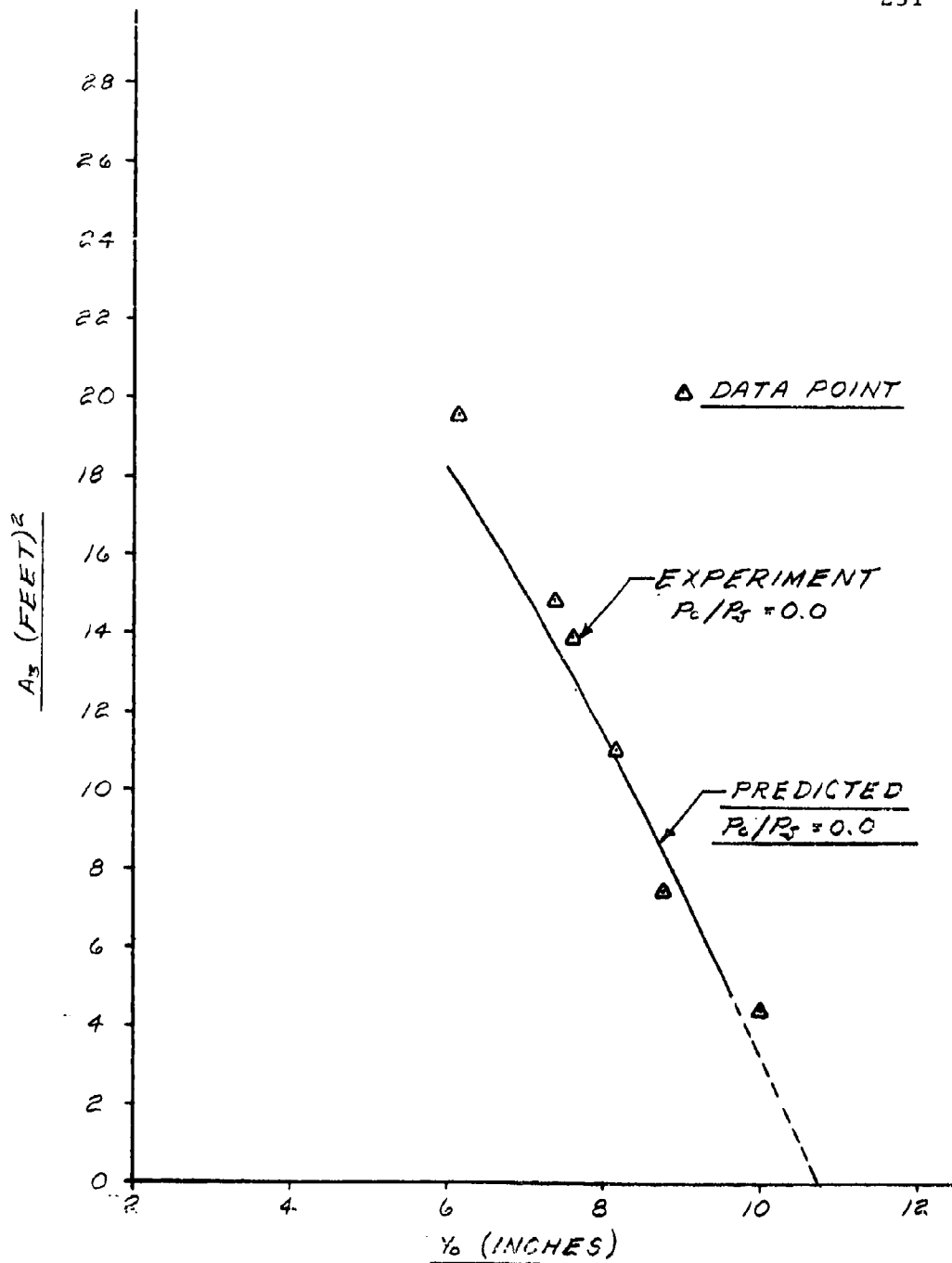
FOOTPRINT AREA vs VEHICLE HEIGHT

FIGURE 8-7

The fan speed was maintained at a constant rpm and the weight supported by the trunk was varied. For low trunk loads the model was partially suspended from a load cell. The load on the trunk was determined by the loss of weight registered by the load cell. For heavier loads, the model was loaded with known quantities of lead weights.

Data was recorded at approximately 1-inch increments over a model height range from 11 inches to 7 inches. At each data point, the model was leveled by adjusting the location of weights and the fan speed was set at 8000 rpm. The trunk height (Y_o) was measured with a scale and the jet height (d) was measured by rods of calibrated thickness. The trunk pressure was measured by a water tube manometer.

The recorded values of jet height (d) and trunk pressure (p_j) at a constant fan speed of 8000 rpm are shown in Figure 8-6.

The effective footprint areas of the trunk were calculated from the weight supported and the trunk pressure.

$$A_3 = \frac{W_A}{p_j} \qquad (8\text{-}2)$$

The resulting experimentally determined values of A_3 versus Y_o are shown in Figure 8-7.

The values of A_3 calculated by the computer program developed in Section 4.5 were also plotted in Figure 8-7. Values of A_3 were computed from the values of ℓ_3 shown in Figures 4-21 and 4-22 using techniques described in Sections 7.3.3 and 7.4.8. In computing A_3, the trunk was divided into three parts — the ends, the sides, and the corners. These three parts are designated by L_e, L_s, and L_k respectively (see Figure 4-8). The respective footprint areas were computed as follows.

$$(A_3)_s = (\ell_3)_s \, L_s \qquad (8\text{-}3)$$

$$(A_3)_e = \frac{(a)_e}{2} \left\{ \left[\frac{e}{2} + (X_o)_e + (\ell_3)_e \right]^2 - \left[\frac{e}{2} + (X_o)_e \right]^2 \right\} \qquad (8\text{-}4)$$

$$(A_3)_k = \frac{(a)_k}{4} \left\{ \left[\frac{e}{2} + (X_o)_e + (\ell_3)_e \right]^2 - \left[\frac{e}{2} + (X_o)_e \right]^2 \right.$$

$$\left. + \left[\frac{e}{2} + (X_o)_s + (\ell_3)_s \right]^2 - \left[\frac{e}{2} + (X_o)_s \right]^2 \right\} \qquad (8\text{-}5)$$

As shown in Equation (7-28), the total footprint area is equal to the sum of the various parts. For the model in Figure 4-8

$$A_3 = 4(A_3)_e + 2(A_3)_s + 4(A_3)_k \qquad (8\text{-}6)$$

Figure 8-8 shows the experimentally determined values of the coefficient C_y. The value of C_y at a given height (Y_o) was determined by the ratio of the flow at that height of the flow at an infinite height.

The value of C_y was also computed from theoretical considerations. For this calculation, the trunk model was divided into three segments: ℓ_1, ℓ_2, and ℓ_3 as shown in Figure 4-2. The flow from the three segments was computed following the procedure outlines in Section 7.3.5. The resulting equations were:

$$C_y = \frac{a_j - A_3 \xi + a_3'}{a_j} \qquad (7\text{-}40)$$

and

$$a_3' = \begin{cases} A_3 \xi \\ 2\, S_3 d\, C_D/C_X \end{cases} \qquad \text{whichever is less} \qquad (7\text{-}36)$$

The values of A_j, ξ, and S_3 are given in Table 8-1. The values of C_X and C_D were experimentally determined in Appendix VI and Section 6.3.2 respectively. The values for d

C_Y vs. Y_0/Y_∞
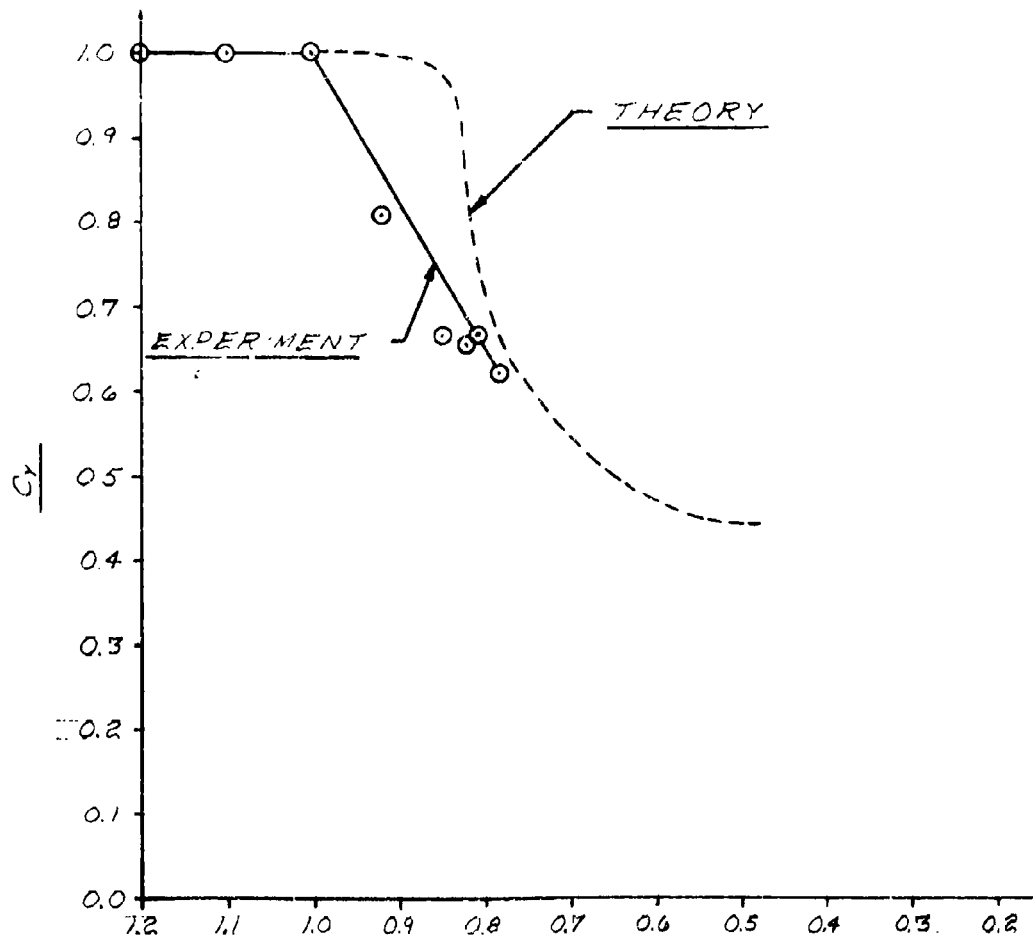
Y_0/Y_∞ $(Y_\infty = 10.5\ INCHES)$

CUSHION DISCHARGE COEFFICIENT vs VEHICLE HEIGHT
FIGURE 8-8

and A_3 versus Y_o are given in Figures 8-6 and 8-7 respectively. The resulting variation of C_v with Y_o is given in Figure 8-8.

8.5   Determination of Trunk Volume

A test was conducted to determine the variation in trunk volume with model height.

The trunk volume in the free (unloaded) condition was determined by graphical integration of the various cross-sectional areas shown in Figure 4-8. The total trunk volume was found to be 25.24 ft^3. The volume of the ducting between the fan and trunk was 1.8 ft^3.

The change in volume with model height was determined from the change in trunk cross-sectional area as the model was statically loaded against the test platform.

A constant fan speed of 8,000 rpm was used for this test. The floor center sections were removed to prevent cushion pressure build-up and to allow access to the inside portion of the trunk. The model height was varied by changing the load which was supported by the trunk. Data points were taken at approximately every 1.5 inches from a model height of 12 inches down to 6.25 inches. The trunk shape was determined at the midpoint of one side and one end for each data point.

The ground tangent points, (x_1, y_o) and (x_2, y_o) in Figure 4-2, were determined by measuring the vertical and horizontal distance relative to the attachment points (o, o) and (a, b).

The contour between an attachment point and a ground tangent point was determined by fitting a copper wire against the trunk. The copper wire was deformed plastically to retain the trunk contour. The inside and outside contours (ℓ_2 and ℓ_1 in Figure 4-2, respectively) were transferred by the copper wire to a full scale drawing of the trunk cross section. The resulting areas were measured with a compensating polar planimeter.

The volume of the trunk was calculated from the side and end cross-sectional areas in a manner similar to that outlined in Section 7.3.4. In order to perform this calculation, the trunk volume was separated into the four parts — the end shape, the corner shape, the side shape, and the fan ducting. These parts are shown in Figure 4-8. It is evident from the figure that the total volume of the trunk is

$$V_j = 4\ V_e + 2\ V_s + 4\ V_k + V_f \tag{8-10}$$

The volume of the end is a volume of revolution. The radius vector between the center of revolution and the centroid of the cross-sectional area is $\overline{r}_e$. The total volume of the two end sections is the product of the angle of revolution, the radius and the cross-sectional area. The result is:

$$V_e = c_e\ \overline{r}_e\ (A_j)_e \tag{8-11}$$

The volume of the two sides is the product of the section length L_s and the cross-sectional area. The result is:

$$V_s = L_s\ (A_j)_s \tag{8-12}$$

The volume of a corner section is more difficult to calculate than the other volumes. It approaches a volume of rotation, however the cross-sectional area and the radius of the centroid vary with the angle of rotation. On one side the cross-sectional area is $(A_j)_e$ and the centroid radius is $\overline{r}_e$. On the other side the cross-sectional area is $(A_j)_s$ and the centroidal radius is $\overline{r}_s$. It is evident that the volume of a single corner section lies in the range

$$a_e\ \overline{r}_e\ (A_j)_e < V_k < a_s\ \overline{r}_s\ (A_j)_s \tag{8-13}$$

In order to approximate the corner volume, the following assumptions were made.

(1) The effective centroidal radius for the corner section is the average of the end and side radii.

$$\bar{r}_k = \frac{\bar{r}_e + \bar{r}_s}{2} \qquad (8\text{-}14)$$

(2) The values of $\bar{r}_e$ and $\bar{r}_s$ do not change with Y_o.

(3) The effective cross-sectional area of the corner section lies somewhere between $(A_j)_e$ and $(A_j)_s$,

$$(A_j)_k = \zeta (A_j)_s + (1 - \zeta)(A_j)_e \qquad (8\text{-}15)$$

where ζ is a fraction between 0.0 and 1.0.

The resulting corner volume is:

$$V_k = a_k \frac{(\bar{r}_e + \bar{r}_s)}{2} \left[\zeta (A_j)_s + (1 - \zeta)(A_j)_e \right] \qquad (8\text{-}16)$$

The total trunk volume may now be written:

$$V_j = 4 \left[a_e \bar{r}_e (A_j)_e \right] + 2 \left[L_s (A_j)_s \right]$$

$$+ 4 \left\{ a_k \frac{(\bar{r}_e - \bar{r}_s)}{2} \left[(1 - \zeta)(A_j)_e + \zeta (A_j)_s \right] \right\} + V_f$$

Factoring the above equation gives:

$$V_j = \left[2a_e \bar{r}_e + 4a_k \frac{(\bar{r}_e + \bar{r}_s)}{2} (1 - \zeta) \right] (A_j)_e$$

$$+ \left[2(L_s) + 4a_k \frac{(\bar{r}_e + \bar{r}_s)}{2} (\zeta) \right] (A_j)_s + V_f \qquad (8\text{-}17)$$

The free volume of the trunk may be written

$$(V_j)_\infty = \left[2a_e \bar{r}_e + 4a_k \frac{(\bar{r}_e + \bar{r}_s)}{2} (1 - \zeta) \right] (A_j)_{e\infty}$$

$$+ \left[2(L_s) + 4a_k \frac{(\bar{r}_e + \bar{r}_s)}{2} (\zeta) \right] (A_j)_{s\infty} + V_f \qquad (8\text{-}18)$$

With the exception of ζ , the values of all variables in the above equation are known and are listed in Table 8-1. Consequently, the equation may be solved for ζ . For the model summarized in Table 8-1 the value of ζ was 0.727.

It is now possible to simplify Equation (8-18) with the following condensation of variables:

$$K_e \equiv 2a_e \bar{r}_e + 4a_k \frac{(\bar{r}_e + \bar{r}_s)}{2} (1 - \zeta) \qquad (8\text{-}19)$$

$$K_s \equiv 2L_s + 4a_k \frac{(\bar{r}_e + \bar{r}_s)}{2} \zeta \qquad (8\text{-}20)$$

For the model described in Table 8-1, the values of these parameters are K_e = 126.6 in. and K_s = 55.5 in.
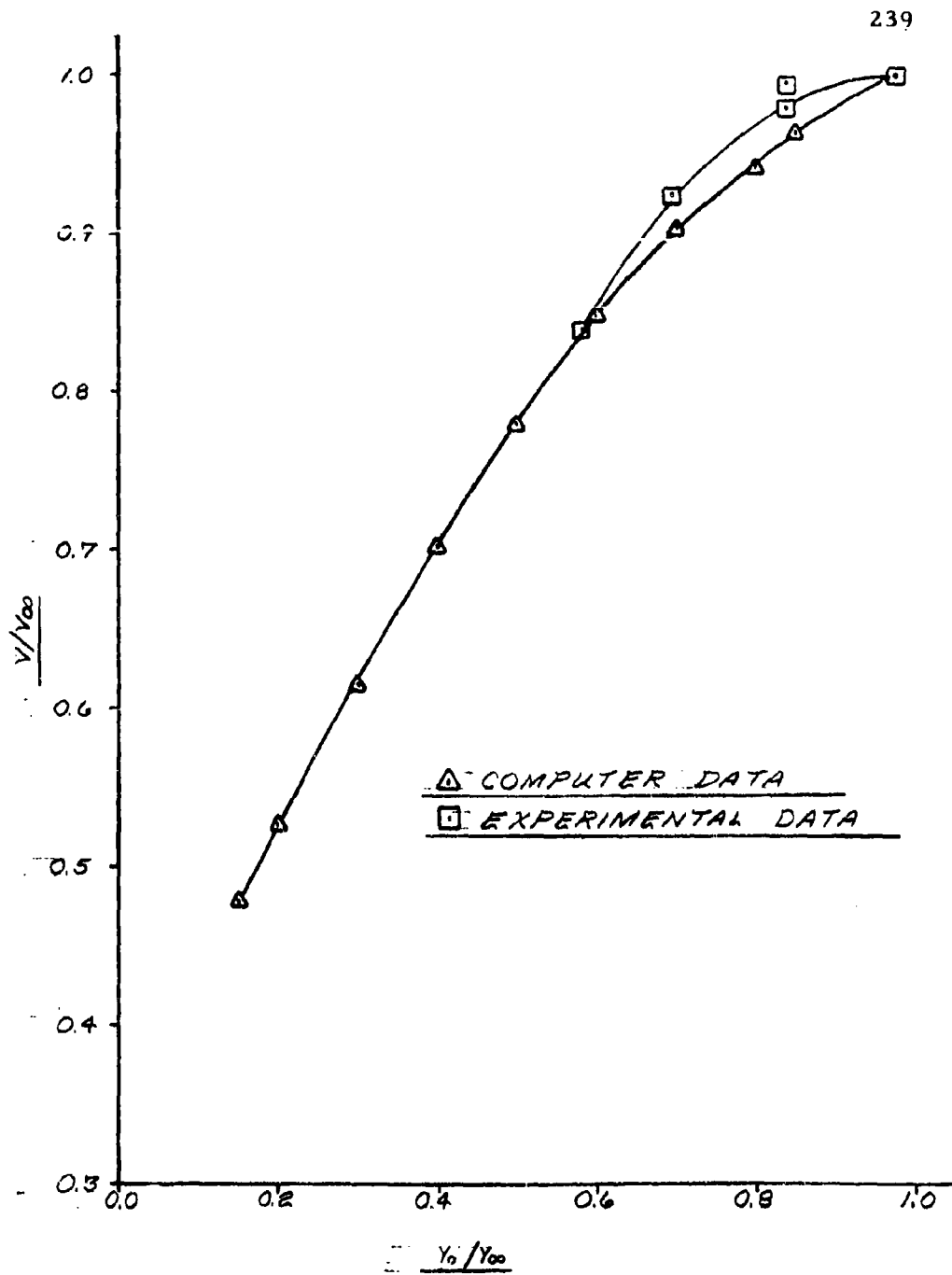
TRUNK VOLUME RATIO vs VEHICLE HEIGHT RATIO

FIGURE 8-9

The general equation for the total volume of the trunk and ducting may be written

$$V_j = K_e (A_j)_e + K_s (A_j)_s + V_f \qquad (8\text{-}21)$$

The volume ratio is

$$\frac{V_j}{(V_j)_\infty} = \frac{K_e (A_j)_e + K_s (A_j)_s + V_f}{(V_j)_\infty} \qquad (8\text{-}22)$$

Figure 8-9 shows the values of $V_j/(V_j)_\infty$ computed from the experimentally determined values of $(A_j)_e$ and $(A_j)_s$. In addition, the values of $V_j/V_{j\,\infty}$ computed from the values of A_j predicted by the computer program developed in Chapter 4 are shown. The computed values of $(A_j)_s$ and $(A_j)_e$ versus Y_o/Y_∞ are shown in Figures 4-23 and 4-24.

8.6 Fan Characteristics

The fan characteristics were determined by measuring the flow from the fan at various speeds and back pressures.

In the calibration tests, the fan and ducting were installed above a plywood plenum chamber of approximately the same volume as the free volume of the trunk. Two convergent conical nozzles with an included angle of 12 degrees were installed on opposite sides of the plenum. The discharge coefficient of the conical nozzles was constant at 0.95 over the range of Reynolds numbers of interest in the test. Data was recorded at 200 rpm increments, at motor speeds ranging between 2200 rpm and 3000 rpm. The back pressure (trunk pressure) was varied by changing the exit area of the convergent nozzles. Since the coefficients for the nozzles were known, the total flow from the fan could be calculated from the formula given in Appendix VI.
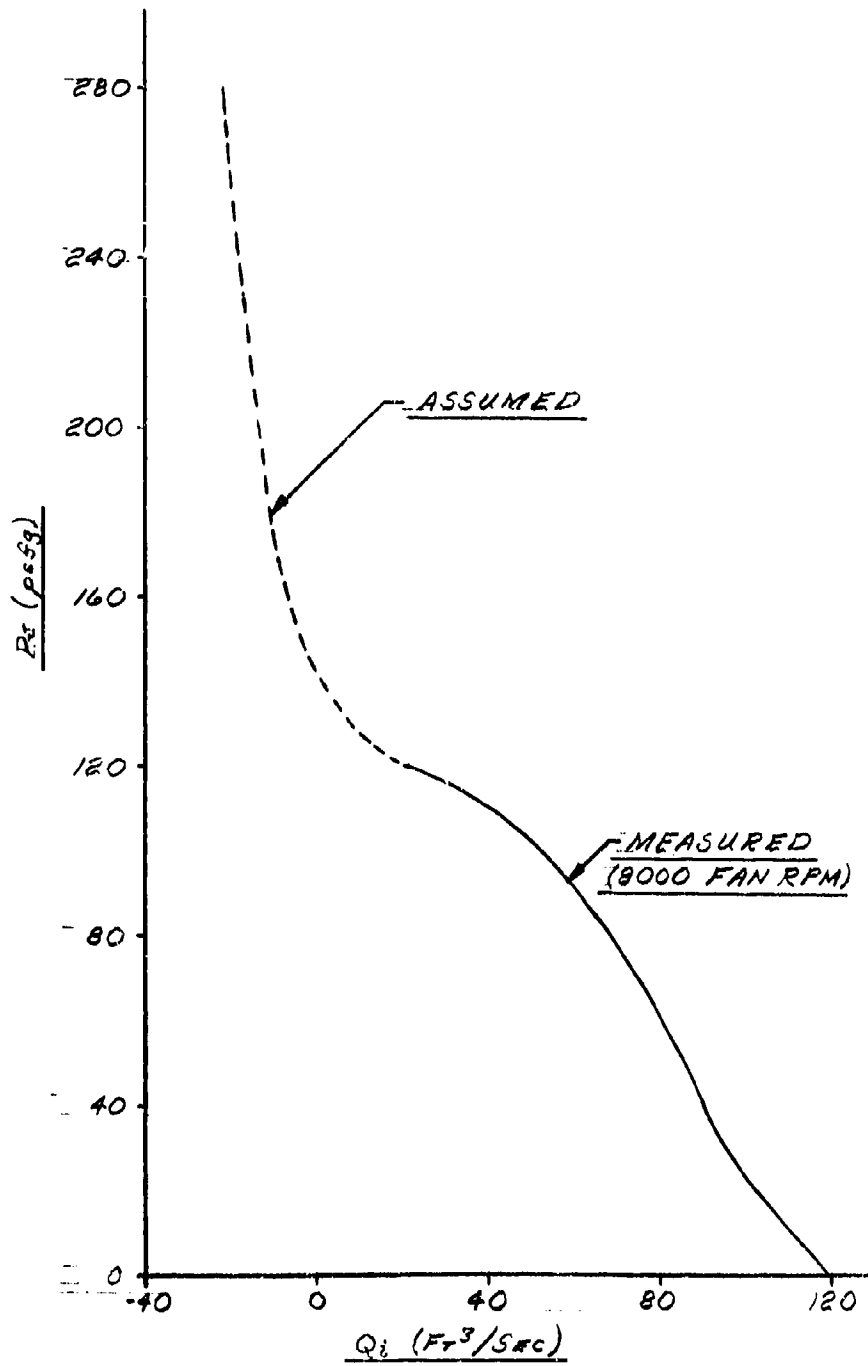
ASSUMED FAN CHARACTERISTICS
FIGURE 8-10

$$Q_i = \sqrt{\frac{2g_0}{\rho} (p_i)} \; a_D \, C_D$$

where

a_D is the total exhaust nozzle area

C_D is the nozzle coefficient of discharge

The resulting fan characteristics of the fan were plotted in Figure 8-3.

The backflow characteristics of the fan were not known. Consequently, it was assumed that at pressures above the stall pressure of the fan, the backflow through the fan was proportional to the square root of the difference between trunk pressure and stall pressure. The resulting relationship was:

$$Q_i = Q_r - \sqrt{\frac{2g_0}{\rho} (P_r - P_j)} \; a_r$$

where

P_r is the stall pressure of the fan for 8000 rpm fan speed

Q_r is the flow at the stall pressure

a_r is the effective flow area associated with fan backflow.

The assumed relationship between Q_i and P_j at pressures above stall pressures is shown in Figure 8-10.

8.7 Dynamic Model Test

In order to verify the dynamic analysis developed in Section 7-2, the dynamic test model was allowed to free fall and impact against the platform. Prior to drop test, the model was suspended above the platform by a nylon belt which incorporated a quick release

mechanism. The height above the platform and the fan rpm were measured prior to drop by a scale and a strobe light, respectively. During the drop and subsequent impact, the following parameters were measured and recorded.

(1) p_c and p_j were measured by Consolidated Electrodynamic Type 4-312 pressure transducers located in the cushion and trunk areas. These instruments had a pressure range of ± 12.5 psi with a linearity of ± 1.0% of the full scale reading. The natural frequency of the instruments was 8,000 cps. The error caused by a 15 g peak sinusoidal vibration from 5 to 2,000 cps was less than ± 0.160% full range/g.

(2)   Vertical acceleration was measured by a model 333 g Stradham Laboratories accelerometer with a± 25 g range, and a linearity of ± 1.0% of full scale reading.

(3)   The vertical displacement was measured by a linear displacement transducer, Model 4040 manufactured by Research, Incorporated. The displacement transducer had a 3.0 ft range, with a linearity of ± 1.0% of full scale reading.

The data was recorded on a direct reading oscillograph, Data Graph Model 5-26 manufactured by Consolidated Electrodynamics Corporation. The paper speed was eighteen inches per second.

The recorded values of trunk pressure, vertical acceleration, and vertical displacement are shown in Figures 8-11, 8-12, and 8-13, respectively, for a typical drop test. For the test results shown, the drop height was one foot and the cushion pressure was zero.
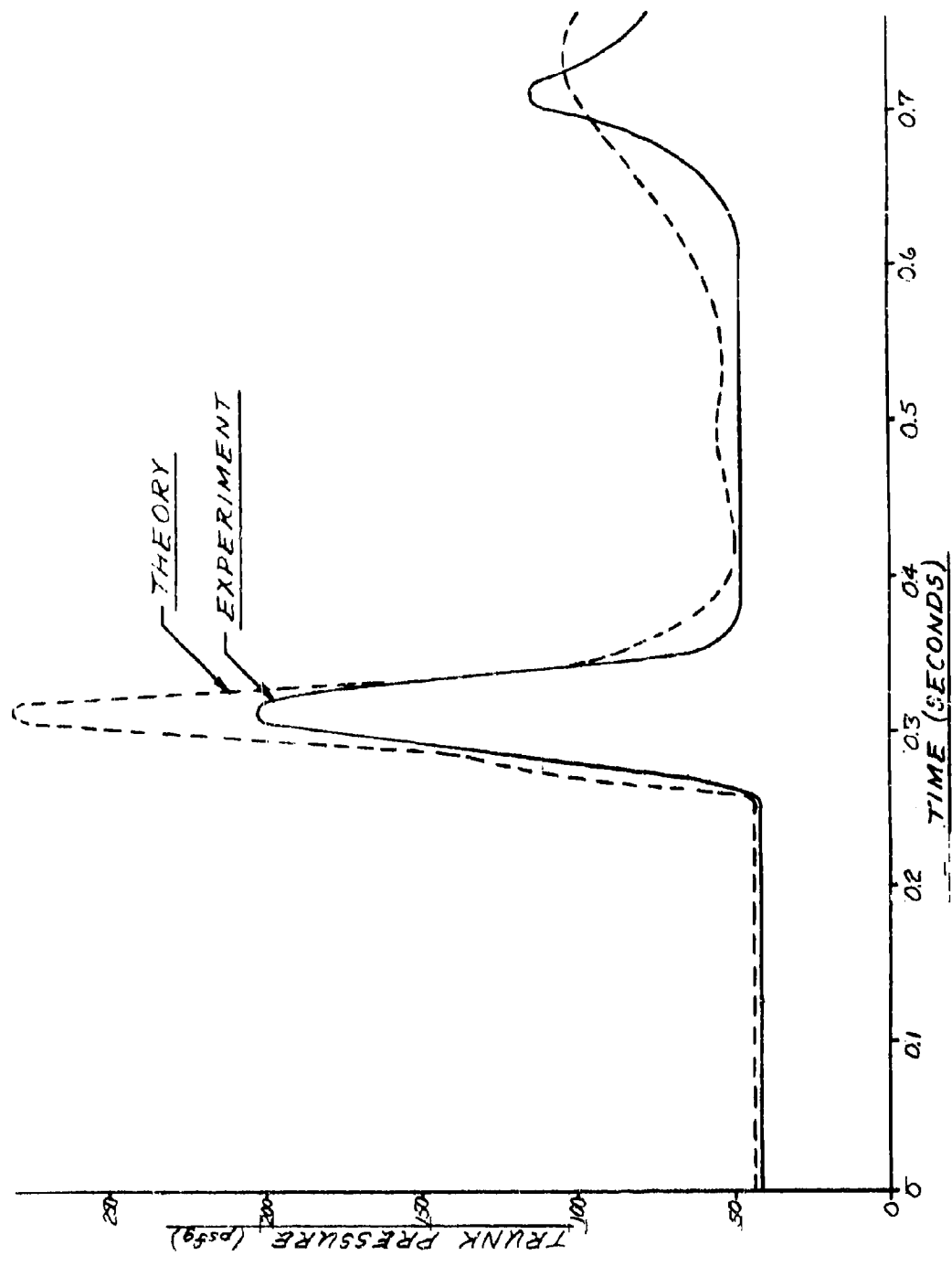
TRUNK PRESSURE DURING DROP TEST

FIGURE 8-11
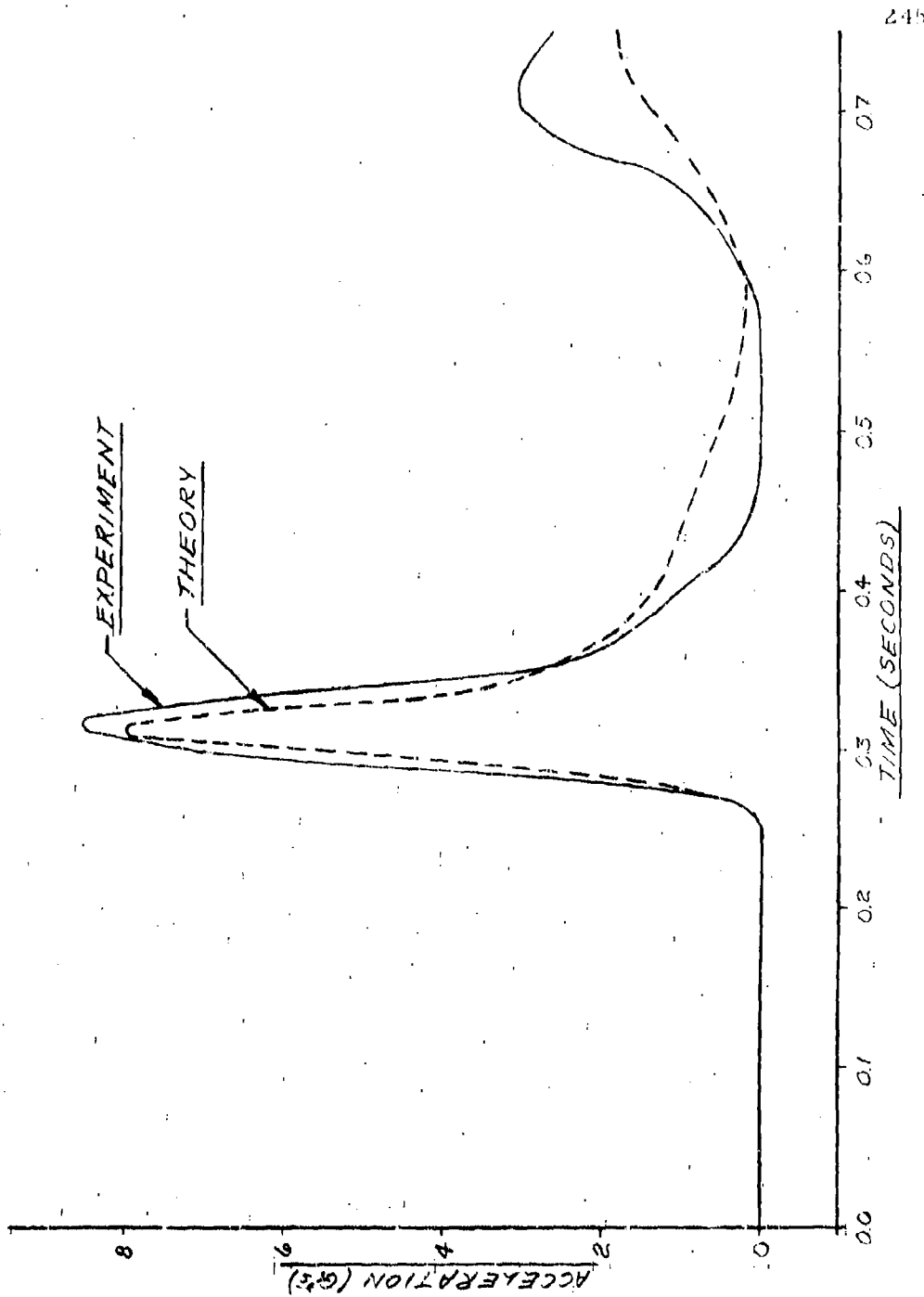
ACCELERATION DURING DROP TEST

FIGURE 8-12
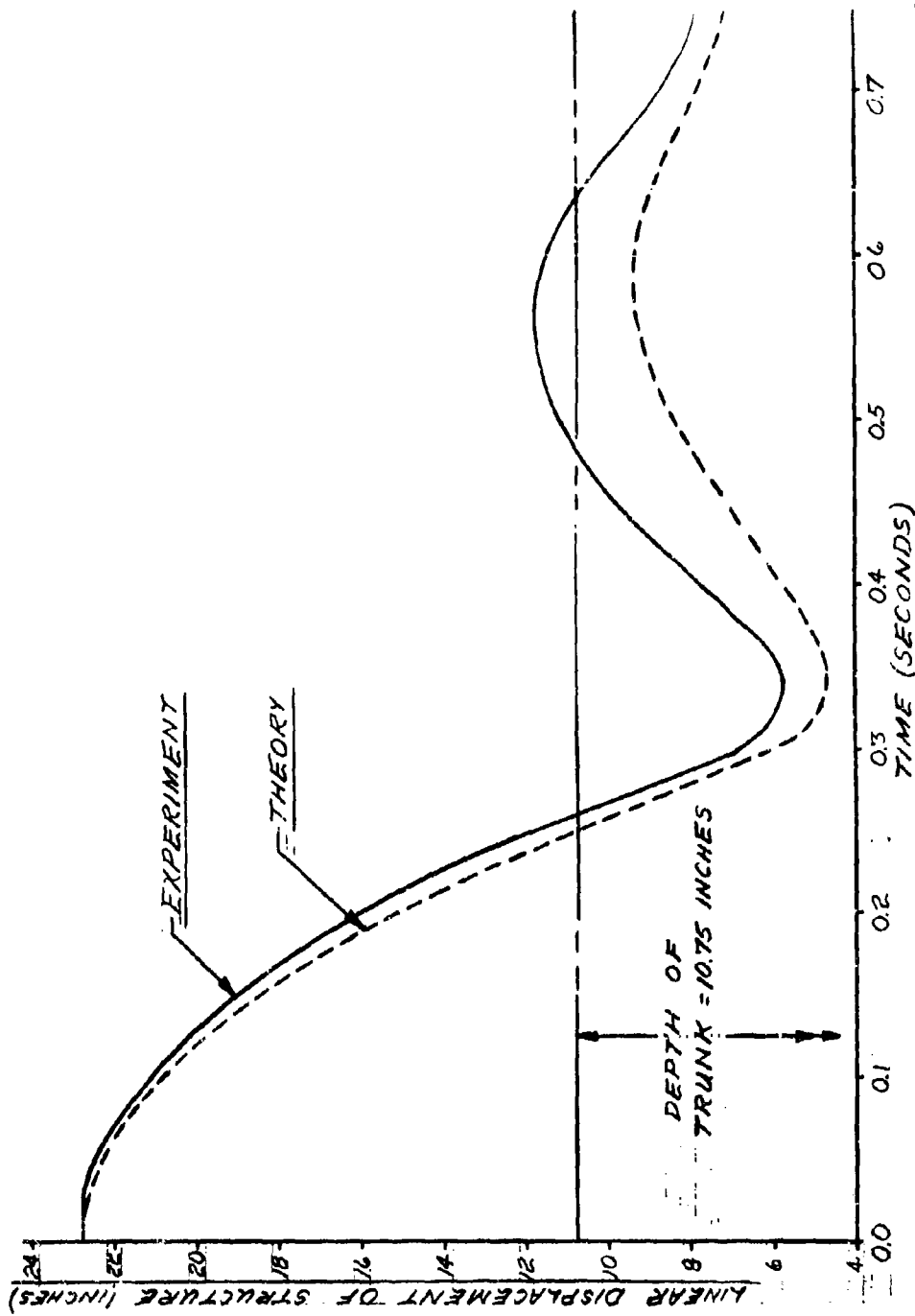
DISPLACEMENT DURING DROP TEST

FIGURE 8-13

246

8.8   Summary of Dynamic Test Results

The model drop test was conducted in order to compare the experimental results with the computer prediction of the dynamic response.

The fan speed at drop was 8,000 rpm and the drop height was one foot. The experimentally determined static characteristics shown in Figures 8-7, 8-8, 8-9, and 8-10 were used as inputs to the computer program.

The variation of trunk pressure with time for the experimental and the computer results are shown in Figure 8-11. The shapes of the two curves are quite similar. However, the peak pressure predicted by the computer was higher than that measured.

Figure 8-12 compares the predicted and measured values of the vertical acceleration. As in the case of the pressures, the curves are similar in shape. However, the experimentally measured acceleration was slightly higher than that predicted.

Figure 8-13 compares the predicted and measured values of displacement. The curves are similar in shape, but the maximum predicted displacement is slightly greater than the measured displacement.

Figures 8-11 through 8-13 show that it is possible to analytically predict the general characteristics of the dynamic response on the model tested. The analysis presented in Section 7.3 represents a valuable design tool for evaluating the effect on dynamic response of changes in the various design variables.

9.1   Design Considerations

In this report, the static and dynamic performance characteristics of the air cushion landing system were considered. The performance characteristics which are associated with static equilibrium include the following:

load capacity

stiffness

obstacle clearance

Additional performance characteristics associated with the dynamic performance of the system include: vertical (landing) energy absorption characteristics, horizontal energy absorption characteristics (braking and frictional drag), and system stability. The horizontal energy absorption and system stability were not considered in this study.

The load capacity is generally a specified design requirement which is determined by the aircraft design.

The system stiffness is dependent upon the trunk shape, trunk pressure, and the configuration of the cushion. It is desired to design the trunk so that pitch, roll, and heave stiffness are adequate. However, it should be noted that trunk stiffness is also an important parameter in designing the air cushion system for landing energy absorption. This consideration may become the overriding factor in specifying the trunk stiffness.

The obstacle clearance is related to the daylight clearance (d), the trunk height (Y_o), and the design of the jets and the trunk. It is generally desired to have large values of d for maximum ground performance but small values of d for minimum power. It is possible,

248

through using a flexible trunk with distributed jets, to provide adequate ground performance for low values of d. The value of d necessary for adequate ground performance for a given trunk and jet configuration must, at present, be determined experimentally. The resulting value of d is an important variable in determining power requirements for adequate ground performance.

The design variables may be subdivided into the following four areas: aircraft, jet system, trunk, and power system.

The aircraft variables include the weight to be supported (W_A), the length (D_2), width (D_1), area (A_C), and the perimeter (S) of the air cushion, and the daylight clearance (d) between the trunk and the ground. Additional variables which enter into the dynamic performance include take-off and landing speeds, loads and attitudes, vertical velocity at touchdown, braking coefficient and braking distance.

The jet system variables include the type of jets (slots, holes, nozzles, etc.), the jet spacing, the number of jet rows (M), the location of the jet rows on the trunk (λ_n), the effective jet thickness (t_n), and the effective jet angle (θ_n).

The trunk variables include the location of attachment points, (o, o) and (a, b), the trunk length (ℓ) and the elastic characteristics of the trunk material (E).

The power system variables include the horsepower input (hp) and the pressure (P_j) versus flow (Q_j) characteristics of the fan.

It is desired to select values for the design variables in such a way that performance requirements are met and the power, weight, and cost of the system are minimized. The design requirements may be specified in terms of aircraft weight, jet height, and trunk stiffness, and maximum allowable deceleration during landing impact.

The relationship between groupings of the design variables are expressed throughout this report in terms of p_c/p_j. It should be noted that when the aircraft is totally supported by the cushion, p_c is completely determined by the supported weight and cushion area. The effect of increasing power is to increase p_j, which in turn increases jet

flow. The major effect of increased flow is to increase the jet height, d. It is evident that the ratio of p_c/p_j is an important parameter which relates the variables of weight, power and jet height. The trunk stiffness and trunk shape are also functions of p_c/p_j. Consequently, the ratio p_c/p_j forms an important link between the dependent and independent variables.

In the following sections, the relationships between the various design variables have been summarized.

9.2   Aircraft Variables

The principal aircraft variables are as follows:

A_c-cushion area

D_1-cushion width

D_2-cushion length

d-daylight clearance (jet height)

S-cushion perimeter

W_A-aircraft weight

Very little design flexibility is generally allowed in the aircraft variables. The cushion area and shape are generally determined by the aircraft design. Similarly, the weight of the aircraft is specified. The jet height is specified by the obstacle negotiation and ground performance requirements.

A relationship between the principal aircraft variables and the power requirements may be developed by combining Equations (2-9) and (3-7). The result is

$$hp = \left(\frac{W_A}{A_c}\right)^{3/2} \frac{S\,d}{550} \left(\frac{2g_0}{\rho}\right)^{1/2} C_{hd} \qquad (9\text{-}1)$$

This relationship shows that among the aircraft variables it is desirable to maximize A_c and minimize S and d for minimum power. This relationship is further

illustrated by Figure 3-5 which shows that the augmentation ratio is increased by increasing cushion area for a fixed value of d.

A further consideration in designing the air cushion system is the pitch and roll stiffness offered by the trunk. It is desired to place the trunk as far from the center of gravity as possible to increase the restoring moment developed by the trunk.

Consequently, it is desired to make the aircraft fuselage as wide as is permitted by aerodynamic and structural considerations. An optimum cushion shape for an air cushion landing system would probably involve a fuselage with a higher width to length ratio than exists in normal aircraft designs.

9.3 Jet System Variables

The jet system variables include:

d - jet height

p_c/p_j — pressure ratio

N — number of jet rows

t — total jet thickness

t_n — jet thickness for individual rows

λ_n — location of individual rows on the trunk

θ_n — effective jet angle for individual rows

In addition, the use of slots versus holes for the jet nozzle must be considered. The diameter and spacing between the holes must be determined if holes are selected.

The selection of p_c/p_j is determined largely by the cushion system stiffness and vertical energy absorption desired. Low values of p_c/p_j give a stiff cushion while high values of p_c/p_j give a soft cushion. The influence of p_c/p_j on power is shown in Figure 3-4(a). The power-height parameter C_{hd} is directly proportional to power for constant vehicle weight,

area, perimeter, and jet height. The curves show that power requirements are relatively insensitive to p_c/p_j for the range of 0.5 to 0.9. Figures 3-4(b) and 3-4(c) also show the effect of jet angle on power requirements. An increase in jet angle from 0° to 30° results in a considerable decrease in power. Further increases have minor influence on power. Negative jet angles and jet orifices to the outside of the trunk low point (X_0, Y_0) were shown in Chapters 5 and 6 to contribute practically nothing to jet height.

The jet thickness t is selected to provide the desired level of p_c/p_j for the design weight, jet height, and power setting.

Front and rear trunk sections generally require more jets than side trunk sections. The reason for this may be seen by comparing Figure 4-21 and Figure 4-22. These figures show that for a given deflection, the end trunk has a longer length flattened against the ground (ℓ_3) than the side trunk. In addition, the rear trunk undergoes extensive flattening during take-off rotation and landing touch-down. Inadequate air lubrication would contribute to plow-in of the front trunk and excessive wear of the aft trunk.

Because of the complexity of the flow beneath the trunk, an optimum spacing and nozzle design cannot at present be predicted analytically. However, the analysis presented in this report is useful in determining trends and extrapolating experimental results. In particular, the power-jet-height parameter (C_{hd}) is a valuable parameter for this purpose.

The C_{hd} parameter was defined by Equation (3-7) in Section 3.6.

$$C_{hd} = \frac{t}{d} \left(\frac{p_j}{p_c} \right)^{3/2} C_Q C_x \qquad (3-7)$$

The values of t/d and C_Q as a function of p_c/p_j may be determined by the simple test described in Chapter 6 on a model section of trunk. The test rig for conducting such a test was shown in Figure 6-1. The test for determining C_x was described in Appendix VI. As

a result of these simple tests, it is possible to plot C_{hd} versus p_c/p_j for particular jet configuration. A comparison of these plots for various jet configurations allows the evaluation of the designs in efficiency of maximizing jet height and minimizing horsepower. It was shown in Equation (9-1) tha horsepower is directly proportional to C_{hd}.

$$hp = \left(\frac{W_A}{A_c}\right)^{3/2} \frac{S\,d}{550} \left(\frac{2g_0}{\rho}\right)^{1/2} C_{hd} \qquad (9\text{-}1)$$

As a consequence it is desirable to select the design which minimizes C_{hd}, provided weight, cost, or other factors do not dictate the selection. Other factors include the necessity to provide "air lubrication" beneath the trunk during landing impact, and to stabilize dynamic oscillations of the trunk under all operating conditions.

A comparison of C_{hd} for two trunk designs is shown in Figure 9-1. In the figure, eight rows of orifices, the design described in Appendix IV, is compared with a design which has four tranverse slots. Both designs had the same total nozzle area. The curve shows tha the slot design is better for low p_c/p_j while the orifice design is better for high p_c/p_j. It is evident from Figure 9-1 that the C_{hd} gives a simple vehicle for comparing competing designs without the need for a complicated analysis.

9.4 Trunk Variables

The trunk variables include:

(o,o) and (a,b) — the trunk attachment points

ℓ — the trunk length

E — the trunk material elasticity

P_j — the trunk pressure

The trunk stiffness may be influenced considerably by choosing appropriate trunk lengths and attachment points. The load supported by the trunk is proportional to P_j (the
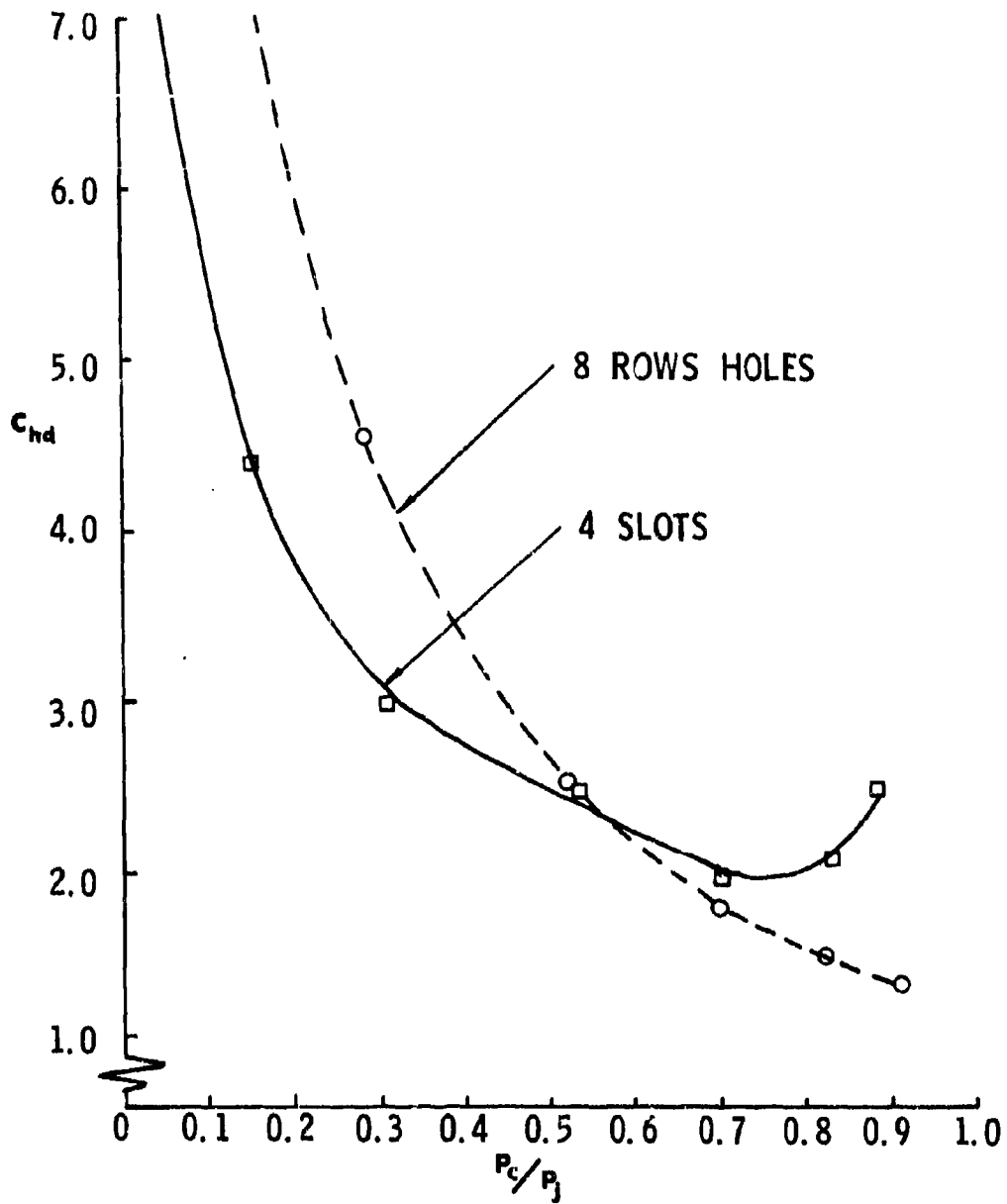
POWER-HEIGHT PARAMETER FOR TWO TRUNK DESIGNS
FIGURE 9-1

trunk pressure) and to ℓ_3 (the length flattened against the ground). The relationships between ℓ_3 and trunk deflection are shown in Figures 4-21 and 4-22; the two trunks having different attachment points. The stiffness variation, scaled up to a C-119 aircraft size trunk, is shown in Figure 9-2. The curves shown in Figure 4-21 and Figure 4-22 are scaled up to produce curves "A" and "B" respectively in Figure 9-2. The following assumptions were made:

> All dimensions are scaled up by a factor of 3.00.
>
> The design p_c/p_j is 0.5.
>
> The trunk is inelastic.
>
> The design trunk pressure is 333 lb/ft^2.
>
> The trunk section is 500" in length.

The stiffness of the two trunk sections was found to be 2000 lb/in. for trunk "A" and 6000 lb/in. for trunk "B". The stiffness of the air spring on the conventional C-119 shock strut is around 4500 lb/in. It is evident from this simple illustration that considerable flexibility exists in designing trunk stiffness by appropriate selection of the trunk variables. In a manner similar to the illustration above, the stiffness for any trunk design may be calculated from the computer program results.

The selection of the trunk material elasticity is based on the difference between the retracted length and the desired inflated length. It is desirable to have a compound elastic curve with two different slopes. A typical curve is shown in Figure 4-14. The material shown has the slope characteristic of the rubber up to the inflated design point and the slope of the fabric reinforcing material above the design point. Such an elastic characteristic allows the material to stretch easily up to the design point but resists further elongation above the design point.

The analysis of the air cushion trunk shape developed in Chapter 4 and the computer programs developed in Appendices I, II, and III provide the capability of predicting the influence of all the trunk variables on the trunk and cushion stiffness. In

addition, the dynamic analysis developed in Chap'ers 7 and 8 provides the capability of evaluating the influence of all trunk design variables except trunk elasticity, on the dynamic response of the vehicle.

9.5   Power System Variables

The power system variables include:

hp - power input

Q_j — air flow rate

P_j — trunk pressure

The flow rate is determined from Equation (3-3), which may be written:

$$Q_j = t\,S\,\sqrt{\frac{2g_0}{\rho}\,P_j}\;C_x\,C_Q \tag{3-4}$$

The coefficient C_Q is a function of p_c/p_j and is shown in Figure 3-2.

The power system must be designed so that the desired flow rate is produced at the design p_j. Further, the fan characteristics should be chosen such that the necessary flow will be produced to maintain p_c/p_j in an acceptable range over the expected variations of p_c caused by changes in the aircraft operating weight. Under landing impact, it is possible for p_j to increase to the point where the fan stalls and reverse flow occurs. The fan should be designed to permit and withstand this condition.

Considering only static conditions, the desired P_j versus Q_j fan characteristics may be obtained from Equation (3-3). This equation gives the required flow for various levels of P_j and p_c/p_j. The value of C_Q as a function of p_c/p_j is given in Figures 3-2, 5-7, and 6-12 for various cushion designs.

In addition, the fan characteristics play an important role in the dynamic response of the system. The fan flow characteristics near and above stall pressure have a profound

influence on the maximum trunk pressure and maximum deceleration during impact. The effect of fan characteristics on dynamic response may be evaluated using the dynamic analysis developed in Chapter 7.

9.6 Power Requirements for the ACLS

The power requirements for the ACLS may be scaled up using Equations (9-1) and (3-7).

$$hp = \left(\frac{W_A}{A_c}\right)^{3/2} \frac{S d}{550} \left(\frac{2 g_0}{\rho}\right)^{1/2} C_{hd} \tag{9-1}$$

$$C_{hd} = \frac{t}{d} \left(\frac{p_j}{p_c}\right)^{3/2} C_Q C_x \tag{3-7}$$

The C_{hd} parameter is dimensionless and independent of scale. This parameter may be easily measured for a given trunk design by model testing. The values of ρ and g_0 are also independent of vehicle size. The remaining variables are dependent on aircraft size and performance requirements. In particular, the value of d is related to the ground performance requirements, and A_c and S are related to aircraft weight. A 2500 pound aircraft equipped with an air cushion landing system has been tested and its take-off, landing and obstacle negotiation performance was excellent as reported in References (3) and (50). If it is assumed that the jet height and C_{hd} of the test aircraft design are satisfactory for larger aircraft, the power requirements for larger aircraft may be estimated from Equation (9-1).

To determine the relationship between the power and aircraft weight, some dependence between weight and fuselage area, and weight and fuselage perimeter, is necessary.
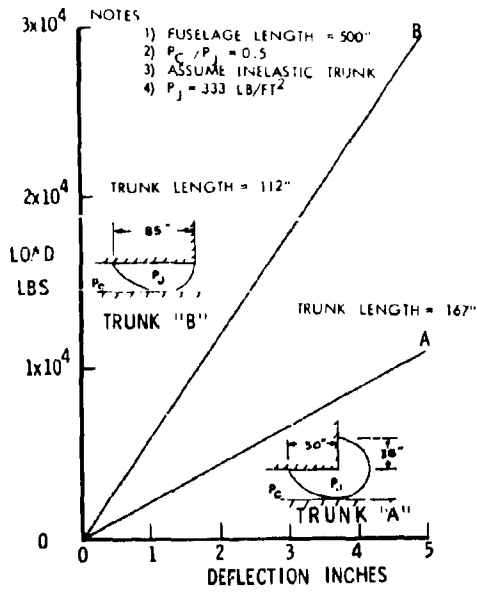
LOAD DEFLECTION CHARACTERISTICS

FIGURE 9-2
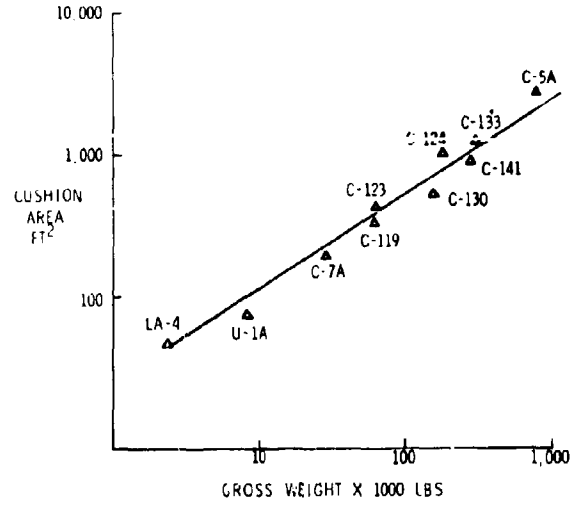
FUSELAGE AREA VS A/C GROSS WEIGHT

FIGURE 9-3
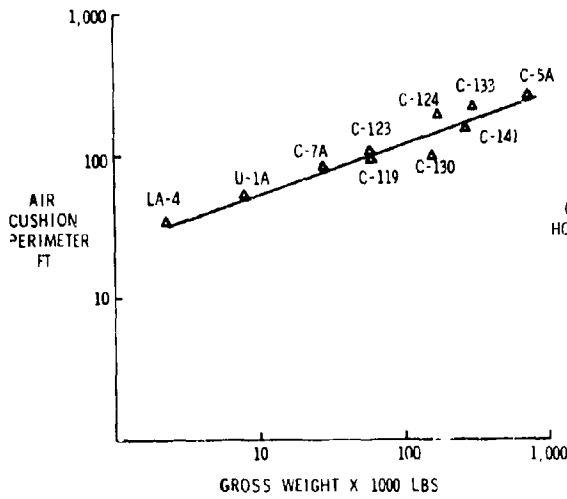
FUSELAGE PERIMETER VS A/C GROSS WEIGHT

FIGURE 9-4
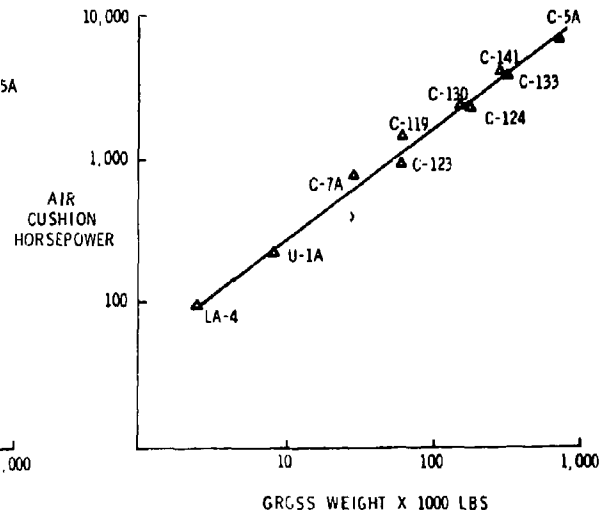
ACLS POWER VS A/C WEIGHT

FIGURE 9-5

Figure 9-3 shows a plot of fuselage area versus weight for various cargo and utility aircraft. A similar plot of fuselage perimeter versus aircraft weight is shown in Figure 9-4.

Using the relationships of Figures 9-3 and 9-4 in Equation (9-1), it is possible to estimate ACLS horsepower as a function of aircraft weight. The resulting power requirements are shown in Figure 9-5.

It should be noted that the results in Figure 9-5 assume a constant jet height and neglect the effect of compressibility and ducting losses. Figure 9-5 shows that ACLS power requirements are proportional to $(W_c)^{5/6}$. At aircraft weights in the 60,000 pound class, approximately 20% of the propulsive power would be required. At weights in the 600,000 pound class, only 15% would be required. It is evident that the power required by the ACLS is only a small fraction of the normal propulsive power and an even smaller fraction of the power required for vertical takeoff. The ACLS offers the aircraft remarkable improvements in ground performance for a modest increase in power.

9.7 Conclusions

As a result of the work reported herein the following conclusions are made:

(1) The corss-sectional area and shape of an air cushion trunk of the general configuration tested (Chapter 6) can be analytically predicted using the analysis in Chapter 4. The agreement between theory and experiment was good for both the free and ground loaded cases.

(2) The classical peripheral jet momentum theories (Chapter 2) do not adequately predict the jet height and flow for a distributed jet of the type used on the aircraft in the air cushion landing system flight test program.[3],[50]

(3)   The flow restrictor theory developed in Chapter 5 gives excellent agreement with experimental results reported in Chapter 6 for jet height, flow and pressure distribution around the trunk for the trunk configuration tested.

(4)   The presently used orifice system is inefficient from the standpoint of jet height. As far as the jet height is concerned, the momentum from the jet exhaust and the flow from the jets on the atmospheric side of the trunk low point are almost totally wasted.

(5)   The dimensionless parameter C_Q provides an accurate compensation for the effect of p_c/p_j on the total flow from the trunk.

(6)   The parameter p_c/p_j was found to be a valuable dimensionless quantity for relating the various dependent and independent variables. Test results reported in Chapter 6 showed that both jet height d and C_Q were dependent on p_c/p_j and relatively independent on the magnitude of p_j alone.

(7)   The trunk shape analysis developed in Chapter 4 for a trunk with free edges gave good agreement with experimental results when applied to the complicated dynamic test model reported in Chapter 8.

(8)   The dynamic analysis developed in Chapter 7 gave good agreement with the dynamic test reported in Chapter 8 for a drop test with $p_c = 0$.

(9)   The trunk shape analysis developed in Chapter 4 provides the capability of analytically evaluating the effect of trunk length, attachment points, material elasticity, cushion pressure and trunk pressure on trunk shape, volume and stiffness.

(10)   The flow analysis developed in Chapter 5 provides the capability of analytically evaluating the effect of jet size, spacing, angle, position on the trunk, cushion pressure, trunk pressure, and trunk shape on the resulting jet height and flow.

(11)   The dynamic analysis developed in Chapter 7 provides the capability of analytically evaluating the influence of aircraft weight, sink velocity, fan characteristics, trunk shape, trunk length, and trunk orifice area and spacing on the dynamic response of the vehicle under landing impact.

(12)   The dimensionless parameter C_{hd} is a valuable vehicle for comparing the relative effectiveness of competing designs for minimizing horsepower and maximizing jet height. The value of C_{hd} for a design may be determined easily by test, thereby eliminating a complicated analysis. The parameter C_{hd} is also valuable for scaling model test results to full size vehicles.

(13)   The air cushion landing system offers a promising area for further development.

Appendix I

FREE TRUNK SHAPE (INELASTIC)

The computer program described in this appendix computes the cross-sectional shape for a free inelastic trunk. The logic is similar to that presented in Section 4.4, but with the restriction that the trunk is inelastic.

The input variables are

a   = x coordinate of upper trunk attachment point

b   = y coordinate of upper trunk attachment point

p_c/p_j = ratio of cushion pressure to trunk pressure

ℓ = trunk length

The program uses a and b to make an initial estimate R_1 and computes $\bar{\ell} = \bar{\ell}(R_1)$. Improved estimates on R_1 are made until $\left| \ell - \bar{\ell} \right|$ >(TOL)(ℓ). TOL is the relative tolerance on $\bar{\ell}$. This tolerance is set at 3×10^{-5}. This can be changed by inserting a new card.

The main program may call three subroutines: function $F(R_1)$ evaluates $\bar{\ell}(R_1) - \ell \equiv F(R_1)$; function $DF(R_1)$ evaluates the derivative of $F(R_1)$; subroutine RTMI uses Mueller's Iteration Method to converge on the solution of $F(R_1) = 0$, once the solution is bounded.

Initially, the program converges on the solution of $F(R_1) = 0$ from the right side using Newton's iteration method.

If the solution is bounded during the Newton iteration process, the Mueller subroutine is called to speed convergence, and a notation is made in the data output to indicate that this subroutine was used.

262

The program has been found to converge for the range of variables which are of practical interest. For extremely small values of ℓ (say $\ell \approx \sqrt{a^2 + b^2}$), an improved initial guess on R_i is necessary. This may be done by inserting a card in the location noted in the program. The variable p_c/p_j is restricted to values less than 1.0.

The output gives the values of all input variables the notation Mueller if the RTMI subroutine was called, and the final values of the following variables: A_j, R_1, R_2, X_o, Y_o, Y_1, Y_2, θ_1, and θ_2.

```
        COMMON /CO/ A,B,PCPJ,L
        COMMON /OER/ C1,C2,YO,XO,Y1,Y2,TH1,TH2,SGN
        REAL L1,L2,L,LO,LN,LMM1,L3
        DATA PI / 3.1415927   /
        EXTERNAL F

C       ****************************************************************
C       TOL IS A RELATIVE TOLERANCE ON LBAR . CAN BE CHANGED BY
C       INSERTING CARD.
C       ****************************************************************

        TOL = 3.E-5
1       READ (5,10) A,B,PCPJ,L
10      FORMAT ( 4E20.4)
        WRITE(6,11) A,B,PCPJ,L
11      FORMAT(1H0///4H A= ,E16.4,10X,4HB = ,E16.4,10X,8HPC/PJ =  ,E16.4,
      1 10X,4HL = ,E16.4)

C       ****************************************************************
C       FIX SIGN ON SQUARE ROOT.
C       ****************************************************************

        SGN  = 1.0
        IF( PI*SQRT(A**2+B**2)/2.0 .LT. L) SGN  = -1.0


C       ****************************************************************
C       RO EQUALS INITIAL GUESS FOR R1.  CAN BE CHANGED BY INSERTING CARD.
C       ****************************************************************

        RO = SQRT(A**2 + B**2)*(1.0 + 10.**(-6))/2.
        RN = RO

C       ****************************************************************
C       CALCULATE K-TH VALUE OF R AND OBTAIN LBAR (R)
C       ****************************************************************

        DO 68 K=1,1000

C       ****************************************************************
C       SUBROUTINE F COMPUTES LBAR -L
C       ****************************************************************

2       PLN= F(RN)
        LN = PLN + L

C       ****************************************************************
C       IS R NEGATIVE OR IS LBAR (R) COMPLEX. IF SO R(K+1)=(R(K+1)+R(K))/2
C       (THIS OCCURS WHEN R(K) IS TOO SMALL)
C       ****************************************************************

        IF(PLN .NE. 10.**15 .AND. RN .GT. 0.)  GO TO 4
        IF( K .EQ. 1) GO TO 70
        RN = (RN+RNM1)/2.0
        GO TO 2
```

```
4       IF(K .EQ. 1) GO TO 5

C       ................................................................
C       DETERMINE IF SOLUTION HAS BEEN BOUNDED.  IF SO SET BOUNDS
C       AND CALL MUELLER ROUTINE.  IF NOT COMPUTE R(K+1) USING
C       NEWTON'S FORMULA.
C       ................................................................

        IF( SIGN(1.,L-LN) .NE. SIGN(1.,L-LNM1))GO TO 100
5       LNM1 = LN

C       ................................................................
C       SUBROUTINE DF COMPUTES LBAR'(R)
C       ................................................................

        DLN = DF(RN)                                                      29
        R1 = RN

C       ................................................................
C       TOLERANCE TEST
C       ................................................................

        IF( ABS(LN-L) .LT. TOL*ABS(L)) GO TO 110
        RNM1 = RN
        RN = RN-(LN-L)/DLN
68      CONTINUE
70      WRITE(6,71)                                                       36
71      FORMAT(17H1 RO COMPLEX ....      )
        STOP
100     IF( RN .GT. RNM1) GO TO 105
        DUM = RN
        RN = RNM1
        RNM1 = DUM
105     WRITE(6,104)                                                      40
104     FORMAT(1H0, 7HMUELLER)
        CALL RTM1 ( R1,LN,F,RNM1,RN,TOL     ,2000,IER)                    41
        IF( IER .EQ. 0) GO TO 110
        WRITE(6,106) IER,R1,LN                                            45
106     FORMAT(1H1,10HIER EQUAL   ,I2,5X,4HSTOP,2E25.6)
        STOP
110     R2 = R1/(1. - PCPJ)
        X07 = X0/A
        L1 = R1*TH1
        L2 = R2*TH2
        L3 = 0.0
        WRITE(6,55) R1,R2,X0,Y0,Y1,Y2,TH1,TH2                             47
55      FORMAT(1H0,5HR1 = ,E16.4,10X,5HR2 = ,E16.4,10X,5HX0 = ,E16.4,10X,
     1   5HY0 = ,E16.4,/1X,5HY1 = ,E16.4,10X,5HY2 = ,E16.4,10X,
     2   6HTH1 = ,E15.4,10X,6HTH2 = ,E15.4 /////////)
        GO TO 1
        END
```

```
      FUNCTION F (R1)
      COMMON /CO/ A,B,PCPJ,L
      COMMON /DER/ C1,C2,Y0,X0,Y1,Y2,TH1,TH2,SGN
      DATA PI / 3.1415927  /

C     ..........................................................
C     IF R(K) IS SUCH THAT L-BAR WILL BE CPMPLEX, THE VALUE
C     OF F = LBAR -L IS SET TO 10**15
C     ..........................................................

      REAL L
      R2 = R1 / (1.0-PCPJ)
      C1 = (R1-B-R2) / A
      C2 = A/2.0 + (B**2)/(2.0*A) - (R1*B)/A
      ASQ = (2.0*R2+2.0*C1*C2)**2 - (4.0*C2**2) * (C1**2 + 1.0)
      IF( ASQ .LT. 0.0) GO TO 25
      SQ = SQRT(ASQ)                                                       5
      Y0 = (-2.0*(R2+C1*C2)+SGN *SQ) / (2.0*(C1**2 + 1.0))

      X0 = C1*Y0+C2
      Y1 = Y0+R1
      Y2 = Y0+R2
      TH2 = ATAN(X0/Y2)                                                   6
      IF( Y2 .EQ. 0.) TH2 = PI/2.0
      IF(TH2 .LT. 0.0) TH2 = TH2 + PI
      PSI = ATAN((B-Y1)/(A-X0))                                          11
      IF( A-X0) 20,23,21
20    PSI = PSI+PI
21    TH1 = PSI+PI/2.0
      F  = R1*TH1 + R2*TH2 - L

C     ..........................................................
C     IF VALUE OF VARIABLES ON EACH ITERATION IS DESIRED, REMOVE
C     C ON THE TWO WRITE STATEMENTS.
C     ..........................................................

C     WRITE(6,22) R1,R2,TH1,TH2,Y0,ASQ,C1,C2,PCPJ,X0,Y1,Y2,A,B,F
      RETURN
23    PSI = PI/2.0
      GO TO 21
25    F = 10.0**15
C     WRITE(6,22) R1,R2,TH1,TH2,Y0,ASQ,C1,C2,PCPJ,X0,Y1,Y2,A,B,F         18
22    FORMAT(1H0/(7E18.5))
      RETURN
      END
```

```
FUNCTION DF(R1)
COMMON /DER/ C1,C2,YO,XO,Y1,Y2,TH1,TH2,SGN
COMMON /CO/ A,B,PCPJ,L
REAL K
K = 1.0 - PCPJ
DC1 = (K-1.0) / (K*A)
DC2 = -B/A
X = R1 / K + C1*C2
Y = C1**2 + 1.0
DX = 1.0/K + C1*DC2 + C2*DC1
DY = 2.0*C1 * DC1
Z = -SGN *SQRT( X**2 - Y*C2**2)
DZ = (1.0 / (2.0*Z)) * ( 2.0*X*DX - (2.0*Y*C2*DC2 + C2**2 * DY))
DYO = (1.0/Y**2) * (-Y * (DX+DZ) + (X+Z)*DY)
DXO = C1*DYO + YO*DC1 + DC2
DY1 = DYO + 1.0
DY2 = DYO + 1.0/K
S = B-Y1
T = A-XO
DST = (1.0/T**2) * (-T*DY1 + S*DXO)
DXOY2 = (1.0/Y2**2) * (Y2*DXO - XO*DY2)
DPSI = DST/ (1.0 + (S/T)**2)
DTH2 = DXOY2 / (1.0 + (XO/Y2)**2)
DTH1 = DPSI
DF = R1 * (DTH1 + DTH2/K) + TH1 + TH2/K
RETURN
END
```

2

RTMI   - EFN   SOURCE STATEMENT - IFN(S) -

```
C                                                                      RTMI0010
C      .................................................................RTMIC020
C                                                                      RTMIC030
C          SUBROUTINE RTMI                                             RTMIC040
C                                                                      RTMIC050
C          PURPOSE                                                     RTMIC060
C             TO SOLVE GENERAL NONLINEAR EQUATIONS OF THE FORM FCT(X)=0 RTMIC070
C             BY MEANS OF MUELLER-S ITERATION METHOD.                  RTMIC080
C                                                                      RTMIC090
C          USAGE                                                       RTMI0100
C             CALL RTMI (X,F,FCT,XLI,XRI,EPS,IEND,IER)                 RTMIC110
C             PARAMETER FCT REQUIRES AN EXTERNAL STATEMENT.            RTMIC120
C                                                                      RTMIC130
C          DESCRIPTION OF PARAMETERS                                   RTMI0140
C             X       - RESULTANT ROOT OF EQUATION FCT(X)=C.           RTMI0150
C             F       - RESULTANT FUNCTION VALUE AT ROOT X.            RTMIC160
C             FCT     - NAME OF THE EXTERNAL FUNCTION SUBPROGRAM USED. RTMIC170
C             XLI     - INPUT VALUE WHICH SPECIFIES THE INITIAL LEFT BOUND RTMIO180
C                       OF THE ROOT X.                                 RTMIC190
C             XRI     - INPUT VALUE WHICH SPECIFIES THE INITIAL RIGHT BOUNDRTMIO200
C                       OF THE ROOT X.                                 RTMI0210
C             EPS     - INPUT VALUE WHICH SPECIFIES THE UPPER BOUND OF THE RTMI0220
C                       ERROR OF RESULT X.                             RTMI0230
C             IEND    - MAXIMUM NUMBER OF ITERATION STEPS SPECIFIED.   RTMI0240
C             IER     - RESULTANT ERROR PARAMETER CODED AS FOLLOWS     RTMI0250
C                       IER=0 - NO ERROR,                              RTMI0260
C                       IER=1 - NO CONVERGENCE AFTER IEND ITERATION STEPS RTMI0270
C                               FOLLOWED BY IEND SUCCESSIVE STEPS OF   RTMI0280
C                               BISECTION,                             RTMIC290
C                       IER=2 - BASIC ASSUMPTION FCT(XLI)*FCT(XRI) LESS RTMI0300
C                               THAN OR EQUAL TO ZERO IS NOT SATISFIED. RTMIC310
C                                                                      RTMIC320
C          REMARKS                                                     RTMIC330
C             THE PROCEDURE ASSUMES THAT FUNCTION VALUES AT INITIAL    RTMIC340
C             BOUNDS XLI AND XRI HAVE NOT THE SAME SIGN. IF THIS BASIC RTMIC350
C             ASSUMPTION IS NOT SATISFIED BY INPUT VALUES XLI AND XRI, THE RTMIC360
C             PROCEDURE IS BYPASSED AND GIVES THE ERROR MESSAGE IER=2. RTMIC370
C                                                                      RTMIO380
C          SUBROUTINES AND FUNCTION SUBPROGRAMS REQUIRED               RTMI0390
C             THE EXTERNAL FUNCTION SUBPROGRAM FCT(X) MUST BE FURNISHED RTMIC400
C             BY THE USER.                                             RTMI0410
C                                                                      RTMI0420
C          METHOD                                                      RTMIC430
C             SOLUTION OF EQUATION FCT(X)=0 IS DONE BY MEANS OF MUELLER-S RTMI0440
C             ITERATION METHOD OF SUCCESSIVE BISECTIONS AND INVERSE    RTMI0450
C             PARABOLIC INTERPOLATION, WHICH STARTS AT THE INITIAL BOUNDS RTMIC460
C             XLI AND XRI. CONVERGENCE IS QUADRATIC IF THE DERIVATIVE OF RTMIC470
C             FCT(X) AT ROOT X IS NOT EQUAL TO ZERO. ONE ITERATION STEP RTMI0480
C             REQUIRES TWO EVALUATIONS OF FCT(X). FOR TEST ON SATISFACTORYRTMIC490
C             ACCURACY SEE FORMULAE (3,4) OF MATHEMATICAL DESCRIPTION. RTMI0500
C             FOR REFERENCE, SEE G. K. KRISTIANSEN, ZERO OF ARBITRARY  RTMI0510
C             FUNCTION, BIT, VOL. 3 (1963), PP.205-206.                RTMIC520
C                                                                      RTMIC530
C      .................................................................RTMI0540
C                                                                      RTMI0550
```

```
        RTMI      -  EFN   SOURCE STATEMENT  -  IFN(S)  -

   11 IF(ABS(XR-XL)-TOL)12,12,13                              RTMI1120
   12 IF(ABS(FR-FL)-TOLF)14,14,13                             RTMI1130
   13 CONTINUE                                                RTMI1140
C     END OF BISECTION LOOP                                   RTMI1150
C                                                             RTMI1160
C     NO CONVERGENCE AFTER IEND ITERATION STEPS FOLLOWED BY IEND  RTMI1170
C     SUCCESSIVE STEPS OF BISECTION OR STEADILY INCREASING FUNCTION  RTMI1180
C     VALUES AT RIGHT BOUNDS. ERROR RETURN.                   RTMI1190
      IER=1                                                   RTMI1200
   14 IF(ABS(FR)-ABS(FL))16,16,15                             RTMI1210
   15 X=XL                                                    RTMI1220
      F=FL                                                    RTMI1230
   16 RETURN                                                  RTMI1240
C                                                             RTMI1250
C     COMPUTATION OF ITERATED X-VALUE BY INVERSE PARABOLIC INTERPOLATIORTMI1260
   17 A=FR-F                                                  RTMI1270
      DX=(X-XL)*FL*(1.+F*(A-TOL)/(A*(FR-FL)))/TOL            RTMI1280
      XM=X                                                    RTMI1290
      FM=F                                                    RTMI1300
      X=XL-DX                                                 RTMI1310
      TOL=X                                                   RTMI1320
      F=FCT(TOL)                                              RTMI1330        41
      IF(F)18,16,18                                           RTMI1340
C                                                             RTMI1350
C     TEST ON SATISFACTORY ACCURACY IN ITERATION LOOP         RTMI1360
   18 TOL=EPS                                                 RTMI1370
      A=ABS(X)                                                RTMI1380
      IF(A-1.)20,20,19                                        RTMI1390
   19 TOL=TOL*A                                               RTMI1400
   20 IF(ABS(DX)-TOL)21,21,22                                 RTMI1410
   21 IF(ABS(F)-TOLF)16,16,22                                 RTMI1420
C                                                             RTMI1430
C     PREPARATION OF NEXT BISECTION LOOP                      RTMI1440
   22 IF(SIGN(1.,F)+SIGN(1.,FL))24,23,24                      RTMI1450
   23 XR=X                                                    RTMI1460
      FR=F                                                    RTMI1470
      GO TO 4                                                 RTMI1480
   24 XL=X                                                    RTMI1490
      FL=F                                                    RTMI1500
      XR=XM                                                   RTMI1510
      FR=FM                                                   RTMI1520
      GO TO 4                                                 RTMI1530
C     END OF ITERATION LOOP                                   RTMI1540
C                                                             RTMI1550
C                                                             RTMI1560
C     ERROR RETURN IN CASE OF WRONG INPUT DATA                RTMI1570
   25 IER=2                                                   RTMI1580
      RETURN                                                  RTMI1590
      END                                                     RTMI1600
```

Appendix II

INELASTIC LOADED TRUNK SHAPE

The computer program described in this appendix computes the cross-sectional loaded shape for an inelastic trunk. The logic is similar to that presented in Section 4.5, but with the restriction $\varepsilon = 0$.

The input variables are:

a   = x coordinate of the upper trunk attachment point

b   = y coordinate of the upper trunk attachment point

p_c/p_j = ratio of cushion pressure to trunk pressure

ℓ = trunk length

y_0 = y coordinate of lower-most segment of the trunk.

         (Note: y_0 is always negative.)

The program solves Equation (4-37) ($\bar{\ell}(R_1) - \ell = 0$) to the desired tolerance using Mueller's Iteration Method. The main program brackets the solution and then calls the Mueller subroutine. The Mueller subroutine may call Function $F(R_1)$ or Function $G(R_1)$.

The subroutines are as follows:

Subroutine RTMI uses Mueller's Iteration Method to converge on the solution of $F(R_1) = \bar{\ell}(R_1) - \ell = 0$.

Note: This is the same subroutine as described in Appendix I and it is not repeated here.

Function $F(R_1)$ evaluates $\bar{\ell}(R_1) - \ell = F(R_1)$.

271

Note: This is not the same $F(R_1)$ subroutine as described in Appendix I because $\ell(R_1)$ is defined differently in the two cases.

Function $G(R_1)$ evaluates $x_1(R_1) - x_2(R_1) = G(R_1)$.

The input variables b and y_0 are used to compute $(R_1)_{MIN}$, the minimum value of R_1 which is possible. This value of R_1 gives the condition $x_1 = a$. The $\bar{\ell}$ associated with the minimum R_1 is then computed. This value of $\bar{\ell}$ is called ℓ_4 and is used in determining the sign on the square root in Equation (4-36). Three possibilities exist:

Case 1 — If $\ell > \ell_4$ then $x_1 > a$ and the sign is plus

Case 2 — If $\ell = \ell_4$ then $x_1 = a$ and the radical is zero

Case 3 — If $\ell < \ell_4$ then $x_1 < a$ and the sign is minus

For cases 1 and 2, $(R_1)_{MIN}$ is a suitable lower bound for the solution of $F(R_1) = 0$. The upper bound is found from Equation (4-40). Once the upper and lower bounds are established the Mueller subroutine is called to converge on the solution.

For case 3, it is necessary to find a lower bound on the equation $F(R_1) = \ell(R_1) - \ell = 0$. The minimum $\ell(R_1)$ occurs when $\ell_3 = 0$ and $x_1 = x_2$. The equation $G(R_1) = x_1(R_1) - x_2(R_2) = 0$ is solved by Mueller's method to determine the value of R_1 for the condition $x_1 = x_2$. The upper bracket for $G(R_1) = 0$ is taken at $x_1(R_1) = a$. The lower bracket for $G(R_1) = 0$ is taken as $x_1(R_1) = 0$. Function $G(R_1)$ is called by the Mueller subroutine in this case. The R_1 obtained from $G(R_1) = 0$ equation is then taken as the lower bracket for the $F(R_1) = 0$ equation. The upper bracket for $F(R_1) = 0$ is taken as $x_1(R_1) = a$. Having bracketed the solution for $F(R_1) = 0$, Mueller's Iteration Method is employed to converge on the solution.

The program has been found to converge for the range of variables of practical interest. Restrictions are as follows:

$$p_c/p_j < 1.0$$

$$y_o < 0$$

y_o must be such that $\ell_3 > 0$. The maximum value of y_o is given by the equilibrium trunk shape program (Appendix I).

The output gives the initial values of all input variables and the final values of the following variables:

R_1, R_2, θ_1, θ_2, y_1, y_2, ℓ_1, ℓ_2, $\overline{X}$, A_j, ℓ_3, x_1, and x_2.

The final value of $F(R_1)$ is also printed under the lable LN.

```
          DICKEN     -  FFN   SOURCE STATEMENT  -  IFN(S)  -

       COMMON/CCM/PCPJ,YO,L,A,B,TH1,TH2,X1,X2,Y1,Y2,PSI,SIGN,T,L4
       REAL L,LX,L4,L3,L1,L2
       EXTERNAL F,G
       PI = 3.1415927

C      *****************************************************************
C      TOL IS A RELATIVE TOLERANCE ON LBAR . CAN BE CHANGED BY
C      INSERTING CARD.
C      *****************************************************************

       TOL = 3.E-5
105    READ(5,1) A,B,PCPJ,L,YO                                           2
1      FORMAT(5E15.4)


C      *****************************************************************
C      RO EQUALS INITIAL GUESS FOR R1.  CAN BE CHANGED BY INSERTING CARD.
C      *****************************************************************

       RO = (B - YO*(1.0 + 10.0**(-6))/2.0                               3
       WRITE(6,2)                                                        4
2      FORMAT( 1H1)
       RNM1 =                AMAX1(-YO*(1. - PCPJ)/2.,(B-YO)/2.)

C      *****************************************************************
C      FIX SIGN ON SQUARE ROOT.
C      *****************************************************************

       SIGN = 1.

C      *****************************************************************
C      SUBROUTINE F IS CALLED TO OBTAIN L4
C      *****************************************************************

       T = F(RNM1)

C      *****************************************************************
C      DETERMINE WHETHER X1 IS GREATER OR LESS THAN A.
C      IF GREATER SIGN IS POSITIVE
C      IF LESS SIGN IS NEGATIVE
C      *****************************************************************
                                                                        5
       IF( L .LT. L4) GO TO 10C

C      *****************************************************************
C      CONDITION X1 GT A.  COMPUTE UPPER BOUND ON R.
C      *****************************************************************

       SQR = SQRT(A**2 + B**2)                                          9
       RN = L/(2.0*PI) + SQR/4.0
       IF(SQR .LE. 2.*L/PI) GO TO 3
       RN = L/PI
       DO 5  I = 1,30
       RN = 10.*RN
       IF(RN*SIN (L/2.*RN) .GE. SQR/2.) GO TO 3                          16
```

```
5       CONTINUE
        WRITE(6,7)                                                      22
7       FORMAT(1H0,12H UPPER BOUND)
        R1 = 0.0
        GO TO 4

C       ****************************************************************
C       USE MUELLER'S METHOD TO COMPUTE R SUCH THAT TOLERANCE
C       ON LBAR IS SATISFIED. (MUELLER ROUTINE CALLS SUBROUTINE F TO
C       COMPUTE LBAR = F(R) - L)
C       ****************************************************************

3       CALL RTMI(R1,LN,F,PKM1 , RN  ,10.0E-5,  60,IER)                 25
        IF(IER .EQ. 0) GO TO 4
        WRITE(6,11) IER                                                 29
11      FORMAT(1H1,14HMUELLER FAILED ,I5)
        R1 = 0
4       R2 = R1 / (1.-PCPJ)
        L3 = X1-X2
        XBAR = (X1 + X2 )/2.0
        L1 = R1*TH1
        L2 = R2*TH2
        AJ = (TH2 * R2* *2)/2.- (X2 + Y2)/2. - L3*YO + (TH1 * R1**2)/2.0 +
     1  (X1 - A)*Y1 + ((X1 - A)*(B - Y1))/2.0
        WRITE(6,500) A,B,PCPJ,YC,L                                      31
500     FORMAT(1HC,4HA = ,F8.3,14X,4HB = ,F8.3,14X,7HPCPJ = ,F8.5,11X,
     1  5HYO = ,F8.3,13X,4HL = ,F8.3 ///)
        WRITE(6,501) R1,R2,LN,TH1,TH2                                   32
501     FORMAT( 1HC,5HR1 = ,F8.3,13X,5HR2 = ,F8.3,13X,5HLN = ,F8.5,
     1  13X,6HTH1 = ,F8.4,12X,5HTH2 = ,F8.4 ///)
        WRITE(6,502) Y1,Y2,L1,L2                                        33
502     FORMAT( 1H0,5HY1 = ,F8.4,13X,5HY2 = ,F8.2,13X,5HL1 = ,F8.4,
     1  13X,5HL2 = ,F8.4 ///)
        WRITE(6,503) XBAR,AJ,L3                                         34
503     FORMAT( 1H0,7HXBAR = ,F8.4,11X,5HAJ = ,F8.2,13X,5HL3 = ,F8.4)
        GO TO 105

C       ****************************************************************
C       CONDITION X1 LESS THAN A.  COMPUTE THE VALUE OF R SUCH THAT
C       X1 = A .  THIS VALUE OF R GIVES THE MAXIMUM VALUE OF L
C       POSSIBLE UNDER THE RESTRICTIONS X2 LT X1, X1 LT A
C       ****************************************************************

100     SIGN = -1.
        RN =(A**2 + B**2 + YO**2 - 2.*YO*B)/(2.*(B-YO) )
        IF(X2 .LE. A) GO TO 111
        SIGN = 1
        WRITE(6,505)                                                    40
505     FORMAT(1HC,129HCONDITION X2 GT X1 AND X1 LT A NOT SOLVED BY THIS
     1  PROGRAM.  EITHER THERE IS NO SOLUTION OR A BETTER GUESS FOR RO
     1  IS REQUIRED  )

C       ****************************************************************
C       USE MUELLERS METHOD TO COMPUTE FINAL UPPER BOUND ON R
C       WHICH IS THE CONDITION THAT L3 = 0. ( MUELLER ROUTINE
```

```
      FUNCTION F(R1)
      COMMON/CCM/PCPJ,VO,L,A,P,TH1,TH2,X1,X2,Y1,Y2,PSI,SIGN,T,L4
      REAL L,L4
      DATA PI /3.1415927/

C     ****************************************************************
C     IF R(X) IS SUCH THAT L-BAR WILL BE COMPLEX, THE VALUE
C     OF F = LBAR -L IS SET TO 10**15
C     ****************************************************************

      R2 = R1 /(1.0 - PCPJ)
      A1 = -VO**2 -2.0*R2*VO
      IF(A1 .LT. -10.**(-4)) GO TO 45                              2
      IF(A1 .LT. 0. ) A1 = 0.
      X2 = SQRT(A1)                                                8
      Y2 = R2 + VO
      TH2 = ATAN(X2/Y2)                                           9
      IF(Y2 .EQ. 0.) TH2 = PI/2.
      IF( TH2 .LT. 0. ) TH2 = TH2 + PI
      L4 = (PI*(P-YO))/ 2.0 + TH2*R2 +ABS( A - X2 )
9     A2 = -(YC+R1-P)**2 +R1**2
      IF(A2 .LT. -10.**(-4)) GO TO 50                            15
      IF(A2 .LT. 0. ) A2 = 0.
      IF( A2 .LT. C.) GO TO 50
      X1= A+SIGN * SQRT(A2)                                      24
      Y1= R1 + YC
      T = (P-Y1) / (A-X1)
      PSI = ATAN(T)                                              25
      IF( A-X1 .GE. 0.) GO TO 10
      PSI = PSI + PI
10    IF(A - X1 .EQ. 0.) PSI = .PI/2.
      TH1 = PI/2. + PSI
      F = TH1*R1 + TH2*R2 +ABS( X1-X2)- L

C     ****************************************************************
C     IF VALUE OF VARIABLES ON EACH ITERATION IS DESIRED, REMOVE
C     C ON FOLLOWING WRITE STATEMENT.
C     ****************************************************************

C     WRITE(6,51) R1,TH1,X1,A,X2,L4,F                           32
51    FORMAT(15H FUNCTION F  R1,F8.4,5X,3HTH1,F8.4,5X,2HX1,F8.4,5X,
     1 1HA,F8.4,5X,2HX2,F8.4,5X,2HL4,F8.4,5X,1HF,F8.4)
      RETURN
45    F = 10.0**15                                              34
      WRITE(6,103)                                              35
103   FORMAT(1HC,12HCOMPLEX IN F  )
      RETURN
50    F = 10.C**15                                              37
      WRITE(6,103)                                              38
      RETURN
      END
```

```
C      CALLS SUBROUTINE C )
C      ************************************************************

11)    CALL RTMI( R1,LN,C,RNM1,RN,1C,CE-6,2000,IER)
       IF( IER .EQ. 0) GC TO 201                                    42
       WRITE(6,11) IER
       GO TO 4                                                      46
201    RN   = R1
       GO TO 3
       END
```

```
      FUNCTICN C(R1)
      COMMON/CCM/PCPJ,YO,L,A,R,TH1,TH2,X1,X2,Y1,Y2,PSI,SIGN,T,L4
      REAL L,L4
      DATA PI /3.1415927/
C
C     ****************************************************************
C     IF R(K) IS SUCH THAT L-BAR WILL BE COMPLEX, THE VALUE
C     IS SET TC 10**15
C     ****************************************************************
C
      R2 = R1 /(1.0 - PCPJ)
      A1 = -YO**2 -2.0*R2*YO
      IF(A1 .LT. -1C.**(-4)) GO TO 45                                    2
      IF(A1 .LT. 0. ) A1 = 0.
      X2 = SQRT(A1)                                                      8
      Y2 = R2 + YO
      TH2 = ATAN(X2/Y2)                                                  9
      IF(Y2 .EQ. C.) TH2 = PI/2.
      IF( TH2 .LT. 0. ) TH2 = TH2 + PI
      L4 = (PI*(P-YO))/ 2.0 + TH2*R2 +ABS( A - X2 )
8     A2 = -(YO+R1-R)**2 +R1**2
      IF(A2 .LT. -1C.**(-4)) GO TO 50                                    15
      IF(A2 .LT. 0. ) A2 = 0.
      X1 = A+SIGN * SQRT(A2)                                             21
      Y1= R1 + YO
      T = (P-Y1) / (A-X1)
      PSI = ATAN(T)                                                      22
      IF( A-X1 .GE. 0.) GO TO 10
      PSI = PSI + PI
10    IF(A - X1 .EQ. 0.) PSI = PI/2.
      TH1 = PI/2. + PSI
      G = X1 - X2 - 10.**(-3)
C
C     ****************************************************************
C     IF VALUE CF VARIABLES CN EACH ITERATICN IS DESIRED, REMOVE
C     C ON FOLLOWING WRITE STATEMENT.
C     ****************************************************************
C                                                                       29
C     WRITE(6,51) R1,TH1,X1,A,X2,L4,G                                   30
51    FORMAT(15H FUNCTION G  R1,F8.4,5X,3HTH1,F8.4,5X,2HX1,F8.4,5X,
     1 1HA,F8.4,5X,2HX2,F8.4,5X,2HL4,F8.4,5X,1HG,F8.4)
      RETURN
45    F = 10.0**15                                                      32
      WRITE(6,104)                                                      33
104   FORMAT(1HC,12HCCMPLEX IN G  )
      RETURN
50    F = 10.0**15                                                      35
      WRITE(6,104)                                                      36
      RETURN
      END
```

ELASTIC FREE TRUNK SHAPE

The computer program described in this appendix computes the cross-sectional shape for a free elastic trunk. The elasticity may be non-linear. The logic is similar to that presented in Section 4.4.

The initial input variables are:

a = x coordinate of upper trunk attachment point, ft.

b = y coordinate of upper trunk attachment point, ft.

p_c/p_j = ratio of cushion pressure to trunk pressure

P_j = trunk pressure lb/ft^2 absolute

ℓ = trunk length of $\epsilon = 0$, ft.

The elasticity of the trunk is defined by 15 points or less from the tension versus strain curve and the derivatives of the end points.

The input variables for the elastic curve are:

NN = number of points selected from the elastic curve (15 points maximum)

ARG = value of tension (R * P_j) at each point, lb/ft.

TAB = value of strain (epsilon) at each point ft/ft or in./in.

DV (1) = the reciprocal of the derivative of elastic curve at left end point, ft/lb

DV (2) = the reciprocal of the derivative of elastic curve at right end point, ft/lb

This program is similar to the program described in Appendix I, except the equation to be satisfied in this case is as follows:

$$F(R_1) = \bar{\ell} - \ell (1 + \epsilon) = 0$$

where $\epsilon = f_1(R_1)$ and $\bar{\ell} = f_2(R_1)$

The program uses the following subroutines:

Function $F(R_1)$ evaluates $\bar{\ell} - \ell (1 + \epsilon) = F(R_1)$

Function $DF(R_1)$ evaluates the derivative of $F(R_1)$.

Subroutine RTM1 uses Mueller's Iteration Method to converge on the solution of $F(R_1) = 0$, once the solution is bounded. This subroutine is listed in Appendix I and is not repeated here.

Subroutine SPLN1 develops the coefficients for a third degree interpolating polynomial between each pair of points which specify the elastic curve. These coefficients are stored in the C matrix whose dimension is 4 (NN — 1).

Subroutine SPLN2 uses the coefficients developed by SPLN1 to interpolate for the value of ϵ at $R_1 \times P_j$. The output of SPLN2 is a five dimensional vector V with the following values:

V (1)	= tension or ($R_1 \times P_j$)	
V (2)	= ϵ	
V (3)	= ϵ'	
V (4)	= ϵ''	
V (5)	= key;	1 = value of V(1) below the table
		2 = value of V(1) in the table
		3 = v of V(1) above the table

These values may be printed out by removing the comment notation from the write statement above statement 409.

The output gives the values of all input variables, the initial guess for R_1, the notation Mueller if the RTM1 subroutine was called, and the final values of the following variables:

ℓ, T_t, ϵ, R_1, R_2, X_o, Y_o, Y_1, Y_2, ϕ_1, ϕ_2, and A_j.

```
      COMMON / MAINE / NN, ARG, TAB, C, PJ, V
      COMMON /CC/ A,B,PCPJ,L
      COMMON /DER/ C1,C2,YO,XU,Y1,Y2,TH1,TH2,SGN
      DIMENSION TAB(15), ARG(15),W(99), C(95),DV(2), V(5)
      REAL L1,L2,L,L3,LN,LNM1
      DATA PI / 3.1415927   /
      EXTERNAL E

C     ***********************************************************
C     TOL IS A RELATIVE TOLERANCE ON LBAR . CAN BE CHANGED BY
C     INSERTING CARD.
C     ***********************************************************

      TOL = 3.E-5

C     ***********************************************************
C     READ DATA FOR TABLE DEFINING EPSILON AS A FUNCTION OF R*PJ AND
C     PASS TO SPLINE INTERPOLATION SUBROUTINE.  DV(1) AND DV(2) ARE
C     THE DERIVATIVES AT THE LEFT AND RIGHT ENDPOINTS RESPECTIVELY.
C     ***********************************************************

      READ(5,62) NN                                                     2
62    FORMAT(I10)
      READ(5,31)    DV                                                  4
3     READ(5,31) (ARG(I),I=1,NN)                                        6
      READ(5,31)(TAB(I),I=1,NN)                                        13
31    FORMAT(8E10.2)
      CALL SPLN1 ( NN,ARG,TAB,1,DV,C, W )                             20
1     READ(5,10) A,B,PCPJ,L,PJ                                         21
10    FORMAT(5F15.4,I5)
      WRITE ( 6,400 )                                                 22
400   FORMAT ( 1H1, 40X, 36H*****    ELASTIC EQ. TR. SHAPE  *****     )
      WRITE ( 6,401 )                                                 23
401   FORMAT ( 1H0, 131( 1H* ) )
      WRITE ( 6,402 ) DV                                              24
402   FORMAT ( 1H0, 5X, 37H*****  DERIVATIVES AT THE END POINTS  ,
     1        19HOF THE TABLE  ***** ,
     2 //  14X, 8HDARG1 = , E20.5, 10X, 8HDARGN = , E20.5 ///// )
      WRITE ( 6,403 ) NN, ( TAB(I), ARG(I), I=1,NN )                 26
403   FORMAT ( 1H0, 5X, 14HTABLE ENTRIES , I2,
     1 //  ( 5X, 2F20.5 ))
      WRITE ( 6,404 ) A, B, PCPJ, L, PJ                              34
404   FORMAT ( 1H0, 5X, 4HA = , E20.5, 20X, 4HB = , E20.5, 20X,
     1 7HPCPJ = , E20.5,  //  6X, 4HL = , E20.5, 20X, 5HPJ = , E19.5 )

C     ***********************************************************
C     FIX SIGN ON SQUARE ROOT.
C     ***********************************************************

      SGN = 1.0
      IF( PI*SQRT(A**2+B**2)/2.0 .LT. L) SGN = -1.0


C     ***********************************************************
```

```
      DIGGES                                                    02/09/70
         FORTRAN    -  FEN   SOURCE STATEMENT  -  IFN(S)  -

C     RO EQUALS INITIAL GUESS FOR R1.  CAN BE CHANGED BY INSERTING CARD.
C     ***********************************************************************
                                                                       35
      RO = SQRT(A**2 + P**2)*(1.0 + 10.**(-6))/2.                      38
      WRITE ( 6,406 ) RC                                               40
406   FORMAT ( 1H0, 5X, 12H****** RO =  , F16.4, 2X, 5H******    //  )
      RN = RO

C     ***********************************************************************
C     CALCULATE K-TH VALUE OF R AND OBTAIN LBAR (R)
C     ***********************************************************************

24    DO 68 K = 1,1000

C     ***********************************************************************
C     SUBROUTINE F COMPUTES LBAR -L(1 + EPS)
C     ***********************************************************************

2     PLN= F(RN)                                                       46
      LN = PLN + L

C     ***********************************************************************
C     IS R NEGATIVE OR IS LBAR (R) COMPLEX. IF SO R(K+1)=(R(K+1)+R(K))/2
C     (THIS OCCURS WHEN R(K) IS TOO SMALL)
C     ***********************************************************************

      IF(PLN .NE. 10.**15 .AND. RN .GT. 0.)  GO TO 4                   47
      IF( K .EQ. 1) GO TO 70
      RN = (RN+RNM1)/2.0
      GO TO 2
4     IF(K .EQ. 1) GO TO 5

C     ***********************************************************************
C     DETERMINE IF SOLUTION HAS BEEN BOUNDED.  IF SO SET BOUNDS
C     AND CALL MUELLER ROUTINE.  IF NOT COMPUTE R(K+1) USING
C     NEWTON'S FORMULA.
C     ***********************************************************************

      IF( SIGN(1.,L-LN) .NE. SIGN(1.,L-LNM1))GO TO 100
5     LNM1 = LN

C     ***********************************************************************
C     SUBROUTINE DF COMPUTES (LBAR(R))'
C     ***********************************************************************

      DLN = DF(RN)                                                     62
      R1 = RN

C     ***********************************************************************
C     TOLERANCE TEST
C     ***********************************************************************

      IF( ABS(LN-L) .LT. TOL*ABS(L)) GO TO 110
      RNM1 = RN
```

```
        RN = RN-((LA-L)/DLN
68      CONTINUE


70      WRITE(6,71)                                                      69
71      FORMAT(17H1 RC COMPLEX ....
        STOP

100     IF( RN .GT. RNM1) GO TO 105
        DUM = RN
        RN = RNM1
        RNM1 = DUM
105     WRITE(6,104)                                                     73
104     FORMAT(1H0, 7HMUELLER)
        CALL RTMI ( R1,LN,F,RNM1,RN,TOL    ,2000,IER)                    74
        IF( IER .EQ. 0) GO TO 110
        WRITE(6,106) IER,R1,LN                                           78
106     FORMAT(1H1,10HIER EQUAL  ,I2,5X,4HSTOP,2E25.6)
        STOP


110     R2 = R1/(1. - PCPJ)
        X07 = X0/A
        BAR = TH1 * R1  +  TH2 * R2
        AJ = (TH2*R2**2)/2. - (X0*Y2)/2.+ (TH1*R1**2)/2.
     1  + (X0-A)*Y1 + ((X0-A)*(B-Y1))/2.
        WRITE ( 6,727 ) BAR, V(1), V(2),AJ                               80
727     FORMAT ( 1H0, 7HLBAR = , E16.5, 10X, 6HTEN = , E16.5, 10X,
     1  6HFPS = , E16.5 , 10X , 5HAJ = , E16.5)
        WRITE(6,55) R1,R2,X0,Y0,Y1,Y2,TH1,TH2                           81
55      FORMAT(1H0,5HR1 = ,F16.4,10X,5HR2 = ,E16.4,10X,5HX0 = ,E16.4,10X,
     1  5HY0 = ,E15.4,/1X,5HY1 = ,E16.4,10X,5HY2 = ,E16.4,10X,
     2  6HTH1 = ,E15.4,10X,6HTH2 = ,E15.4 //  )
        GO TO 1
        END
```

```
DICGES                                                      02/09/70
        FTN        -  EFN   SOURCE STATEMENT  -  IFN(S)  -


        FUNCTION F (R1)
        CCMMON / MAINE / NN, ARG, TAB, C, PJ, V
        COMMCN /CC/ A,B,PCPJ,L
        CCMMON /DER/ C1,C2,YO,X0,Y1,Y2,TH1,TH2,SGN, PJDEPS
        DIMENSICN C(99),ARG(15),TAB(15),V(5)
        DATA PI / 3.1415927   /
        REAL L

C       ***************************************************************
C       IF R(K) IS SUCH THAT L-BAR WILL BE COMPLEX, THE VALUE
C       OF F = LHAR -L IS SET TO 10**15
C       ***************************************************************


C       ***************************************************************
C       SPLN2 INTERPOLATES FCR EPS AT R1*PJ.
C       ***************************************************************


        V(1) = R1 * PJ
        CALL SPLN2 ( NN, ARG, TAB, C, V  )

C       ***************************************************************
C       IF VALUE OF VARIABLES ON EACH ITERATICN IS DESIRED, REMOVE
C       C ON THE TWO WRITE STATEMENTS.
C       ***************************************************************

C       WRITE ( 6,409 )  V, R1, PJ                                   2
409     FORMAT ( 1HC, 5X, 27H.....  SPLINE OUTPUT  .....
       1 // (5E25.7) )
        EPS = V(2)
        DEPS = V(3)
        PJDEPS = PJ * DEPS


        R2 = R1 / (1.0-PCPJ)
        C1 = (R1-B-R2) / A
        C2 = A/2.0 + (B**2)/(2.0*A) - (R1*B)/A
        ASQ = (2.0*R2+2.0*C1*C2)**2 - (4.0*C2**2) * (C1**2 + 1.0)
        IF( ASQ .LT. 0.0) GO TO 25
        SQ = SQRT(ASQ)                                               7
        YO = (-2.0*(R2+C1*C2)+SGN *SQ) / (2.0*(C1**2 + 1.0))

        X0 = C1*YC+C2
        Y1 = YO+R1
        Y2 = YO+R2
        TH2 = ATAN(X0/Y2)                                           8
        IF( Y2 .EQ. 0.) TH2 = PI/2.0
        IF(TH2 .LT. 0.0) TH2 = TH2 + PI
        PSI = ATAN((B-Y1)/(A-X0))                                   13
        IF( A-XC) 20,21,21
20      PSI = PSI+PI
21      TH1 = PSI+PI/2.0
        F   = R1*TH1 + R2*TH2 - L* (1.0 + EPS)
C       WRITE(6,22) R1,R2,TH1,TH2,YC,ASQ,C1,C2,PCPJ,X0,Y1,Y2,A,B,F
```

```
      DIGGES
         FIN        -  FFN   SOURCE STATEMENT  -  IFN(S)  -

      RETURN
23    PSI = PI/2.0
      GO TO 21                                                              20
25    F = 10.0**15
C     WRITE(6,22) R1,R2,TH1,TH2,YO,ASQ,C1,C2,PCPJ,XC,Y1,Y2,A,B,F
22    FORMAT(1H0/(7F18.5))
      RETURN
      END
```

```
FUNCTION DF(R1)
COMMON /DER/ C1,C2,YO,XC,Y1,Y2,TH1,TH2,SGN, PJDEPS
COMMON /CC/ A,B,PCPJ,L
REAL K,L
K = 1.0 - PCPJ
DC1 = (K-1.0) / (K*A)
DC2 = -B/A
X = R1 / K + C1*C2
Y = C1**2 + 1.0
DX = 1.0/K + C1*DC2 + C2*DC1
DY = 2.0*C1 * DC1
Z = -SGN *SQRT( X**2 - Y*C2**2)                                                2
DZ = (1.0 / (2.0*Z)) * ( 2.0*X*DX - (2.0*Y*C2*DC2 + C2**2 * DY))
DYO = (1.0/Y**2) * (-Y * (DX+DZ) + (X+Z)*DY)
DXO = C1*DYC + YO*DC1 + DC2
DY1 = DYO + 1.0
DY2 = DYO + 1.0/K
S = B-Y1
T = A-XO
DST = (1.0/T**2) * (-T*DY1 + S*DXO)
DXCY2 = (1.C/Y2**2) * (Y2*DXC - XO*DY2)
DPST = DST/ (1.0 + (S/T)**2)
DTH2 = DXCY2 / (1.0 + (XO/Y2)**2)
DTH1 = DPST
DF = R1 * (DTH1 + DTH2/K) + TH1 + TH2/K - L*PJDEPS
RETURN
END
```

```
      SUBROUTINE SPLN1 (N,X,Y,J,D,C,W)                          SPLN1
      DIMENSION X(1),Y(1),D(2),C(1),W(1)                        SPLN1
C     ----------------------------------------------------------SPLN1
C                OVER THE INTERVAL X(I) TO X(I+1), THE INTERPOLATING   SPLN.
C                POLYNOMIAL                                     SPLN1
C                   Y=Y(I)+A(I)*Z+B(I)*Z**2+E(I)*Z**3           JPLN1
C                WHERE Z=(X-X(I))/(X(I+1)-X(I))                 SPLN1
C                IS USED. THE COEFFICIENTS A(I),B(I) AND E(I) ARE COMPUTED SPLN1
C                BY SPLN1 AND STORED IN LOCATIONS C(3*I-2),C(3*I-1) AND  SPLN1
C                C(3*I) RESPECTIVELY.                           SPLN1
C                WHILE WORKING IN THE ITH INTERVAL,THE VARIABLE Q WILL   SPLN1
C                REPRESENT Q=X(I+1) - X(I), AND YI WILL REPRESENT  SPLN1
C                Y(I+1)-Y(I)                                    SPLN1
C     ----------------------------------------------------------SPLN1
C                                                               SPLN1
      Q=X(2) - X(1)                                             SPLN1
      YI =Y(2) - Y(1)                                           SPLN1
      IF (J.EQ.2) GO TO 100                                     SPLN1
C     ----------------------------------------------------------SPLN1
C                IF THE FIRST DERIVATIVE AT THE END POINTS IS GIVEN,  SPLN1
C                A(1) IS KNOWN, AND THE SECOND EQUATION BECOMES  SPLN1
C                MERELY B(1)+E(1)=YI - Q*D(1).                  SPLN1
C     ----------------------------------------------------------SPLN1
      C(1)=Q*D(1)                                               SPLN1
      C(2)=1.0                                                  SPLN1
      W(2)=YI-C(1)                                              SPLN1
      GO TO 200                                                 SPLN1
C     ----------------------------------------------------------SPLN1
C                IF THE SECOND DERIVATIVE AT THE END POINTS IS GIVEN  SPLN1
C                W(1) IS KNOWN. THE SECOND EQUATION BECOMES     SPLN1
C                A(1)+E(1)=YI-C.5*Q*Q*D(1). DURING THE SOLUTION OF  SPLN1
C                THE 3N-4 EQUATIONS;A1 WILL BE KEPT IN CELL C(2)  SPLN1
C                INSTEAD OF C(1) TO RETAIN THE TRIDIAGONAL FORM OF THE  SPLN1
C                COEFFICIENT MATRIX.                            SPLN1
C     ----------------------------------------------------------SPLN1
  100 C(2)=0.0                                                  SPLN1
      W(2)=0.5*Q*Q*D(1)                                         SPLN1
  200 M=N-2                                                     SPLN1
      IF(M.LE.0) GO TO 350                                      SPLN1
C     ----------------------------------------------------------SPLN1
C                UPPER TRIANGULARIZATION OF THE TRIDIAGONAL SYSTEM OF  SPLN1
C                EQUATIONS FOR THE COEFFICIENT MATRIX FOLLOWS--  SPLN1
C     ----------------------------------------------------------SPLN1
      DO 300 I=1,M                                              SPLN1
      AI=C                                                      SPLN1
      Q=X(I+2)- X(I+1)                                          SPLN1
      H=AI/Q                                                    SPLN1
      C(3*I)=-H/(2.0-C(3*I-1))                                  SPLN1
      W(3*I)=(-YI-W(3*I-1))/(2.0 - C(3*I-1))                    SPLN1
      C(3*I+1)=-H*H/(H-C(3*I))                                  SPLN1
      W(3*I+1)=(YI-W(3*I))/(H-C(3*I))                           SPLN1
      YI=Y(I+2)- Y(I+1)                                         SPLN1
      C(3*I+2)=1.0/(1.0-C(3*I+1))                               SPLN1
  300 W(3*I+2)=(YI-W(3*I+1))/(1.0-C(3*I+1))                     SPLN1
C     ----------------------------------------------------------SPLN1
```

```
C               F(N-1) IS DETERMINED DIRECTLY FROM THE LAST EQUATION    SPLN1
C               OHTAINED ABOVE, AND THE FIRST CR SECOND DERIVATIVE       SPLN1
C               VALUF GIVEN AT THE END POINT.                            SPLN1
C          ----------------------------------------------------------SPLN1
350       IF(J.FQ.1) GO TO 400                                          SPLN1
          C(3*N-3)=(Q*Q*D(2)/2.0-W(3*N-4))/(3.0- C(3*N-4))              SPLN1
          GO TO 500                                                     SPLN1
400       C(3*N-3)=(Q*D(2)-YI-W(3*N-4))/(2.0-C(3*N-4))                  SPLN1
500       M=3*N-6                                                       SPLN1
          IF(M.LF.0) GO TO 700                                          SPLN1
C          ----------------------------------------------------------SPLN1
C               RACK SOLUTICN FCR ALL COEFFICENTS FXCEPT                 SPLN1
C               A(1) AND P(1) FOLLOWS--                                  SPLN1
C          ----------------------------------------------------------SPLN1
          DO 600 II=1,M                                                 SPLN1
          I=M-II+3                                                      SPLN1
600       C(II)=W(I)-C(I)*C(I+1)                                        SPLN1
700       IF(J.FQ.1) GC TO 800                                          SPLN1
C          ----------------------------------------------------------SPLN1
C               IF THE SECOND DERIVATIVE IS GIVEN AT THE END PCINTS,     SPLN1
C               A(1) CAN NOW BF COMPUTED FROM THE KNOWN VALUES OF        SPLN1
C               9(1) AND F(1). THEN A(1) AND P(1) ARF PUT INTO THEIR     SPLN1
C               PROPER PLACES IN THE C ARRAY.                           SPLN1
C          ----------------------------------------------------------SPLN1
          C(1)=Y(2) - Y(1)-W(2)-C(3)                                    SPLN1
          C(2)=W(2)                                                     SPLN1
          RETURN                                                       SPLN1
800       C(2)=W(2)-C(3)                                                SPLN1
          RETURN                                                       SPLN1
          END                                                          SPLN1
```

```
      SUBROUTINE SPLN2 (N,X,Y,C,V)
      DIMENSION X(1),Y(1),C(1),V(5)
      V(5)=2.0
      LIM=N-1
C                        ------------------------------------------------
C                        DETERMINE IN WHICH INTERVAL THE INDEPENDENT
C                        VARIABLE,V(1),LIES.
C                        ------------------------------------------------
      DO 10 I=2,LIM
10    IF(V(1).LT.X(I)) GO TO 20
      I=N
      IF(V(1).GT.X(N)) V(5)=3.0
      GO TO 30
20    IF(V(1).LT.X(1)) V(5) =1.0
C                        ------------------------------------------------
C                        Q IS THE SIZE OF THE INTERVAL CONTAINING V(1).
C                        ------------------------------------------------
C                        Z IS A LINEAR TRANSFORMATION OF THE INTERVAL
C                        ONTO (0,1) AND IS THE VARIABLE FOR WHICH
C                        THE COEFFICIENTS WERE COMPUTED BY SPLN1.
C                        ------------------------------------------------
30    Q=X(I)-X(I-1)
      Z=(V(1)-X(I-1))/Q
      V(2)=((Z*C(3*I-3)+C(3*I-4))*Z+C(3*I-5))*Z+Y(I-1)
      V(3)=((3.*Z*C(3*I-3)+2.0*C(3*I-4))*Z+C(3*I-5))/Q
      V(4)=(6.*Z*C(3*I-3)+2.0*C(3*I-4))/(Q*Q)
      RETURN
      END
```
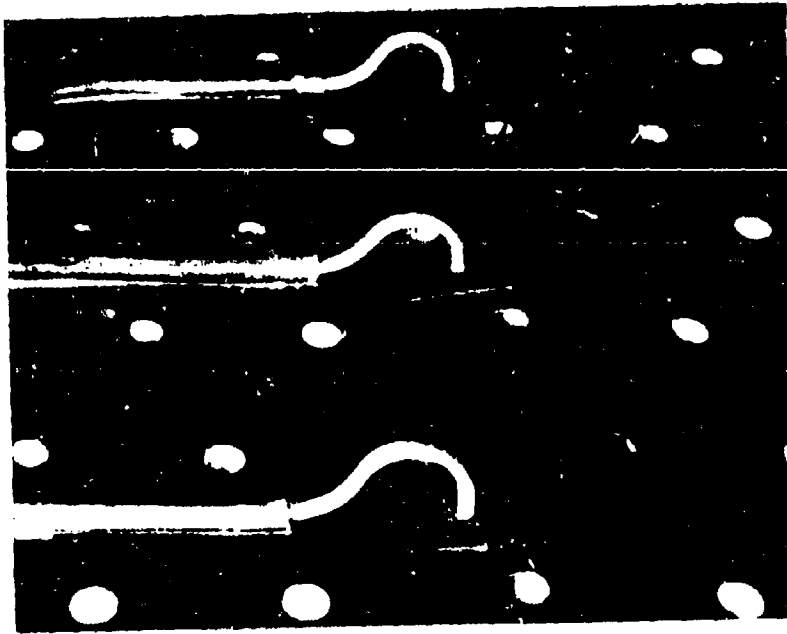
Appendix IV

TRUNK CONSTRUCTION

The trunk section was made of a nylon-hypalon material. The dimensions of the piece of material, before fabrication of the trunk, were 59-1/2 inches by 33 inches. Approximately four inches of the length was used for attaching the trunk to the model structure; the unpressurized length of the trunk became 55-1/2 inches. One-half inch of the material was folded over and sewn along each edge of the trunk to increase the stiffness of the edge (see Figure IV-1). A strip of trunk material 1-1/2 inches wide was sewn along either edge of the trunk to act as a sealing flap. When the trunk was inflated, pressure inside the trunk pressed the flap against the walls, resulting in an effective seal. A nylon string inside the fold of the flap was used as a drawstring to slightly decrease the length of the free edge of the flap. The final width of the test specimen was 32 inches.

The trunk was perforated with 192 holes of 5/16 inch diameter. The holes were arranged in 8 rows of 24 holes each, as shown in Figure IV-1. The centerline of the outside row of holes was located 31 inches from the outside attachment point. A 1/16 inch diameter hole was punched at each of the pressure tap locations indicated in Figure IV-1.
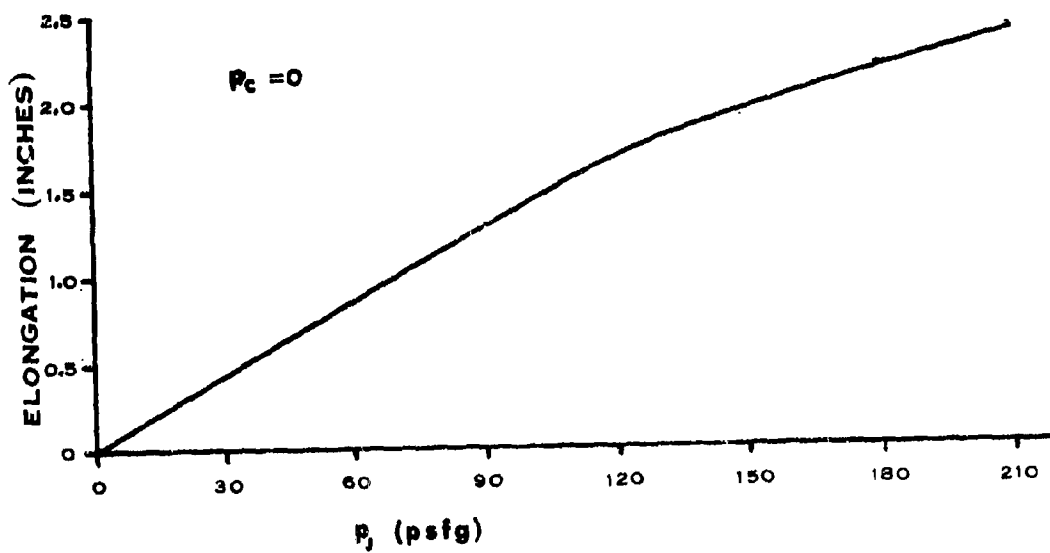
The pressure taps used to measure static pressure on the outside of the trunk are shown in Figure IV-2. A 2-inch length of 1/8 inch O.D. copper tubing was flared and flattened at one end to give a thin flat flange. The tubing was bent, as shown, and cemented to the trunk over the 1/16 inch hole with a prepunched square piece of trunk material. Plastic tubing was connected to the copper tubing, and cemented to the trunk for a short distance. Thus, motion of the copper tubing and a corresponding deflection of the trunk surface were prevented. The outside surface of the trunk had nothing protruding to disrupt the flow, and the area in which the pressure was measured was a smooth continuation of the trunk contour.

Sealing Flap

Trunk

String

Trunk Seal

1 1/4"

1 1/4"

3"

3"

◊ - Pressure Tap Location

Jet Pattern
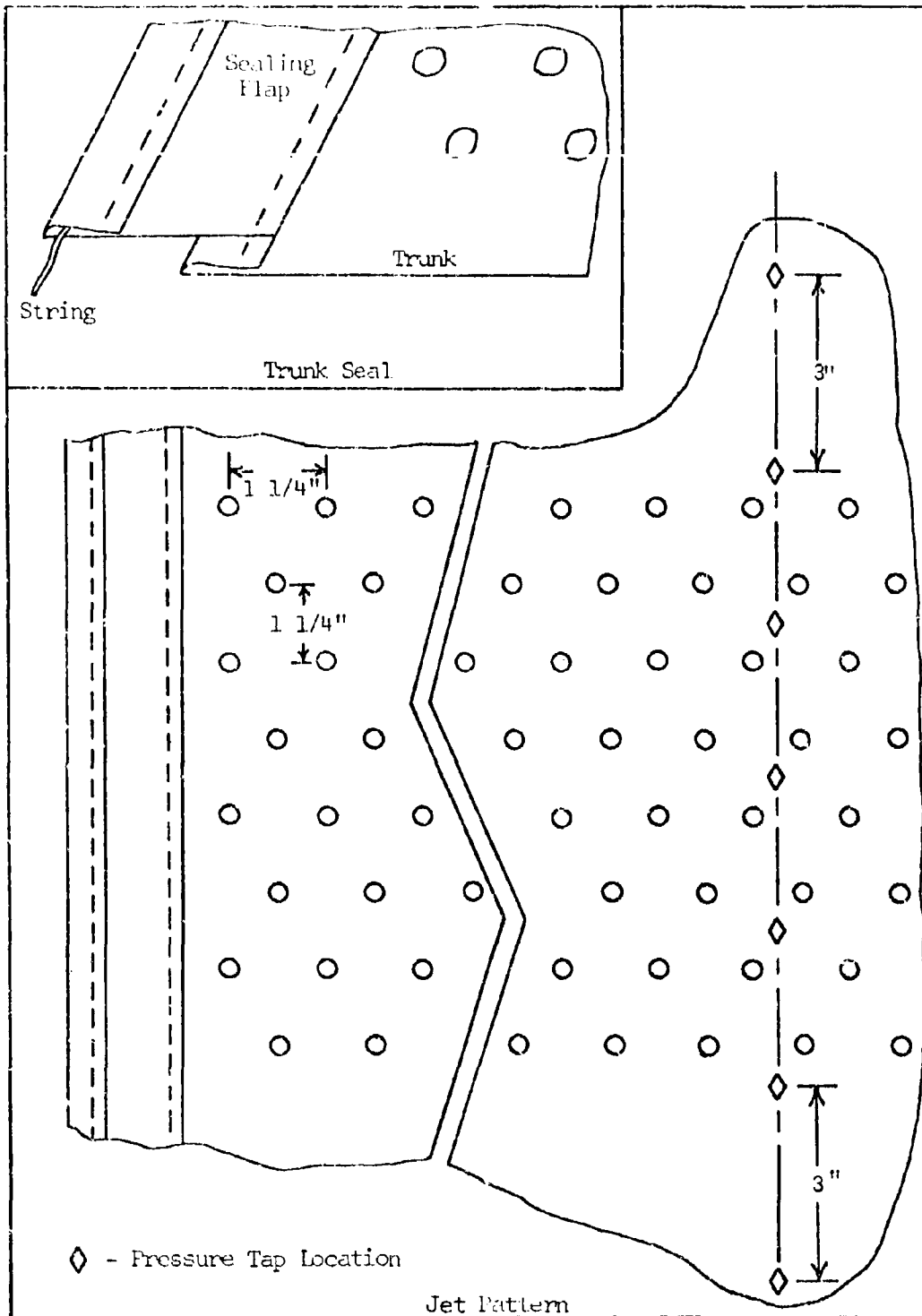
TRUNK SPECIMEN DETAILS

FIGURE IV-1

TRUNK PRESSURE TAPS
FIGURE IV-2

$P_c = 0$

TRUNK MATERIAL ELONGATION
FIGURE IV-3

A section of the trunk material was tested for tension-elongation in a tensile test machine. The results were used to predict the elongation of the trunk at various pressure levels. Figure IV-3 shows the resulting pressure-elongation curve for the trunk under test. Equation (4-1) was used to relate the tension to the trunk pressure. All results presented in Chapter 6 were corrected for trunk elongation.

Appendix V

DETERMINATION OF FLOW LEAKAGE

The flow leakage in the model was measured as a function of trunk pressure to enable corrections to be made to subsequent flow calculations.

Before the holes had been punched in the trunk, the trunk was attached to the model and inflated. In this manner, a measurement of the flow leakage between the trunk section and the walls of the model was made. A 1.2 inch orifice was used for flow measurement because the flow rate was quite low. The flow leakage measurements are presented in Figure V-1.

295
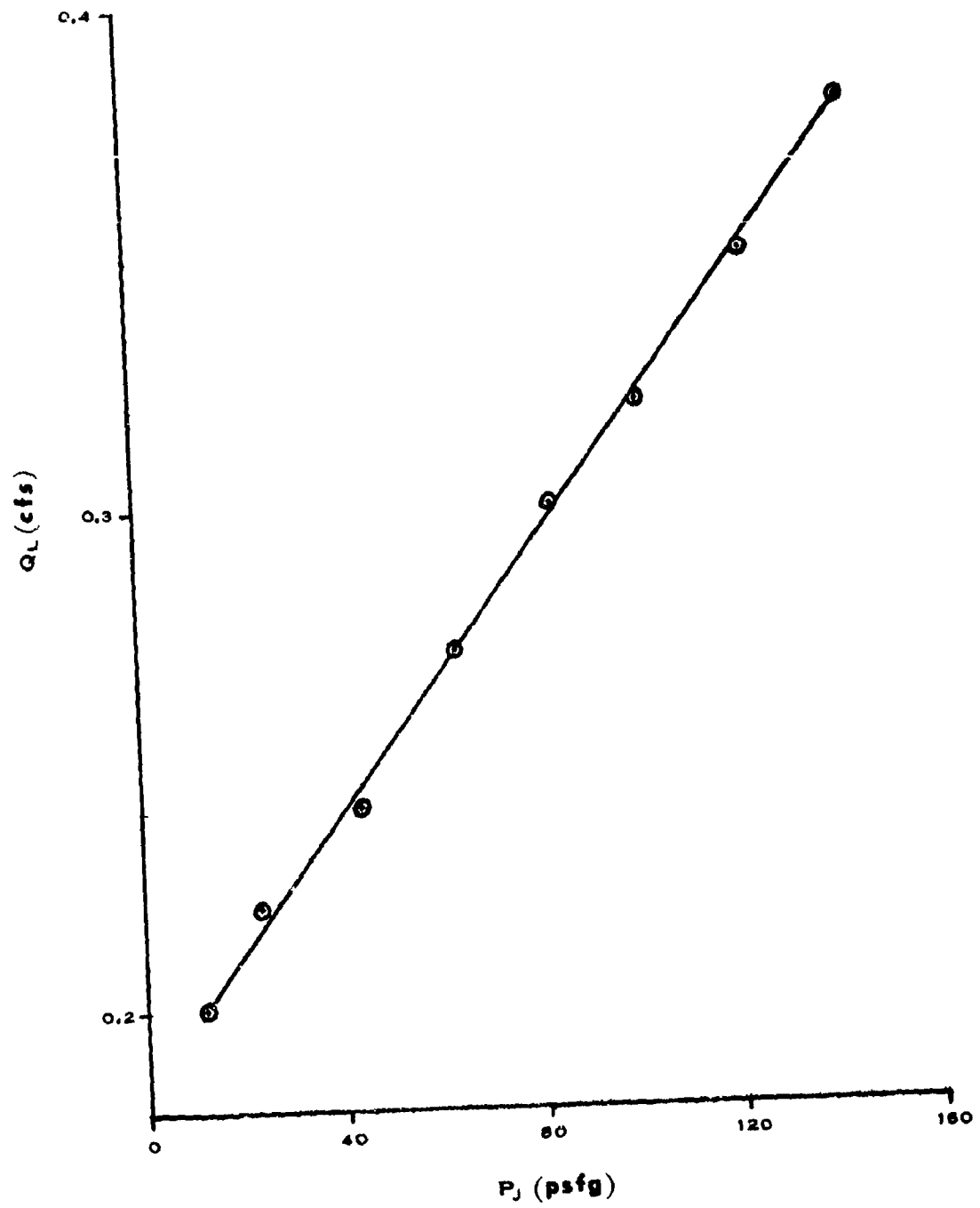
LEAKAGE VARIATION WITH TRUNK PRESSURE
FIGURE V-1

Appendix VI

COEFFICIENT OF DISCHARGE OF TRUNK

The coefficient of discharge of the trunk (C_x) is the flow coefficient for the entire orifice area of the trunk (a_j), in the absence of cushion pressure.

With the movable floor removed from the model, the air gap between the trunk and the bottom of the model was sufficiently large that no restriction was presented to trunk flow. Thus, the pressure on the outside of the trunk was equal to atmospheric pressure. The system was operated throughout an extended range of trunk pressures, 10-140 psf, and the data required for flow calculations were recorded.

The ideal rate of flow through the holes would be that predicted by a combination of the laws of conservation of energy and mass.

$$Q_{id}(cfs) = \sqrt{\frac{2g_o}{\gamma} p_j} \; (a_j) \tag{VI-1}$$

The coefficient of discharge of the trunk is herein defined as the ratio of actual jet flow, when there is no cushion present, to the ideal jet flow.

$$C_x = \frac{Q_j}{\sqrt{\frac{2g_o}{\rho} p_j} \; a_j} \tag{VI-2}$$

To make the results applicable to subsequent runs when a cushion exists under part of the trunk, C_x was plotted as a function of P_x/P_j. P_x is defined as the average of the absolute cushion pressure and atmospheric pressure.

297
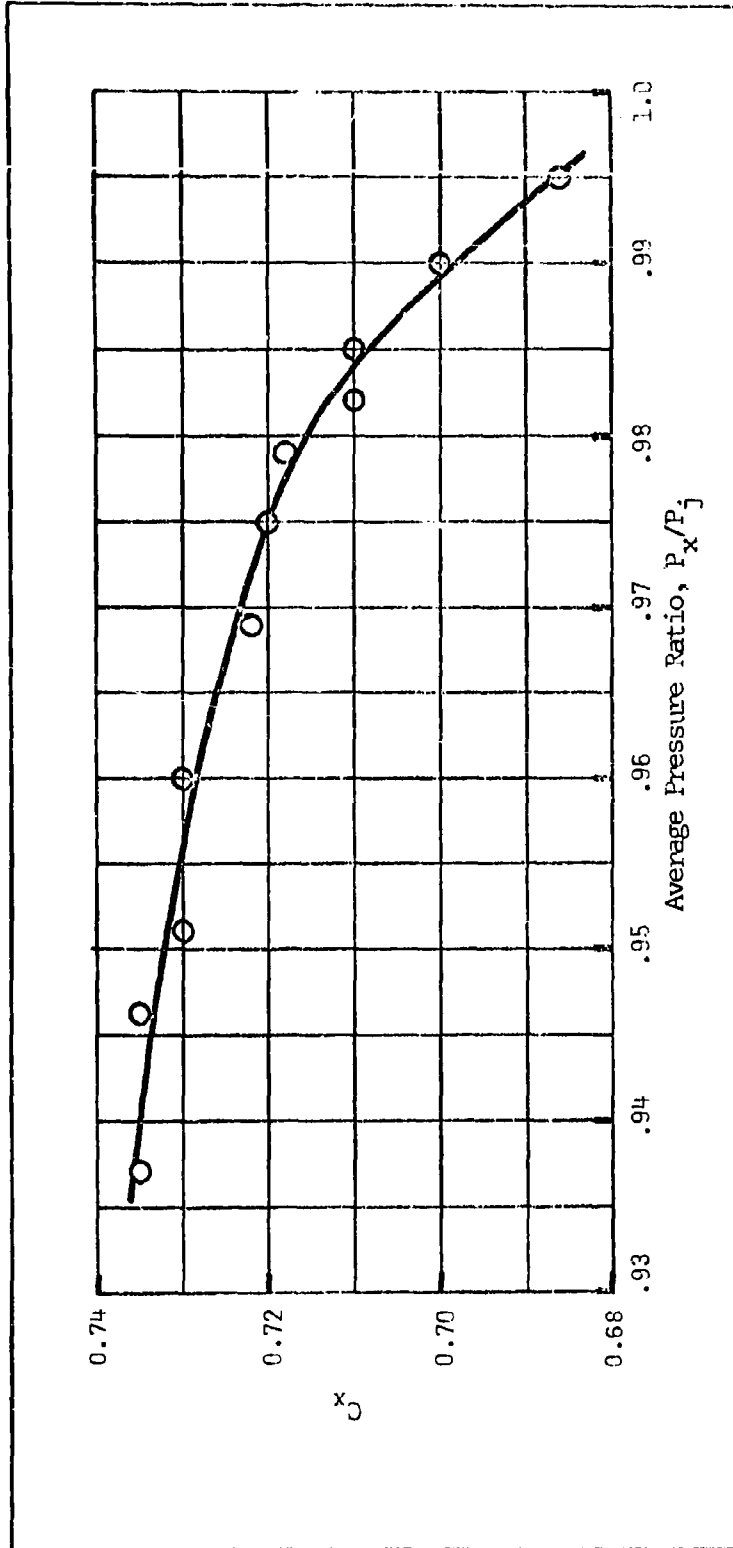
TRUNK DISCHARGE COEFFICIENT vs

AVERAGE PRESSURE RATIO

FIGURE VI-1

REFERENCES

1. T. D. Earl, AFFDL-TR-67-32, "Air Cushion Landing Gear Feasibility Study," Bell Aerosystems Company, Mar 1967.

2. T. D. Earl and R. H. Cooper, AFFDL-TR-68-124, "Air Cushion Landing Gear for Aircra , Bell Aerosystems Company, August 1968.

3. C. Stauffer, AFFDL-TR-69-32, "Ground Flight Test Report of Air Cushion Landing Gear (LA-4)," Bell Aerosystems Company, Apr 1969.

4. D. J. Perez and H. K. Brewer, AFFDL-TM-69-11-FDFM, "Air Cushion Landing Gear Skid Brake Heat Transfer Study," AF Flight Dynamics Laboratory, Feb 1969.

5. K. H. Digges and D. J. Perez, "Air Cushion Landing System for STOL Aircraft," AF Flight Dynamics Laboratory, V/STOL Technology and Planning Conference, 25 Sep 1969.

6. D. J. Perez, "Implications of Air Cushion Landing System on STOL Aircraft,' AF Flight Dynamics Laboratory, 1969.

7. J. Taylor, "All the World's Aircraft," McGraw-Hill Publishing Co., 1964.

8. A. Harting, "A Literature Survey on the Aerodynamics of Air Cushion Vehicles," AGARD Report No. 565, 1969.

9. T. D. Earl, "AGARDograph on Ground Effect Machines," AGARDograph No. 67, Jan 1962.

10. J. C. M. Frost, "Flow Phenomena of the Focused Annular Jet, Symposium on Ground Effect Phenomena," Princeton University, Oct 1959.

11. J. C. M. Frost, "The Canadian Contribution to the Ground Cushion Story," Canadian Aeronautical Journal, October 1961.

12. R. K. Greif and W. H. Tolhurst, " Large Scale Wind Tunnel Tests of a Circular Planform Aircraft with a Peripheral Jet for Life, Thrust and Control," NASA TN D-1432, Feb 1963.

13. J. B. Chaplin, "The Development of a Multi-Cell Plenum Concept," AIAA Paper 64-188, May 1964.

14. W. Z. Stepniewski, "Performance Possibilities of Subsonic Airplanes Taking-Off and Landing on the Ground Cushion," Symposium on Ground Effect Phenomena, Princeton University, Oct 1959.

15. W. Z. Stepniewski, "The Subsonic VTOL and GETOL in Perspective," Aerospace Engineering, Oct 1959.

16. S. Montuoro, "Preliminary Results of an Experimental Investigation of Various Annular Jet Configurations in Ground Effect," Atti del Ve Congresso Aeronautico Europeo, Venezia, Sep 1962.

17. W. Z. Stepniewski and F. J. McHigh, "Performance Considerations of Ground Effect Take-Off and Landing (GETOL) Transport Aircraft," New York Academy of Sciences, Vol 107, Article 1, Mar 1963.

18.   W. Z. Stepniewski, et al., "Research Program to Determine the Feasibility and Potential of the Ground Effect Take-Off and Landing (GETOL) Configuration," Vol 1, US Army Transport Research Command, TCREC Technical Report 62-63.

19.   Convair's "GETOL Flight," Feb 1963.

20.   W. D. Reeder and F. W. McDonald, "GETOL Aircraft, A Research Status Report," Institute of Aerospace Sciences, IAS Paper 62-182, Jun 1962.

21.   Ph. Poisson-Quinton, "Two-Dimensional Studies of a Ground Effect Platform," Symposium on Ground Effect Phenomena, Princeton University, Oct 1959.

22.   Ph. Poisson-Quinton, "Influence of the Proximity of the Ground on the Aerodynamic Characteristics of V/STOL Aircraft Using Jets," AGARDograph 46, Symposium on V/STOL Aircraft, Part II, Jun 1960.

23.   K. Dau, "Characteristics of a Rectangular Wing with a Peripheral Jet in Ground Effect," Part I, University of Toronto, Institute of Aerophysics, UTIA TN-56, Sep 1961.

24.   J. M. Davis, "Characteristics of Rectangular Wing with a Peripheral Jet in Ground Effect," Part II, University of Toronto, Institute of Aerophysics, UTIA TN-59, May 1962.

25.   K. Dau, et al., Aerodynamics of a Rectangular Wing with a Peripheral Jet for Air Cushion Take-Off and Landing," Canadian Aeronautics and Space Journal, Mar 1965.

26. A. W. Carter and L. H. Person, "Investigation of the Free-Flight Characteristics and Handling Qualities of a Ground Effect Machine," NASA TN-D-3885, Apr 1967.

27. "New Developments in Air Cushion Vehicles," Hovering Craft and Hydrofoil.

28. R. McLeavy, "Jane's Surface Skimmer Systems," 1967-68 1st Edition Sampson Low, Marston, London, 1967.

29. R. McLeavy, "Jane's All The Worlds Surface Skimmer Systems," 69th Edition.

30. G. D. Boehler, "Aerodynamic Theory of the Annular Jet," Institute of Aerospace Sciences, IAS Report 59-77, Jan 1959.

31. H. R. Chaplin and B. Stephenson, "Preliminary Study of the Hovering Performance of Annular Jet Vehicles in Proximity to the Ground," David Taylor Model Basic, DTMB Aero Report 947, Sep 1958.

32. T. Strand, Inviscid, "Incompressible Flow Theory of Static, Peripheral Jets in Proximity to the Ground," Journal of the Aerospace Sciences, Jan 1961.

33. F. F. Ehrich, "The Curtain Jet," Journal of the Aerospace Sciences, Nov 1961.

34. M. J. Cohen, "Peripheral Jets in Proximity of the Ground," Journal of Applied Mechanics, Dec 1966.

35. T. P. Bligh, "The Potential Flow Solution of the Peripheral Jet of an Air Cushion Vehicle, Applicable to all H/t Ratios," University of Witwatersrand Report 30, Dec 1965.

36.   J. T. Diez Roche, "The Preipheral Jet Theory," Proceedings of the 11th International Congress of Applied Mechanics, Munich, Aug and Sep 1965.

37.   H. H. Richardson and K. M. Captain, "Simplified Static Performance Characteristics of Low-Pressure Plenum and Peripheral Jet Fluid Suspensions," Massachusetts Institute of Technology, Jan 1968.

38.   H. R. Chaplin, "Effect of Jet Mixing on the Annular Jet," David Taylor Model Basin, DEMB Aero Report 953, Feb 1959.

39.   H. R. Chaplin, "Theory of the Annular Nozzle in Proximity to the Ground," David Taylor Model Basin, DTMB Aero Report 923, Jul 1957.

40.   R. Stanton Jones, "Some Design Problems of Hovercraft," Institute of Aerospace Sciences, IAS Paper 61-45, Jan. 1961.

41.   A. J. Burgess, "A Two-Dimensional Static Stability Theory for an Air Cushion Vehicle with a Central Stability Jet," Department of Aeronautics and Astronautics, A.A.S.U. Report No. 256, University of Southampton, Great Britain, May, 1964.

42.   V. Khanzhonkov, "Calculated Parameters of Air-Cushion Devices with Nozzle Device at Hovering Condition," Translation by Institute of Foreign Technology, WPAF Base, FTD-RT-23-1277-67, 15 Jan 1968.

43.   T. Fujita, "Double Jet Theory," Working Paper No. 7, Vehicle Research Corp., Pasadena, Calif., 2 May 1962.

44. S. B. Gates, "A Crude Theory of Hovercraft Performance at Zero Tilt", Royal Aircraft Establishment RAE Technical Note Aero 2800, Nov. 1961.

45. J. B. Esgar and W. C. Morgan, "Analytical Study of Soft Landings on Gas-Filled Bags," NASA TR R-75, Mar. 1960.

46. S. D. Conte, "Elementary Numerical Analysis," McGraw-Hill, 1965, p. 65, p. 222.

47. L. K. Spink, "Principles and Practices of Flow Meter Engineering," (Ninth Edition), Forboro, Massachusetts: Foroboro Company, 1967.

48. ASME Research Committee on Fluid Meters, "Fluid Meters, Their Theory and Application," (Fifth Edition), New York: American Society of Mechanical Engineers, 1959.

49. L. S. Han, "Air Cushion Pressure During Stiff-Operation for Air Cushion Landing Systems", AFFDL Technical Report, AFFDL-TR-71-4, May 1971.

50. C. L. Stauffer, "Water Operations and Overland Braking Test Report of Air Cushion Landing System (LA-4)," Technical Report AFFDL-TR-69-125, Textron's Bell Aerosystems Co., 1969.